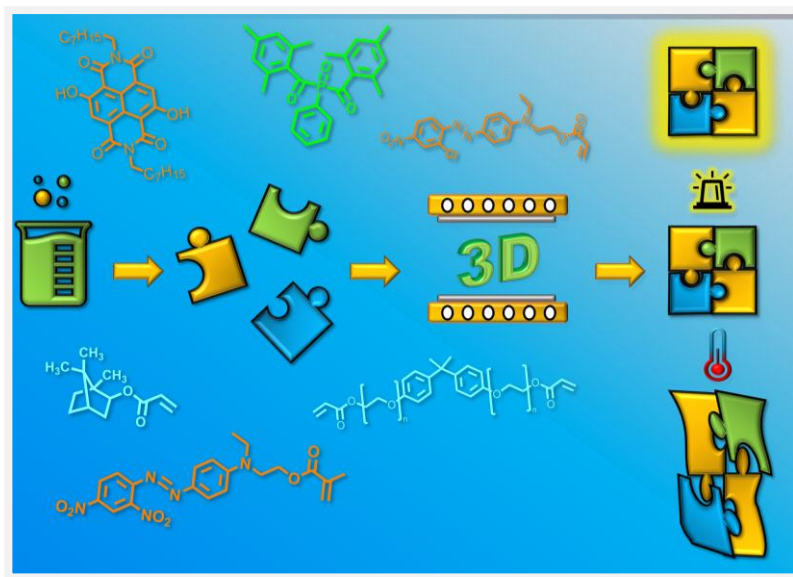**Università degli Studi di Torino**
Doctoral School of the University of Torino
PhD Programme in Chemical and Materials Sciences 34 Cycle

Functional 3D printed polymeric materials exploiting engineered dyes and pigments

Matteo Gastaldi

Supervisor:
Prof. **Claudia Barolo**

Co-Supervisors:
Prof. **Marco Zanetti**
Prof.ssa **Silvia Bordiga**
Dott. **Ignazio Roppolo**

Università degli Studi di Torino

Doctoral School of the University of Torino

PhD Programme in Chemical and Materials Sciences 34 cycle

Functional 3D printed polymeric materials exploiting engineered dyes and pigments

Candidate: **Matteo Gastaldi**

Supervisor: Prof. **Claudia Barolo**

Jury Members: Prof. **Pierangiola Bracco**
                   Università di Torino
                   Department of Chemistry

                   Prof. **Marco Sangermano**
                   Politecnico di Torino
                   Department of Applied Science and Technology

                   Prof. **Francesca Brunetti**
                   Università di Roma "Tor Vergata"
                   Department of Electronics Engineering

Head of the Doctoral School: Prof. Alberto Rizzuti
PhD Programme Coordinator: Prof. Bartolomeo Civalleri

Torino, 2022

Abstract

Polymeric materials have found growing applications, thanks to their peculiar mechanical and chemical properties that make these materials advantageous in uncountable applications. They still show some limits, such as poor electrical and thermal conductivity, absence of emitting properties and the impossibility of tuning their properties as needed. Moreover, recycling remains a problem not wholly overcome, and many plastic materials are dumped in landfills every year.

Here, the attention focuses on providing innovative functionalities to generally inert polymeric matrices, opening their uses as sensors. Dyes are synthesised and inserted into polymers, allowing them to change their properties under suitable external stimulations. Secondly, recent innovations in additive manufacturing will enable the production of complex-shaped devices quickly without wasting raw materials and requiring complex-forming techniques.

New research in 4D printing is demonstrated here, joining these two fields, in which the 4th dimension is time or some external stimulations. First, carbon nanotubes and graphite nanoplates are exploited to confer piezoresistive properties to a non-conductive polymeric matrix. Small quantities of suitable dyes are then used to obtain light-emitting materials, act as downshifter polymers, and shift their emission by changing the temperature. New applications of well-known azodyes are also described here as functional materials that can confer shape-memory properties, light-tunable elastic modulus or even gas permeability. Besides temperature and light, pH stimulation is also exploited through dyes dispersed into the polymeric matrix, which changes their absorption and emission spectra in different acidic or basic conditions. The attention was focused on the organic synthesis of these chromophores, both on the printing process that can be improved in final resolutions and on fidelity to the virtual project introducing these functional moieties. Preliminary results are described here, paving the way for future developments of these techniques, which represent one of the possible ways to exploit polymers more sustainably.

Table of contents

List of Figure

detection fluorescence of the slice was obtained from the 3D printed hybrid structure (scale bar 1 mm).

List of Table

List of abbreviations

3DP	Three-dimensional Printing
ABS	Acrylonitrile-Butadiene-Styrene
ACN	Acetonitrile
AM	Additive Manufacturing
AN-PDLLAPTMEG	Poly(D,L-lactide)-poly-(tetramethylene oxide) glycol copolymers
ATRP	Atom Transfer Radical Polymerization
BEDA	Bisphenol A ethoxylate diacrylate
BEMA	Bisphenol A ethoxylate dimethacrylate
CAD	Computer-aided design
CB	Carbon Black
CNTs	Carbon Nanotubes
DBU	1,8-Diazabicyclo[5.4.0]undec-7-ene
DCM	Dichloromethane
DLP	Digital Light Processing
DMA	Dynamic Mechanical Analysis
DMSO	Dimethyl Sulfoxide
EtOAc	Ethyl Acetate
EtOH	Ethanol
FFF	Fused Filament Fabrication
GNP	Graphite Nanoplatelets
HDDA	1,6-Hexanediol diacrylate
HMBT	2-(2-Hydroxy-5-Methylphenyl)benzotriazole
HMPP	2-Hydroxy-2-Methylpropiophenone
IBA	Isobornyl acrylate
MeOH	Methanol
MWCNTs	Multiwall Carbon Nanotubes
PA	Polyamide
PA12	Polyamide 12
PC	Polycarbonate
PCL	Poly(ε-caprolactone)
PEGDA	Poly(ethylene glycol) diacrylate
PHR	Per Hundred Resin
PI	Photoinitiator
PLA	Polylactide
PS	Polystirene
QY	Quantum Yield
RP	Rapid Prototyping
SDS	Sodium dodecyl sulphate

SEM	Scanning Electron Microscopy
SLA	Stereolithography
SLS	Selective Laser Sintering
SMPs	Shape-memory Polymers
TCDMA	Tricyclo[5.2.1.02,6]decanedimethanol diacrylate
TEA	Triethylamine
THF	Tetrahydrofuran
TPO	Diphenyl(2,4,6-trimethylbenzoyl)phosphine oxide
TPP	Two Photon Polymerization
TPU	Thermoplastic polyurethane
Tr	Transmission rate
V3DP	Vat 3D Printing
VP	Vat Photopolymerization
XPS	X-Ray Photoelectron Spectroscopy

Scaffolds of all synthesized molecules

3

4

5

6

7

8

9 L =

10 L =

12

13

14-17; 26-28; 31
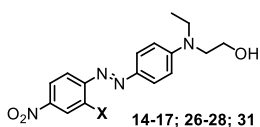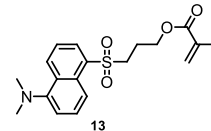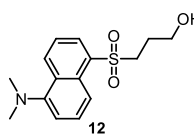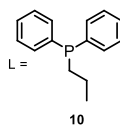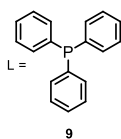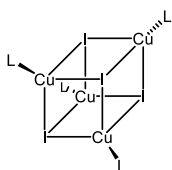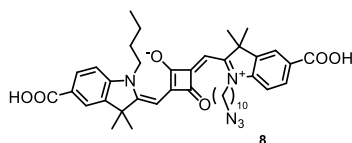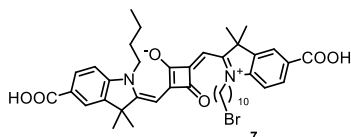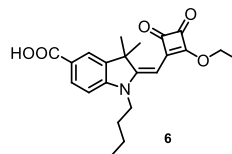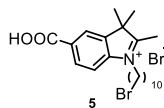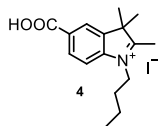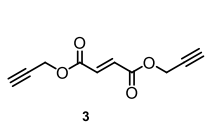
X = H (**14**), Cl (**15**), OCH$_3$ (**16**), NO$_2$ (**17**), F (**26**), Br (**27**), I (**28**)

18-21; 29-32
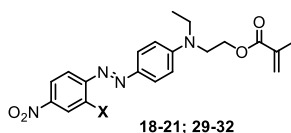
X = H (**18**), Cl (**19**), OCH$_3$ (**20**), NO$_2$ (**21**), F (**29**), Br (**30**), I (**31**)

22-25
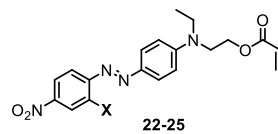
X = H (**22**), Cl (**23**), OCH$_3$ (**24**), NO$_2$ (**25**)

32

33

34
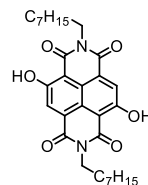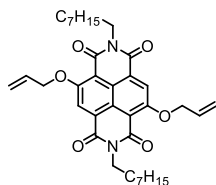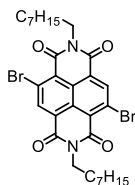
Scaffolds of monomers and photoinitiators
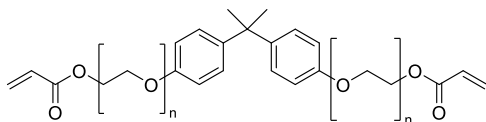
Bisphenol A ethoxylate diacrylate (BEDA)
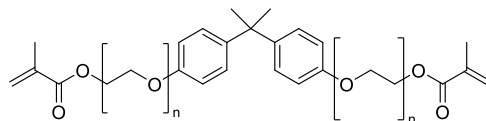
Bisphenol A ethoxylate dimethacrylate (BEMA)
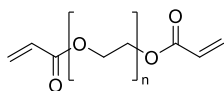
Poly(ethylene glycol) diacrylate (PEGDA)
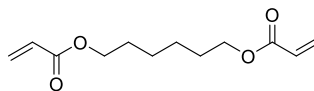
1,6-Hexanediol diacrylate (HDDA)
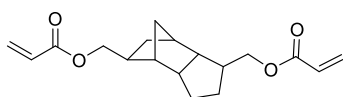
Tricyclo[5.2.1.0^{2,6}]decanedimethanol diacrylate (TCDMA)
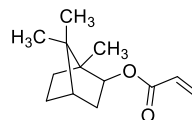
Isobornyl acrylate (IBA)
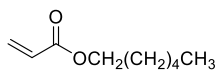
Hexyl acrylate (HA)
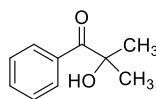
2-Hydroxy-2-methylpropiophenone (HMPP)
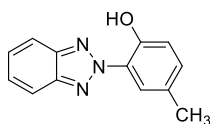
2-(2-Hydroxy-5-methylphenyl)benzotriazole (HMBT)
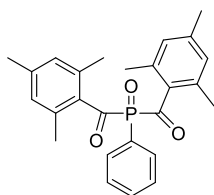
Phenylbis(2,4,6-trimethylbenzoyl)phosphine oxide (BAPO)
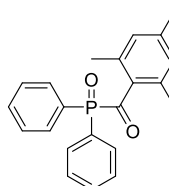
Diphenyl(2,4,6-trimethylbenzoyl)phosphine oxide (TPO)

1. Introduction

The invention of Additive Manufacturing (AM), and in particular the Stereolithography, dates back to the early 1980s when Charles Hull patented for the first time an "Apparatus for production of three-dimensional objects by stereolithography". It was the 11th of March 1986, and from this date, many improvements have been carried out by companies and scientists. Innovative technologies overcome many limits, increasing printing speed and resolution and reducing raw materials waste. Initially, less attention was devoted to mechanical properties, which is an essential issue with developing tougher or elastomeric materials for vat 3D printing (V3DP). They became helpful in the last years, not only for prototyping but directly in many production processes, due to the significant advantages of complex shapes achievable[1], high resolutions and fidelity to the virtual project,[2] saving of raw materials and energy,[3] reduced times and costs.[4] Moreover, the customizability of these techniques opens the way for using 3DP in the fabrication of biomedical devices.[5,6] Among all available materials, ceramics[7] and metals[8] can be applied in 3D printing techniques. However, polymers are the most used ones, and they represent the broadest category in terms of available materials and different properties.[9] Many printing configurations can be applied on thermoplastic and thermoset polymers, from sintering powders to melting filaments and photopolymerization under UV irradiation.[10]

The addition of some functionalities to polymers came from the necessity to have materials that can actively respond under different stimuli, changing mechanical or chemical properties, to better adapt to different conditions.[11] Polymers with tunable features enlarge the possible uses of these materials, spacing from biomedicine to optics, electronics and sensors. Usually, these 3D printed smart polymers can be produced by introducing inorganic fillers dispersed into the matrix, using metal nanoparticles,[12,13] carbon nanotubes (CNTs),[14] inorganics,[15] graphene[16] or carbon black[17] and magnetic compounds.[18] Different stimuli can be exploited to respond by

1

exposing these materials to IR or light irradiation, magnetic or electrical fields, increasing the temperature or changing the pH of the solution.

On the other hand, fillers may introduce new issues such as increased viscosity, stability and sedimentation or dispersion, and even modification of mechanical properties. Instead, organic molecules or metalorganic complexes can be used without affecting printing parameters, and they can be synthesized by introducing different functional groups. This large variety of molecules, able to give tunable, reversible, and specific behaviour, is beginning the research process. Only a few promising results can be found in the recent literature.

In this way, the fourth dimension in 3D printing can be added, related to the possibility for these devices to have peculiar tunable properties that can change as a function of time. The production of "living" and dynamic materials, which can be programmed using external forces and stimuli according to the desired application, became possible.[19,20] For these reasons, the term 4D printing is usually referred to as shape-memory polymers (SMPs), but it can also be used more extensively to include all stimuli-responsive polymers.[21]

2. Aim of the thesis

Polymeric materials have known an exponential increase in their production and applications in the last-half century due to the low price of raw materials, their peculiar mechanical and chemical properties, and the possibility for thermoplastic ones to be recovered and re-utilized many times. Thermoset or composite materials are polymers that cannot be recovered at the end of their use, and wastes have to be incinerated or stocked in waste dumps. Moreover, during traditional manufacturing methods, wastes are usually produced, and they concur to increase the number of plastic wastes annually produced.

The limited properties of polymers in terms of thermal, electrical and light conductivity and the impossibility of tuning their mechanical and chemical properties represent limits in the applicability of these materials. Fillers are usually introduced to overcome these drawbacks, producing composites with the required characteristics for each purpose.

In this thesis, the reduction of raw material wastes is achieved by using innovative and emerging 3D printing techniques as production methods to obtain complex-shaped final objects, which are impossible to achieve with the traditional processes. The material is deposited only where needed in these techniques, avoiding waste production.

An investigation about the typical way of conferring innovative properties to polymeric matrices introducing inorganic fillers as active species is carried out, describing preliminary results aiming to obtain electrical-conductive polymeric compounds. CNTs and GNPs are introduced to obtain piezoresistive thermoplastic materials that can change their electrical conductivity under external compressions. Moreover, the resulting composite can be easily processed by obtaining homogeneous formulations printable through the FFF 3D printing technique.

The high quantities of inorganic fillers needed to obtain fast and reversible changing of piezoresistive properties under compression and the elevated prices of these materials represent the main drawbacks of this method. The palette of available inorganic fillers is still limited, and only a few peculiar properties can be conferred,

reducing the material's homogeneity and mechanical or chemical features. Additionally, recycling composite materials, even thermoplastic polymers, becomes more difficult.

The attention is then focused on using organic and metalorganic dyes to overcome these problems. Here, an investigation of innovative uses of these dyes is conducted and their engineering to improve final properties. In this way, their use as active moieties in 3D printed polymeric matrices becomes possible, opening the possibility of changing mechanical or chemical properties under appropriate external stimuli, such as light or pH. Moreover, they can be solubilized into liquid photoreactive monomers that can be photopolymerized under light irradiation using the innovative DLP 3D printing method. In this geometry, the printer can focus the light in very precise areas in which the polymerization starts, while the other parts remain liquid and can be recycled. Furthermore, DLP printers are versatile, and it is possible to tailor the properties of the final product. In this context, dyes play an essential role since they can help control the photopolymerization process, achieving better resolutions and CAD fidelity.

The post-functionalization process of an external surface of a DLP 3D printed polymeric device is carried out, by exploiting some reactive functional groups that are not involved in the photopolymerization reaction. The results demonstrate the possibility of introducing useful dyes and connecting them after the printing process, which is beneficial for photosensitive dyes, that can be degraded under LED 3D printer irradiation. Moreover, the emitting properties of dyes are preserved.

Dyes can also be introduced directly into liquid formulations, and they can be 3D printed, trapping them as dispersed moieties into the polymeric matrix. Engineering them with photoreactive groups can also be covalently connected to the polymeric chains, avoiding their leaching during use. Both ways are here investigated to obtain fast and reversible stimuli-responsive polymers.

One of the first examples of these innovative materials here reported deals with 3D printed polymeric waveguides, usually produced with expensive procedures and complex synthesis. The goal is to produce polymeric emitting waveguides using light-emitting dyes, absorb harmful and powerful UV irradiation, and downshift it in a visible

light that can be conducted through the polymeric matrix without lateral dispersions. Metalorganic complexes are first examined to obtain such materials, with promising results in quantum yield, downshifting properties, and light conductivity into a transparent 3D printed waveguide. Moreover, their ability to change the emitting wavelengths with temperature allows their use as cryogenic thermometers. Limitations in solubility, dispersibility and leaching can be avoided using photopolymerizable organic emitters. Nevertheless, these compounds suffer from low quantum yield and photo and thermal stability that require improvements before a possible industrial application.

Light can also activate chemical or mechanical processes, as usually occurs for azobenzene dyes that can undergo cis/trans isomerization under irradiation. These well-known dyes are used here as key-role players in changing the mechanical or chemical properties of the polymeric matrix. Beyond cis/trans isomerization reaction, these compounds rise in temperature under green laser irradiation, reaching high values in a few seconds and in a very localized area. Thanks to these properties, the final material can tune its modulus fast and reversible, finding interesting applications as SMPs, which are materials that can modify their shapes under light irradiation. Moreover, by functionalizing them with groups having different steric hindrance or electronic effects, changes in gas permeability can be observed and tuned under light irradiation.

Beyond light, pH is another valuable stimulus here exploited, used to obtain a fast and reversible response from a 3D printed polymeric device, finding applications as sensors. The production of devices that change colours according to different pH values helps control liquid and gas-phase reactions.

In this project, demonstrations of possible applications of low amounts, cheap, and easy to synthesize engineered dyes are provided, conferring at the same time innovative functionalities and allowing direct control of the intrinsic properties of the final material. These processes are reversible and easy to manage, exploiting ordinary external stimuli, such as light, temperature or pH. Few research works have been conducted due to the only recent innovations in photo-based 3D printers. Many studies have to be done to

enlarge the palette of available functional and smart 3D printable polymers. As reported by Yue et al., "The development of highly photo-responsive materials that can convert light into mechanical work in an efficient manner remains a research challenge", which was the inspiration source for this thesis.[22]

3. 3D Printing techniques

The invention of AM, usually called three-dimensional printing (3DP) or rapid prototyping (RP), coincides with the first patent registered by Charles Hull in the 1980s.[23] The slowness of the printing process (1-2 months) and the presence of imperfections and defects in the final devices forced researchers to improve more and more these techniques in these few years.

Nowadays, 3D printing has become one of the most promising techniques applied not only for prototyping but also in the production processes of many companies. This revolutionary method's advantages rely on the high versatility of this technique, the progressive printers' price knocks off and the considerable saving of raw materials, together with the possibility to produce items with a complex structure.[24]

The versatile applicability of 3DP devices ranges from electronics, mechanics, aerospace, and biomedical engineering.[25–28] In the automotive and aerospace industries, for example, many parts and architectural models can be created, and gun prototyping and manufacturing processes for the military have already been established.[25] The production of dental implants and prosthetic devices and the food industry and fashion have also emerged.[29]

The first common stage in all 3DP techniques is preparing a computer-aided design (CAD) that represents a virtual model of the final product to be printed. The printer then slices this CAD into many 2D layers with a defined thickness, and they will represent each step of the printing process. In this way, the additional material is added only where necessary.

The most common AM techniques are listed in Figure 1, subdivided according to the starting material used, and better described in Table 1 with the related advantages and drawbacks in the following paragraphs, with an overview of the printable materials for each configuration.[2,30]
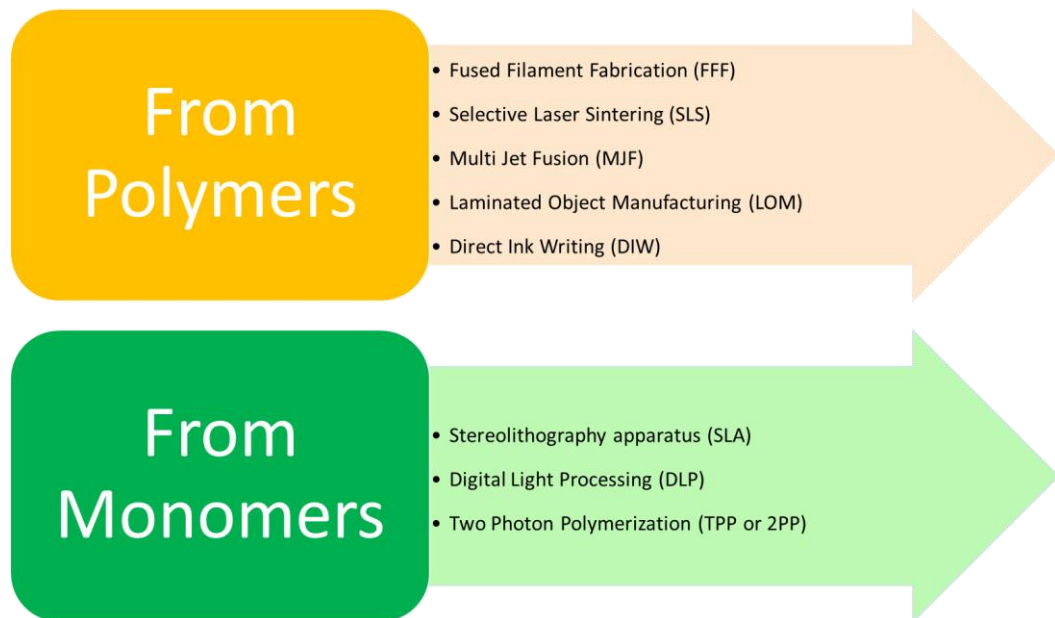
Figure 1 - *List of all principal 3D printing techniques divided by the materials used to start the printing process.*

Table 1 – *Advantages and drawbacks of the main 3D printing techniques.*

3DP technique	Printable materials	Pros	Cons	Resolution
FFF	Thermoplastic polymers (PA, PC, PLA, PS, PC) Composites (CNTs, Graphene, Graphite) Biocompatible materials (PLA)	High speed Low cost Multimaterial Large availability of materials	Low resolution Vertical anisotropy Presence of voids Reduced mechanical properties High temperature needed	100 μm -1 cm
SLS	Metals Ceramics Composites	Relatively inexpensive Good mechanical properties Unsintered powders act as supports High resolutions Large availability of materials	Low speed High power laser is necessary High dependency on particle size Rough surface	50 – 100 μm
DIW	Polymers Hydrogels Biocompatible materials	Rapid self-healing after the extrusion Low-cost technology	The ink must show a reduction in viscosity under applied shear stress Low printing speed	~ 250 μm

SLA	Photopolymers (acrylates, methacrylates, thiols, alkenes, alkynes)	Excellent resolutions Good surface finish High versatility Customized objects Good mechanical properties	No recyclability Medium-low speed A limited number of printable photopolymers	0.1 – 200 μm
DLP	Photopolymers (acrylates, methacrylates, thiols, alkenes, alkynes)	Excellent resolutions Good surface finish High versatility Customized objects Good mechanical properties	No recyclability Medium-low speed A limited number of printable photopolymers	0.1 – 200 μm
TPP	Photopolymers (acrylates, methacrylates)	Excellent resolutions Excellent surface finish Very small objects	Slow speed Elevated costs It no easy to use A limited number of printable materials	< 100 nm

3.1 Fused Filament Fabrication (FFF)

FFF is one of the most employed 3DP techniques; it is easy to use and offers the possibility to print large dimension objects. This type of printing was developed in the early 1990s by Scott Crump and opened the way to using thermoplastic polymers in the 3DP.[31]

Thin filaments of thermoplastic polymers (usually of 1.75 or 3 mm) are introduced in the extruder that can heat the material above its melting point (for semi-crystalline polymers) or glass transition temperature (for amorphous materials) and deposit it only where necessary, according to the CAD project.[9] When the first layer is completed, the head lifts up on Z-direction, and another layer is printed on the previous one. The final quality and the time required to carry out the whole process depending on the printing parameters, which must be specified initially. Among others, the filament's temperature and speed are fundamental factors to be optimized.[32–34]

Many commercial polymers can be applied, such as acrylonitrile-butadiene-styrene copolymers (ABS), polyamides (PA), polycarbonate (PC) and polylactide (PLA).[35] In this technique, many fillers, fibres and metallic particles can be easily added to tune the properties of these materials and also multi-material devices can be prepared using

9

multiple extruders.[12,29,36] Instead, organic dyes are usually avoided due to the high temperatures needed to melt the polymeric filament that can cause their thermal degradation.

FFF suffer from limited spatial resolution, principally due to the impossibility of extruding submicron-size structures, and the presence of voids might reduce the mechanical properties of the final devices.[1] Moreover, it requires time and, eventually, post-processing to obtain a smooth surface.[9] Nevertheless, its significant advantages in terms of low printing costs, the large availability of processable materials and the possibility to print multi-materials simultaneously made it the most exploited technique worldwide.[37]

3.2 Selective laser sintering (SLS)

Patented in 1992 by Carl Deckard[38], SLS is composed of a high-power laser employed to sinter glasses, polymeric powders, ceramics or even metals. The CAD project guides the laser that controls which areas have to be irradiated and the exposure time. When the first layer is done, the building stage goes down by one thickness step, a new layer of powder is deposited, and the laser scans the surface again: the final device is printed layer-by-layer with a maximum speed of about 35 mm/h.[8,39,40] Only a few polymers can be melted with the laser and processed, such as polyamide 12 (PA12), polystyrene (PS) and polycarbonate (PC), and this represent the main limitation of this technique.[40,41] Among different parameters, the most important ones to be set for good final resolutions are temperature, the powder's capability to absorb laser wavelength, the laser irradiation intensity, the size of the powders and the viscosity of the melted polymers. The high melting enthalpy and the powders' low thermal conductivity prevent the particles from melting close to the irradiated areas.

SLS doesn't need support for more complicated structures because non-sintered powders can also support top layers: these powders are completely recovered at the end of the process. The high printing speed and the large printable areas made SLS one of the most exploited for industrial purposes.[41] Also, in this case, much research was pursued to enlarge the palette of available materials, introducing graphite,

nanocomposites and even high-temperature-resistant polymers.[40] While no examples are reported about using organic dyes in this 3DP technique due to their low photo and thermal stability under laser irradiation.[35]

3.3 Direct Ink Writing (DIW)

Like FFF, DIW is based on printing high viscosity or shear-thinning inks.[2] A syringe containing the printable resin deposit the material under a pneumatic compression or a screw, forming a thin filament with controlled viscosity, temperature and pressure.[35] As already reported, the filament is deposited only in the areas identified by the project. Usually used for biological applications, many printable materials are available nowadays, spacing from ceramics and composites to polymers.[42–44] Extruding pressure and temperature must be finely controlled to obtain excellent resolutions, homogeneity and fidelity to the CAD project.[45–50] Nanoparticles, CNTs or composites can be printed using DIW, but also some organic functional dyes were recently introduced in these printable inks.[44,51] A post-functionalization process can be used at the end of the process to obtain a photo or thermal crosslinked devices to keep the shape optimally.

3.4 Photopolymerization Techniques

The photopolymerization process is a well-known and deeply studied mechanism of polymerization that takes place under light irradiation, usually with very high speed and resolutions.[35] The most exploited light source is in the ultraviolet range, but near-infrared or visible regions of the spectra can be easily used as irradiation sources.[52–56] Photoinitiators are added and dissolved in a liquid formulation to absorb radiation and generate radicals or cations that react with functional monomers starting the polymerization process.

The liquid formulations are made of photoreactive monomers (e.g., acrylate or methacrylate), and they can be mono, bi or multifunctional to produce thermoset polymers. These are insoluble in solvents and the same liquid formulation. This represents an essential element for 3D photopolymerization techniques since 3D printed parts can be built even if in continuous contact with 3D ink.

Stereolithography (SLA), digital light processing (DLP) and two-photon polymerization (TPP) are the three most important techniques. Usually, in literature, these are reported under the term of vat photopolymerization (VP) techniques. In the following paragraphs, all advantages and drawbacks are reported with a brief description of the printing process. In general, the exposure time and the power of the light source are the fundamental parameters to be optimized to obtain the best results, the temperature of the process, and the viscosity of the formulation. The irradiation intensity controls XY resolution, while the vertical resolution depends on the light penetration depth that can be controlled with a photon absorber, which can prevent the undesired polymerization.[9]

3.4.1 Stereolithography (SLA)

In the SLA configuration, a tank is filled with a liquid formulation, and a UV laser (usually at 385 nm or 405 nm) scans the surface according to a CAD project, starting the polymerization only in the irradiated areas, obtaining a first layer of the final thermoset polymeric device. The building stage is completely immersed in the liquid formulation, and the final device grows upside down in a layer-by-layer manner. When the first layer is done, the platform is lowered by one thickness layer, and after a few seconds, a new layer is printed in the same way. At the end of the process, a post-curing step in a UV oven is necessary to cure the residual reactive groups and enhance mechanical properties completely.[57] The high precision and resolution (20 μm compared to 50-200 μm of other techniques)[67] are due to a micromirror that focuses the LED irradiation in very small areas. The whole printing process is influenced by many factors such as the irradiation time, the power of the LED irradiance, and the concentration of the photoinitiator. The low cost of the printers, the reactive monomers and the capability to obtain complex shapes with high accuracy in a fast way made SLA advantageous with respect to other 3DP techniques.[52,58,59] The major limits are related to the reduced availability of printable monomers and materials, reducing possible applications. Moreover, the Z-dimension of the final object is limited, and it has to coincide with the

maximum dimension of the instrument's tank.[58,60,61] Multimaterial printing is only possible in the Z direction by changing the resin, which is not possible on the *XY* plane.

3.4.2 Digital Light Processing (DLP)

The digital evolution of SLA is DLP, in which some limits are overcome. The LED irradiation comes from the bottom of the reservoir, overtaking the Z-dimension limit of SLA. Here, there are no limitations to the maximum height achievable by the final object. Then, the light is reflected and focused only where needed, thanks to the micromirror device (DMD), which comprises thousands of movable micromirrors that can modulate the light quickly.[62] In this configuration, the whole layer can be polymerized at the same time, reducing the time needed to end the process.[24,60]

The procedure is the same previously reported for SLA. In this case, the stage is suspended above the resin reservoir, and when the first layer is created, the platform rises, and a layer of uncured resin fills the gap, and another layer is formed. Moreover, when the platform rises, the uncured resin can drain away, enhancing XY resolution and avoiding problems of liquid resin trapped in the final device.[52] The so printed object is created upside down, and the resin can easily drain and be reused.[9]

The limited palette of available materials joined with the possibility of printing only tiny objects, is the major limitation of DLP in industrial applications.

3.4.3 Two-Photon Polymerization (TPP)

Göppert-Mayer suggested the idea of the TPP in 1931, and it was based on the theory that two photons can be absorbed at the same time in a very tiny area, allowing the starting of the photopolymerization process.[63] With the invention of the laser, a source of high-intensity coherent light, the TPP became possible[64], and in 1997, the first 3DP structure printed with this technique was produced.[65,66] A cleanroom is mandatory for this peculiar technology, and chemical or plasma etching on the support is needed.

Despite other photopolymerization techniques, TPP uses the simultaneous absorption of two photons whose sum of energies is the same as the energy difference between

the ground and the excited states. The femtosecond pulsed laser is highly focused on the liquid resin. Here, the probability that two photons can be absorbed simultaneously is high in the focus, while it's very low outside.[67] The very high resolution, possible under 100 nm[68], is compensated by a low printing speed. The absence of an efficient photoinitiator and the tiny, printable objects limited TPP only in academic research.[69]

4. Functional 3DP materials: the state of the art

Functional materials are generally described in the literature as materials able to respond under an external stimulus, such as light irradiation (UV, visible, IR), changes in the external or internal temperature, pH, or even external stresses and forces applied. Additives and fillers can be added to the printable formulations to reach this goal. [59,70,71,71]

Focusing the attention only on the FFF and DLP techniques, their uses will be described in the following chapters. A description of the composition of 3D printable formulations is reported, focusing on the additives that can be introduced to improve some mechanical or chemical properties. The importance of 3DP functional materials is demonstrated by the increasing attention of many researchers worldwide and the number of papers published in recent years. In the following paragraphs, some examples about state of the art are reported, focusing on the additives introduced and the final possible applications of the 3DP devices.

4.1 Polymer-based composite

Polymer-based composites have set up more opportunities to explore new applications and innovative functions for polymers.[72] The necessity to join high performances and sustainability while maintaining at the same time low costs and very good accessibility forces researchers to find new ways to produce these advanced functional materials.[73] Many industries also require this goal to expand the application fields of AM.[74] Usually, the addition of fillers and inorganics can lead to a drastic reduction in mechanical properties, such as tensile strength and density.

4.1.1 FFF formulation

In FFF, the starting material is represented by thermoplastic polymers in the form of filaments that can be melted without degradation. Polyolefins, ABS, and PC, are the most common materials, but PLA plays a crucial role in FFF due to its biodegradability and biocompatibility. Due to the low shrinkage after the solidification, amorphous polymers are generally preferred with respect to the semi-crystalline ones.[1] The intrinsic defects of the so 3DP devices can easily be overcome by introducing inorganic fillers or organic functional dyes. The first ones are commonly added by dispersing them before the filament extrusion, improving mechanical features, electrical and thermal conductivities or conferring the magnetic responsiveness to the polymer. A the same time, organic dyes can be used to change the optical properties, such as the absorption and emission spectra producing thermochromic or emitting polymers.

4.1.1.1 Inorganic Fillers

The most exploited inorganic fillers include carbon fibres (CFs), glass fibres (GF), carbon black (CB), hydroxyapatite, graphene platelets (GP) and CNTs.[36] Relevant applications of CFs are reported in the literature as reinforcing materials, as reported by Matsuzaki et al.[75] In this paper, they reported using this type of material to enhance the mechanical properties of the tensile modulus and the tensile strength. In the same way, Gao et al.[76] used CFs to reduce the anisotropy of the 3DP object and to enhance the tensile strength. Instead, Zhong et al.[77] reported the use of short glass fibres. The reduction of flexibility counterbalances the significant increase in strength of the resulting filaments.[77]

CB are extensively used for the same purposes as previously reported[2] and only a few years ago as a material able to confer shape-memory properties to the matrix.[17] The ability to heat the material under visible or directly under sunlight is fully exploited to obtain devices that can be deformed and recover the original shape under irradiation. The same purpose was obtained using magnetite to induce the recovery of the initial shape using a magnetic and alternating field.[78]

Nikzad et al.[79] developed a method to introduce metal particles, such as iron or copper powders, to produce 3D printable composites with desirable thermo-mechanical properties. Significant advantages are also obtained from a mechanical point of view, increasing the stiffness and dynamic mechanical tests thanks to the use of FFF and the introduction of fillers.

Hydroxyapatite is also introduced as a reinforced filler to enhance the biocompatibility of the 3DP device.[15,78] An extensive evaluation of graphene's use in different forms is deeply studied and reported by Li et al.[16]

CNTs are probably the most exploited additives during the last few years due to their ability to simultaneously induce good thermal, electrical, and mechanical properties. These properties are induced by their high strength, high aspect ratio, and low weight, producing very performing polymers with low quantities of CNTs. The high cost and the difficulties in the producing methods can limit this compound's use.[80,81]

Natural fibres are other important fillers which have obtained increasing attention in the last few years. Principally obtained from industrial wastes,[82,83] this type of material plays an active role in costs and environmental impact reduction as well as in density decrease and as reinforcing materials to improve stiffness and mechanical properties.[1] The limited uses of these organic fillers reside in the low thermal stability[84] and the possibility of developing aqueous vapours under heating.[85]

4.1.1.2 Organic Dyes

Few examples of organic dyes in FFF are actually reported in the literature due to their possible thermal degradation during the extrusion process. Mechanochromic spiropyrans are introduced as dyes able to change their colour under applied stress. This class of compounds can isomerize under stress isomerizing from the spiropyran form to the merocyanine one, with the relative change of colour, as reported in Figure 2.[86] Peterson et al.[87] reported the use of these compounds covalently connected to the polymeric chains via copolymerization with poly(ε-caprolactone) (PCL). The polymers are printed at 110°C without any evidence of thermal degradation to obtain an almost totally transparent product. The reversible changes in colour under elongation and UV

irradiation are then evaluated, getting promising results in the use of this device as a sensor for mechanical stresses.

Spiropyran

Colourless

Merocyanine

Purple

Figure 2 - Isomerization of colourless spiropyran to purple merocyanine under mechanical stress or UV irradiation.

Another example of the application of organic dyes in FFF is alkoxyphenyl N-substituted naphthalene diimides (Figure 3), reported by Dharmarwardana et al.[88,89] These papers described different compounds in a biodegradable and inexpensive PLA polymeric matrix to produce a negative thermochromism effect changing the external temperature from -173°C to 140°C. Controlling the length of the alkoxyphenyl chain length, it is possible to modulate the activation of this effect at different temperatures.

Figure 3 - Scaffold of alkoxy phenyl N-substituted naphthalene diimides.

Finally, photonic crystals are also introduced in FFF printable formulation as an alternative to other organic dyes. In these compounds, some light propagation frequencies are forbidden, and in this way, they can give a colour proper to the crystalline nanostructure. After the printing process at 200°C, these moieties can rapidly self-assemble to produce nanostructure able to reflect violet and emit yellow light. Moreover, the reflected light can be modulated by changing the molecular weight.[90]

4.1.2 DLP formulation

As previously reported, each formulation is mainly composed of photoreactive monomers, photoinitiators and eventually dyes. This composition is typical of all the VP techniques. Updated reviews about the commercially available or recently developed photocurable monomers are recently reported.[9,58] Acrylates or methacrylates are the

principal monomers usually used; nevertheless, the first suffer from very strong internal stresses and shrinkages that can reduce the final resolution,[52] while the second ones are less reactive and their curing rate is slow.[91] Another type of formulation used is thiol-ene systems, which show low shrinkage, few stresses, and high conversions.[92,93] Enhanced mechanical properties can be achieved by introducing allyl ethers to reduce the influence of C-S-C bonds weakness.[94]

Photoinitiators are species able to absorb some irradiation wavelengths to generate radicals or cations that can start the polymerization reaction. This component can affect the polymerization rate, the conversion of the functional groups and the threshold to start the process.[69,95] Moreover, the light penetration into the liquid formulation and the curing depth also affect XY and Z-resolution. The curing depth (C_p) is defined as follows:

$$C_p = D_p \ln\left(\frac{E}{E_c}\right)$$

in which E is the laser exposure on the resin, E_c is the critical exposure under a specific laser wavelength, and D_p is the penetration depth[96]

$$D_p = \frac{1}{2.3\ \varepsilon[I]}$$

where ε is the molar extinction coefficient of the photoinitiator and *[I]* its concentration.

The resolution can be improved by tuning the concentration and type of photoinitiator and the exposure time, the wavelength, and the light source.[97]

Finally, inorganic fillers or organic dyes can be added to improve the mechanical features or to confer innovative properties and, particularly for dyes, enhance the final resolution, and avoid overcuring on the XY plane and in the Z direction. In fact, dyes can usually confine the photopolymerization process only in the irradiated areas individuated by the CAD project.[60]

4.1.2.1 Inorganic Fillers

As reported previously, CNTs show excellent properties also in DLP 3DP devices. Cortés et al.[14] described the use of CNTs in very low concentrations (< 0.3 wt.%) as electrically

conductive material to induce the heating through the Joule effect and the consequent shape memory recovery. The introduction of CNTs is commonly exploited in many other applications.[51,98–100]

Metal nanoparticles, such as silver[13,101] or paramagnetic iron oxide [102,103], can be even generated in situ by thermal treatment at high temperatures. The process is performed under vacuum to avoid thermal degradation. [104] The electrical properties are then tested, showing promising results. Beyond metals, other inorganics can be added to improve mechanical properties, such as boehmite[105] and carbon fibres.[106] This type of material is largely reviewed.[12,15,16,107,108]

4.1.2.2 Organic Dyes

Organic dyes are traditionally introduced to enhance the final resolution, acting as a light absorber to avoid lateral and vertical overcuring of the liquid resin. Usually, Sudan I[62,109] or Reactive Orange 16[91] are used for these purposes, thanks to their very good solubility in printable monomers and the efficiency to absorb light also in very low quantities (0.1 wt.%).

Beyond this application, some dyes were introduced to confer peculiar properties usually not characteristic of the polymeric matrix. Some azodyes (Figure 4) are used to change Young's modulus of 3DP devices under laser irradiation.[60] These two compounds differ in the absence (**A**) or the presence (**B**) of a photopolymerizable group. The authors showed the possibility of using a high-power irradiation source at 532 nm to reduce the elastic modulus for matrices made of bisphenol A ethoxylate methacrylate (BEDA) containing only 0.2 wt.% of each azodye. In this case, for compound **A**, the modulus reduction is about 27%, while with compound **B** is 75%. Rising the temperature to 48°C, this matrix showed an opposite behaviour, and, with compound **B**, the elastic modulus increases by 620% under irradiation. An increased elastic modulus value is obtained at room temperature, changing the polymeric matrix. Bisphenol A ethoxylate dimethacrylate (BEMA) has a T_g of about -38°C (while BEDA is around 46°C), with 0.1

wt.% of **A,** the elastic modulus increased by 18%. At the same time, with compound **B,** the improvement is about 58%.
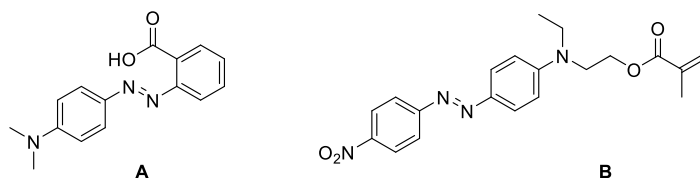
Figure 4 – Structures of A) Methyl Red azodye and B) Disperse Red 1 (DR1) azodye with a methacrylic photopolymerizable group.

The same azodyes are used as switchable moieties, which can undergo reversible *cis/trans* isomerization under light irradiation, to induce changes in gas permeability of 3DP membranes.[110] The authors reported that the CO_2 permeability was increased by 14% for polyethylene glycol diacrylate (PEGDA) containing 0.2 wt.% of A under green laser irradiation. In comparison, the same membrane containing 0.2 wt.% of **B** can increase the CO_2 permeability by about 70% in a total reversible manner. Moreover, the good selectivity for CO_2 with respect to O_2 under laser irradiation is also demonstrated, and it is about 30 times higher for CO_2 than O_2. In this direction, a demonstrator was also 3D printed as a device able to separate a mixture of different gases.

Anthracene is also an interesting molecule used in DLP printer configuration. In this case, it shows the possibility of undergoing [4 + 4] cycloaddition under UV light irradiation with a wavelength > 300 nm. At the same time, the reversible reaction can be obtained by irradiating the material with a light wavelength < 300 nm. This moiety was inserted in poly(D, L-lactide)-poly-(tetramethylene oxide) glycol copolymers (AN-PDLLAPTMEG) to obtain material able to be deformed once heated and to maintain the new shape at a temperature under its T_g. The recovery of the initial structure becomes possible under UV irradiation or heating, producing a double responsive material.[111] Moreover, anthracene can change its emission before and after irradiation, and the final device can be helpful for information storage and sample anticounterfeiting.

5. Experimental method

5.1 CNTs and graphite

The polymeric matrix selected to produce piezoresistive materials is a commercial TPU (Elastollan 1185 A 10 000) purchased from BASF. Two different types of non-functionalized MWCNTs (Nanoamor) were used: the first one presented a diameter <8 nm, a length of 10-30 μm, 95% of purity and a specific surface area of 500 m^2/g. The second type showed 50-80 nm of diameter, 10-20 μm of length, and 40 m^2/g of specific surface area. GNP (xGnP Graphene Nanoplatelets, grade M) presented a length of about 5 μm with a specific surface area of 120-150 m^2/g.

All solvents and reagents were purchased from Merck and VWR and used as received.

A mini extruder (HAAKE MiniLab II micro compounder) was used to mix MWCNTs or GNP with TPU using the same conditions optimized to avoid thermal degradation, reported in Table 2.

Table 2 - Optimized extruding parameters.

Parameter	Optimal condition
Temperature of the mixing chamber	210°C
Mixing time	3 minutes
Fillers adding time	9 minutes
Screw rotation speed	200 rpm
Max quantity of TPU	7 g

All fillers are mixed with hexanol and then added into the extruder. The solvent is removed by evaporation during mixing in the hot head of the extruder.

DSC measurements were performed with a Q200 (TA Instrument) from -75°C to 220°C under N$_2$ constant flux with a heating ramp of 20°C/min. TGA analyses were carried out with a Q600 (TA Instrument) from 30°C to 800°C under N$_2$ atmosphere with a heating ramp of 20°C/min.

The final filaments were obtained using 3DEVO NEXT 1.0 Filament Maker, which allowed the possibility to choose the optimal temperatures, filament flows, and cooling rate for all samples.

5.2 Organic molecules

5.2.1 Post-functionalization process

In this section, both the 3D printable and reactive monomer both dyes used for the post-functionalization process are synthesized according to the following procedures.

All reagents are solvents were purchased from Sigma-Aldrich, Merck, Fluka, Riedel de Haen and Alfa Aesar and used without further purification, unless otherwise noted. All solvents were purchased from VWR, Carlo Erba and Sigma-Aldrich and used without other purification. Nuclear magnetic resonance ^{1}H NMR (200 MHz and 600 MHz) and ^{13}C NMR (151 MHz) experiments were conducted using a Bruker AVANCE 200 (^{1}H operating frequency 200 MHz) and a JEOL ECZ-R instrument (^{1}H operating frequency 600) MHz.

Photorheology tests were performed with an Anton Paar rheometer (Physica MCR 302) in parallel plates. The rheometer is coupled with a Hamamatsu LC8 lamp emitting in the visible range with a cut-off filter below 400 nm (intensity 10 mW cm^{-2}). It is equipped with a glass-bottom plate and an upper one aluminium (∅ 25 mm). During the test, the sample is illuminated from below the glass plate; the light is turned on after 1 min to stabilize the system. The value of G' as a function of the irradiation time was measured for all the prepared samples.

ATR spectra were collected with a Nicolet iS50 FT-IR spectrometer (Thermo Scientific) equipped with an attenuated total reflection (ATR) accessory (Smart iTX). The spectra were collected first on a drop of the liquid photocurable formulations and then on the 3D printed samples after curing UV.

DMA analyses (Triton Technology TTDMA) were carried out on 3D printed films (5 × 20 × 0.3 mm) in order to investigate the thermomechanical properties of the final materials in a range of -40 to 70°C with a heating rate of 3°C/min at a frequency of 1 Hz and a strain of 20 μm.

XPS measurements have been performed by means of a PHI Versaprobe 5000 (Physical Electronics – Chanhassen, MN – USA), equipped with a monochromatic Al k-alpha source (1486.6 eV).

A 3D DLP Printer (3DLPrinter-HD 2.0 provided by Robot Factory) furnished with a projector (resolution of 50 µm in X and Y directions - 1920 × 480 × 1080 pixels) with a LED power density at 10 mW cm^{-2} was used to print all samples. The Z resolution can be varied from 10 to 100 µm.

Synthesis of bis(propargyl) fumarate (3):

All synthetical steps were carried out in dried glassware under an inert Argon atmosphere. Propargyl alcohol **2** (7.55 mL, 131 mmol) was solubilized in anhydrous dichloromethane (DCM) in a three-neck round-bottom flask under stirring. Triethylamine (TEA) (21.88 ml, 157.2 mmol) was added, and the mixture was cooled to 0 °C. A solution of fumaryl chloride **1** (5.65 mL, 52.4 mmol) in anhydrous DCM (30 mL) was added dropwise over 45 minutes through a dropping funnel. Then the temperature was raised to 25°C, and the reaction was stirred for 24 h, washed sequentially with a saturated solution of ammonium chloride (3 x 250 mL), and saturated sodium bicarbonate (2 x 240 mL) and brine (1 x 80 mL). The organic fractions were collected, dried under Na$_2$SO$_4$, filtered, and the solvent was evaporated under reduced pressure. The crude material was recovered as a dark brown solid, and it was purified with silica gel flash chromatography (100% ethyl ether, isocratic eluent) to obtain a brown-white solid. Yield 81.0% (42.44 mmol, 8.16 g).

^{1}H NMR (600 MHz, Chloroform-*d*): δ 6.93 (s, 2H), 4.80 (d,J = 2.5 Hz, 4H), 2.52 (t, J = 2.5 Hz, 2H).

^{13}C NMR (151 MHz, Chloroform-*d*): δ 163.99, 133.69, 75.89, 75.39, 52.64.

Synthesis of 4-((1-(10-azidodecyl)-5-carboxy-3,3-dimethyl-3Hindol-1-ium-2-yl)methylene)-2-(((E)-1-butyl-5-carboxy-3,3-dimethylindolin-2-ylidene) methyl)-3-oxocyclobut-1-en-1-olate – azide terminated squaraine dye (8) (Figure 5).
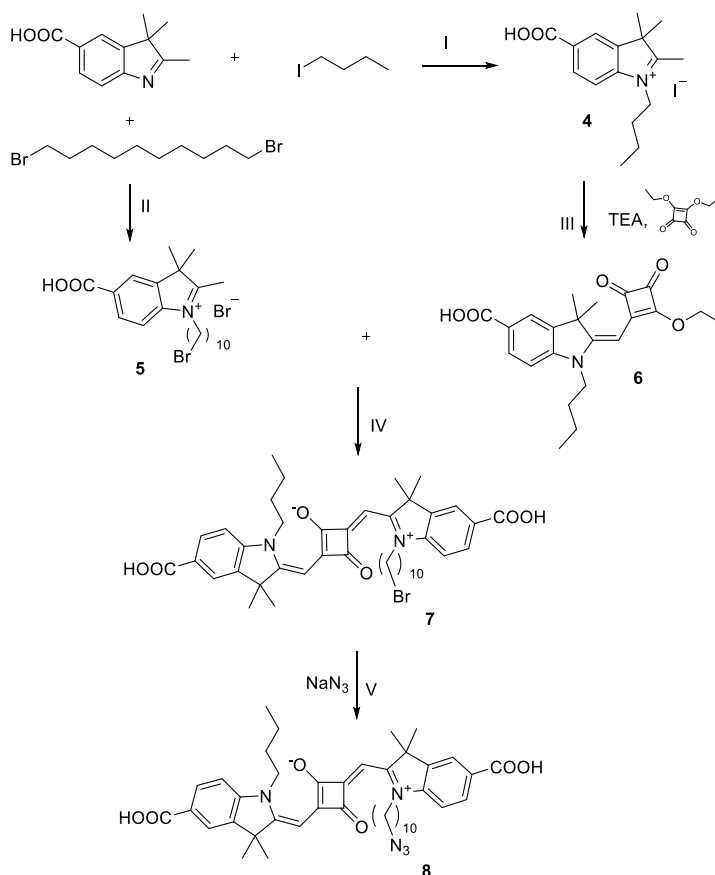
Figure 5 *- Synthetis of azide-terminated squaraine. (I) Anhydrous ACN, MW: T = 155 °C, t = 20 min. (II) Anhydrous ACN, MW: T = 165 °C, t = 60 min. (III) EtOH, MW: T = 90 °C, t = 13 min. (IV) BuOH/toluene, MW: T = 160 °C, t = 60 min. (V) DMF, MW: T = 100 °C,t = 20 min.*

Synthesis of 1-butyl-5-carboxy-2,3,3-trimethyl-3H-indol-1-ium iodide (4).

The procedure followed is the same as reported by N. Barbero et al.[112]

2,3,3-Trimethyl-3H-indole-5-carboxylic acid (2.50 g, 12.3 mmol), 1-iodobutane (5.6 ml, 49.2 mmol) and 9 ml ACN.Yield: 86% (4.10 g, 10.6 mmol). Yield: 86% (4.10 g, 10.6 mmol). All characterizations are in agreement with the literature.

Synthesis of 1-(10-bromodecyl)-5-carboxy-2,3,3-trimethyl-3H-indol-1-ium bromide (5).

2,3,3-trimethyl-3H-indole-5-carboxylic acid (0.500 g, 2.46 mmol) was inserted in a vial equipped with a magnetic stirrer. The vial was sealed, and 1,10-dibromodecane (3.69 g, 2.76 ml, 12.3 mmol) and 8 ml of anhydrous ACN were added dropwise. Argon was fluxed

24

for 15 minutes, and then the reaction was carried out in a microwave (165°C, 60 minutes). The solvent was removed under vacuum, and the product was recovered with ethyl ether, filtered and washed five times with ethyl ether. Yield 73% (0.903 g, 1.80 mmol).

^{1}H NMR (200 MHz, DMSO-d_6) δ (ppm) = 8.40 (s, 1H), 8.13 (m, 2H), 4.48 (t, 2H), 3.51 (t, 2H), 2.89 (s, 3H), 1.77 (t, 2H), 1.58 (s, 6H), 1.26 (m, 14H).

Synthesis of 1-butyl-2-((2-ethoxy-3,4-dioxocyclobut-1-en-1-yl)methylene) -3,3-dimethylindoline-5-carboxylic acid (6).

1-butyl-5-carboxy-2,3,3-trimethyl-3H-indol-1-ium (0.100 g, 0.258 mmol) was inserted in a vial equipped with a magnetic stirring. Ethanol (3 ml), 3,4-diethoxycyclobut-3-ene-1,2-dione (0.088 g, 0.08 ml, 0.52 mmol) and triethylamine (0.078 g, 0.11 ml, 0.78 mmol) were added. The reaction was conducted with the microwave (90°C, 13 minutes). The resulting mixture was evaporated under vacuum, and ethyl ether was added to recover the product. The solvent was evaporated under reduced pressure, and the so obtained solid was washed with ethyl ether (3x15 ml). The filtrate was evaporated, the liquid was diluted with DCM, and purified by flash column chromatography (EtOAc/Petroleum ether 3:7). Yield: 49% (48.5 mg, 0.126 mmol).

^{1}H NMR (200 MHz, DMSO-d_6) δ (ppm) = 7.93 (s, 1H), 7.865 (d, 1H, J = 6.0 Hz), 7.24 (d, 1H, J = 8.0 Hz), 5.44 (s, 1H), 4.82 (m, 2H), 3.93 (t, 2H, J = 8.0 Hz), 1.56 (s, 6H), 1.41 (m, 4H), 0.88 (t, 3H, J = 8.0 Hz).

^{13}C NMR (50 MHz, DMSO-d_6) δ (ppm) = 192.88, 188.93, 187.24, 172.51, 167.10, 146.40, 140.28, 130.38, 124.42, 122.76, 108.67, 82.192, 70.04, 46.962, 42.12, 28.05, 26.47, 19.39, 15.56, 13.54.

ESI-MS: 382.44 (M-1).

Synthesis of 4-((1-(10-bromodecyl)-5-carboxy-3,3-dimethyl-3H-indol-1-ium-2-yl)methylene)-2-((-1-butyl-5-carboxy-3,3-dimethylindolin-2-ylidene)methyl)-3-oxocyclobut-1-en-1-olate (7).

1-(10-bromodecyl)-5-carboxy-2,3,3-trimethyl-3H-indol-1-ium bromide (0.145 g, 0.289 mmol) and 1-butyl-2-((2-ethoxy-3,4-dioxocyclobut-1-en-1-yl)methylene)-3,3-dimethylindoline-5-carboxylic acid (0.111 g, 0.289 mmol) were dissolved in a vial employing a solution of 2 mL of butanol and toluene (1:1). The vial was sealed, and the reaction was carried out with the microwave (160°C, 1 hour). The green-blue liquid was recovered with ethyl ether, and the solvent was evaporated. The product was re-crystallised by butanol, and the obtained solid was filtered under vacuum, washed with ethyl ether and dried on the vacuum stove (40°C, 2 hours). Yield: 24% (0.052 g, 0.069 mmol).

^{1}H NMR (200 MHz, DMSO-d_6) δ (ppm) = 8.03 (s, 2H), 7.96 (d, 2H, J = 8.0 Hz), 7.43 (d, 2H, J = 8.0 Hz), 5.90 (s, 2H), 4.12 (t, 4H, J = 6.0 Hz), 3.47 (t, 2H, J = 7.0 Hz), 1.70 (m, 12H), 1.23 (m, 20H), 0.94 (t, 3H, J = 8.0 Hz).

^{13}C NMR (50 MHz, DMSO-d_6) δ (ppm) = 180.92, 170.18, 167.46, 146.35, 141.96, 130.69, 126.29, 123.66, 119.66, 110.67, 88.04, 48.97, 35.55, 32.66, 29.16, 28.46, 27.92, 26.90, 26.45, 20.04, 14.16.

ESI-MS: 759.20 (M-1).

Synthesis of 4-((1-(10-azidodecyl)-5-carboxy-3,3-dimethyl-3H-indol-1-ium-2-yl)methylene)-2-((-1-butyl-5-carboxy-3,3-dimethylindolin-2-ylidene)methyl)-3-oxocyclobut-1-en-1-olate (8):

4-((1-(10-bromodecyl)-5-carboxy-3,3-dimethyl-3H-indol-1-ium-2-yl)methylene)-2-((-1-butyl-5-carboxy-3,3-dimethylindolin-2-ylidene)methyl)-3-oxocyclobut-1-en-1-olate (0.025 g, 0.033 mmol) and sodium azide (0.0024 g, 0.036 mmol) were added in a vial and dissolved in 1 mL of DMF. The vial was sealed and the reaction was carried out with the microwave (100°C, 20 minutes). The product was recovered with DCM and it was washed with deionized water (2x50 mL) and brine (1x50 mL). Then the product was dried with Na$_2$SO$_4$, filtered and the solvent was evaporated under vacuum. Yield: 63% (0.016 g, 0.021 mmol)

^{1}H NMR (200 MHz, DMSO-d_6) δ (ppm) = 8.03 (s, 2H), 7.96 (d, 2H, J = 8.0 Hz), 7.43 (d, 2H, J = 8.0 Hz), 5.90 (s, 2H), 4.12 (t, 4H, J = 6.0 Hz), 3.47 (t, 2H, J = 7.0 Hz), 1.70 (m, 12H), 1.23 (m, 20H), 0.94 (t, 3H, J = 8.0 Hz)

The compound solubility in CDCl$_3$ proved too low to record a ^{13}C NMR spectrum.

HR-ESI-MS: calculated 720.3839, found 720.3763 (M-1).

Post-functionalization process:

Compound 8 was used to functionalize the surface of the polymeric matrix, exploiting the click chemistry reaction between the azide terminal group with alkyne ones that remain still available after the photopolymerization process. The post-functionalization procedure followed was the same one reported by A. B. Hughes et al. based on the use of Cu-catalyst.[113] The sample was introduced in a mixture of t-BuOH : H$_2$O (1 : 2), in which 0.1 mmol of squaraine was dissolved. Cu(O) powder was added, and after 2 hours, the sample was removed, washed with ethanol (3 x 5 mL) and dried under a nitrogen stream.

5.2.2 Fluorophores for 3D printing

In this work, all monomers and photoinitiators used are listed below.

- BEDA EO/phenol 2
- HDPP

5.2.2.1 Metalorganic complexes

All reagents are solvents were purchased from Sigma-Aldrich, Merck, Fluka, Riedel de Haen and Alfa Aesar and used without further purification, unless otherwise noted. All solvents were purchased from VWR, Carlo Erba and Sigma-Aldrich and used without other purification. Nuclear magnetic resonance ^{1}H NMR (200 MHz and 600 MHz) and ^{13}C NMR (151 MHz) experiments were conducted using a Bruker AVANCE 200 (^{1}H operating frequency 200 MHz) and a JEOL ECZ-R instrument (^{1}H operating frequency 600) MHz.

A DLP 3D printer (Asiga DLP-3D printer Max-UV) with a nominal X-Y pixel resolution of 27 µm and a minimum Z resolution control of 1 µm was employed to obtain 3D printed samples. The light intensity was fixed at 25 mW cm^{-2} and a layer's thickness of 25 µm, with 3 layers of burn-in (15 seconds of irradiation) and all other layers under normal irradiating time (10 seconds). The printing process was performed at 25°C, and at the end, all sides were post-cured under UV irradiation for 5 minutes each side in a UV over (provided by RoboFactory) with light intensity at 10 mW cm^{-2}.

UV-Visible absorption spectra were recorded with a Varian Cary 300 spectrophotometer in a range of 250 – 750 nm. Photoemission spectra, luminescence lifetimes and quantum yields were acquired with a HORIBA Jobin Yvon IBH Fluorolog-TCSPC spectrofluorometer, equipped with a Quanta-φ integrating sphere. All measurements were performed on 3D printed polymeric samples.

DSC measurements were performed with a Q200 (TA Instrument) ranging from -20 to 80°C with a heating ramp of 20°C/min and a cooling process with a rate of 10°C/min in N_2 atmosphere. TGA were carried out with a Q600 (TA Instrument) in a range of 30-650°C with a heating ramp of 10°C/min in air.

ATR-FTIR spectra were registered with a Nicolet iS50 Spectrometer equipped with an attenuated total reflection. The range of 4000–500 cm^{-1} was scanned (32 scans per spectra, resolution 2 cm^{-1}).

Photorheological tests were performed in real-time during irradiation using an Anton Paar rheometer (Physica MCR 302) equipped with a Hamamatsu LC8 lamp (light emission in the UVA range, intensity 25 mW cm^{-2}). The measurements were carried out in a plate-plate geometry equipped with a quartz bottom plate. The gap between the plates was 200 µm. Oscillatory measurements were performed at 25 °C, at a constant frequency (1 Hz) and amplitude (1%). Amplitude sweep test (from 0.01% to 100%, frequency 1 Hz) was preliminarily performed to evaluate the linear viscoelastic range.

The precision of the 3D printing process was evaluated using an E4 3D scanner (3Shape) with a scanning accuracy of 4 µm.

The light propagation efficiency was investigated by employing a high flux density 365 nm surface mount ceramic package UV LED with an integrated flat glass lens (LZ4– 04UV0R OSRAM) as the optical power source. The current source and voltage meter is a KEITHLEY 2602 A SourceMeter. The spectrometer is an AcalBFi USB4000 preconfigured for applications from 200 to 850 nm, and the multimode optical fibre is an FT600EMT with a numerical aperture of 0.39 and diameter of 600 μm.
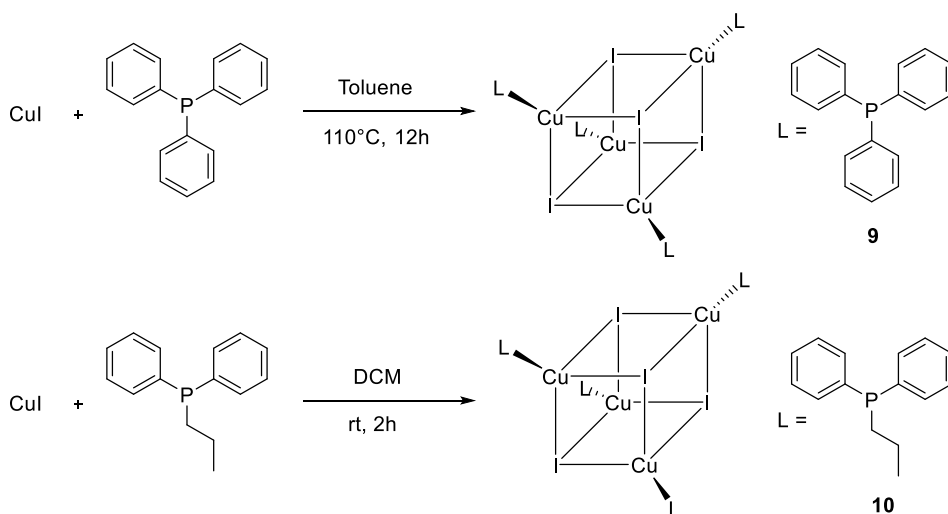
Figure 6 *- Synthesis of copper-iodine based clusters for 3D printing.*

Synthesis of copper-iodine based complex with triphenylphosphine as ligand (9) (Figure 6):

The procedure is the same as previously reported.[114] All glassware was dried overnight before use, and the air was removed with Schlenk equipment. CuI (2.6 mmol, 0.500 g) was suspended in 50 mL of toluene, and triphenylphosphine (2.6 mmol, 0.700 mg) was added. The reaction was left for 12 hours at 110°C under stirring, then the mixture was filtered, the solvent was removed under vacuum, and the solid was recovered as white crystals. Yield 52.4% (0.343 mmol, 0.617 g).

The NMR characterization matches the one reported in the literature.

Synthesis of copper-iodine based complex with diphenylpropylphosphine as ligand (10) (Figure 6):

The procedure is the same as previously reported.[115] All glassware was dried overnight before use, and the air was removed with Schlenk equipment. CuI (4.4 mmol, 0.840 g) was suspended in 20 mL of DCM and diphenylpropylphosphine (4.4 mmol, 1.0 g) was added. The solution was stirred for 2 hours, then it was filtered, and the solvent was removed under vacuum. The resulting white powder was purified by flash chromatography (PE/EtOAc 4:1). Yield 65.1% (0.859 mmol, 1.99 g).

The NMR characterization matches the one reported in the literature.

5.2.2.2 Organic fluorophores

All reagents are solvents were purchased from Sigma-Aldrich, Merck, Fluka, Riedel de Haen and Alfa Aesar and used without further purification, unless otherwise noted. All solvents were purchased from VWR, Carlo Erba and Sigma-Aldrich and used without other purification. Nuclear magnetic resonance ^{1}H NMR (200 MHz and 600 MHz) and ^{13}C NMR (151 MHz) experiments were conducted using a Bruker AVANCE 200 (^{1}H operating frequency 200 MHz) and a JEOL ECZ-R instrument (^{1}H operating frequency 600) MHz.

A DLP 3D printer (Asiga DLP-3D printer Max-UV) with a nominal X-Y pixel resolution of 27 µm and a minimum Z resolution control of 1 µm was employed to obtain 3D printed samples. The light intensity was fixed at 30 mW cm^{-2} and a layer's thickness of 25 µm, with burn-in layers' thickness of 0.300 mm (20 seconds of irradiation) and all other layers under normal irradiating time (15 seconds) with a thickness of 0.05 mm. The printing process was performed at 25°C, and at the end, all sides were post-cured under UV irradiation for 5 minutes each side in a UV over (provided by RoboFactory) with light intensity at 10 mW cm^{-2}.

UV-Visible absorption spectra were recorded with a Varian Cary 300 spectrophotometer in a range of 410 – 650 nm. Photoemission spectra, luminescence lifetimes and quantum yields were acquired with a HORIBA Jobin Yvon IBH Fluorolog-

TCSPC spectrofluorometer, equipped with a Quanta-φ integrating sphere. All measurements were performed on 3D printed polymeric samples.

Differential scanning calorimetry (DSC) measurements were performed with a Q200 (TA Instrument) ranging from -20 to 80°C with a heating ramp of 20°C/min and a cooling rate of 10°C/min in N_2 atmosphere. Thermal gravimetric analyses (TGA) were carried out with a Q600 (TA Instrument) in a range of 30-650°C with a heating ramp of 10°C/min in air.
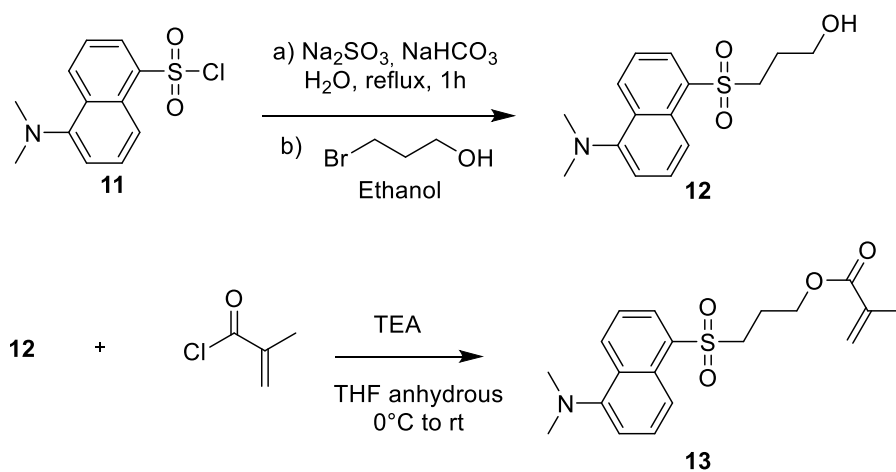
Figure 7 – Synthesis of methacrylated fluorophores for 3D printing.

Synthesis of 3-((5-(dimethylamino)naphthalen-1-yl)sulfonyl)propan-1-ol (12) (Figure 7):

Na2SO3 (11.12 mmol, 1.402 g) and NaHCO3 (11.12 mmol, 0.934 g) were dissolved in 15 mL of H2O in a round bottom flask. The temperature was raised to 95°C, and under vigorous stirring, **11** (5.56 mmol, 1.50 g) was added dropwise over an hour. After the last addition, the mixture was left for one hour under reflux, and then the flask was cooled to room temperature and water was removed employing a freeze drier. The solid product was dissolved in 25 mL of ethanol under stirring, and 3-bromopropanol (5.56 mmol, 0.773 g) was added dropwise. The mixture was left for 24 h under reflux, and the reaction was monitored by TLC (DCM : EtOAc 7:3, Rf = 0.4). Once the complete reaction

was reached, the solvent was removed under vacuum, and the solid was dissolved in DCM (30 mL) and washed with brine (4 x 20 mL). The organic fractions are collected, dried with Na_2SO_4 and filtered. The solvent was removed under vacuum to obtain a yellow solid purified by crystallization from DMF and ethyl ether. The yellow solid obtained after the crystallization was washed with ethyl ether. Yield 46.8% (2.60 mmol, 0.763 g).

^{1}H NMR (600 MHz, Chloroform-*d*): δ 8.60 (d, J = 8.5 Hz, 1H), 8.37 (d, J = 8.6 Hz, 1H), 8.29 (dd, J = 7.3; 1.3 Hz, 1H), 7.59 (m, 2H), 7.20 (d, J = 7.6 Hz, 1H), 3.72 (q, J = 5.7 Hz, 2H), 3.45 (m, 2H), 2.89 (s, 6H), 1.98 (m, 2H).

^{13}C NMR (151 MHz, Chloroform-*d*): δ 152.29, 134.26, 131.59, 130.62, 130.45, 129.96, 128.92, 123.51, 118.47, 115.44, 60.72, 52.85, 45.48, 25.84.

ESI-MS (m/z): calculated 293.11, found 294.04 [M + H]$^+$

λ (EtOH abs.) = 342 nm

ε (EtOH abs.) = 3.548*10^3 L mol^{-1} cm^{-1}

Emission: 522 nm (Excitation 325 nm)

Quantum yield (φ): 47.15% (excitation 345 nm, emission 370-650 nm)

Stokes shift: 180 nm

3-((5-(dimethylamino)naphthalen-1-yl)sulfonyl)propyl methacrylate (13) (Figure 7):

In an anhydrous round bottom flask under argon atmosphere, **12** (0.68 mmol, 0.200 g) was dissolved in 8 mL of anhydrous THF under stirring. The temperature was cooled down to 0°C then TEA (0.82 mmol, 0.11 mL) and freshly distilled methacryloyl chloride (0.89 mmol, 0.086 mL) were added. The reaction was left for 12 h at room temperature, and it was monitored by TLC (DCM:MeOH 95:5, Rf = 0.84). Once the complete conversion was reached, EtOAc (50 mL) was added, and the mixture was filtered. The solvents were removed under vacuum, and the resulting solid product was dissolved in DCM and washed with brine (3 x 30 mL). The aqueous fractions were extracted with DCM, and all organic fractions were collected, dried with Na_2SO_4 and filtered. The organic solvent was removed under vacuum, and the water residues were removed by

freeze-drying. The product was recovered as a yellow solid. Yield 45.9% (0.313 mmol, 0.113 g).

^{1}H NMR (600 MHz, Chloroform-*d*): δ 8.61 (dt, J = 8.5, 1.1 Hz, 1H), 8.35 (dt, J = 8.6, 0.9 Hz, 1H), 8.30 (dd, J = 7.3, 1.3 Hz, 1H), 7.59 (ddd, J = 8.6, 7.4, 1.2 Hz, 2H), 7.20 (dd, J = 7.7, 0.9 Hz, 1H), 5.95 (dq, J = 2.0, 1.0 Hz, 1H), 5.50 (dq, J = 2.0, 1.0 Hz, 1H), 4.15 (t, J = 6.2 Hz, 2H), 3.44 – 3.39 (m, 2H), 2.90 (s, 6H), 2.13 – 2.06 (m, 2H), 2.01 (dd, J = 1.6, 1.0 Hz, 1H), 1.83 (dd, J = 1.6, 1.0 Hz, 3H).

^{13}C NMR (151 MHz, Chloroform-*d*): δ 167.00, 152.37, 135.90, 133.94, 131.72, 130.76, 130.40, 129.99, 128.95, 125.98, 123.53, 118.30, 115.45, 62.24, 52.54, 45.48, 22.62, 18.26.

ESI-MS (m/z): calculated 361.456, found 362.11 [M + H]$^+$

λ (EtOH abs.) = 344 nm

ε (EtOH abs.) = 4.393*10^3 L mol^{-1} cm^{-1}

Emission: 522 nm (Excitation 325 nm)

Quantum yield (ϕ): 41.55% (excitation 345 nm, emission 370-650 nm)

Stokes shift: 178 nm

5.2.3 Azodyes

All reagents are solvents were purchased from Sigma-Aldrich, Merck, Fluka, Riedel de Haen and Alfa Aesar and used without further purification, unless otherwise noted. All solvents were purchased from VWR, Carlo Erba and Sigma-Aldrich and used without other purification. Nuclear magnetic resonance ^{1}H NMR (200 MHz and 600 MHz) and ^{13}C NMR (151 MHz) experiments were conducted using a Bruker AVANCE 200 (^{1}H operating frequency 200 MHz) and a JEOL ECZ-R instrument (^{1}H operating frequency 600) MHz.

The DLP 3D printer is an Asiga Freeform Pico Plus 39 DLP printer that uses a LED light source (405 nm) with an intensity of 22 mW cm^{-2} (XY resolutions of 39 mm, the layer thickness is adjustable from 10 to 100 mm). Optimized parameters are reported in the following chapters.

DSC measurements were performed with a Q200 (TA Instrument) ranging from 0 to 80°C with a heating ramp of 20°C/min and a cooling process with a rate of 10°C/min N_2 atmosphere. TGA were carried out with a Q600 (TA Instrument) in a range of 30-700°C with a heating ramp of 10°C/min in air.

Photorheological tests were performed in real-time during irradiation using an Anton Paar rheometer (Physica MCR 302) equipped with a Hamamatsu LC8 lamp (light emission in the UVA range, intensity 25 mW cm^{-2}). The measurements were carried out in a plate-plate geometry equipped with a quartz bottom plate. The gap between the plates was 200 μm. Oscillatory measurements were performed at 25 °C, at a constant frequency (1 Hz) and amplitude (1%). Amplitude sweep test (from 0.01% to 100%, frequency 1 Hz) was preliminarily performed to evaluate the linear viscoelastic range.

UV-Visible absorption spectra were recorded with a Varian Cary 300 spectrophotometer in a range of 250 – 750 nm. Photoemission spectra, luminescence lifetimes and quantum yields were acquired with a HORIBA Jobin Yvon IBH Fluorolog-TCSPC spectrofluorometer, equipped with a Quanta-φ integrating sphere. All measurements were performed on 3D printed polymeric samples.

The precision of the 3D printing process was evaluated using an E4 3D scanner (3Shape) with a scanning accuracy of 4 μm.

DMA evaluated the thermomechanical properties of the printed materials. 3D printed films were prepared and tested using a Triton Technology TTDMA.

A continuous-wave laser beam (doubled-frequency Nd:YAG source, emission wavelength 532 nm, max power 160 mW) has been used to illuminate the sample. The illumination spot had a diameter of about 3.6 mm.

5.2.3.1 Photoinduced tunable properties polymers with azobenzene dyes

The monomer and photoinitiator listed below were used for all formulations used in these works.

- BEDA EO/phenol 2

- BAPO

In Figure 8, the synthetical pathway and all dyes synthesized used in this work are reported.
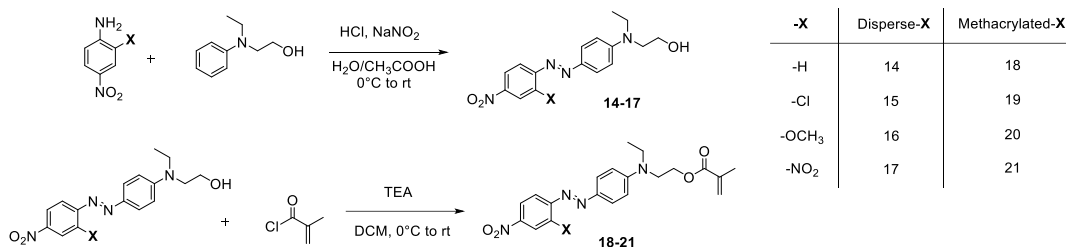
Figure 8 - *Synthetical pathway to produce ortho-functionalized azodyes with a photopolymerizable methacrylic functional group.*

Compound **14** is commercially available, and it was purchased from Sigma-Aldrich and used without further purifications. The procedure reported in the literature[116,117] was followed to obtain compounds **15** and **17,** as all characterizations agreed with the reported data.

Compound **16** was synthesized as follows. 2-Methoxy-4-nitroaniline (2.0 g, 11.9 mmol) was dissolved in 50 mL of a 1:1 solution of H_2O and acetic acid under stirring; then, the temperature was brought to 0°C. Sodium nitrite (0.985 g, 14.3 mmol) was dissolved in 5 mL of water and added dropwise. After 30 minutes, a solution of N-ethyl-N-hydroxyethylaniline in 10 mL of water and 2 mL of methanol was added under vigorous stirring. After 30 minutes from the last addition, the temperature was brought to room temperature, and after 2 hours, the product was filtrated, washed with cold water and dried. The product was then purified on a silica gel column with an eluent PE/EtOAc 7:3. The product was recovered as a dark red powder with a yield of 90% (3.53 g, 10.7 mmol).

^{1}H-NMR (600 MHz, Chloroform-*d*) δ 7.92 – 7.87 (m, 4H), 7.71 – 7.66 (m, 1H), 6.79 (d, J = 9.0 Hz, 2H), 4.09 (s, 3H), 3.89 (t, J = 5.9 Hz, 2H), 3.61 (t, J = 5.9 Hz, 2H), 3.56 (q, J = 7.1 Hz, 2H), 1.25 (t, J = 7.1 Hz, 4H).

^{13}C-NMR (151 MHz, Chloroform-*d*) δ 155.79, 151.67, 148.39, 147.01, 144.55, 126.54, 117.53, 116.70, 111.68, 107.79, 77.37, 77.16, 76.95, 60.45, 56.85, 52.52, 46.12, 12.25.

λ$_{max}$ (EtOH): 490 nm

ε (L mol^{-1} cm^{-1}): 30.5 x 10^3

HRMS: calculated 344.1485, found 345.1557 (M+1)

Compounds **18** and **19** were synthesized according to the procedures reported in the literature, and their characterizations agreed with the results reported.[118,119]

Compounds **20** and **21** were synthesized as follows. All glassware was dried before use, and all reactions were performed under an inert atmosphere (Ar). The azodye was dissolved in anhydrous THF, and the solution was put in an ice bath to reach 0°C. Methacryloyl chloride (1.1 eq.) and TEA (1.2 eq.) were added through a syringe, and after 20 minutes, the ice bath was removed, and the temperature was brought to room temperature. The reaction was left under stirring overnight and was monitored with TLC (PE:EtOAc 7:3). The solution was filtered, the solvent was removed under vacuum, maintaining the temperature below 30°C, and then EtOAc was added and extracted three times with water and one time with brine. The organic fractions were collected, dried with Na$_2$SO$_4$ and filtered. The product was then purified on a silica gel column with an eluent PE/EtOAc 7:3. The product was recovered as dark red powders.

20: yield 93%.

^{1}H-NMR (600 MHz, Chloroform-*d*) δ 7.93 – 7.86 (m, 4H), 7.69 (d, *J* = 8.6 Hz, 1H), 6.81 (d, *J* = 1.5 Hz, 2H), 6.14 – 5.59 (m, 2H), 5.59 (p, *J* = 1.6 Hz, 1H), 4.37 (t, *J* = 6.2 Hz, 2H), 4.09 (s, 3H), 3.73 (t, *J* = 6.2 Hz, 2H), 3.54 (q, *J* = 7.1 Hz, 2H), 1.94 (t, *J* = 1.3 Hz, 3H), 1.26 (t, *J* = 7.1 Hz, 4H).

^{13}C-NMR (151 MHz, Chloroform-*d*) δ 167.41, 155.76, 151.24, 148.37, 146.94, 144.58, 135.96, 126.49, 117.50, 116.63, 111.54, 107.74, 61.83, 56.80, 48.85, 45.70, 18.45, 12.36.

λ$_{max}$ (EtOH): 490 nm

HRMS: calculated 412.1747, found 413.1819 (M+1)

21: yield 82%

^{1}H-NMR (600 MHz, Chloroform-*d*) δ 8.39 (d, *J* = 2.4 Hz, 1H), 8.15 (dd, *J* = 8.9, 2.4 Hz, 1H), 7.97 – 7.92 (m, 2H), 7.78 (d, *J* = 8.9 Hz, 1H), 6.85 – 6.80 (m, 2H), 6.14 – 5.59 (m, 2H), 4.38 (t, *J* = 6.3 Hz, 2H), 3.75 (t, *J* = 6.3 Hz, 2H), 3.56 (q, *J* = 7.1 Hz, 2H), 1.94 (s, 3H), 1.27 (t, *J* = 7.1 Hz, 3H).

^{13}C-NMR (151 MHz, Chloroform-d) δ 167.44, 153.21, 151.85, 147.30, 144.56, 135.95, 134.14, 127.10, 126.50, 126.17, 122.76, 118.17, 111.68, 77.37, 61.74, 48.91, 45.86, 18.49, 12.41.

λ_{max} (EtOH): 520 nm

HR-ESI-MS: calculated 427.1492, found 450.1384 (M + Na$^+$)

5.2.3.2 Light-induced shape-memory 3D printed polymers

The monomer and photoinitiator listed below were used for all formulations used in these works.

- Tricyclo[5.2.1.02,6]decanedimethanol diacrylate (TCDMDA) as comonomer
- Poly(ethylene glycol) diacrylate (PEGDA, average Mn 575) as comonomer
- Isobornyl acrylate (IBA) as comonomer
- Hexyl acrylate (HA) as comonomer
- BAPO as photoinitiator

In Figure 9, the synthetical pathway and all dyes synthesized used in this work are reported.

-X	Disperse-X	Acrylated-X
-H	14	22
-Cl	15	23
-OCH$_3$	16	24
-NO$_2$	17	25
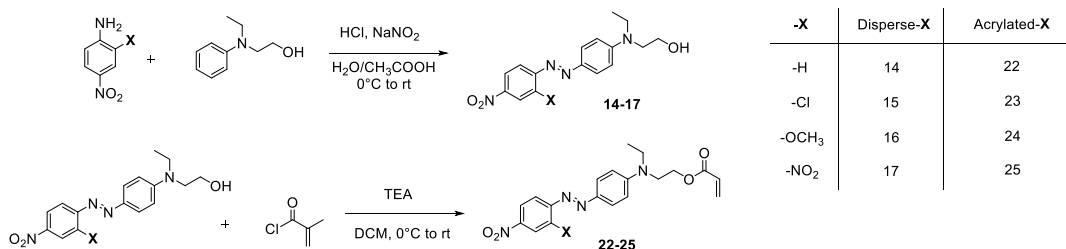
Figure 9 - *Synthetical pathway to produce ortho-functionalized azodyes with a photopolymerizable acrylic functional group.*

Synthesis of compounds **14-17** is reported in the previous chapter.

Compounds **22** and **23** were synthesized following the reported procedure[120], and their characterization agrees with the reported data. Yield **22**: 92%, **23**: 90%.

Acrylated azodyes **24** and **25** were synthesized according to the following procedure. The azodye (**16** or **17**) was put in a dried round bottom flask under an inert Ar atmosphere and completely dissolved with anhydrous THF under stirring. The flask was put in an ice bath, and 1.1 eq of triethylamine (TEA) was added by a syringe. Then freshly distilled acryloyl chloride (1.2 eq) was added dropwise over 15 minutes, and after 30 minutes from the last addition, the ice bath was removed, and the reaction was left for 24 h, monitoring with TLC (EP/EtOAc 1:1). When the reaction is completed, the solution is filtrated and washed with EtOAc to recover the desired product; the solvents were distilled under vacuum at a temperature below 30°C. The solid was recovered with EtOAc, put in a separation funnel, and extracted 3 times with water and 2 times with brine. The organic fractions were combined, and the solvent was distilled under vacuum at 30°C. Instead, the aqueous fractions were extracted again with EtOAc until they became clear. The final product was obtained as a dark red solid. Yields: **24**: 92%, **25**: 87%.

24: yield 92%

^{1}H NMR (600 MHz, Chloroform-*d*) δ 7.96 – 7.86 (m, 4H), 7.69 (d, *J* = 8.6 Hz, 1H), 6.83 – 6.79 (m, 2H), 6.41 (dd, *J* = 17.2, 1.4 Hz, 1H), 6.12 (dd, *J* = 17.3, 10.4 Hz, 1H), 5.86 (dd, *J* = 10.4, 1.3 Hz, 1H), 4.38 (t, *J* = 6.2 Hz, 2H), 4.08 (s, 3H), 3.72 (t, *J* = 6.2 Hz, 2H), 3.54 (q, *J* = 7.1 Hz, 2H), 1.26 (t, *J* = 7.1 Hz, 3H).

^{13}C-NMR (151 MHz, Chloroform-*d*) δ 166.11, 155.77, 151.19, 148.38, 146.93, 144.60, 131.66, 128.03, 126.48, 117.49, 116.63, 111.52, 107.75, 61.56, 56.81, 48.91, 45.80, 12.38.

HR-ESI-MS: calculated 398.1590, found 399.1663 (M + 1)

25: yield 87%

^{1}H NMR (600 MHz, Chloroform-*d*) δ 8.39 (d, 1H), 8.15 (dd, *J* = 8.9, 2.4 Hz, 1H), 7.94 (d, *J* = 9.1 Hz, 2H), 7.77 (d, *J* = 8.9 Hz, 1H), 6.82 (d, *J* = 9.2 Hz, 2H), 6.42 (dd, *J* = 17.4, 1.3 Hz, 1H), 6.13 (dd, *J* = 17.3, 10.5 Hz, 1H), 5.87 (dd, *J* = 10.4, 1.3 Hz, 1H), 4.39 (t, *J* = 6.3 Hz, 2H), 3.74 (t, *J* = 6.3 Hz, 2H), 3.56 (q, *J* = 7.1 Hz, 2H), 1.27 (t, *J* = 7.1 Hz, 3H).

^{13}C-NMR (151 MHz, Chloroform-d) δ 166.06, 152.55, 149.42, 146.60, 146.06, 144.52, 131.84, 127.91, 127.31, 120.06, 119.70, 111.80, 61.38, 49.00, 46.02, 12.39.

HR-ESI-MS: calculated 413.1335, found 436.1228 (M + Na^{+})

5.2.3.3 3D printed azo-based membranes for gas permeability

The monomer and photoinitiator listed below were used for all formulations used in these works.

• BEDA E/O phenol 2 as monomer

• BAPO as a photoinitiator

In Figure 10, the synthetical pathway and all dyes synthesized used in this work are reported.

-X	Disperse-X	Methacrylated-X
-H	14	18
-F	26	29
-Cl	15	19
-Br	27	30
-I	28	31
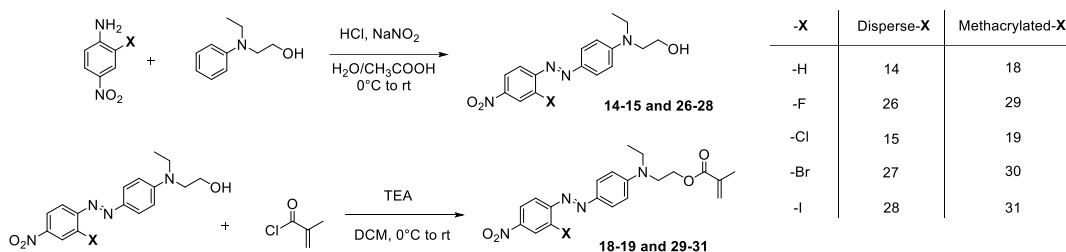
Figure 10 - *Synthetical pathway to produce ortho-functionalized azodyes with a photopolymerizable methacrylic functional group.*

Compounds **26**-**28** are synthesized according to the following procedure. The aniline was dissolved in 50 ml of H2O/CH3COOH (1:4) solution under stirring in a round bottom flask. The mixture was heated until it became clear, then the flask was put in an ice bath, and the temperature was monitored to reach 0-5°C. NaNO$_2$ (1.1 eq) was dissolved in deionized water, brought to 0-5°C and added dropwise to the aniline solution. After 30 minutes, the N-Ethyl-N-hydroxyethylaniline (1.2 eq) was dissolved in H$_2$O, and 1 mL of

HCl was added: this solution was dripped in the first one under vigorous stirring. The reaction was left for 3 h and then was poured into crushed ice to obtain a red precipitate that was filtered, washed with cold water and dried. Yields: **26**: 84%, **27**: 92%, **28**: 81%.

26:

^{1}H-NMR (600 MHz, Chloroform-*d*) δ 8.09 – 8.03 (m, 2H), 7.89 (d, J = 9.3 Hz, 2H), 7.82 (dd, J = 8.8, 7.5 Hz, 1H), 6.79 (d, J = 9.4 Hz, 2H), 3.90 (t, J = 6.0 Hz, 2H), 3.62 (t, J = 6.0 Hz, 2H), 3.57 (q, J = 7.2 Hz, 2H), 1.26 (t, J = 7.1 Hz, 3H).

^{13}C-NMR (151 MHz, Chloroform-*d*) δ 159.03, 157.31, 152.18, 147.54, 145.54, 144.36, 126.87, 119.89, 118.40, 113.04, 112.88, 111.66, 60.37, 52.47, 46.14, 12.20.

HR-ESI-MS: calculated 332.1285, found 333.1357 (M + 1)

27:

^{1}H NMR (600 MHz, Chloroform-*d*) δ 8.53 (d, *J* = 2.4 Hz, 1H), 8.16 (dd, *J* = 8.7, 2.4 Hz, 1H), 7.91 (d, *J* = 9.4 Hz, 2H), 7.71 (d, *J* = 8.9 Hz, 1H), 6.79 (d, *J* = 9.5 Hz, 2H), 3.90 (t, *J* = 4.2 Hz, 2H), 3.62 (t, *J* = 5.9 Hz, 2H), 3.57 (q, *J* = 7.2 Hz, 2H), 1.26 (t, *J* = 7.1 Hz, 3H).

^{13}C NMR (151 MHz, Chloroform-*d*) δ 154.12, 152.26, 147.29, 144.33, 129.12, 123.97, 123.40, 118.08, 111.75, 60.42, 52.54, 46.22, 12.25.

HR-ESI-MS: calculated 392.0484 and 394.0464 (M^{79}Br and M^{81}Br), found 393.0557 395.0538 [(M^{79}Br + 1) and (M^{81}Br + 1)].

28:

^{1}H NMR (600 MHz, Chloroform-*d*) δ 8.80 (d, *J* = 2.4 Hz, 1H), 8.24 (dd, *J* = 8.8, 2.4 Hz, 1H), 7.95 (d, *J* = 9.4 Hz, 2H), 7.66 (d, *J* = 8.9 Hz, 1H), 6.82 (d, *J* = 9.3 Hz, 2H), 3.90 (t, *J* = 6.9 Hz, 2H), 3.64 (t, *J* = 5.9 Hz, 2H), 3.59 (q, *J* = 7.1 Hz, 2H), 1.27 (t, *J* = 7.1 Hz, 3H).

^{13}C NMR (151 MHz, Chloroform-*d*) δ 155.70, 152.24, 147.47, 144.11, 134.99, 127.29, 124.35, 117.22, 111.82, 99.92, 60.46, 52.56, 46.24, 12.28.

HR-ESI-MS: calculated 440.0345, found 441.0418 (M + 1)

Azodyes **26**-**28** were put in a dried round bottom flask under an inert Ar atmosphere and completely dissolved with anhydrous THF under stirring. Then the flask was put in an ice bath, and 1.1 eq of triethylamine (TEA) was added by a syringe. Then freshly distilled methacryloyl chloride (1.2 eq) was added dropwise for 15 minutes, and after 30 minutes from the last addition, the ice bath was removed, and the reaction was left for 24 h monitoring with TLC (EP/EtOAc 1:1). When the reaction is completed, the solution is filtrated and washed with EtOAc to recover the desired product; the solvents were distilled under vacuum at a temperature below 25°C. The solid was recovered with EtOAc, put in a separation funnel, and extracted 3 times with water and 2 times with brine. The organic fractions were combined, and the solvent was distilled under vacuum at 25°C; instead, the aqueous fractions were extracted again with EtOAc until they became clear. The final product was obtained as a dark red solid. Yields: **29**: 88%, **30**: 91%, **31**: 85%.

29:

^{1}H-NMR (600 MHz, Chloroform-*d*) δ 8.12 – 8.04 (m, 2H), 7.92 (d, J = 8.6 Hz, 2H), 7.87 – 7.81 (m, 1H), 6.82 (d, J = 9.3 Hz, 2H), 6.13 – 6.08 (m, 1H), 5.63 – 5.57 (m, 1H), 4.37 (t, J = 6.2 Hz, 2H), 3.74 (t, J = 6.2 Hz, 2H), 3.56 (q, J = 7.1 Hz, 2H), 1.94 (dd, J = 1.6, 1.0 Hz, 3H), 1.27 (t, J = 7.1 Hz, 3H).

^{13}C-NMR (151 MHz, Chloroform-d) δ 167.43, 159.13, 157.41, 151.84, 144.53, 135.97, 126.91, 126.45, 119.96, 112.94, 111.66, 61.79, 48.91, 45.82, 18.47, 12.41.

HR-ESI-MS: calculated 400.1547, found 401.1620 (M + 1)

30:

^{1}H-NMR (600 MHz, Chloroform-*d*) δ 8.55 (d, *J* = 2.4 Hz, 1H), 8.18 (dd, *J* = 8.8, 2.4 Hz, 1H), 7.94 (d, *J* = 8.9 Hz, 2H), 7.73 (d, *J* = 8.9 Hz, 1H), 6.82 (d, *J* = 8.7 Hz, 2H), 6.11 (s, 1H), 5.60 (s, 1H), 4.38 (t, *J* = 6.2 Hz, 2H), 3.74 (t, *J* = 6.3 Hz, 2H), 3.56 (q, *J* = 7.1 Hz, 2H), 1.94 (s, 3H), 1.27 (t, *J* = 7.1 Hz, 4H).

^{13}C-NMR (151 MHz, Chloroform-*d*) δ 167.40, 154.06, 151.83, 147.34, 144.43, 135.94, 129.09, 127.11, 126.45, 124.01, 123.38, 118.09, 111.69, 61.70, 48.91, 45.87, 18.46, 12.40.

HR-ESI-MS: calculated 460.0746 and 462.0726 (M^{79}Br and M^{81}Br), found 461.0819 and 463.0801 [(M^{79}Br + 1) and (M^{81}Br + 1)].

31:

^{1}H NMR (600 MHz, Acetone-*d*$_6$) δ 8.79 (d, *J* = 2.4 Hz, 1H), 8.34 (dd, *J* = 8.9, 2.4 Hz, 1H), 7.95 (d, *J* = 9.5 Hz, 2H), 7.74 (d, *J* = 8.8 Hz, 1H), 7.03 (d, *J* = 9.3 Hz, 2H), 6.08 (dq, *J* = 1.9, 1.0 Hz, 1H), 5.64 (p, *J* = 1.6 Hz, 1H), 4.43 (t, *J* = 5.9 Hz, 2H), 3.90 (t, *J* = 5.9 Hz, 2H), 3.69 (q, *J* = 7.1 Hz, 2H), 1.93 – 1.87 (m, 3H), 1.28 (t, *J* = 7.1 Hz, 3H).

^{13}C NMR (151 MHz, Acetone-*d*$_6$) δ 166.70, 155.65, 152.47, 147.59, 143.83, 136.34, 134.68, 126.96, 125.38, 124.48, 117.09, 111.99, 99.26, 61.90, 48.59, 45.44, 17.62, 11.65.

HR-ESI-MS: calculated 508.0607, found 531.0500 (M + Na$^+$)

5.2.4 NDI-OH

All reagents are solvents were purchased from Sigma-Aldrich, Merck, Fluka, Riedel de Haen and Alfa Aesar and used without further purification, unless otherwise noted. All solvents were purchased from VWR, Carlo Erba and Sigma-Aldrich and used without other purification. Nuclear magnetic resonance 1H NMR (200 MHz and 600 MHz) and 13C NMR (151 MHz) experiments were conducted using a Bruker AVANCE 200 (1H operating frequency 200 MHz) and a JEOL ECZ-R instrument (1H operating frequency 600) MHz.

A DLP 3D printer (Asiga DLP-3D printer Max-UV) with a nominal X-Y pixel resolution of 27 μm and a minimum Z resolution control of 1 μm was employed to obtain 3D printed samples. The light intensity was fixed at 25 mW cm^{-2} and a layer's thickness of 25 μm, with 3 layers of burn-in (15 seconds of irradiation) and all other layers under normal irradiating time (10 seconds). The printing process was performed at 25°C, and at the end, all sides were post-cured under UV irradiation for 5 minutes each side in a UV over (provided by RoboFactory) with light intensity at 10 mW cm^{-2}.

UV-Visible absorption spectra were recorded with a Varian Cary 300 spectrophotometer in a range of 250 – 750 nm. Photoemission spectra, luminescence lifetimes and quantum yields were acquired with a HORIBA Jobin Yvon IBH Fluorolog-TCSPC spectrofluorometer, equipped with a Quanta-φ integrating sphere. All measurements were performed on 3D printed polymeric samples.

Differential scanning calorimetry (DSC) measurements were performed with a Q200 (TA Instrument) in a range from -20 to 80°C with a heating ramp of 20°C/min and a cooling process with a rate of 10°C/min in N_2 atmosphere. Thermal gravimetric analyses (TGA) were carried out with a Q600 (TA Instrument) in a range of 30-650°C with a heating ramp of 10°C/min in air.

The precision of the 3D printing process was evaluated using an E4 3D scanner (3Shape) with a scanning accuracy of 4 μm.

Different DLP 3D printable monomers were exploited and listed below for this work.

- PEGDA 250 Da
- PEGDA 575 Da
- PEGDA 700 Da
- HDDA
- BEDA EO/phenol 2
- BEMA EO/phenol 15

A UV absorber was used to compare the formulation without the active chromophore to obtain the formulation's printability with good resolutions. The moiety selected was 2-(2-Hydroxy-5-methylphenyl)benzotriazole (HMBT) obtained from Sigma-Aldrich and used without further purifications.

Other chemicals and solvents listed below were used in this work.

- Ammonia solution 25 wt%
- DBU
- Ethylene glycol

- Toluene

- Acetonitrile

- Propylene carbonate

- Dimethylformamide

- Acetone

- Isopropanol

- Ethanol

For the dye used in this work, the procedure described below was followed to obtain a chromophore able to change its colour and emission by changing the pH of the aqueous solution in which it was dipped.
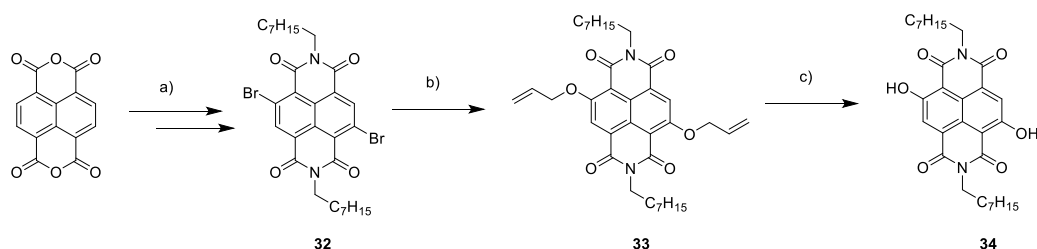
Figure 11 - *Synthetical way to synthesize NDI-OH.*

Synthesis of 4,9-dibromo-2,7-dioctylbenzo[lmn][3,8]phenanthroline-1,3,6,8(2H,7H)-tetraone (32) (Figure 11).

Compound **32** was synthesized following the same procedure reported by Modarelli et al.[121] The chemical characterization was in agreement with the reported data.

Synthesis of 4,9-bis(allyloxy)-2,7-dioctylbenzo[lmn][3,8]phenanthroline-1,3,6,8 (2H,7H)-tetraone (33) (Figure 11).

A freshly prepared solution of AllylONa in allyl alcohol (240 μL of a solution 1 M of NaH in allyl alcohol) was added dropwise to a solution of **32** (50 mg, 0.08 mmol) in dry CH_2Cl_2 (8 mL). The mixture was stirred at rt for 7 h. Then, CH_2Cl_2 was added, and the organic layer was washed with brine and water, dried over Na_2SO_4 and concentrated *in vacuo*.

The crude was purified by flash chromatography (CH$_2$Cl$_2$/Hexane 3:2), affording **33** as a yellow solid (13 mg, 28%).

^{1}H-NMR (600 MHz, CDCl$_3$): 8.47 (s, 2H), 6.18 (ddt, ^{3}J(H,H) = 17.2, 10.6, 5.2 Hz, 2H), 5.72 (dq, ^{3}J(H,H) = 17.2 Hz, ^{2}J(H,H) = 1.2 Hz, ^{4}J(H,H) = 1.4 Hz, 2H), 5.45 (dq, , ^{3}J(H,H) = 10.6 Hz, ^{2}J(H,H) = 1.2 Hz, ^{4}J(H,H) = 1.4 Hz, 2H), 5.02 (dt, , ^{3}J(H,H) = 5 Hz, ^{4}J(H,H) = 1.5 Hz, 4H), 4.15 (t, ^{3}J(H,H) = 7.8 Hz, 4H), 1.73 (qt, ^{3}J(H,H) = 7.8 Hz, 4H), 1.42 (qt, ^{3}J(H,H) = 7.7 Hz, 4H), 1.36 (qt, ^{3}J(H,H) = 7.6 Hz, 4 H), 1.32-1.25 (m, 12 H), 0.87 (t, ^{3}J(H,H) = 6.8 Hz, 6H).

^{13}C-NMR (150 MHz, CDCl$_3$): δ 162.53, 161.27, 159.80, 131.60, 127.80, 123.88, 120.12, 119.47, 111.36, 71.61, 43.44, 31.96, 29.46, 29.36, 28.14, 27.31, 22.79, 14.79.

MS (ESI, CH$_2$Cl$_2$/MeOH): 603 ([M+H]$^+$), 1204 ([2M]$^+$), 1227 ([2M + Na$^+$]).

Synthesis of 4,9-dihydroxy-2,7-dioctylbenzo[*lmn*][3,8]phenanthroline-1,3,6,8 (2*H*,7*H*)-tetraone (34) (Figure 11).

To a solution of **33** (13 mg, 0.02 mmol) and Pd(PPh$_3$)$_4$ (1.3 mg, 0.001 mmol) in dry CH$_2$Cl$_2$ (3 mL), phenylsylane (17.3 mg, 0.16 mmol) was added. The mixture was stirred under Argon at rt for 12 h. Volatiles were removed *in vacuo,* and the reaction crude was purified by flash chromatography (CH$_2$Cl$_2$/Hexane 1:1), affording **34** as a yellow solid (6 mg, 53%).

^{1}H-NMR (600 MHz, CDCl$_3$): 12.38 (s, 2H), 8.30 (s, 2H), 4.17 (t, ^{3}J(H,H) = 7.7 Hz, 4H), 1.73 (qt, ^{3}J(H,H) = 7.6 Hz, 4H), 1.42 (qt, ^{3}J(H,H) = 7.6 Hz, 4H), 1.36 (qt, ^{3}J(H,H) = 7.4 Hz, 4 H), 1.32-1.25 (m, 12 H), 0.87 (t, ^{3}J(H,H) = 6.9 Hz, 6H).

^{13}C-NMR (150 MHz, CDCl$_3$): δ 168.55, 166.42, 161.92, 160.68, 127.25, 123.94, 106.96, 40.75, 31.93, 29.38, 29.32, 28.09, 27.19, 22.77, 14.24.

6. Results and discussion

In the following paragraphs, each application of fillers and dyes into 3D printable formulations is described in detail. The first part deal with piezoresistive materials suitable for FFF 3D printers and appliable as sensors. In this section, we studied the preparation processes to obtain optimal formulations without applying them directly in 3D printing: this last part is actually under investigation.

DLP 3D configuration is applied to all other parts, introducing dyes differently. Firstly, an innovative and less exploited post-functionalization process is investigated in which the reactive dye is covalently linked to the polymeric matrix after the printing process. This way shows advantages in using dyes that do not show very good photostability. Still, it is by far the least used process due to the limited availability and difficulty of leaving unreacted functional groups after the photopolymerization process induced by the 3D printer.

In the following chapters, dyes are added, solubilizing them directly into liquid formulations. They can be used as dispersed moieties or covalently connected through the use, where possible, of photoreactive functional groups. This second way helps avoid the leaching of dyes during the use of the final objects, particularly when in contact with water or other solvents. In some cases, differences in mechanical properties between dispersed or linked dyes are noticed and described.

6.1 Addition of inorganic fillers to confer innovative properties

This section focused our attention on introducing inorganic fillers in a thermoplastic polymer that can find application in FFF 3D printer configuration.

6.1.1 3D printable thermoplastic elastomers with piezoresistive properties conferred by inorganic fillers

Some preliminary studies on the use of MWCNTs and GNP fillers in FDM 3D printing are described, focusing on the preparation procedure of printable formulations and

their optimal concentration of fillers to obtain the best results. This work aims to confer piezoresistive properties to a TPU matrix by using different fillers. The optimal concentration, the different types of available fillers, and the optimal mixing parameters are evaluated here, opening the field for future studies and improvements.

The introduction of nanocomposites in a polymeric matrix is becoming one of the most relevant research topics over the last decade. These nanofillers are usually introduced in an inert polymeric matrix to confer innovative properties that can change in response to an external stimulus, such as temperature, pressure and strain, for different applications as sensors.[122–126] Among other fillers, MWCNTs are the most exploited due to their performing properties as reinforcing and high thermal and electrical conductive filler.[127,128] At the same time, GNPs represent a useful material that shows very high electrical and thermal conductivity and lower mass density than other fillers, making them ideal candidates for applications in polymeric materials. Furthermore, the production of GNPs requires less expensive and intricate apparatus than CNTs with a consequent reduction in costs, and they can be derivate from many natural resources. All these advantages make GNPs valid substitutes for high-priced CNTs in many applications.[129] Production methods and properties of GNPs are in-depth reviewed by Kim et al.[130]

In this work, we compared MWCNTs and GNPs to understand better the optimal concentration of fillers to obtain a piezoresistive material, able to change its conductivity under external mechanical stress. Moreover, a study about the best mixing method to obtain a homogeneous composite material with some peculiar characteristics, such as flexibility, thermal stability and high conductivity, was carried out to make this material processable by FDM 3D printers.

Different concentrations (5.0 wt.%, 10.0 wt.% and 15.0 wt.%) of fillers are introduced in the extruder. The resulting filaments are then characterized by TGA and DSC analysis to evaluate the effect of different fillers and their concentration on the chemical and mechanical properties of the polymeric matrix. Moreover, from TGA thermograms, the

47

real concentration of fillers can be evaluated by evaluating the losses of fillers that may occur during the loading in the extruder.

TGA analysis

All measurements were performed from 30°C to 800°C in N_2 atmosphere. As depicted in Figure 12, the introduction of an increasing concentration of MWCNTs affects the starting of thermal degradation (as is better evident in Figure 13), caused by the enhanced thermal conductivity conferred by the filler, as well as CNTs introduce a secondary degradation step. This second step is probably due to the formation of more stable carbonic residues caused by the degradation of TPU, both to the stabilizing effect of CNTs when inserted in a polymeric matrix.[131–133]
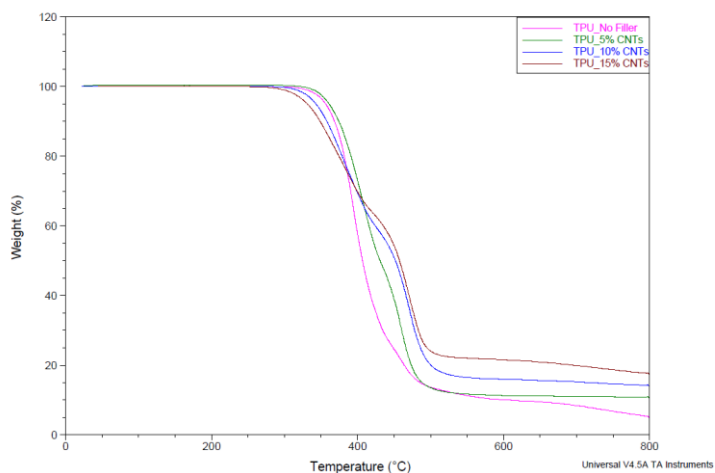
Figure 12 *- TGA thermograms under N_2 flux of TPU with increasing concentration of CNTs.*
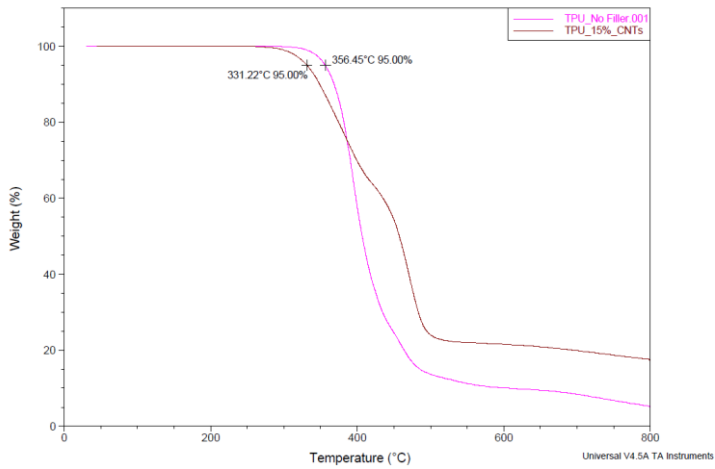
Figure 13 - *TGA thermograms under N_2 flux for TPU without CNTs (purple line) and with 15 wt.% of CNTs (dark-red line). The concentration of fillers affects the start of thermal degradation.*

The same considerations reported for CNTs remain valid also for GNPs. Still, in this case, the effect of filler on the thermal degradation of the polymer is less evident, as demonstrated in Figure 14 and Figure 15.
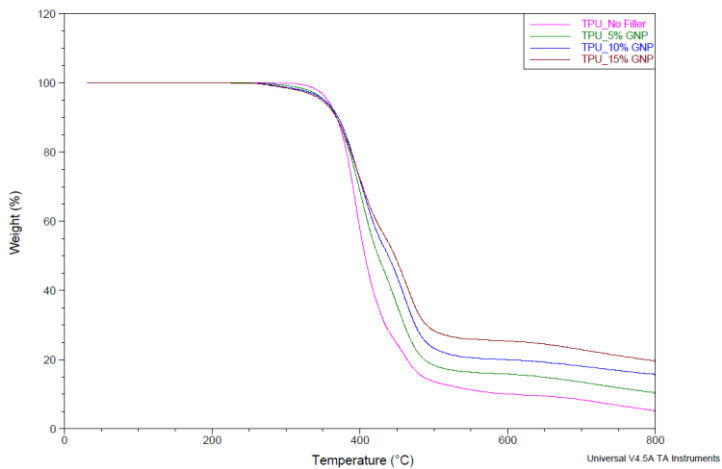
Figure 14 - *TGA thermograms under N_2 flux of TPU with increasing concentration of GNPs.*
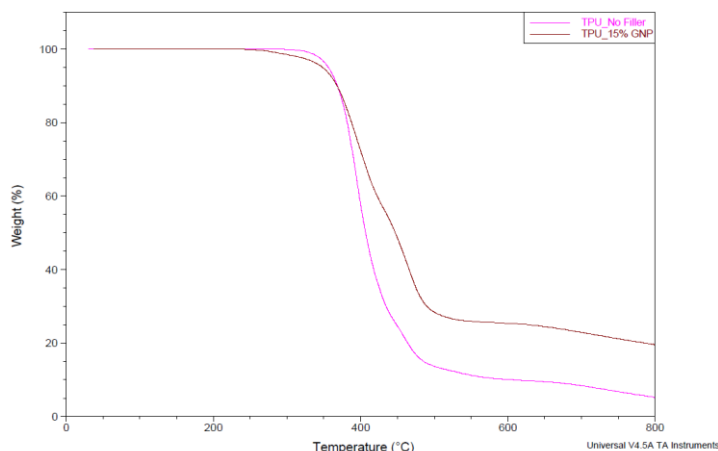
Figure 15 - *TGA thermograms under N₂ flux for TPU without GNPs (purple line) and 15 wt.% of CNTs (dark-red line). The concentration of fillers affects the start of thermal degradation.*

The results obtained from TGA measurements can be useful for calculating the real quantity of fillers introduced in the formulation. Residues at 795°C are used for all calculations due to each thermogram's stability in that region. The calculation of the real concentration of fillers is reported below.

$$wt.\% \ of \ filler = \frac{R - R_{TPU}}{R_{Filler}}$$

Where R is the residue of each sample at 795°C, R_{TPU} is the residue at 795°C for pure TPU, and R_{Filler} is the residue at 795°C for pure filler (MWCNTs or GNPs). The values found are reported below from thermograms of pure TPU, MWCNTs and GNPs (Figure 119, Appendix II).

R_{TPU} = 5.39%

R_{MWCNTs} = 81.73%

R_{GNPs} = 74.84%

In Table 3, the temperatures in which a 5.0% of weight loss ($T_{5.0\%}$) in TGA thermograms are reported with the calculation of the real concentration of each filler compared to the theoretical one.

Table 3 - *Theoretical concentrations of fillers compared to the calculated one. $T_{5.0\%}$ reports the temperature in which a 5.0% of weight loss is registered.*

Type of filler	Theoretical concentration (wt.%)	Calculated concentration (wt.%)	$T_{5.0\%}$
MWCNTs	5.00	6.63	344.88
	10.0	10.8	343.12
	15.0	15.0	331.22
GNPs	5.00	6.89	351.83
	10.0	13.9	351.80
	15.0	19.2	348.39

As reported, the real concentration can assume different values from the theoretical one due to problems during the loading of the fillers; this is particularly evident for GNPs.

DSC analysis

The homogeneity of the filler dispersions can be evaluated from DSC thermograms. Each measure was conducted from -75°C to 220°C with a heating ramp of 20°C/min. The transition temperature for pure TPU can be observed at -37.98°C, followed by a melting signal with a maximum of 166.81°C. During the cooling process, a crystallization peak is visible at 77.46°C (Figure 16).
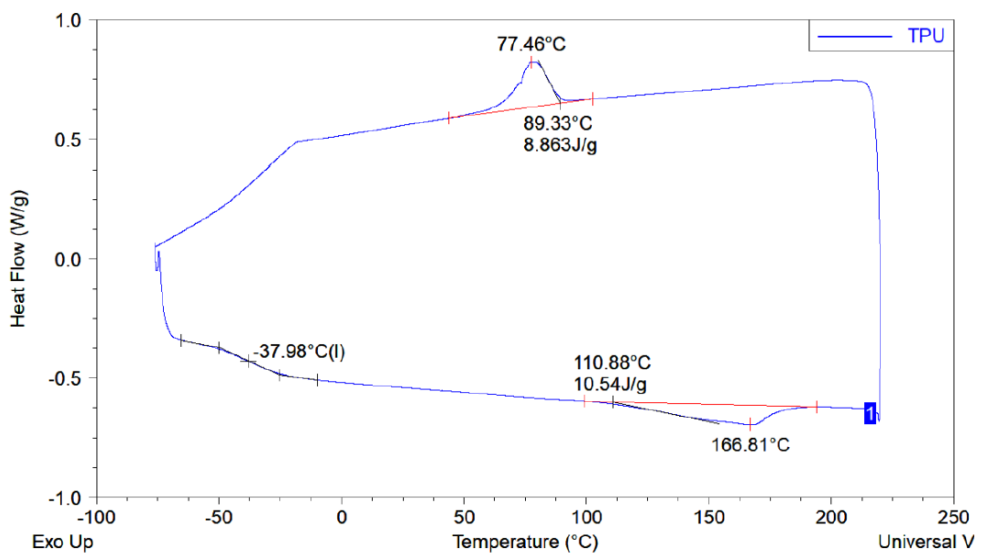
Figure 16 - *DSC thermogram of pure TPU.*

Comparing the thermogram of pure TPU with the ones for MWCNTs and GNPs is visible a shift of crystallization peaks to higher temperatures due to the nucleating action of these fillers. Moreover, a broadening of the crystallization peaks is caused by the different viscosity of the loaded samples than pure TPU. For both fillers, an adequate shift can be observed that suggests an excellent dispersion in the polymeric matrix (Figures 17a and 17b).
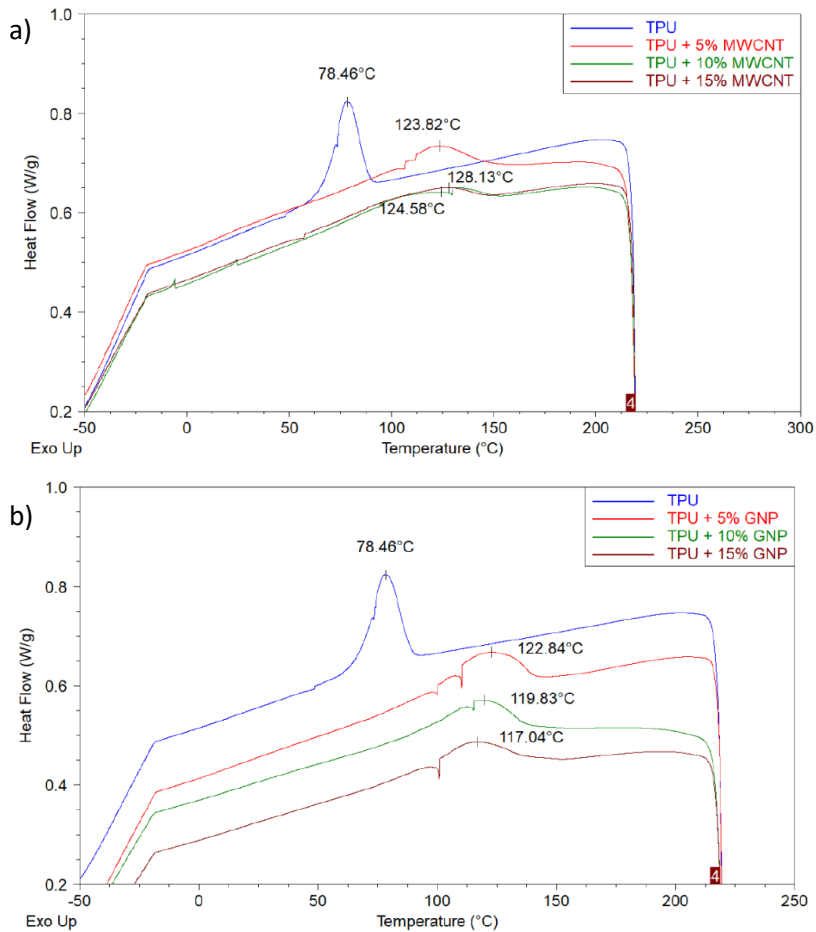
Figure 17 - *Crystallization peaks of DSC thermograms of A) MWCNTs and B) GNPs loaded TPU, compared to the pure one.*

After the extruder's mixing process, good dispersion and homogeneity are reached for all samples.

SEM analysis

The correct and homogeneous dispersion of the fillers can also be evaluated with SEM. Some cryofractures were produced into the polymeric sample treating them at 77K: this preliminary process is necessary to avoid the "skin effect" of polymers. The fillers are incorporated into the matrix when a ductile fracture occurs. The reported images demonstrate a good dispersion for all the fillers involved in this study (Figures 18 and 19).
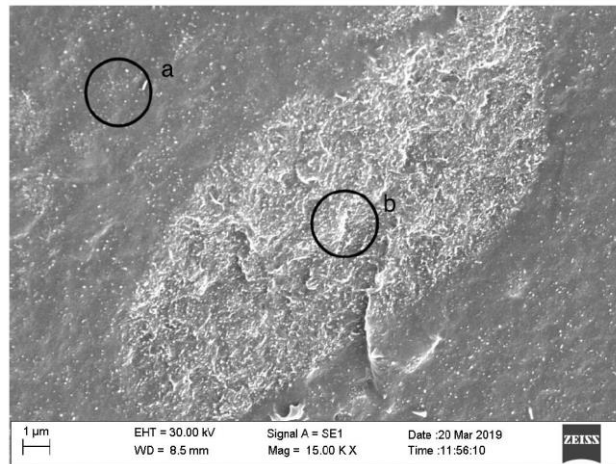
Figure 18 – TPU with 10 wt.% of MWCNTs in which a good dispersion of fillers (a) can be compared to an area of aggregates (b).
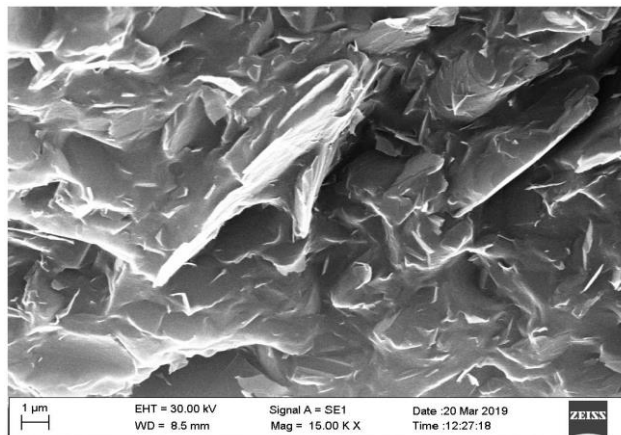
Figure 19 - TPU with 15 wt.% of GNPs.

Resistivity measures

Before proceeding with piezoresistivity measures, all polymeric samples were subjected to a film-forming process with a heated mechanical press at 180°C. Then, some rectangular samples were obtained, and on their surface, metal-conductive connectors were applied to measure the changes in resistivity under an external load applied (Figure 20). All these analyses were carried out in collaboration with Eltek s.p.a.
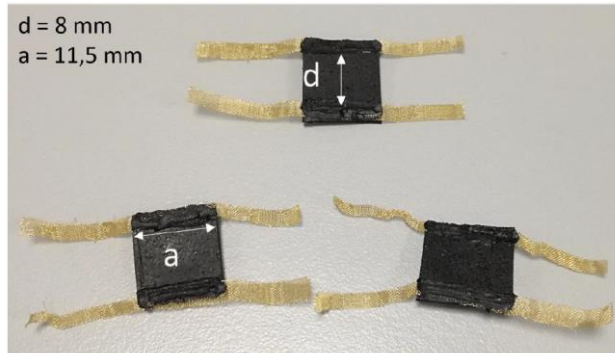
Figure 20 – *Polymeric samples with metal-conductive connectors applied.*

The experimental setup is depicted in Figure 21, in which the sample is connected to the resistivity meter and is visible under a mechanical press able to apply an external compression (3.4 N on a 36 mm^2 area).
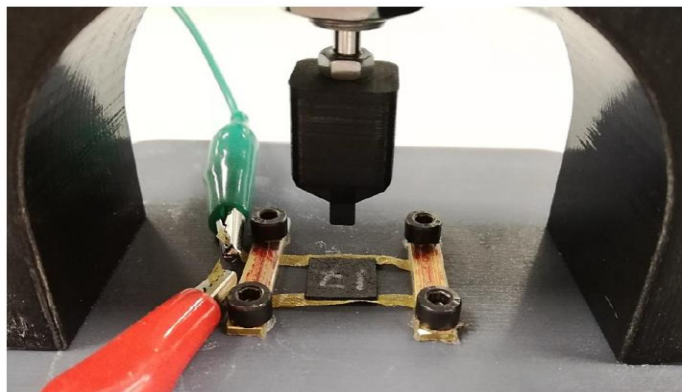
Figure 21 – *Experimental setup to evaluate changes in resistivity under external pressure applied.*

The most promising formulations contain 5.0% of MWCNTs, 10.0% and 15.0% of GNPs, and they represent the only ones deeply investigated in this study. High concentrations of MWCNTs (up to 5.0%) result in very high production costs, while high concentrations

of GNPs are necessary to obtain promising results with reduced costs and good mechanical properties. As depicted in Figure 22, different repetitions of the same samples are tested, and all of them are placed in other parts of the graph. Very low resistivity values are observed for 5.0% of CNTs and 15.0% of GNPs, while more elevated values for 10.0% of GNPs. For these reasons, the first two samples are the most promising ones, but the one with 15.0% of GNPs shows reduced production costs.
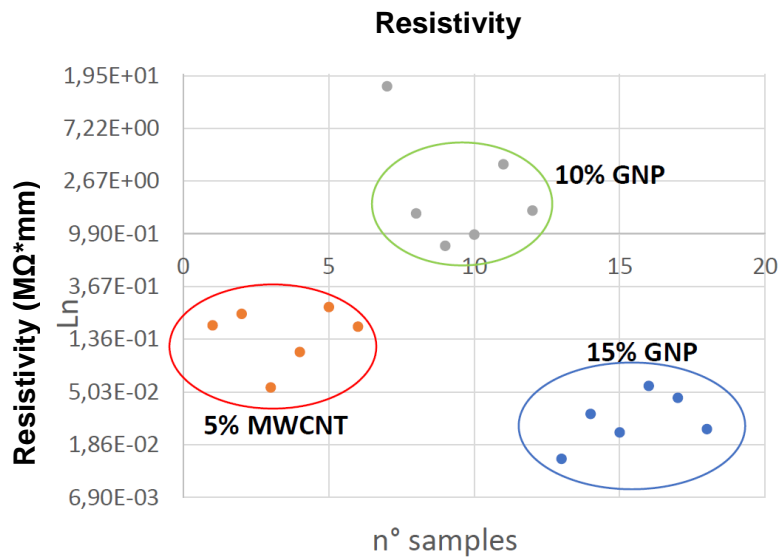
Figure 22 – Resistivity measures were repeated on different samples loaded with 5.0% of MWCNTs (red), 10% (green) and 15% (blue) of GNPs.

All samples are subjected to loaded and unloaded cycles of the external compression. These measurements are repeated four times per sample. As reported in Figure 23, samples with 5.0% of CNTs and 10% of GNPs show the best mechanical properties in terms of the number of cycles that can be performed while maintaining unaltered resistivity values. The samples with 15.0% of GNPs show at the same time reduced values of resistivity but also reduced mechanical performances. The high quantity of GNPs causes the breaking of the polymeric films after a few loading cycles.
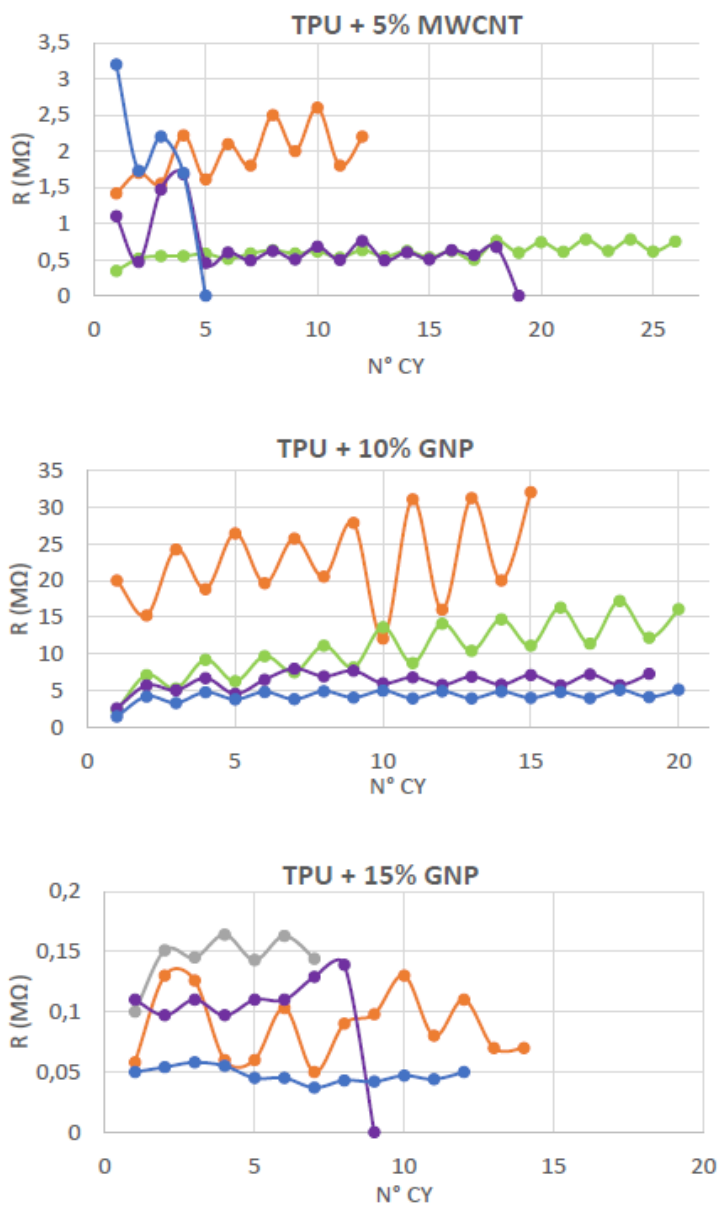
Figure 23 – Number of cycles that can be obtained before rupture of the polymeric sample. From top to bottom: 5.0% wt. of MWCNT, 10.0 wt.% and 15.0 wt.% of GNP.

6.2 Uses of dyes in DLP 3D printer configuration

In this chapter, all DLP 3D printer configuration applications are described in detail, emphasising the uses and the stimulus chosen to activate the peculiar property conferred by the dyes.

6.2.1 Post-functionalization process
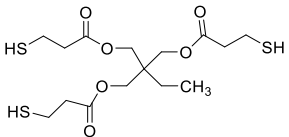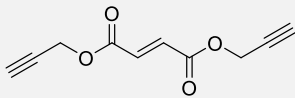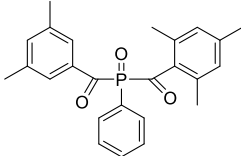
The first and less exploited way to introduce functional moieties in 3D printing involves a post-functionalization process. Some residual functional groups, unreacted after the printing process, are used to covalently link dyes.

This process is particularly interesting for introducing bio-functional molecules onto different polymeric matrices. Available groups are exploited to generate covalent bonds [134] and take advantage of carboxylic groups to functionalize acrylate 3D printed polymers[135] or through post-printing surface-initiated ATRP modification.[136] A wide range of exploitable post-functionalization reactions can be used to link chemical moieties, conferring peculiar and innovative properties to the surface of 3D printed objects.[137,138] In this work[139], we focus on the photopolymerization reaction between thiol and alkyne monomers, employing these two functional groups to produce 3D printed polymeric devices. Modulating the ratio of thiol and alkyne functional groups in the liquid monomer's mixture makes it possible to generate surfaces that react with different chemical species. In developing off-stoichiometric formulations, the excess of SH (thiol) or YNE (alkyne) functionalities not involved in the cross-linked network results is available for various post-functionalization processes. Thiol-yne polymerization has attracted the attention of many researchers[140–143], and in the last years, this process has been of particular interest in the photopolymerization field[144] due to its many advantages respect the common traditional polymerization methods.[145,146]

Three formulations were prepared by mixing the alkyne with trifunctional thiol monomers. Different ratios of these two components were chosen to obtain

stoichiometric (EQ), alkyne-excess (YNE) or thiols-excess (TH) formulations (Table 4). In all the formulations, 1 phr of BAPO, as photoinitiator (PI), was solubilized with acetone.

Table 4 - Composition (wt.%) of the formulations prepared.

	Formulations (wt %)		
	EQ	YNE	TH
Thiol monomer			
	77	70	84
Alkyne monomer			
	23	30	16
BAPO (PI)			
	1	1	1

In Figure 24, the reactions between the two synthesized monomers are reported. An ideal step-growth reaction occurs for TH and EQ formulations, while for YNE a homopolymerization of the alkyne/alkene moieties can also occur.
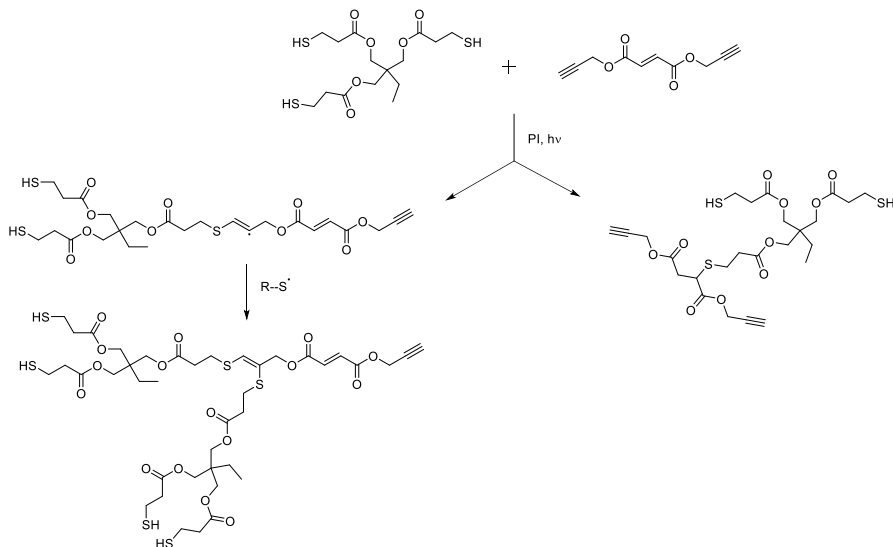
*Figure 24 - Thiol-yne and thiol-ene reactions that can occur between the two monomers. Material from: I. Roppolo, F. Frascella, M. Gastaldi, M. Castellino, B. Ciubini, C. Barolo, L. Scaltrito, C. Nicosia, M. Zanetti, A. Chiappone, Polym. Chem. **2019**, 10, 5950.*

The reactivity of each formulation is tested through photorheology measures. After 60 s, a UV lamp is switched on, and the start of the photopolymerization reaction is evaluated by the increase of G'. As depicted in Figure 25, the formulation containing an excess of thiol is the most reactive, while the YNE one requires more time to start and complete the photopolymerization. This can be adduced to the low amount of thiol monomers that act as a crosslinker and allow rapid growth of the polymeric chains.
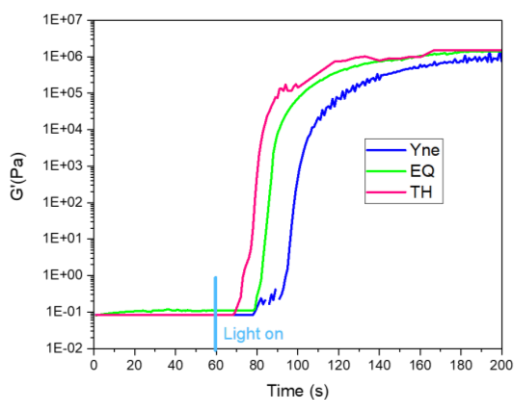
*Figure 25 – Photorheology measurements. Material from: I. Roppolo, F. Frascella, M. Gastaldi, M. Castellino, B. Ciubini, C. Barolo, L. Scaltrito, C. Nicosia, M. Zanetti, A. Chiappone, Polym. Chem. **2019**, 10, 5950.*

The curing behaviour is necessary to find the optimal parameters for the 3D printing process with all the reported formulations (Table 5). In particular, layer exposure time represents the irradiation time necessary to complete the entire layer's photopolymerization (50 µm).

Table 5 - Optimal 3D printing parameters for 50 µm thickness layer.

Sample	Layer exposure time (sec)
YNE	15
EQ	6
TH	5

To fully characterize the resulting polymeric matrices for each pure formulation, some flat samples (5 × 20 × 0.3 mm) were 3D printed to be tested in FT-ATR, DMA and XPS measurements. FT-ATR is necessary to evaluate the conversion of reactive groups, comparing the liquid formulation with the 3D printed polymeric samples. As reported in Table 6, for EQ formulation, both thiol and triple bonds can't reach complete conversion: this is probably related to monomers' reduced mobility once the photopolymerization occurs. This represents a limit in using EQ formulation in 3D printing due to the high amount of unreactive monomers. Instead, the TH formulation reaches a complete conversion of triple bonds, able to react with thiol monomers, and for the YNE formulation in which almost all thiol groups are converted, leaving a high number of triple bonds unreacted.

Table 6 - Conversion of reactive groups of monomers in the formulation. The values are calculated by observing the decrease of the thiol (2570 cm^{-1}), alkyne (2130 cm^{-1}) and alkene (1640 cm^{-1}) peaks in ATR spectra.

Sample	-SH conversion (%)	-C≡C- conversion (%)	-C=C- conversion (%)
EQ	60	52	72
YNE	80	37	63
TH	48	98	100

XPS analysis is carried out on 3D printed polymeric samples to support these results. According to the literature,[147–151] the attribution of each chemical shift to the relative chemical bond is given, as depicted in Figure 26.
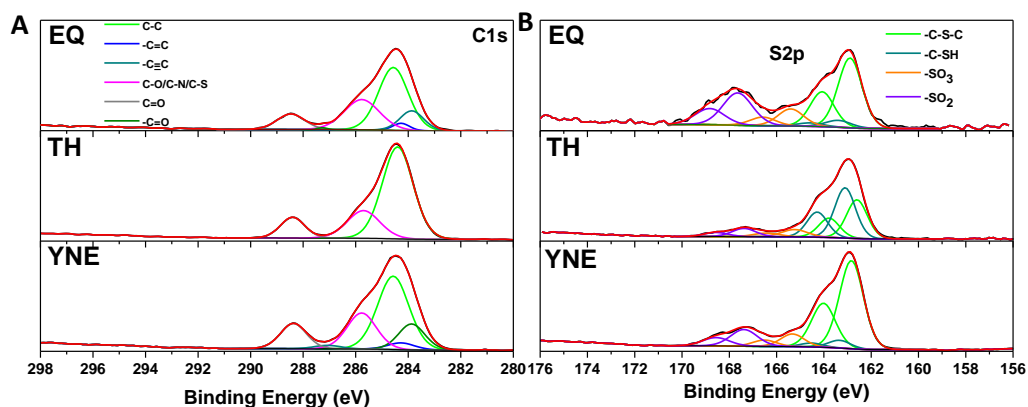
Figure 26 *-HR XPS spectra for EQ, TH and YNE samples: (A) C 1s peaks and (B) S 2p doublets with their deconvolution curves. Material from: I. Roppolo, F. Frascella, M. Gastaldi, M. Castellino, B. Ciubini, C. Barolo, L. Scaltrito, C. Nicosia, M. Zanetti, A. Chiappone, Polym. Chem.* ***2019****, 10, 5950.*

A comparison between the results obtained from ATR and those from XPS is not possible due to the different in-depth sensitivity of these two techniques. Nevertheless, good accordance can be observed between the two sets of data obtained (Table 7): the YNE sample is the one that shows a higher amount of % of triple bonds due to their low conversion during photopolymerization. Instead, TH sample shows less than 0.1% of double and triple bonds, which means that all these functional groups reacted during photopolymerization, as reported in ATR measurements.

Table 7 *-Chemical bonds % evaluated using HR XPS spectral deconvolution for S 2p (unbound thiol –SH) and C 1s (–CuC– and –CvC– chemical shifts) photoelectron peaks.*

Sample	-SH (%)	-C≡C- (%)	-C=C- (%)
EQ	5.5	11.9	3.0
YNE	5.7	13.8	3.7
TH	46.7	<0.1	<0.1

Different thermal-mechanical behaviours can be observed from DMA measurements. Glass transition temperatures increase, increasing the alkyne content in the formulation, starting from 8°C for the TH sample to 34°C for the YNE one (Figure 27): this is due to the rigidity given by alkyne monomers. The final mechanical properties can be tuned to reach the desired values by introducing different quantities of the two monomers. Moreover, a bilayer specimen composed of YNE and TH formulations was

also printed, changing the reservoir with the resin during the printing process. This experiment demonstrates the possibility of printing different materials one on the other, maintaining at the same time their peculiar mechanical properties separated. No delamination or adhesion problems can be observed between the two printed parts, and a good final resolution is achieved.
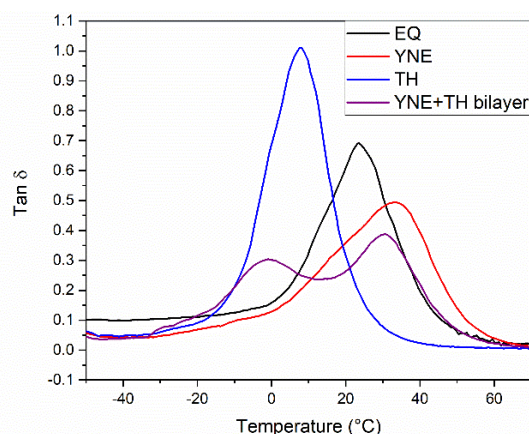
Figure 27 *- Tan δ plot obtained by DMA on flat specimens produced with the three formulations and on one bilayer specimen built with the two OSTY formulations one after the other (TH and YNE). Material from: I. Roppolo, F. Frascella, M. Gastaldi, M. Castellino, B. Ciubini, C. Barolo, L. Scaltrito, C. Nicosia, M. Zanetti, A. Chiappone, Polym. Chem. **2019**, 10, 5950.*

Non reacted functional groups can be exploited to functionalize the surface after the 3D printing process. As reported by Hoffman et al.[152] unreacted triple bonds can be used to graft an azide-terminated dye. Here, the post-functionalization reaction occurs between the alkyne available groups on the surface of a 3D printed object with a squaraine dye functionalized with a terminal azide group. To achieve this proof of concept, a complex 3D printed structure is produced combining different formulations: the bottom part is made of YNE formulation while the top one with an excess of TH monomers.

The whole 3D printed object is post-functionalized following the procedure previously reported and the results are depicted in Figure 28. To evaluate the presence of reactive triple bonds available on the surface, the colour of the matrix has to change from native white to blue, the typical colour of the squaraine dye. Due to the lack of available triple bonds, the 3D printed object made of TH formulation remains white, while the EQ one

assumes a light blue colour that becomes more intense for the YNE one. The same situation is also observed for the 3D printed complex object made of TH (upper part) and YNE (bottom part). To better evaluate the behaviour of the linked dye, some fluorescence images are registered under irradiation. As is pointed out in Figure 28E, an intense emission of the squaraine is visible only in the YNE part and only barely in the TH one.
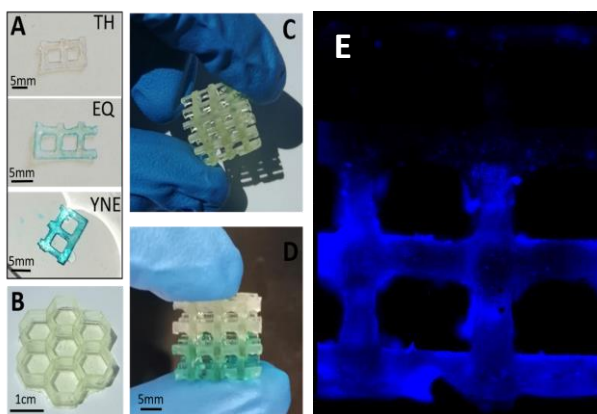
*Figure 28 -Images of the 3D printed objects. (A) The post functionalization step with the squaraine dye for TH, YNE EQ formulations. (B) Structure built with EQ formulation, (C) hybrid structure with YNE at the bottom and TH at the top formulations. (D) Result of the post functionalization process on the same structure. (E) Widefield optical detection fluorescence of the slice was obtained from the 3D printed hybrid structure (scale bar 1 mm). Material from: I. Roppolo, F. Frascella, M. Gastaldi, M. Castellino, B. Ciubini, C. Barolo, L. Scaltrito, C. Nicosia, M. Zanetti, A. Chiappone, Polym. Chem. **2019**, 10, 5950.*

In this work, we have demonstrated that thiol-yne photopolymerization can be successfully employed in 3D printing to produce devices with high fidelity to the CAD virtual project and good resolution in order of mm or less. At the same time, it is possible to exploit functional groups on the surface of the 3D printed polymeric matrix to graft dyes and confer new functionalities to polymers with potential future applications in biomedicine.

6.2.2 Light-emitting fluorophores for 3D printing

This study describes some preliminary results using organic fluorophores with high quantum yield and Stokes shift in the DLP 3D printing technique. The use of these types of organic molecules was investigated recently by Frascella et al.[153] to produce 3D

printed polymeric waveguides able to guide the luminescence up to an angle of 40°C without no degradation of the dye during the irradiation. Moreover, the dye's sensitivity to different solvent polarities enables these waveguides as sensors. The ability of methacrylate dyes to copolymerize as a side-chain functional group avoids their leaching into the organic solvent.

The recent interest in polymeric waveguides is related to the wide range of applications concerning sensors,[154–157] communications,[158] photonic integrated circuits,[159] biomedicals[160,161] and optics.[162] Traditionally, polymeric waveguides are produced employing conjugated polymers, able to emit light thanks to the long-range π-electron conjunction. The high costs, the usually complex synthetical procedures, the non-trivial relationships between structure and properties and the limits of manufacturing methods represent the main drawbacks of this technique.[163–165] A different and innovative helpful method to produce polymeric waveguides concerns photoluminescent fillers, which can be organic or inorganic, in an optically inert polymeric matrix. This loading method can achieve reduced costs and greater ease of processing.[166]

Recently, polymeric waveguides have been produced employing the loading method joined with additive manufacturing, using FFF or DIW printing techniques.[167–170] In the applied formulations, transition metals,[171] rare earth,[172,173] organo-lanthanide complexes[174] or organic molecules[175] are generally introduced. Only a few authors reported using SLA or DLP 3D printing techniques to obtain emitting polymers with an accurate final resolution.[97,153,176]

6.2.2.1 Thermochromic waveguides based on metalorganic complexes

In the first part of this work,[177] we applied some metalorganic complexes in DLP 3D printing to produce polymeric waveguides. These compounds are very known in literature due to their peculiar properties of high luminescence and quantum yields and their thermal-depending photophysical properties.[178–182] Among other properties, these compounds show a very high Stokes shifts that was the most useful characteristic

for obtaining polymeric waveguides. In fact, the ability to absorb in the UV range and emit in the visible one preserves the transparency of the polymeric matrix without conferring a colour. Their low toxicity, high availability and ease of synthesis make these compounds ideal for many applications.

Six different formulations of the two copper clusters synthesized were prepared, changing their concentration (0.1, 1.0 and 5.0 wt.%). Each cluster was added as a solid powder in a vial (10 mL) containing a BEDA liquid monomer. DCM (1.0 mL) was added to reduce the formulation's viscosity and enhance the solubilization of the cluster, avoiding the formation of aggregates. All vials were stirred for 1 hour at 50°C and then sonicated for 1 hour more to achieve a homogeneous solution. Following the same procedure, the blank formulation containing no cluster was prepared and used as a reference for all measures. Before starting the printing process, 1.0 wt.% of photoinitiator was added, and the solutions were sonicated for 5 minutes. Here we chose 2-methylpropiophenone (HMPP) as a photoinitiator. Its UV shifted absorption spectrum makes this compound ideal for maintaining the transparency of the matrix without influencing the photopolymerization process.

In this work, the insoluble fraction was measured by evaluating the weight loss of 3DP components after 24 h of chloroform extraction. These measurements are necessary to demonstrate a good printability and high conversion of acrylic double bonds after the printing and post-curing process. The precision of the 3D printing process was evaluated using an E4 3D scanner (3Shape) with a scanning accuracy of 4 µm.

As an optical power source, the light propagation efficiency into the PWGs was evaluated using a high flux density 365 nm surface mount ceramic package UV LED with an integrated flat glass lens (LZ4–04UV0R OSRAM). The current source and voltage meter is a KEITHLEY 2602 A SourceMeter. The spectrometer is an AcalBFi USB4000 preconfigured for applications from 200 to 850 nm, and the multimode optical fibre is an FT600EMT with a numerical aperture of 0.39 and diameter of 600 µm.

Two different kinds of copper-iodine based clusters were synthesized, and they differ in the synthetic procedure required. Compound **9** shows a higher quantum yield and a

shifted absorbance peak in the UV range, but it's more challenging to synthesize, and it requires more time, toxic solvent, and high temperature than cluster **10**.

Moreover, **9** shows some solubility issues due to its intrinsic insolubility in almost all solvents, and a good and stable dispersion can be achieved only for 0.1 wt.%. For all other concentrations, insoluble powders are visible under a 365 nm UV lamp (Figures 29a and 29b). Instead, compound **10** shows very good solubility for all concentrations, as depicted in Figures 29a and 29b. As reported in the literature,[114] these clusters can emit only in solid-state, but they lose this property in solution: this is also demonstrated by emission spectra for both clusters at 1.0% in the liquid monomer (Figure 120, appendix III).

Figure 29 *– Formulations of monomer, photoinitiator, DCM and different concentrations of **9** and **10** under (a) ambient illumination and (b) under 365 nm UV lamp. The yellow emission of compound powder detects the insolubilized copper cluster. The vials in a) and b) are in the following order (from left to right): blank formulation, 0.1%, 1.0% and 5.0% of compound **9**; 0.1%, 1.0% and 5.0% of compund **10**. c) Polymeric films with 1.0 % of both copper clusters **9** (left) and **10** (right). d) Emission of polymeric films with 1.0 % of **9** (left) and **10** (right) under 365 nm light. Material from: M. Gastaldi, I. Roppolo, A. Chiappone, C. Garino, A. Fin, M. Manachino, P. Sirianni, G. Viscardi, L. Scaltrito, M. Zanetti, S. Bordiga, C. Barolo, Additive Manufacturing **2022**, 49, 102504.*

Some preliminary photopolymerization tests were carried out to evaluate the possibility of obtaining a homogeneous polymeric matrix. Polymeric films were produced under an Argon atmosphere irradiating the liquid formulation with UV light. Only the sample containing 1.0% of **9** showed precipitation of the cluster, clearly visible in Figures 29c and 29d under ambient and UV light. At the same time, all films appear homogeneous and transparent under ambient illumination (Figure 30), except for 5.0% of **9**, which shows aggregates.
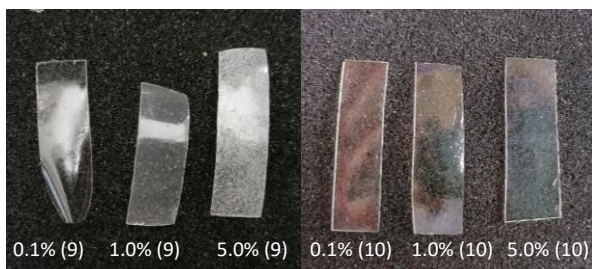
Figure 30 - *Polymeric films with increasing concentrations of **9** and **10**. Material from: M. Gastaldi, I. Roppolo, A. Chiappone, C. Garino, A. Fin, M. Manachino, P. Sirianni, G. Viscardi, L. Scaltrito, M. Zanetti, S. Bordiga, C. Barolo, Additive Manufacturing **2022**, 49, 102504.*

For these reasons, compound **9** cannot be further investigated for applications in 3D printing, despite its higher emission than compound **10**.

Based on previously reported results, using a conventional UV irradiation source, the introduction of up to 5.0 wt.% of the copper cluster doesn't affect the acrylic double bond conversion as well as the transparency of the resulting polymeric matrix. From UV-visible spectra of the polymeric film containing 1.0 wt% of compound **10**, the sample starts to absorb under 400 nm. At the same time, as demonstrated in Figure 31a, the HMPP spectrum overlaps the one reported for the copper cluster to allow fine control of the photopolymerization process and avoid overcuring phenomena that can reduce the final resolutions. The samples' peculiar transparency is preserved after the post-curing process (Figure 121, appendix III).
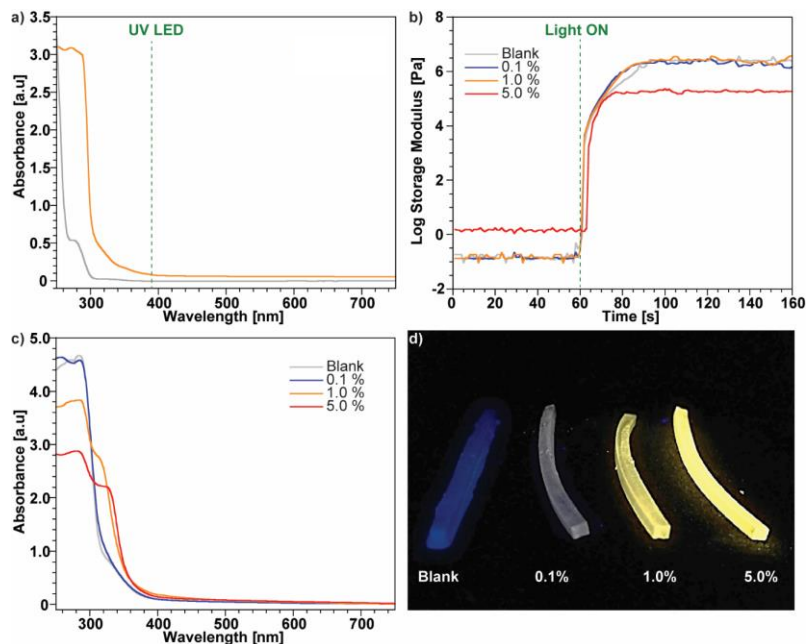
Figure 31 -. a) UV-Visible spectra of 3DP polymeric film containing 1.0 % of *10* (orange) overlapped to UV spectrum of photoinitiator in CAN (gray). The straight dashed green line represents the UV emission of the DLP 3D printer (385 nm). b) Photorheological curves of liquid formulations containing increasing concentrations of *10*. The formulation without a copper cluster represented the reference (Blank). c) UV-visible spectra of 3D printed films containing different concentrations of *10*. d) Picture 3DP polymeric strips with an increasing concentration of *10* under UV (365 nm) light. Material from: M. Gastaldi, I. Roppolo, A. Chiappone, C. Garino, A. Fin, M. Manachino, P. Sirianni, G. Viscardi, L. Scaltrito, M. Zanetti, S. Bordiga, C. Barolo, Additive Manufacturing *2022*, 49, 102504.

Photorheological tests were conducted to evaluate the effect of dyes on the photopolymerization rate. Using the same LED power of the 3D printer (25 mW cm^{-2}), no effect of cluster **10** on the photopolymerization rate is observable up to a concentration of 5.0% (Figure 31b). In this case, the liquid formulation shows a higher storage modulus (G') due to the higher viscosity conferred by the introduction of the cluster. Moreover, a delay in the start of the photopolymerization reaction can be noticed only for the formulation containing 5.0% of compound **10** and a lower value of G' reached after the irradiation. These phenomena can probably be attributed to reduced acrylic double bond conversion value and a less efficient photopolymerization process. This is due to the concurrent absorption of the UV irradiation between the cluster and the photoinitiator. In fact, by reducing the intensity of the LED used during the photorheological tests (setting the value to 0.5 mW cm^{-2}), an apparent effect of the

addition of cluster in the delayed start of polymerization reaction can be noticed Figure 32a. From all these data, the printability of each formulation containing a concentration of less than 5.0% of compound **10** is demonstrated, and the high transparency of the matrix before and after the post-curing process (Figure 32b).
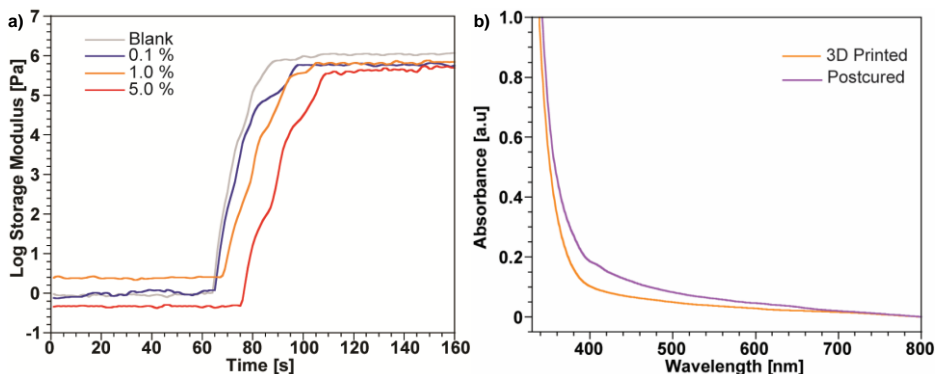
*Figure 32 – a) Photorheology tests at 2 % of UV power (0.5 mW cm^{-2}) on resins containing increasing concentrations of **10**. Blank is the formulation without any copper clusters. A visible delay in the start of the photopolymerization reaction is visible in the formulation containing 5.0 % of **10**. b) UV-Vis spectra of 3D printed polymeric films before (orange) and after (purple) the post-curing process. Material from: M. Gastaldi, I. Roppolo, A. Chiappone, C. Garino, A. Fin, M. Manachino, P. Sirianni, G. Viscardi, L. Scaltrito, M. Zanetti, S. Bordiga, C. Barolo, Additive Manufacturing **2022**, 49, 102504.*

3D printing parameters were experimentally optimized. A slice thickness of 25 µm, the minimum resolution of the printer, is necessary to obtain a very good final resolution and fidelity to the CAD virtual project and 3 burn-in layers to enhance the adhesion of the object to the printer's platform. These 3 layers are overcured, irradiating them for 15 seconds each, while all other layers are photopolymerized, exposing them to 10 seconds of UV irradiation.

Employing these optimized parameters, some films and polymeric waveguides were printed using all formulations containing an increasing concentration of **10** (0.1, 1.0 and 5.0 wt.%). The high transparency in the visible range is preserved for all formulations, as demonstrated in Figure 31c from UV-vis spectra of the 3D printed and post-cured polymeric films. As depicted in Figure 31d, good profiles can be obtained without precision due to the overcuring effect. Moreover, increasing the quantity of clusters introduced in the liquid formulation makes the higher luminescence visible with naked eyes. The blank sample and the one containing 0.1% of **10** show a blue emission due to

the emitting properties of the polymeric matrix. This emission is completely covered by the emission of the cluster for higher concentrations.

To maintain good mechanical and thermal properties without any reduction in the photopolymerization reaction kinetics, achieving at the same time suitable emitting properties, the optimal concentration of cluster **10** is 1.0 wt.%, as reported in Table 8.

Table 8 - *Double bond conversions of 3DP films are reported after the post-curing process in a UV oven for 5 s on each side. Glass transition temperature (T_g) and the temperature at which the polymeric sample lose 5.0% of the initial weight (T_5) are described for each formulation.*

Compound 10 content (wt.%)	-C=C- bond conversion (%)	Insoluble fraction (%)	T_g (°C)	T_5 (°C)
0 (blank)	80	99	35.4	313
0.1	79	99	48.4	274
1.0	78	99	43.5	288
5.0	70	95	47.1	247

Acrylic double bond conversions were evaluated through ATR-FTIR instrumentation ranging from 4000 to 500 cm^{-1}. Each value was determined by reducing the peak centred at 980 cm^{-1} normalized by the aromatic signal at 1550 cm^{-1}. All results are reported in Figure 33, in which the liquid and photopolymerized formulations are compared. The presence of **10** doesn't affect the double bond conversion, except for the 5.0% formulation, in which a noticeable reduction in the conversion can be observed. These results agree on which ones are reported in the literature for UV-cured coatings (without using a 3D printer).[178] The low values obtained in this work can be explained considering that the 3D printer used a very short time of irradiation as well as that the photopolymerization process suffers from oxygen inhibition. For these reasons, higher conversions can be found in the literature for samples polymerized under inter atmosphere and longer irradiation times. However, the reported results are compatible with the 3D printing DLP process, as demonstrated by the very low amount of unreacted monomer evaluated by the gel content measurements. These analyses evaluated the loss in weight of 3DP films after 24 h of chloroform extraction.
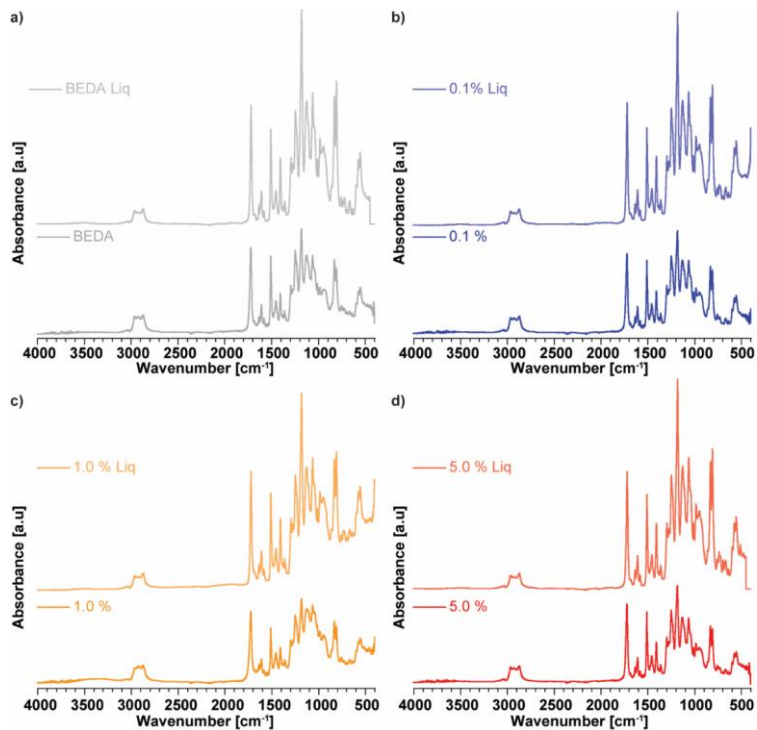
Figure 33 *- ATR-FTIR spectra of liquid formulation (top) and 3DP post cured films (down) of (a) blank BEDA without copper complex, (b) with 0.1 %, (c) 1.0 % and (d) 5.0 % of **10**. Material from: M. Gastaldi, I. Roppolo, A. Chiappone, C. Garino, A. Fin, M. Manachino, P. Sirianni, G. Viscardi, L. Scaltrito, M. Zanetti, S. Bordiga, C. Barolo, Additive Manufacturing **2022**, 49, 102504.*

DSCs were conducted from -20 °C to 80 °C with a heating ramp of 20 °C/min and a cooling ramp of 10 °C/min, while TGA analyses were carried out from 30 °C to 650 °C in air, employing a heating rate of 10 °C/min. All thermograms are reported in Figures 122 and 123 in Appendix III. It's observable that the introduction of the cluster causes an increase in the glass transition temperature of all samples, probably due to the increased hindering of movements of the polymeric chains by the cluster. At the same time, an increase in the stiffness of the loaded materials can be noticed from DSC thermograms. On the other hand, the thermal stability, evaluated by TGA, is not affected by the introduction of copper clusters.

From all these results, the best promising formulation is the one containing 1.0% of cluster **10**. This is the only one further explored in this study in terms of photoluminescence and the final device's production.

In Figure 34a, the absorbance and emission spectra of polymeric 3D printed films containing 1.0% of compound **10** are reported, demonstrating the very high Stokes shift, also maintained in the 3D printed polymeric matrix. No damage to the cluster is reported after the printing or the post-curing process.
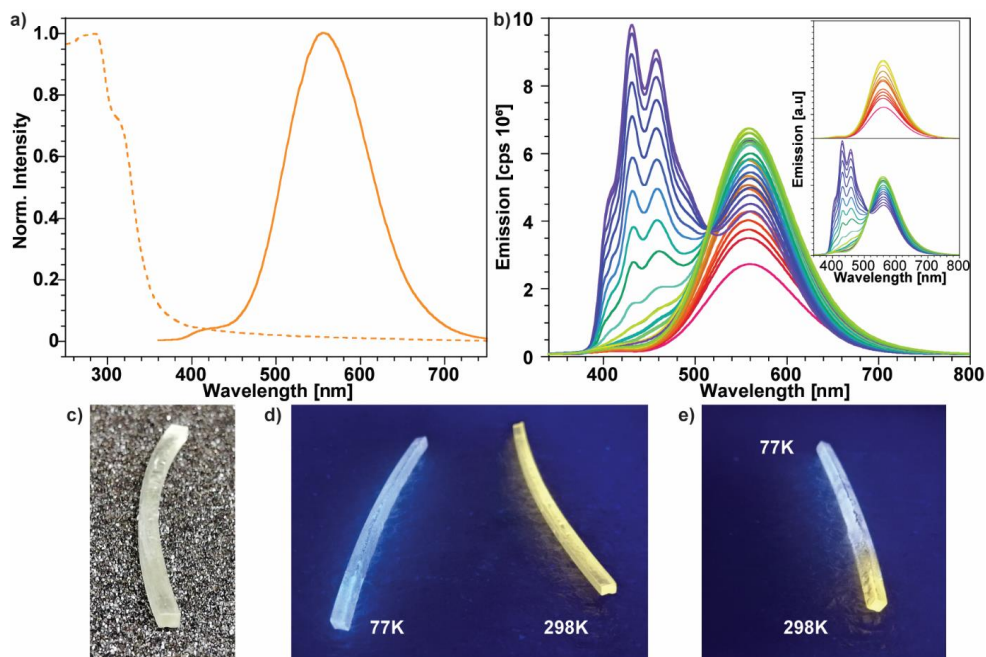
Figure 34 - *a) Absorption (dashed) and emission (solid) spectra of 3DP film containing 1.0 % of* **10**. *b)*
Temperature-dependent luminescence spectra of 2 (λ_ex = 330 nm, temperature from room temperature to
77 K). The two insets reported the separated first (top) and second (bottom) emission wavelengths. 3DP
polymeric waveguide under ambient light (c), under UV (365 nm) light at different temperatures (77 K and
298K) and partially immersed in liquid nitrogen (e). Material from: M. Gastaldi, I. Roppolo, A. Chiappone,
C. Garino, A. Fin, M. Manachino, P. Sirianni, G. Viscardi, L. Scaltrito, M. Zanetti, S. Bordiga, C. Barolo,
Additive Manufacturing **2022**, *49, 102504.*

At the same time, the peculiar thermochromic properties of these compounds are also maintained when inserted as dispersed filler between polymeric chains (Figure 34b). The printed composite displays a single bright yellow luminescence at room temperature under UV excitation (330 nm). This low-energy band (LE) is attributed to a ''cluster-centred'' triplet excited state (3CC) and is independent of the nature of the ligand. Lowering the temperature to 77 K, a structured deep-blue emission appears at higher energy (high-energy band, HE) alongside the LE band. The HE band is assigned to an iodide-to-phosphine ligand charge-transfer transition (XLCT).[183] This thermochromism is perfectly reversible, warming up the sample, which returns to emit

72

yellow light. Changing the temperature, an isosbestic point at 520 nm can be observed, indicating a thermal equilibrium between the LE and HE excited states. This implies a very high coupling of the two states, leading to a perfectly controlled thermochromic luminescence in an extensive temperature range.

The calculated value decreases the quantum yield (QY), reducing the quantity of the cluster in the matrix, from 60% for the formulation containing 5.0% of **10** to 30-10% for 1.0% and 0.1%. Only the value found for the higher concentration can be compared with the one reported in the literature for the pure crystalline compound.[114,115,179] The other two values probably are affected by the concurrent absorption of the polymeric matrix at the exciting wavelength, as demonstrated by the emission spectrum of the blank sample, as reported in Figure 124 in Appendix III.

An evaluation of the HE and LE excited state's lifetimes has also been evaluated by time-correlated single-photon counting. The measured lifetimes for the two emissions are τLE(RT/77 K) = 9 µs, τ^1HE(77 K) = 0.6 ms, τ^2HE (77 K) = 3.3 ms, in accordance with the phosphorescent nature of the two triplet excited states. These results agree with ones reported in the literature for compound **10** embedded in an acrylate polymeric matrix, demonstrating the preservation of the cluster integrity during the whole printing and post-curing process.

The thermochromic behaviour of the resulting functionalized polymeric waveguide, which appears transparent under ambient illumination (Figure 34c), is visible by naked eyes under a 365 nm UV lamp. Different emission properties can be noticed when comparing the sample (Figure 34d) or partially (Figure 34e) immersed in liquid nitrogen with the one at room temperature. This property opens the way for using these compounds as cryogenic optical sensors.

Some complex 3D printed shapes were obtained and investigated by 3D scanning to test the final resolution achievable through the optimised parameters. As demonstrated in Figure 35a, a light diffuser containing the 1.0% of complex **10** can be printed, maintaining the possibility of being lighted with UV irradiation (Figure 35b) and showing a very good fidelity to the CAD project (Figure 125, Appendix III). In this case,

displacements at about ± 0.050 mm in the green zones and ± 0.100 mm in the yellow and light blue ones are pointed out by the 3D scanner and depicted in Figure 35c. Evident defects are visible in the bottom parts that are the first printed: these first layers are overcured to start the polymerization in areas outside the CAD project and guarantee good adhesion of the object to the growing 3D printer platform; without them, the 3D printing process can't proceed. Regarding the inner parts, those are blind points for the 3D scanner, so that volume cannot be considered meaningful for fidelity evaluation.
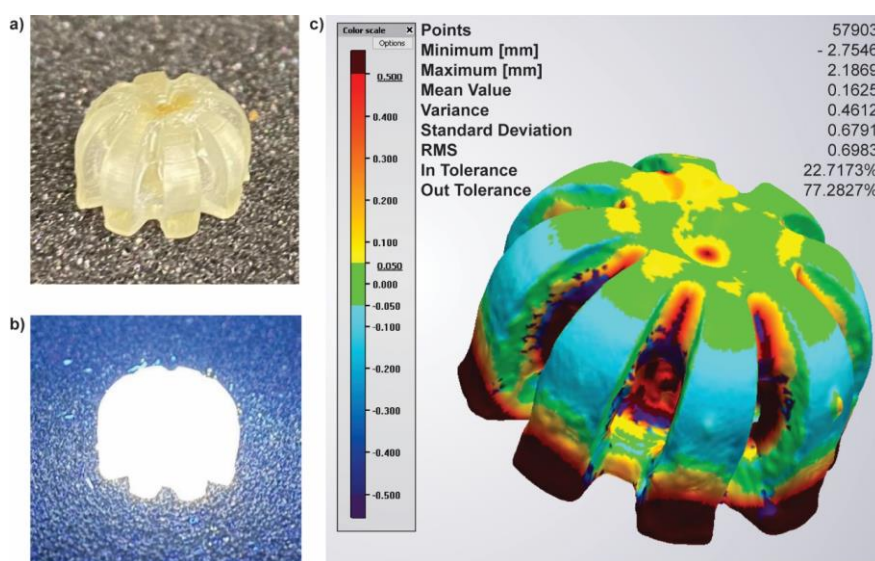
Figure 35 - *3DP light diffusor with 1.0 % of complex **10** under (a) ambient and (b) 365 nm UV illumination. c) 3D image obtained employing the 3D scanner to evaluate the displacements between the CAD project and the 3D printed device. Material from: M. Gastaldi, I. Roppolo, A. Chiappone, C. Garino, A. Fin, M. Manachino, P. Sirianni, G. Viscardi, L. Scaltrito, M. Zanetti, S. Bordiga, C. Barolo, Additive Manufacturing **2022**, 49, 102504.*

Some 3D printed waveguides are then fabricated to evaluate the efficiency in converting UV irradiation into visible light as well as the capability to guide light through the polymeric matrix. Waveguides of 2, 3 and 5 cm in length, which is the maximum that can be reached with a DLP configuration printer, were printed and tested using two configurations, called "direct" and "side" configurations. For the direct one, the irradiation and the detector were in the same direction of the polymeric waveguide. In contrast, for the side configuration, the irradiation was perpendicular to the waveguide (sketch representations of the two configurations are depicted in Figure 126 in

Appendix III). All waveguides were irradiated using a 365 nm centred LED, which emission spectra are reported in Figure 127 in Appendix III. The measurement conditions, the voltage used, and the relative incident power density are reported in Table 40 in Appendix III. The emission spectra for both configurations are reported in Figures 36a and 36b. For direct pumping configuration, a clear decrease in the LED intensity and the relative increase of the visible irradiation along the length is reported in Figure 36a. In this type of configuration, the LED peak is detectable. Still, it decreases in intensity with the distance due to the progressive absorption of the irradiation by the copper cluster, and the visible irradiation consequently increases.

On the other hand, the LED emission cannot be detected for side pumping configuration since the shorter length. Moreover, the direct pumping irradiation reduces the visible emission according to the increase of waveguide length, probably connected with the lateral dispersion. In contrast, the emission is maintained almost constant for side geometry but less intense. The shoulder of the emission spectra depicted in Figure 36b is related to the emission properties of the blank polymeric matrix, whose spectra for both configurations are reported in Figure 128 in Appendix III.
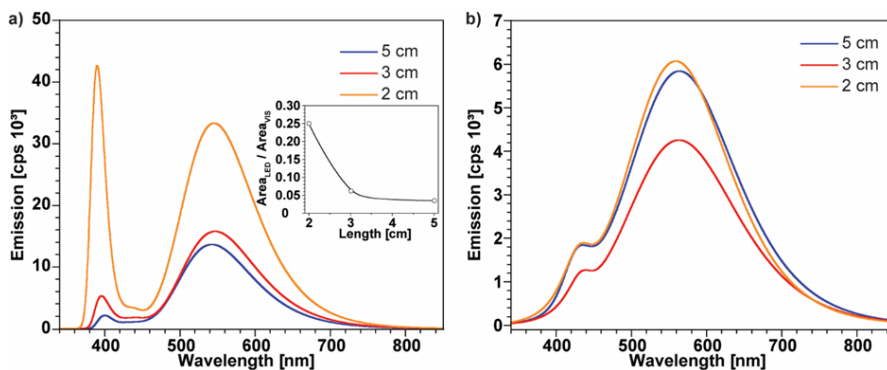
Figure 36 – *Emission spectrum of (a) direct and (b) side pumping configurations of polymeric waveguides with different lengths. In the inset of (a), the ratios between LED and visible emission are reported. Material from: M. Gastaldi, I. Roppolo, A. Chiappone, C. Garino, A. Fin, M. Manachino, P. Sirianni, G. Viscardi, L. Scaltrito, M. Zanetti, S. Bordiga, C. Barolo, Additive Manufacturing* **2022**, *49, 102504.*

Some preliminary studies were also conducted simulating temperature changes for the direct configuration setup, using a Peltier cell to cool the polymeric waveguides from 40°C to almost 13°C (the experimental setup is reported in Figure 129 in Appendix III).

An increase in the emitting properties can be observed reducing the temperature, as demonstrated visually in Figure 37a or by the correlation between the area of each peak and the temperature measured, reported in Figure 37b. According to the data reported in the literature, this is an expected result, but the increase is observable, even remaining in the almost common everyday temperature range.
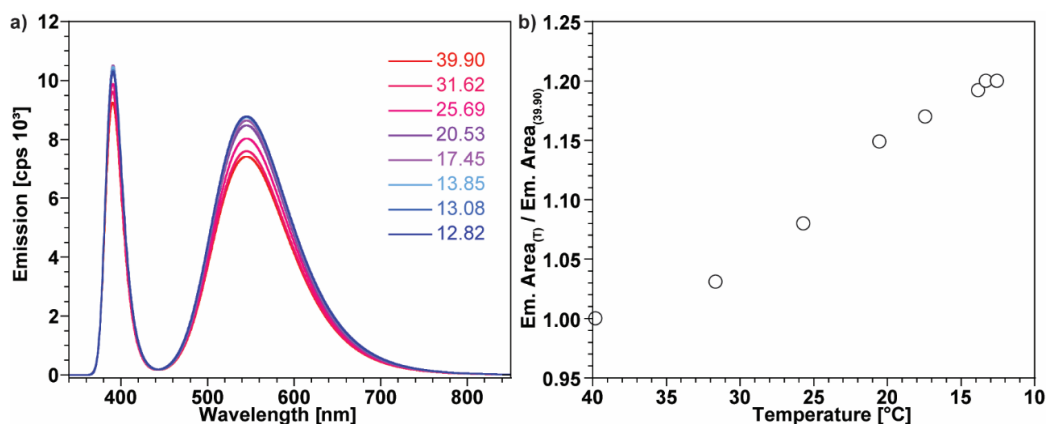
Figure 37 – (a) Emission spectra at different temperatures (reported in the legend (°C)) for 2 cm length polymeric waveguide containing 1.0% of compound 10. B) The normalized emission areas at each temperature over the 39.90°C area. Material from: M. Gastaldi, I. Roppolo, A. Chiappone, C. Garino, A. Fin, M. Manachino, P. Sirianni, G. Viscardi, L. Scaltrito, M. Zanetti, S. Bordiga, C. Barolo, Additive Manufacturing 2022, 49, 102504.

Some promising and preliminary results are obtained in this work, applying copper-based complexes to be incorporated into a liquid 3D printable formulation and maintaining their optical and thermal properties at the end of the process. The possibility of avoiding the use of toxic and rare earth metals, reducing costs and avoiding expensive synthesis represents a first step in producing polymeric waveguides with good efficiency and transparency. The high resolution, achievable thanks to the positive effects of the clusters, and the possibility to print complex objects open the field of applications for these types of materials and the 3D printing contributions. Nevertheless, some improvements can be investigated, mainly to avoid lateral light dispersion with the production of suitable claddings.

6.2.2.2 3D printable organic and engineered fluorophores for DLP printer

Organic dyes can also be developed as downshifter light emitters and applied in polymeric waveguides. Their high solubility and the possibility to functionalize them with photopolymerizable groups allow their use in high concentrations, avoiding leaching during use. We synthesized and investigated different organic light emitters applied in liquid 3D printable formulations to investigate their final properties and efficiency as polymeric waveguides. In this case, only preliminary results were achieved. The effective use in a polymeric waveguide is not tested yet: this aspect is actually under investigation, and the thermal and photostability under UV irradiation.

In this second part of fluorophores for 3D printing, we synthesized compounds **12** and **13**, as previously reported, and we prepared some formulations containing each of these organic molecules. We intended to evaluate the emitter's behaviour when dispersed (**12**) or covalently connected (**13**) to the polymeric chains. Also, in this case, HMPP was used as a photoinitiator due to its ability to absorb at the same range as the LED's printer (385 nm), presenting no competition with the organic dyes or giving colour the final polymeric device. We prepared two concentrated formulations, **A** for compound **12** and **B** for compound **13**. Then we used these to obtain other two diluted formulations for each combination (**A1**, **A2** and **B1**, **B2**). **A3** and **B3** were obtained by diluting A2 and B2, respectively. All data are reported in Table 9.

__Table 9__ - Components and their quantity (grams and wt.%) for each formulation.

Formulation	Concentration of organic dye (mmol/l)	Component of the formulation	Quantity of each component (g)	Composition (wt.%)
A1	23.5088	BEDA	1.988	99.29
		12	0.012	0.61
A2	0.2272	BEDA	5.820	98.93
		A1	0.057	0.97
		HMPP	0.006	0.10
A3	0.1136	BEDA	11.964	99.42
		A1	0.058	0.48
		HMPP	0.012	0.10
A4	0.0284	BEDA	3.50	87.40
		A3	0.500	12.50

		HMPP	0.004	0.10
B1	25.8618	BEDA	1.984	99.18
		13	0.016	0.82
B2	0.1746	BEDA	6.576	99.22
		B1	0.045	0.68
		HMPP	0.007	0.10
B3	0.05820	BEDA	12.414	99.67
		B1	0.028	0.23
		HMPP	0.012	0.10
B4	0.01940	BEDA	3.200	88.79
		B3	0.400	11.11
		HMPP	0.004	0.10

Each formulation was sonicated for 20 minutes to achieve homogeneity, and the addition of 0.5 mL of acetone helped reduce viscosity. The 3D printing parameters were experimentally optimized to reach good adhesion, calibrating the quantity of burn-in layers and polymerized layers to the growing platform, avoiding overcuring phenomena. The optimized parameters are reported in Table 10.

Table 10 - Optimized 3D printing parameters.

Burn-in thickness	0.300 mm
Burn-in time	20.0 s
Layer thickness	0.05 mm
Normal exposure time	15.0 s
Temperature	25.0°C
LED printer intensity	30 mW/cm^2

Moreover, a blank formulation composed only of BEDA monomer and HMPP as PI was prepared in the same way and used as a reference in all measures.

At the end of the 3D printing process, all samples were washed with water and ethanol, dried and post-cured 5 minutes on each side using a UV oven.

As depicted in Figures 130 and 131 reported in Appendix III, both films containing compounds 12 and 13 showed broad absorption spectra, ranging from up to 290 to almost 400 nm. Evaluating the emission spectra, we found that the best excitation wavelength was 380 nm, at which the best emission was achieved. The same excitation

wavelength was used to irradiate all diluted samples obtaining the following emission spectra, reported in Figure 38 (for compound **12**) and Figure 39 (for compound **13**).
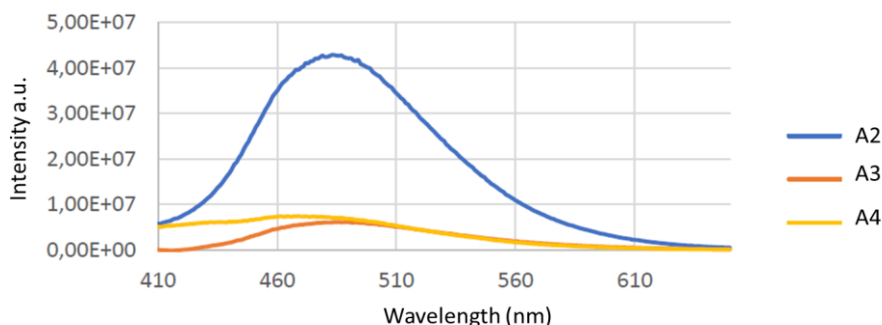
Figure 38 - *Emission spectra of 3D printed polymeric films containing a decreasing concentration of* ***12***.
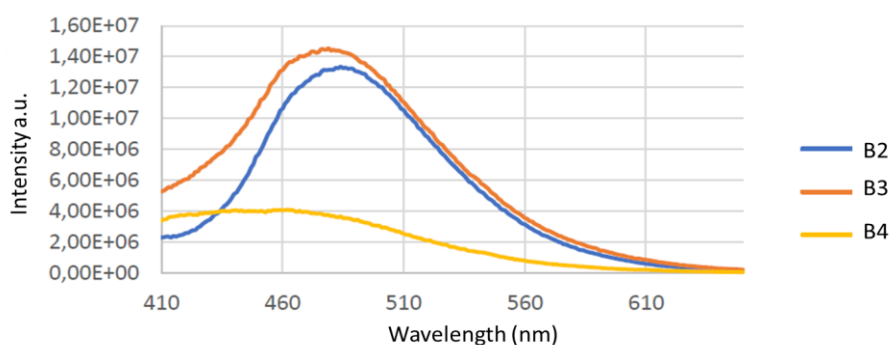
Figure 39 - *Emission spectra of 3D printed polymeric films containing a decreasing concentration of* ***13***.

We noticed a hypsochromic shift when the organic emitter's concentration decreases, particularly for **A3** and **B3** compositions, as depicted in Table 11, in which all absorption maxima are listed. As expected, the best intensity of the emission spectra is observed for the compositions containing higher contents of emitters, without no observable variations between the dispersed and the covalently linked emitter.

Table 11 - *Maxima of the emission spectra for all 3D printed polymeric films containing different concentrations of* ***12*** *and* ***13***.

	Sample	λ_{max} emission (nm)
	A2	483
12	A3	486
	A4	469
	B2	484
13	B3	479

We evaluated the Stokes shift in the liquid state and the difference in emission between the liquid and the solid state to evaluate if some differences occur after the photopolymerization process (Figure 40 for compound **12** and 41 for compound **13**).
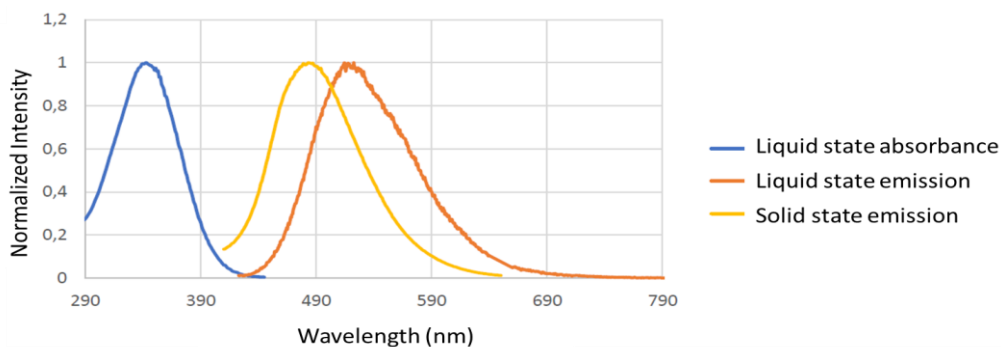
Figure 40 - *Absorption (blue) and emission (orange) spectra of liquid formulations containing compound **12**. In yellow, the emission spectrum of 3D printed polymeric film in which a clear hypsochromic shift of 38 nm with respect to the liquid emission is observable.*
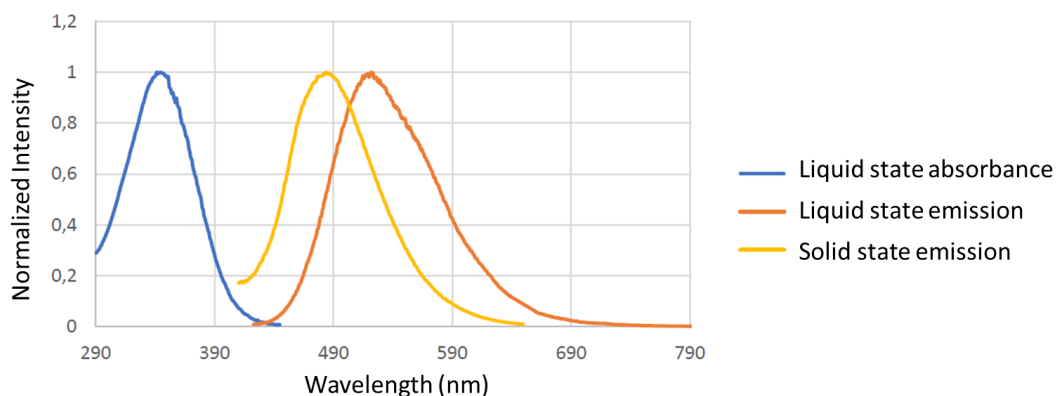
Figure 41 - *Absorption (blue) and emission (orange) spectra of liquid formulations containing compound **13**. In yellow, the emission spectrum of 3D printed polymeric film in which a clear hypsochromic shift of 38 nm with respect to the liquid emission is observable.*

As observable from the previously reported spectra, all samples show almost the same emission, without differences between methacrylate and dispersed organic emitters. No differences in the calculated quantum yield (φ) can be detected (Table 12).

Table 12 - Quantum yield (%) for all diluted samples using 380 nm as excitation wavelength, covering a range of emission from 370 nm to 650 nm employing the integrating sphere.

	Sample	φ (%)
	A2	15.0
12	A3	5.0
	A4	2.7
	B2	14.1
13	B3	3.6
	B4	0.8

The decreasing quantum yield found reducing the concentration of the organic dye is due to the concurrent absorbance of the polymeric matrix, and no auto-quenching phenomena were observed at the reported concentrations. This means that higher quantities of dyes can be introduced to enhance the quantum yield and the final efficiency of the 3D printed devices. Moreover, the thermal stability was not affected by the introduction of the dyes as demonstrated by TGA thermograms (Figure 132 in Appendix III), in which no significant reductions of the thermal stability are noticed for the samples containing the higher concentration of functional dyes, as listed in Table 13.

*Table 13 - Thermal stability for the higher concentrated samples (**A2** and **B2**) and their final residues at 800°C under an N_2 atmosphere with a heating ramp of 10°C/min.*

Sample	Temperature to lose 5.0% of the initial weight (°C)	Residues at 800°C (%)
Blank	352.70	3.791
A2	353.04	3.993
B2	353.88	4.700

We ideated and produced a 3D printed complex object using a diluted **B1** solution (1:10). We printed a cross composed of the BEDA monomer and the functional

methacrylate dye, immersed in a cube made of blank resin, according to the CAD project reported in Figure 42.
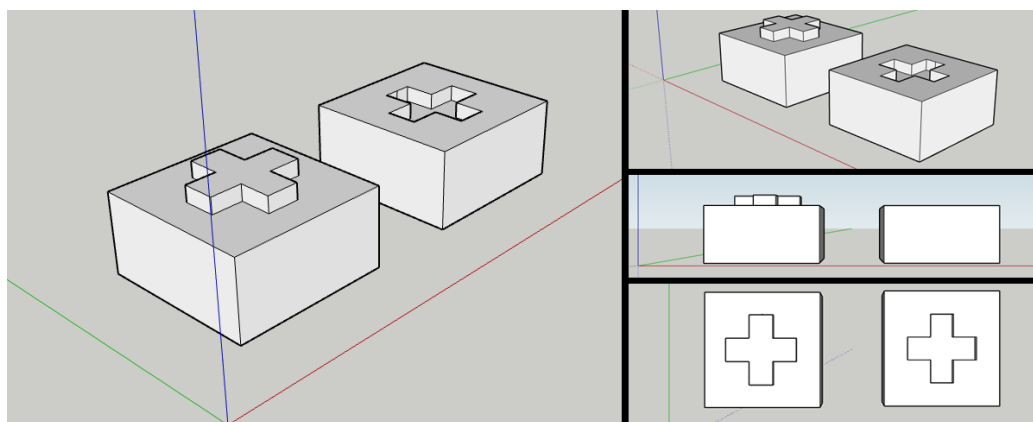
Figure 42 – CAD project of the final 3D printed device in which the cross is composed of light emitter methacrylated dye and the rest of the cube only of blank resin.

To achieve this result, the tank containing the functional resin was substituted during printing with another one containing the blank ink. In the following Table 14 are listed all printing parameters used for both formulations: no burn-in is needed for the luminescent parts because the initial layers are composed of the blank formulation.

Table 14 - Optimized 3D printing parameters for both blank and luminescent formulations.

Parameter	Blank formulation	Dye functionalized formulation
Burn-in exposure time	20.0 s	-
Normal exposure time	15.0 s	15.0 s
Layer thickness	100 μm	50 μm
LED irradiation intensity	30 mW/cm^2	30 mW/cm^2

A transparent device was 3D printed and post-cured using these parameters, as demonstrated in Figure 43a. Under 380 nm LED, the cross at the middle of the printed cube emits light, as clearly reported in Figure 43b.
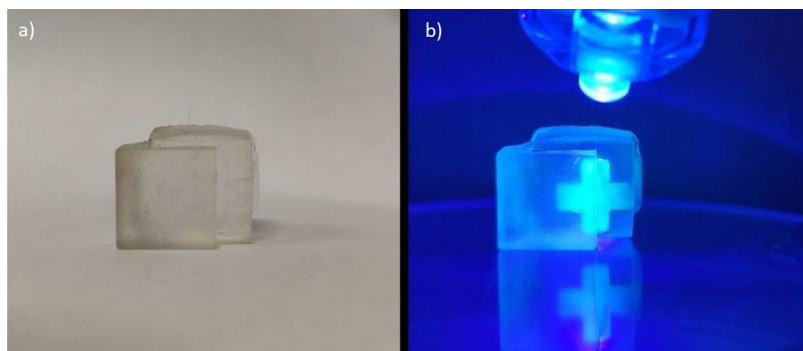
Figure 43 – *(a) 3D printed device containing two different resins: the whole cube is composed of a blank formulation, while a cross is printed using the luminescent resin in the middle. The transparency is demonstrated under ambient illumination. (b) The final 3D printed device under 380 nm LED irradiation in which the polymeric matrix's transparency is pointed out and the luminescent cross at the middle of the cube, activated under UV irradiation.*

The production of 3D printed waveguides is under investigation. Two other important aspects of using these materials have to be considered: the possibility of leaching the functional dyes under organic solvents action and their photostability under UV light irradiation. The possible absence of leaching can path the way to using these polymers as sensors. The importance of photostability is related to the lifetime of the final devices.

These promising results obtained both with metalorganic complexes and organic functional dyes can open in the next future the field of applications of these smart 3D printed materials, able to join both an innovative functionality conferred by the dye as well as a complex shape, achievable with 3D printing.

6.2.3 Functional azodye-based polymers activated under light

6.2.3.1 Photoinduced tunable properties of azodye-based polymers

Azodyes chromophores are well-known chromophores, deeply studied in the literature for many years. Able to undergo *cis/trans* isomerization under heat or light irradiation (Figure 44a), these compounds represent functional photo-switchable dyes that can be quickly introduced as dispersed or covalently connected side or main chain groups to the polymeric matrix. Under dark conditions, these dyes are usually in their

most stable *trans* form; overcoming an energy barrier, which value strongly depends on the structure and functional groups introduced, can induce isomerization to the unstable *cis* one. The reversible reaction usually takes place spontaneously, releasing heat.[184–187] Commonly, azodyes can be classified into three categories (Figure 44b), which differ in the absorption wavelength and thermal back relaxation from *cis* to *trans* isomers. Unsubstituted azodyes usually are characterized by an absorbance maximum in the UV range, showing high stability in dark conditions for the *cis* isomer, while amino-substituted azodyes are usually red-shifted in absorbance of the *trans* isomer, and the *cis* one has a lifetime around minutes. The final type, commonly called pseudo-stilbene azodye, is characterized by fast (in seconds or less) thermal reconversion from *cis* to *trans* and a red-shifted absorption maximum into the blue-green or even yellow visible region. Due to push-pull functional groups at the two ends of the structure, these dyes show overlapped absorption bands between the *trans* and *cis* isomers that allow the use of the same wavelength to activate the isomerization.[188]
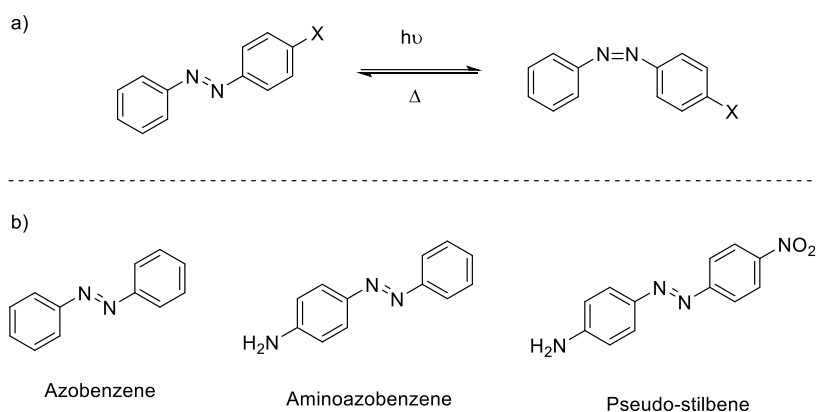
Figure 44 – a) Cis/trans isomerization of azodyes and b) different types of azobenzene dyes.

The photophysical properties of these azodyes can be easily tuned by introducing some functional groups [189], which can act as electron donors or acceptor functionalities. They can generate different grades of steric hindrance and influence the *cis/trans* isomerization process. This great versatility, joined with different synthetical pathways already available to synthesize, makes these compounds promising in their use as functional materials, particularly when exploited in polymeric matrices.[188] The

introduction of azodyes into polymers originates new smart materials that can be controlled in their movements by light. The *trans/cis* isomerization process causes a decrease in the distance between the two ends of the molecule, passing from 10 to 6 Å. This change causes a significant nanoscale force that can be exploited to generate movements and change the materials' optical properties.[190] Some chemical and mechanical properties can also be tuned using azodyes, as recently reported by Aprahamian et al.[191] In this article, they can tune the glass transition temperature (T_g) of some polyacrylate- and polymethacrylate- based polymers with azodye as side-chain functional groups. A ΔT_g about +22°C can be observed under light irradiation for a peculiar type of azodye as well as a photo-hardening effect is also caused by the *cis/trans* isomerization. Sensors and actuators are obtained in this way, efficiently inducing the conversion of light into mechanical work.[22,192]

Among others, the exploitation of push-pull pseudostilbene-azodyes is of particular interest due to the easy synthesis of these compounds, the possibility to tune the *cis/trans* isomerization using the same wavelength and their photo and thermal stability. Moreover, innovative and peculiar properties can be conferred, as reported in the literature, by introducing different functional groups in the ortho position with respect to the azo bridge (X position in Figure 45).[193,194]
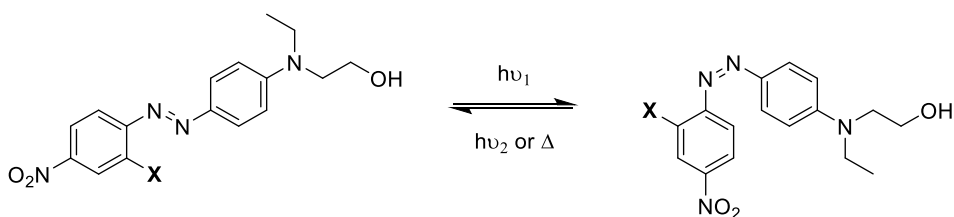
Figure 45 *- Scaffolds of push-pull azodyes with X as ortho functional group as trans (left) and cis (right) isomers.*

In the following chapters, azodyes bearing different functional groups are synthesized and used as side-chain monomers, exploiting the methacrylic functionality specially introduced. All the polymeric devices were obtained through the photopolymerization of acrylic or methacrylic monomers in a DLP 3D printing configuration. The fields of

application are quite broad, spacing from photothermal induced actuators, tunable gas permeation membranes and shape-memory polymers.

In this work, all synthesized azodyes (0.1 wt.%, 10.0 mg) were dissolved in BEDA liquid monomer (10 g) under stirring and sonication until homogeneous solutions were obtained. BAPO photoinitiator (2.0 wt.%, 200.0 mg) was dissolved in acetone (2 mL) and added to the solution. The resulting mixture was then stirred and sonicated for 30 minutes under dark conditions (a similar procedure was followed for a blank (BEDA) sample without adding any dyes). This last formulation is used as a reference for all further measurements. We experimentally optimised the parameters of the 3D printing process, as reported in Table 15.

Table 15 - *Optimized 3D printing parameters according to the azodye used in the BEDA formulation.*

	BEDA	18	19	20	21
Slice thickness (μm)	25.0	25.0	25.0	25.0	25.0
Burn-In time (s)	1.5	5.0	5.0	5.0	7.0
Normal exposure time (s)	1.5	3.5	3.5	3.5	4.5

This work aims to synthesise and evaluate the properties conferred to the polymeric 3D printed matrix using different azodyes. In particular, an essential aspect in assessing the ortho functional groups' steric hindrance and electronic effects on the mechanical properties of 3D printed polymeric devices. All chromophores were functionalized with acrylic or methacrylic photopolymerizable groups, with which a covalent link between the dye and the polymeric chains can be obtained.

Regarding the preparation of each formulation, a minimal quantity of each azodye is introduced in the liquid preparations to avoid modifications in the mechanical properties of the resulting polymer and preserve the printability of the formulations. Increasing the concentration, the light penetration of the 3D printer's LED can be hampered, preventing the photoinduced polymerization process. A few millilitres of acetone helps reduce the formulation's viscosity and enhances the solubilization of the dye and the photoinitiator, achieving homogeneous solutions. During the printing process, the evaporation of the solvent occurs spontaneously, without affecting the resulting mechanical properties.

Once optimized the 3D printing parameters, avoiding overcuring phenomena, some rectangular strip samples were printed and tested using DMA analysis to evaluate their mechanical behaviour in stress/strain test and under an oscillating force applied. Moreover, an evaluation of the green laser effects on the mechanical properties of the polymers was carried out with an available sample holder, exploring the possibility of tuning these features under irradiation. In particular, based on previously reported work,[60] the intention is to investigate the possibility of these azodyes undergoing *cis/trans* isomerization under light irradiation when inserted as covalently liked dyes in a polymeric crosslinked matrix. This phenomenon can be a possible explanation for many reported light-activated behaviours of polymers containing azodyes.

The first observed effect is in modifying the glass transition temperature (T_g), evaluated through DMA, from the ratio (denominated tan δ) between the storage and the loss moduli and DSC. As reported in Table 16 and graphically in Figure 46, a shifting in the maximum of the *tan δ* can be observed, representing each sample's Tg.

Table 16 - *Glass transition temperatures with DMA and DSC instruments, the steric hindrance as A-value for each functional group and thermal degradation from TGA analysis (T_5 correspond to the temperatures at which the samples lose 5.0 % of weight).*

Sample	T_g (°C) - DMA	T_g (°C) - DSC	A-Value	T_5 (°C)
BEDA	35.7	50.3	-	356.77
18	38.0	36.0	0.00	364.66
19	41.1	50.2	0.43	373.13
20	46.2	50.7	0.60	357.48
21	49.3	48.4	1.10	366.74

This small quantity of dye can raise the T_g from 35.7°C for the blank sample (BEDA) up to 49°C for **21**: these differences were completely levelled in DSC measurements (Figure 133 in Appendix IV). These results may be caused by the introduction of functional groups with an increasing steric hindrance that can reduce the mobility of the polymeric chains and shift the T_g to higher temperatures. Moreover, the addition of this small quantity of azodyes didn't affect the thermal stability, as demonstrated by TGA thermograms (Figure 134 in Appendix IV) and by the temperature in which the samples lost 5.0% of the initial weight (T_5 in Table 16).
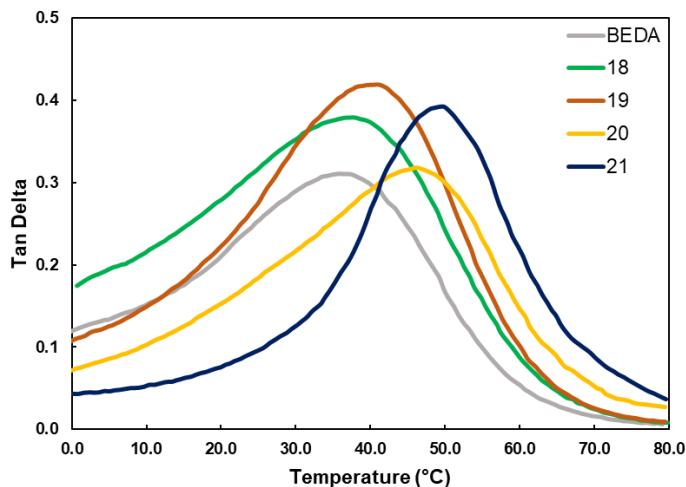
Figure 46 - DMA analysis to evaluate the T_g of the samples at the maximum of the tan delta.

Due to the well-known *cis/trans* isomerization of azodyes usually induced by light, light-induced mechanical or chemical modifications were investigated using an open DMA sample holder introducing a 532 nm laser irradiation. The laser is a focused light source that can be easily managed to irradiate specific areas of a device. The laser power, the distance from the polymeric object and the irradiance can be tuned according to the particular use. The 532 nm wavelength is chosen based on previous work[60], in which some changes in elastic modulus were noticed under laser irradiation. In that work, a comparison between the effects of methacrylate Disperse Red 1 and dispersed Methyl Red was carried out, demonstrating as, under light, the elastic modulus can be reduced or enhanced according to the polymeric matrix and the dye introduced.

Moreover, this wavelength is useful for all samples because it is near their maximum absorptions (Figure 47a). In particular, the samples with electron-withdrawing groups show a bathochromic shift nearer to the 532 nm laser wavelength. In Figure 47b, an evaluation of the molar absorption coefficient in the solution is given. This graph shows that all compounds show very high molar extinction coefficient values at 532 nm. At the same time, all azodyes have a minimum in the absorption spectra at 405 nm (green dashed line in Figure 47c), which is the wavelength used by the 3D printer. That means

a very low competition in printer's LED absorbance occurs between dyes and photoinitiator (see BAPO absorption spectrum in Figure 135 in Appendix IV). A further demonstration is provided in Figure 47c, in which the spectrum of a solution made of compound **17** and 2.0 wt.% of photoinitiator is reported, guaranteeing a fast printing, no overcuring defects and good final resolutions.
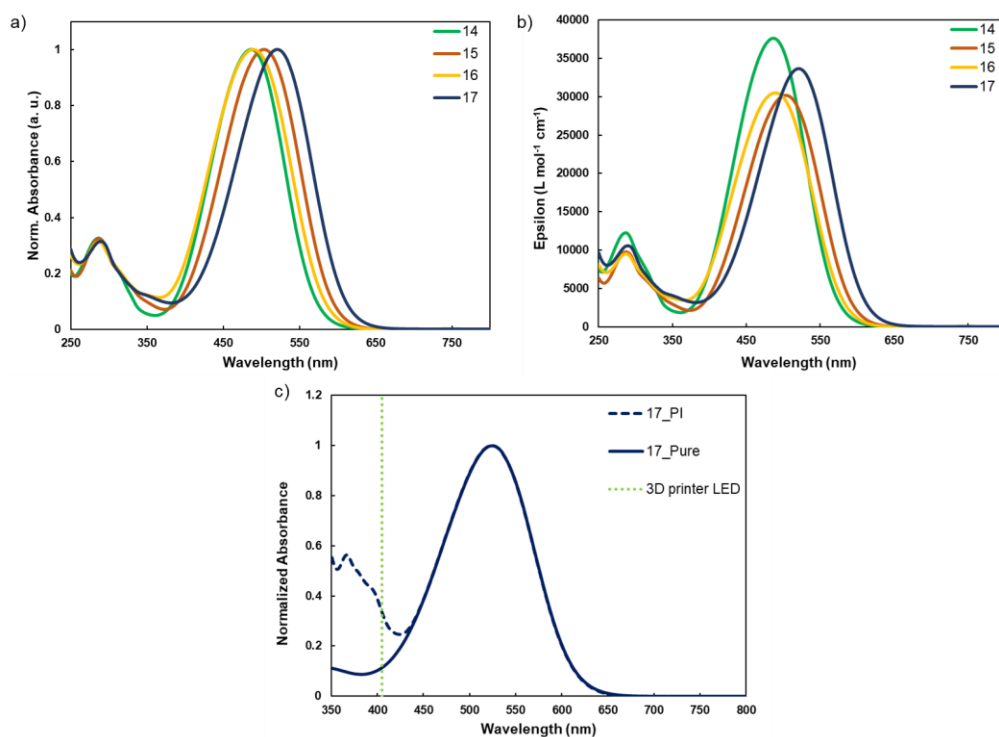
*Figure 47 - a) Normalized UV-vis absorption spectra of azodyes in EtOH. b) Molar absorption coefficient at a different wavelength of all azodyes in solution (EtOH). c) Comparison between UV-vis spectra of compound **17** with (**4_PI**) and without (**4_Pure**) the addition of photoinitiator in EtOH solution. The dashed green line shows the emission of printer LED (405 nm).*

Mechanical properties of the 3D printed samples were tested using DMA. Firstly, stress and strain experiments are carried out to evaluate modifications in the elastic modulus before, during, and after laser irradiation. In Figure 48, the resulting curves before, during and after laser irradiation are depicted, showing an initial linear correlation between applied stress and strain. A slight deformation occurs once the laser is switched on and partially recovered at the end of the process in dark conditions. Analysing the slope of each linear segment, the value of elastic modulus can be extrapolated.
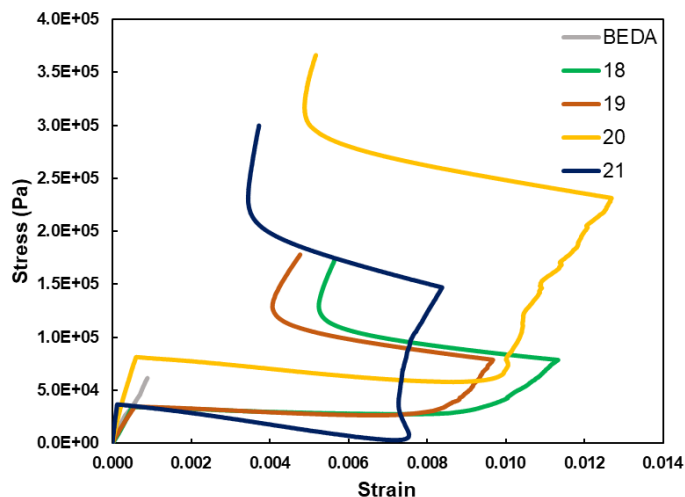
Figure 48 *- Stress/strain curves before, during and after laser irradiation.*

As reported in Table 17, introducing this minimal quantity (0.1 wt.%) of azodye in a 3DP polymeric matrix has an important initial effect in raising the elastic modulus from 69 MPa BEDA sample up to 300 MPa for **21**.

Table 17 *- Elastic modulus before, during and after laser irradiation. The value reported is obtained from the slope of the linear segment.*

	Elastic modulus (MPa)				
	BEDA	**18**	**19**	**20**	**21**
Laser OFF	64.74	69.24	263.00	135.75	304.63
Laser ON	-	27.41	47.17	39.59	61.98
Modulus reduction (%)	-	60.4	82.0	70.8	79.7

Switching off the laser, a modulus reduction from 60% up to 80% can be noticed for each sample, and this effect is connected only to the presence of the azodyes. No changes in elastic modulus can be seen on the BEDA sample. The value remains unaltered during laser irradiation, and a little deformation occurs due to the stress applied. The whole process is almost entirely reversible, and it can be repeated many times, reaching the exact value of elastic modulus.

Using the same configuration of DMA, it is also possible to evaluate the elastic modulus by applying oscillating stress. Measurements were carried out in quasi-static conditions (load ramp 0.1 N min^{-1}) and at room temperature. A preliminary observation can be

noticed in Figure 49, where the initial value of elastic modulus increased, adding 0.1 wt.% of each azodye compared to the BEDA sample. The value raises from 228 MPa up to 1100 MPa (Table 18): the best results were obtained by exploiting **21** as an additive during 3D printing (the results for each sample are reported in Figure 136 in Appendix IV).
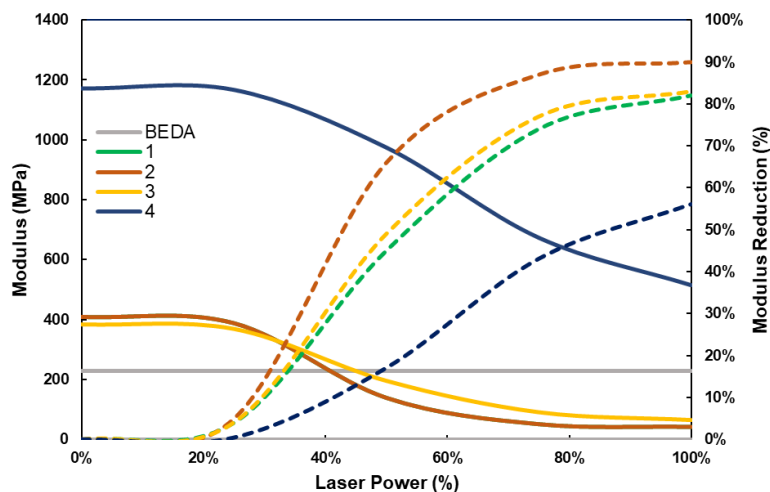
Figure 49 - *Modulus reduction (in MPa and %) under increasing laser power irradiation.*

Then, introducing laser irradiation, up to 80% of modulus reduction can be achieved for all samples under more than 75% of laser power. This process was totally reversible and repeatable, as depicted in Table 18. Compound **21** is the only sample that can reduce its modulus only by 56%, but it is the only one that shows a very high initial modulus.

Table 18 - *Modulus reduction (in MPa and %) for each sample under laser irradiation.*

	% Laser power	Modulus	% Reduction
BEDA	0%	228.18	-
	25%	-	-
	50%	-	-
	75%	-	-
	100%	-	-
H	0%	297.92	0
	25%	286.74	4
	50%	164.72	45
	75%	77.42	74
	100%	53.17	82
Cl	0%	410.33	0
	25%	389.56	5

	50%	140.59	66
	75%	52.63	87
	100%	43.43	90
	0%	384.66	0
	25%	369.55	4
OCH₃	50%	195.50	49
	75%	90.27	77
	100%	63.93	83
	0%	1172.40	0
	25%	1168.03	0.4
NO₂	50%	975.24	17
	75%	673.59	43
	100%	514.86	56

As demonstrated in Figure 49, the most evident effects can be obtained using a laser power between 50% and 75%, while reduced modifications occur at 25% and 100%. These results find an explanation evaluating the radiance of the laser irradiation versus its power, reported in Figure 50. In this graph, 25% of the radiance corresponds to 212 W/m^2, while at 50%, the radiance value went to 2.149 W/m^2 reaching the maximum of 3.284 W/m^2 at 100% of its power.
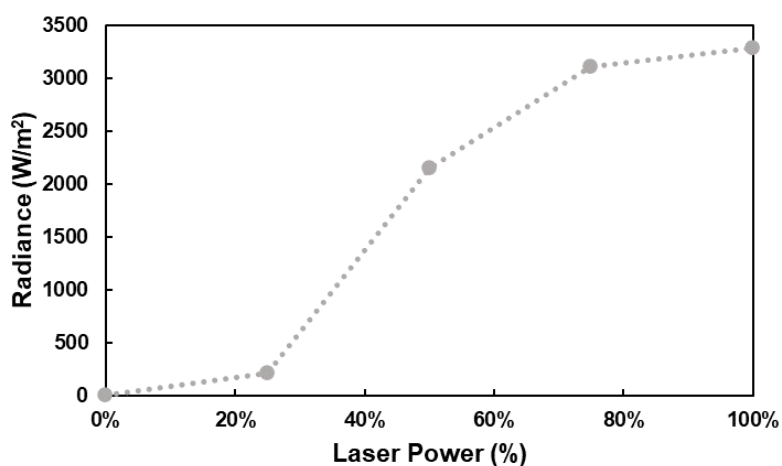
Figure 50 - Radiance in W/m² increasing the laser power.

We chose compound 21 as the most promising one from all reported data. First, it shows the most shifted absorbance spectrum to the laser emitting wavelength and one of the highest molar absorption coefficients among synthetized azodyes. Secondly, it can raise the T_g and the elastic modulus of the polymeric sample to very high values.

Third, evaluating the reduction in the elastic modulus under laser irradiation, we noticed the highest difference in absolute value, passing from about 1.200 MPa to 500 MPa. In comparison, other samples reduced the value from 300-400 MPa to more or less 20-50 MPa. For all these reasons, we chose compound **21** as the most promising one, and all other characterizations are focused only on 3D printed samples containing this dye.

To evaluate the real effect of laser irradiation on the properties of the final polymer, a thermal camera was exploited to obtain infrared images, evaluating the possibility of heating the sample under the light. A comparison between the blank sample and the azo based one is reported in Figure 51, in which the rise in temperature under laser irradiation is demonstrated. When the laser is switched on at 100% of its power, the room temperature is kept for the blank sample (Figure 51a and 51c) for all laser power (Figure 137 in Appendix IV), while up to 100°C is reached for the sample containing **21** (Figure 51b and 51d). Moreover, the temperature rises very fast and only in a localized part of the sample, where the laser's spot is focused.
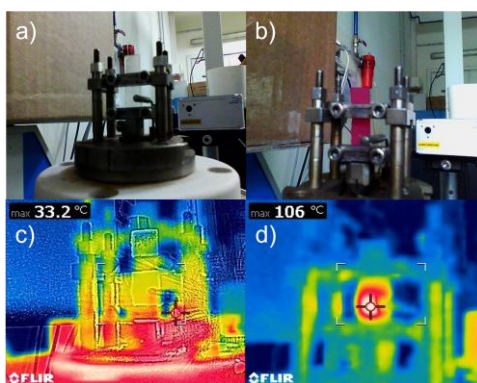
Figure 51 - *Experimental setup with open DMA and laser source for (a) BEDA blank sample and (b) sample containing compound* ***21***. *Thermal images under laser irradiation at 100% of its power for (c) BEDA blank sample and (d) sample containing compound* ***21***.

The same experiments employed liquid formulations composed of BEDA liquid monomer and compounds **17** and **21**. The temperature was evaluated by inserting a thermocouple directly into the liquid solution, using BEDA without dyes as a reference. No changes in temperature were observed for all samples, which remained at room temperature employing 25% and 50% of the laser power. Under 75% and 100%, the temperature increases about a few degrees, as reported in Table 19.

% laser	Sample		
	BEDA	17	21
	Temperature (°C) detected		
0	23.2	23.8	23.8
25	23.2	23.8	23.8
50	23.2	23.8	24.0
75	23.4	24.4	24.8
100	23.4	25.2	26.2

The examination of temperature, which seems to be the only effect to cause a drastic reduction in elastic modulus, was carried out using DMA analysis during which temperature is stepped increased. Each temperature value chosen corresponds to the same value reached under increasing laser irradiation, registered with the thermal camera, reported in Figures 138 and 139 in Appendix IV and Table 20. The same experiments employed compounds **21** (Figure 52a) and **17** (Figure 52b), respectively methacrylate or dispersed in the polymeric matrix. A comparison of the maximum modulus decrease, the time required to reach a stable value, and the initial absolute values of the modulus obtained by introducing copolymerized or dispersed azodyes are carried out, also evaluating the effects of laser irradiation on both samples is reported in Figure 52c.

*Table 20 – Temperature values reached by compounds **21** (methacrylate) and **17** (dispersed) under increasing % of laser power.*

% Laser Power	Temperature for methacrylated (21) (°C)	Temperature for Dispersed (17) (°C)
0	25.3	26.9
25	27.0	27.5
50	55.9	32.6
75	84.9	42.1
100	106	54.6

Figure 52a and Table 21 for compound **21** show that the modulus slowly decreases under heating, employing more than 10 minutes to reach new stable values. They seem

to follow a linear regression in which the modulus linear decreases under temperature increase (Figure 140 in Appendix IV).

***Table 21** - Temperature and its relative modulus (in MPa and % of reduction) of 3D printed samples with methacrylate (**21**) and dispersed (**17**) azodyes.*

Compound 21			Compound 17		
Temperature (°C)	Modulus (MPa)	Modulus reduction (%)	Temperature (°C)	Modulus (MPa)	Modulus reduction (%)
RT	1359.38	-	RT	427.43	-
26.44	1348.65	0	28.0	332.57	22
55.42	226.72	83	32.0	250.25	41
89.63	7.59	99	45.1	75.37	82
107.3	2.66	100	53.1	41.21	90

The final value is three orders of magnitude less than the same reached under 100% of laser irradiation with a reduction of about 100% at 107.3°C. A possible explanation for this phenomenon is probably correlated to the different heating processes. Under laser irradiation, the heating is focalised in a tiny area, and the modulus reduction involves only the irradiated parts while the rest of the object maintains an unaltered modulus. Instead, heating the whole sample causes a homogeneous modulus reduction that involves the whole device, which can reach the same reduced value of elastic modulus in all its parts. Using laser irradiation, some advantages can be pointed out: the heating process is faster, gives more stable results, and is entirely reversible without compromising the material. Moreover, it is not required to heat the whole volume, avoiding thermal degradation.
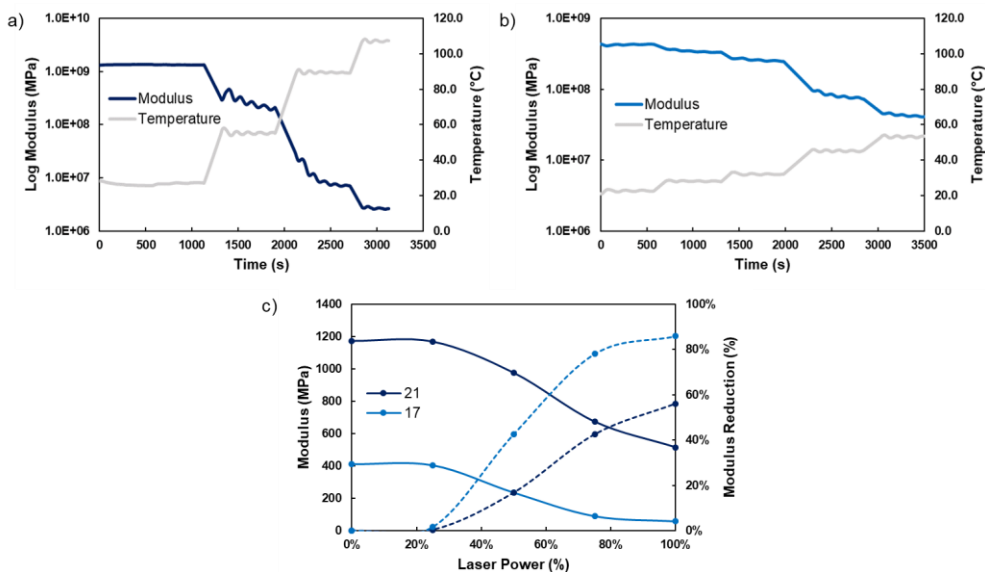
Figure 52 – *Effects of changes in temperature on a) methacrylated (21) or b) dispersed (17) azodyes in a 3D printed polymeric sample, evaluating employing DMA. c) Comparison between the modulus of the two samples and the resulting effects under laser irradiation.*

To evaluate the effect of the azodye as a side-chain functional group or as a dispersed moiety, the same experiments were carried out using the dispersed azodye without the methacrylic functional group. Analysing the increasing temperature under laser irradiation through the thermal camera, an increase only of 54°C is noticed (Figure 139 in Appendix IV). We used the same temperature values reported to analyse the modulus reduction for the **17**. As depicted in Figure 52b, the modulus reduction under increasing temperature is shown. The initial value of around 400 MPa is reduced at 54°C by about 90% (Table 21 for compound **17**). These differences can be ascribed to the initial value of the elastic modulus achieved for each sample. Compound **21** makes the matrix high-crosslinked, and consequently, its elastic modulus shows high initial values. The temperature reached under laser irradiation is not high enough to cause the same modulus reduction obtained for the sample containing compound **17**. The initial value of elastic modulus is very low below the blank sample.

In Figure 52c, a comparison between the two tested samples is reported. In particular, the initial value of **17** is about 400 MPa. In contrast, **21** is about 1100 MPa, and the

reduction under laser irradiation is up to 80% for the first one, higher than the covalently connected azodye.

The heating of the polymeric sample can explain the modulus reduction under laser irradiation. As reported, the huge increment of temperature can be sufficient to reduce the elastic modulus for all samples. These data show no effect of the *cis/trans* isomerization of the azodyes inserted in the polymeric 3D printed matrix. There is no proof of the possibility of these dyes undergoing isomerization in a polymeric matrix in literature. Here we demonstrated that the energy given by laser could be released very fast as thermal heating of the sample, reaching relative high temperatures.

In conclusion, new azodyes with electron donor or attractor functional groups were synthesized very easily. They can be added to polymeric 3D printed devices in very low quantities, obtaining considerable changes in the mechanical properties of the final device. An increment in the glass transition temperature and a significant increase in elastic modulus for each sample is observed, demonstrating as **21** shows the best changes in all these properties.

All these dyes increase the final 3D printing resolution. They can't be released during use, thanks to the methacrylic functional groups being able to react by linking dyes with polymeric chains in a covalently way. Moreover, they have a minimum effect on the 3D printing time required to complete the process, and their low cost doesn't affect the final convenient price of each 3D printed device. All samples show a fast and reversible response under laser irradiation, heating to a very high temperature in a few minutes.

No evidence of the *cis/trans* isomerization effects will be demonstrated due to the impossibility of separating the absorption spectra of the two moieties. A possible explanation for all results resides in the impossibility for these dyes to pass from *trans* to *cis* isomer. The energy given by laser can be released through thermal heating and light emission. In fact, the liquid formulations of azodyes in the BEDA monomer do not show any thermal heating under irradiation. A possible explanation is related to the fast cis/trans isomerization that can dissipate the energy absorbed from the laser. To demonstrate these hypotheses, thermal images were recorded. At the same time, these

types of dyes are usually used as a light absorber, able to reduce the overcuring both on *XY*-plane and in *Z*-direction.

The double effect as moieties can enhance the final resolution and tune the elastic modulus, and the temperature of the polymeric matrix is demonstrated. Then, heating the sample only in very localized areas can be intriguing for many applications, avoiding possible thermal degradation.

These cheap and easy to produce materials can be useful for many applications, such as sensors or actuators that can be activated from a distance by light irradiation, even in sealed systems. Avoiding high temperatures to heat all devices, no thermal degradations are caused. Moreover, light is the most simple, safe and tuneable stimulus that is easy to manage with relatively low costs.

6.2.3.2 Light-induced shape-memory 3D printed polymers

Based on the results reported in the previous paragraph, we established our idea of using azodye-based polymers, able to be heated under light irradiation in very localized areas, to activate some peculiar and innovative properties. Among others, shape-memory materials (SMMs) represent a variety of different materials able to memorize a macroscopic shape, be deformed and fixed in another temporary one under external stress and finally recover the original structure under thermal, electrical or light stimulations.[195] SMMs have attracted the increasing attention of researchers due to their potential applications as sensors, actuators and smart devices.[196] The beginning of SMMs is related to discovering this property in metals, particularly in an AuCd alloy in 1951.[197] Other necessary research in shape-memory alloys (SMAs) are reported in the following years.[198–201] Nevertheless, low recoverable strains, high stiffness, costs and challenging processing conditions are drawbacks that limit the use of metals as SMMs.

On the other hand, polymers are very attractive materials for their peculiar properties, such as low costs, high flexibility, and versatility, making them very interesting materials for producing shape-memory polymeric devices. Shape-memory polymers (SMPs) can

be easily deformed under an external stimulus, usually by heating above their glass transition temperature (T_g) for amorphous polymers or their melting temperature (T_m) for semicrystalline ones.[195,196] Above this temperature, polymers can be deformed by applying stresses. Then, the temperature is decreased to fix the new shape, often called temporary shape, that is stable until an external stimulus is applied to induce original shape recovery.[202] Usually, thermal-induced SMPs are the most exploited ones. Nevertheless, the use of temperature presents some drawbacks, such as the necessity to heat the whole volume and some thermal degradations that can take place, limiting the devices' applicability.[203–206]

The temperature can be raised by exploiting the Joule's effect by applying magnetic or electric fields that can activate the process.[207–210] Along with temperature, other stimuli can induce the shape effect, such as water, moisture, solvent, pH or oxidation/reduction reactions.[211–214]

Among others, light is very attractive. Using this stimulus, a photothermal or photoresponsive behaviour can be activated.[215] Generally, the first can be generated by adding inorganic fillers, representing the most common method to heat the sample using an adequate wavelength (IR, visible or UV). Metals, such as gold,[216] silver[217] and titanium[218] nanoparticles can be actively used in a very efficient manner, as well as carbon nanotubes,[219] carbon fibres,[220] carbon black,[221] graphene[222] and even rare earth complexes.[223] The photoresponsive effect can be achieved through species able to react under light irradiation, such as cinnamic acid (that can undergo [2 + 2] cycloaddition under light irradiation)[224] or using azobenzene dyes in the form of liquid crystal (LC) (able to transform light in mechanical energy through cis/trans isomerization[225,226] or other active moieties).[35,187] The use of azodyes in polymers was deeply investigated in the last years to act as moieties able to induce photo-softening or photo-fluidization due to their intriguing peculiar properties.[227–230]

In this work, some acrylate push-pull type azodyes with different functional groups are synthesized and introduced in a liquid 3D printable formulation composed of different acrylate monomers. The concentration and 3D printing parameters are optimized to

achieve optimal final resolutions, fidelity to the CAD project and an efficient shape recovery process, activated by a 459 nm high power density LED. Based on the previously reported experiments, relatively high temperatures can be reached under irradiation without thermal or photo degradations. To the best of our knowledge, this is the first time an organic dye has been applied to induce a light-activated shape memory process. Light is usually used to heat a DLP 3DP device using carbon nanotubes or metal nanoparticles.[14,103,231] Different functional groups can change the time required to complete the process. The fast response of the 3DP devices will be demonstrated with the possibility of printing a complex-shaped object with very good resolutions and the ability to act in response to visible light.

With this innovative application of azodyes, we would also demonstrate that these types of dyes can be used for their well-known *cis/trans* isomerization and as components that can absorb light to transform it in mechanical work. The open debate about the possibility of *cis/trans* isomerization in a polymeric matrix is still open. Here, the heating under light irradiation seems to confirm the slow speed or the impossible isomerization of this type of push-pull azodyes when inserted as covalently connected functionality to the polymeric chains.[192,230,232,233]

This project was developed in collaboration with prof. Eva Blasco from Heidelberg University was based on her preliminary study during the period abroad.[234] The reported formulation was deeply studied and reported in the literature, and its composition is described in Table 22.

Table 22 *– Composition of the formulation used in this project.*

Component	Wt.%
BAPO	1.92
TCDMDA	18.50
PEGDA 575	6.98
IBA	70.70
HA	1.90

The formulation was left for 24h under vigorous stirring in a round bottom flask closed with a stopper and covered by aluminium foils to prevent light irradiation and the start of photopolymerization.

Shape-memory properties were tested on mechanically deformed 3DP polymeric devices. To confer the temporary shape, all objects are immersed for 5 minutes in 80°C hot water, immediately deformed by applying mechanical stress and fixed under cold water. The shape recovery was evaluated by irradiating the polymeric device with a 459 nm LED with a 2.0 cm distance between the light source and the sample.

The synthesised azodyes are characterized by electron attractors and donor groups connected through a π-conjugated organic linker.[70] As reported in the literature, the position near the azo bridge is the most important one, functionalizing it, some properties can be conferred.[194] Exploiting an acrylic functional group, these dyes are covalently connected to the polymeric chains as side-chain groups, avoiding their release during use. Based on our previous work, this study investigates the possibility of inducing shape memory properties in a 3D printed device using visible light irradiation, which can be absorbed by the azodyes and raise the temperature to 80°C to activate the recovery of the initial shape. Moreover, electron-withdrawing and donor functional groups can lead to differences in optical absorbance and the relative time needed to obtain the correct temperature and complete shape recovery.

The optimal concentration of azodyes that can be introduced in the liquid formulation was experimentally determined by evaluating the time required to complete the photopolymerization process for each sample under a UV LED with a wavelength ranging from 380 nm to 390 nm. We tested this process employing compound **23,** increasing the concentration from 0.1 to 2.0 wt.%, and the results are reported in Table 23.

Table 23 - *Evaluation of the optimal concentration of azodye **23** in the liquid formulation. The LED irradiation time is the time required to complete the photopolymerization process under 380-390 nm UV light.*

Compound 23 (wt.%)	LED irradiation time (s)
0.0	1.5
0.1	3.5
0.2	4.5
0.3	6.0
0.4	8.5
0.5	9.5
1.0	>15
2.0	>15

As can be noticed, increasing the concentration of the azodye, longer exposure times are required to obtain completely solidified samples due to the reduction in light penetration in the bulk solution. Concentrations up to 0.4% don't allow to complete the photocuring process, and some parts of the final samples remain liquid.

Some shape-memory tests were carried out on these preliminary photopolymerized samples to evaluate the real effect of such a low concentration of azodyes. All the resulting completely photocured solid samples (from 0.1 to 0.4 wt.% of azodyes) were deformed in hot water, and the temporary shape conferred was fixed by cooling down to 15°C employing cold water. Then, they were irradiated with 459 nm LED, registering the time required to return to the original form: 1 minute is needed to recover 100% of the original shape for all samples. Similar results were found for all azodyes synthesized, and the high concentrations do not affect the shape-memory recovery, which always requires the same time to be completed. From all these reported results, we fixed the optimal concentrations to 0.1 wt.%, obtaining a fast photopolymerization process and rapid shape-memory effect.
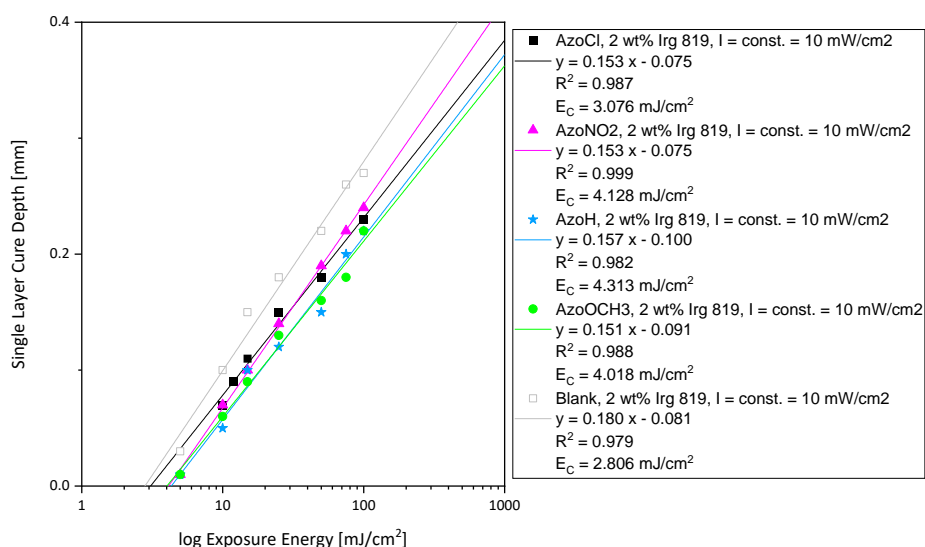
Figure 53 – *Calculation of the curing behaviour for each formulation, obtaining optimal printing parameters.*

Optimal 3D printing parameters were experimentally found by evaluating the curing behaviour (Figure 53), finding the best parameters reported in Table 24.

Table 24 - *Optimized 3D printing parameters (Blank is the formulation without dyes, used as reference).*

Sample	Irradiation Time (s)	LED Intensity (mW/cm²)
Blank	1.1	
22	2.0	
23	1.5	10.0
24	2.0	
25	1.75	

Once the best printing parameters were fixed, some specimens were produced to evaluate the final *XY* resolution, defined as the minimum feature size on the *XY* plane. This represents the most critical parameter that determines the quality of a 3D printed object. It is more difficult to obtain respect than Z-direction resolution, in which the thickness of the final object can easily calculate. For this reason, we printed samples, as reported below in Figure 54 as an example, in which different lines were printed with a prefixed length. Similar devices were also printed to test the 50 μm resolution.
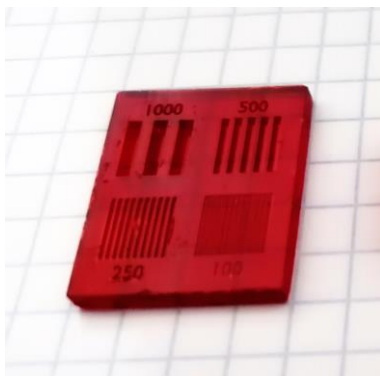
*Figure 54 - Resolution test on a 3D printed sample containing compound 0.1 wt.% of **23**. In the four sections, different resolutions are reported: 1000 µm, 500 µm, 250 µm and 100 µm.*

Measuring their length with an optical microscope, the final *XY* resolution can be obtained compared with the ideal one, as reported in Figure 55 for one of the samples (all resolutions are depicted in Figure 141 in Appendix V).
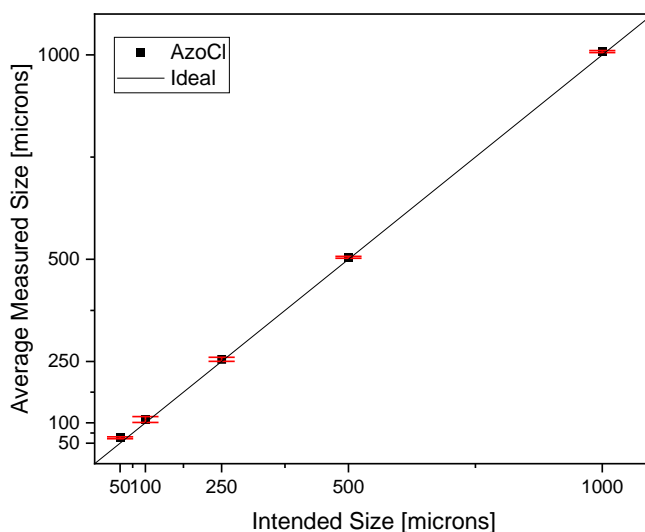
*Figure 55 - Final XY resolution of 3D printed sample in which compound **23** was copolymerized. The good final resolutions are highlighted by the very narrow error bars and the position of all points close to the ideal line.*

Some pictures registered with an optical microscope are reported in Figures 142 to 144 in Appendix V to demonstrate the good results of the obtained *XY* resolutions.

Exploiting compound **23** and their optimized 3D printing parameters previously described, an evaluation of the fidelity between the CAD project and the actual 3D printed object was investigated. As the Pisa Tower reported in Figure 56a, a complex-

104

shaped object was printed and examined through a 3D scanner to achieve this purpose. The obtained image overlapped with the CAD project to evaluate the displacements in each part of the object (Figure 56b). As can be noticed from the colour scale, all printed columns on the side of the tower show very low displacements, in the order of ±0.050 mm, while the yellow and blue regions are pretty similar to the theoretical shape (± 0.100 mm). Red regions represent the less coherent parts that correspond to the base, affected by an overcuring process to guarantee the adhesion on the growing platform.
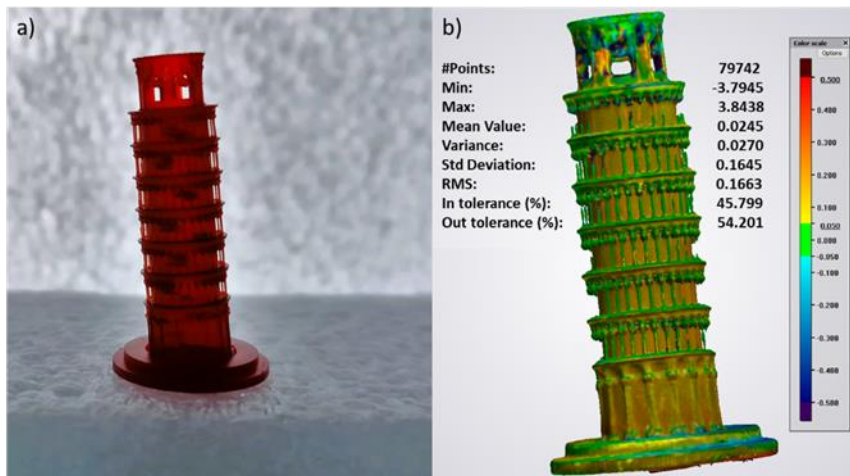
Figure 56 – a) 3D printed Pisa Tower and b) comparison between the real object and the CAD project. The displacements are shown as colour according to the legend reported.

All displacements are reported in Figure 56b, in which it can be noticed that a significant part of the real object remains in a range of ± 0.200 mm from the CAD project. The worst parts are the top, where some details were lost during printing and the tower's base.

These results demonstrate the high precisions and fidelity reachable using azodyes and the optimized printing parameters, through with objects with complex and detailed shapes that can be easily printed. Nevertheless, to use these samples as SMPs, these matrices' mechanical and chemical properties must be investigated. The activation of the shape-memory recovery process requires overcoming the glass transition temperature.[20,235] This value can be obtained for each sample through DMA. For this type of test, some samples as strips of 29.40 mm in length, 7.83 mm in width and 0.90 mm thick were 3D printed and used to evaluate the mechanical properties and the glass

transition temperatures (T_g) of each azodye-based polymer. These experiments were aimed to estimate the temperature at which the shape-memory process can be activated. Two different Tg were found from the results of heating the polymeric samples from 0°C to 110°C two different T_g were found (Figure 145 in Appendix V). The first order T$_g$ is the most important one. It is about 80°C: this temperature represents the threshold that must be overcome to activate the shape-memory process and is due to the IBA component of the formulation (all values are reported in Table 25). While the second-order transition temperature is centred at about 30°C for all samples, it is probably due to the presence of TCDMDA. All other components are present in too low concentrations and are not visible in DMA measurements; as well as, no relevant modifications in the first-order transition temperature occur with the introduction of azodyes.

Table 25 – *First and second-order transition temperature for all 3D printed samples.*

Sample	First-order transition temperature (°C)	Second-order transition temperature (°C)
Blank	81.1	31.9
22	76.4	25.9
23	80.0	30.2
24	77.3	31.1
25	80.6	26.2

At the same time, from TGA thermal analyses, no relevant effects can be noticed with the introduction of azodyes in the second-order glass transition temperatures. In contrast, the thermal stability (Figure 146 in Appendix V) was reduced by about 40 – 50 °C compared to the blank sample. Nevertheless, all samples show high stability under 130°C, demonstrating the possibility of being heated over 80°C without degradation.

DMA analyses were also performed under LED irradiation, introducing the light source directly 2 cm from the opened sample holder. The current of the LED was changed for each cycle from 1.0 A to 1.5 A and 2.0 A, and the LED was switched on and off when a stable value of modulus was reached. The registration in the variation of the storage modulus before and during the LED irradiation was reported in Figure 57, and the

reversibility of the process. As depicted, the blank sample is not affected by the irradiation, and no programmed changes in the mechanical properties can be ascribed to the LED. On the other side, all azo-based samples showed a clear reduction in the G' values when the light source was switched on and complete recovery of the initial values in the dark.

Moreover, by increasing the current of the LED power supply, a faster response can be observed by evaluating the slop of the first derivatives for each modulus reduction. More reduced values of storage modulus (E') were reached. These processes are reversible for all samples and can be repeated without damaging the polymeric sample. After each cycle, an increase in the dark modulus values for all samples can be noticed due to geometric variations in the sample size. Under oscillating DMA stresses, the samples change their lengths, which is a parameter used to calculate the resulting modulus.
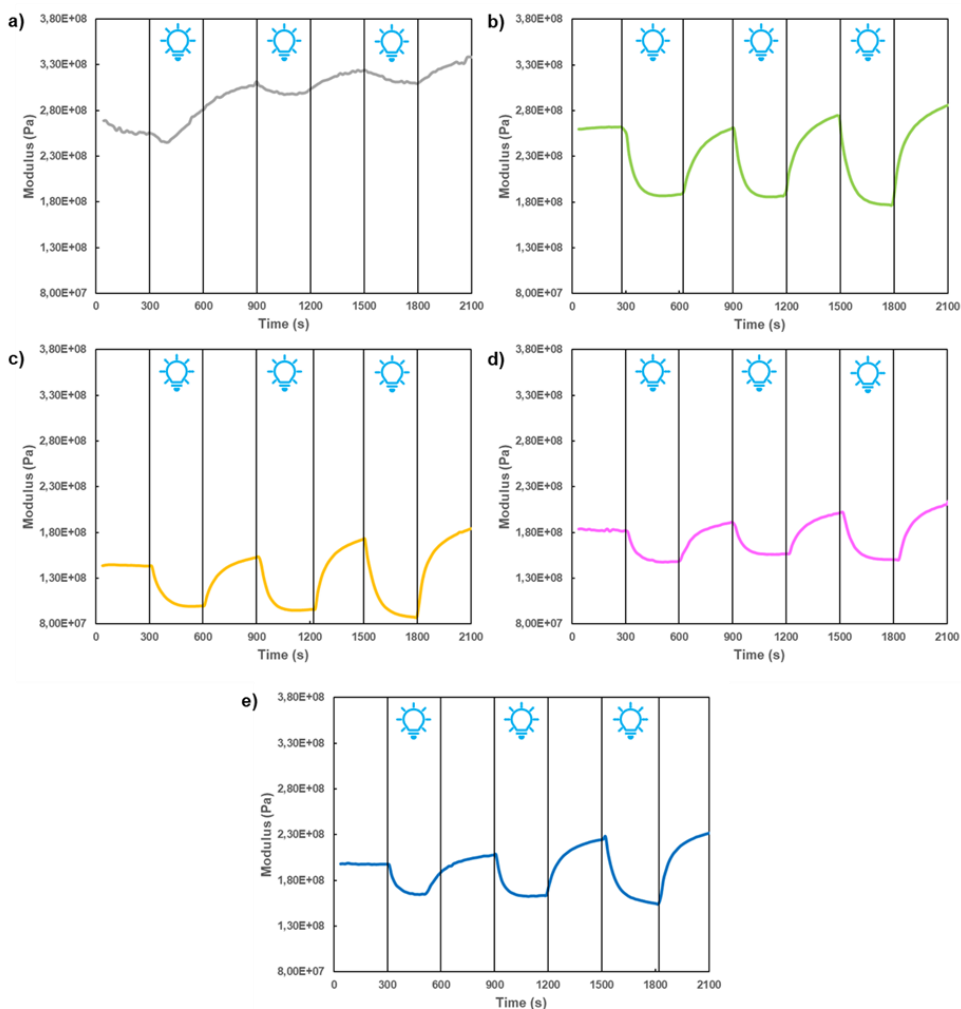
Figure 57 *- DMA analyses under LED irradiation with an increasing current of the LED power supply for 3D printed polymeric samples of a) blank formulation or containing compounds b) **22**, c) **23**, d) **24**, e) **25**.*

Similar specimens used in DMA were also exploited to test the shape memory recovery under 459 nm LED irradiation. In these experiments, the sample was first dipped in hot water at 80°C, and it was left inside for 5 minutes. Then it was deformed, and its temporary shape was fixed using cold water at 15°C. It was exposed to LED irradiation from a 2 cm light source distance to activate the process. A parameter was calculated as the angle formed between the two ends of the strip, as reported in Figure 147 in Appendix V. For samples containing azodyes 22 and 24, the time required to complete the process is about 6 and 7 minutes. In contrast, for **23** and **25,** the process was faster,

108

taking only 4 minutes to achieve the 100% of shape recovery. The complete process for the 3D printed rectangular strips containing azodye **23** is reported in Figure 58a, in which the shape recovery is visible under increasing time irradiation.
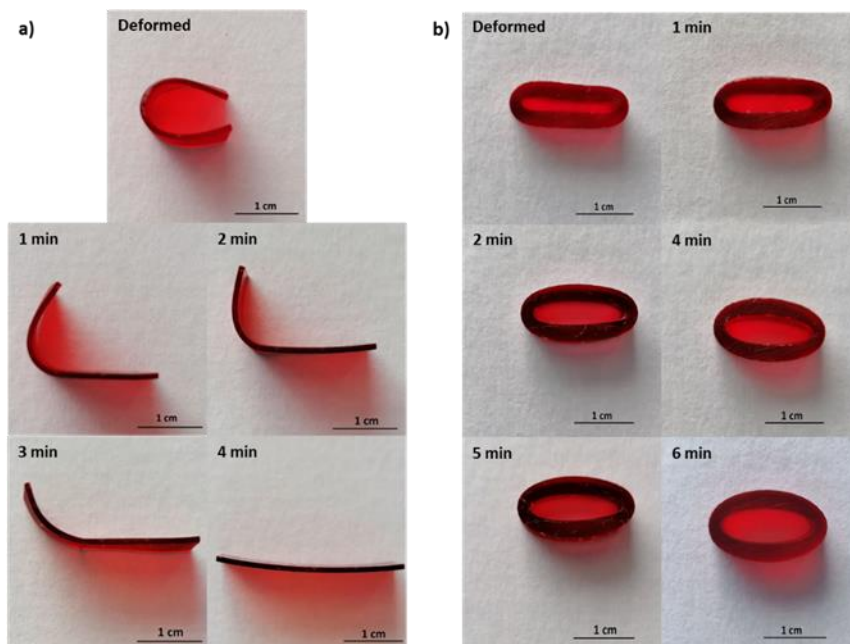
Figure 58 - *a) Shape-memory recovery (%) of each azo-based 3D printed rectangular strip over light irradiation exposure time. The sample was deformed in hot water (80°C), bent, fixed dipped in cold water (15°C). Under light irradiation, the sample containing **23** starts to recover the initial shape after 1 min, 2 min, and 3 min reaching the initial shape at 4 min. b) Shape-memory recovery (%) of each azo-based 3D printed ring over light irradiation exposure time. The sample was deformed in hot water (80°C), bent, fixed dipped in cold water (15°C). Under light irradiation, the sample containing **23** starts to recover the initial shape after 1 min, 2 min, 4 min, and 5 min reaching the initial shape at 6 min.*

More complex objects were printed to test their ability to recover the initial shape under LED irradiation. This test aims to evaluate the shape-memory recovery of massive objects without causing damage and to measure the time required to complete the process. For these reasons, 3D printed frames were obtained with 9.80 mm of width, 17.9 mm of length, and 5.03 mm of thickness, exploiting the previously reported optimised parameters. As shown in Figure 58b, all samples required almost 6 minutes to achieve up to 90% of shape recovery, except for compound 22, which requires more than 10 minutes.

All samples show good shape-memory properties, without damage after more than 15 cycles of deformation and recovery under LED irradiation.

At the same time, objects like Pisa Tower, which shows a massive structure and a considerable height, can be tested by irradiating it after deformation in hot water. As depicted in Figure 59, a very fast shape recovery response is observed without introducing cracks or damages during this process.

Figure 59 – Deformation of Pisa Tower under 5 minutes of LED irradiation.

These results demonstrate the possibility of using these materials as light-activated shape-memory devices, with a fast and reversible response under UV light irradiation. To better understand the causes behind this behaviour, an evaluation of the temperature reached during irradiation was carried out. Some opened rings were printed using two different formulations: the red rings are made of azo-based formulation containing compound **23**, while the white-transparent ones with the blank formulation. With these rings, a chain was built in an open (Figure 60a) or, by deforming each ring, in a close form (Figure 60b). Thermal images and videos were recorded to evaluate the heating under LED irradiation, positioning the cursor on the hottest spot present in the image. Focusing the LED irradiation on a white ring, a rising temperature was noticed only on the red rings, reaching 59°C in 2 minutes (Figure 60c), opening themselves very fast. On the contrary, white rings remain closed, meaning that no heating occurs under LED irradiation (Figure 148, Appendix V).
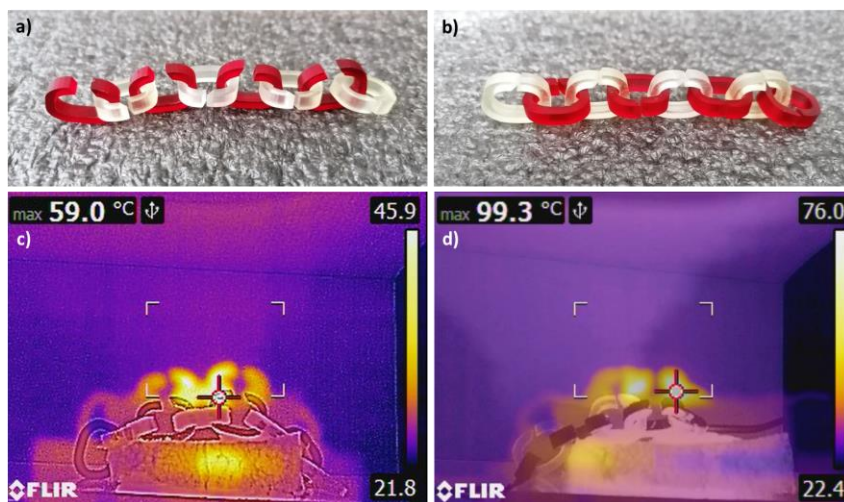
Figure 60 - a) 3D printed chain composed of red rings, which contain compound **23**, and transparent rings, made of the blank formulation. All rings were closed by dipping them in hot water (80°C), and their temporary shape was fixed under cold water. b) The 459 nm LED irradiation was focused on a blank ring.

In addition, by focusing the LED irradiation on one of the red rings, a higher temperature can be easily reached, arriving up to 90°C in just 1 minute, until a maximum of 99°C (Figure 60d): in this case, the recovery process requires only 1.30 min to be completed.

With this innovative application of azodyes, we would also demonstrate that these dyes can be used for their well-known cis/trans isomerization and as components that can absorb light to transform it in mechanical work. The open debate about the possibility of *cis/trans* isomerization in a polymeric matrix is still open. Here, the heating under light irradiation seems to confirm the slow speed or the impossible isomerization of this type of push-pull azodyes.

6.2.3.3 3D printed azo-based membranes for gas permeability

Gas membrane separation plays a key role in many industrial processes, and its main limitations reside in the low selectivity and stability, particularly at high temperatures.[236] The possibility of employing membranes with reversible and tunable selectivity controllable by light irradiation represents a significant innovation in this field. Hassan et al.[237] reported the synthesis of side-chain liquid crystalline polymers to produce an oxygen-permeable membrane. Under heating, the permeability increases,

allowing the gas transmission rate to fine-tune. Kameda et al.[238] used a push-pull azobenzene-based polymer to create a membrane that can reversibly change its permeability to helium under light irradiation. Głowacki et al.[239] used dispersed azobenzene molecules in a polymer to obtain a photo-switchable membrane for nitrogen, and Shi et al.[240] demonstrated the different permeability under external irradiation of a polyethersulfone membrane with a host-guest complex between azobenzene and *β*-cyclodextrin. Other stimuli-responsive membranes are made of metalorganic frameworks (MOFs) with azobenzene dyes as pendant groups.[241,242]

Recently, the use of azobenzene moieties in a polymeric matrix with the DLP technique, aiming at producing a membrane that can tune its CO_2 permeability in response to visible laser irradiation, was reported.[110] The authors described the use of poly(ethylene glycol) diacrylate (PEGDA) with Methyl Red (MR) and Dispersed Red I (DR1), two azodyes. The first was used as dispersion, while the second was functionalized with a methacrylic group to be polymerized as a side-chain group. During a green laser (532 nm) irradiation, the permeability to CO_2 increases by 70% due to the azo photoisomerization and the consequent different free volume formation. This change in the permeability properties can be easily recovered by switching the laser off reversibly. Based on these initial results in this work, novel push-pull methacrylate azodyes are synthetized with the series of halogens (F, Cl, Br and I) as functional groups. These dyes are then introduced in a liquid formulation containing an acrylic monomer to obtain 3DP polymeric membranes exploiting the DLP configuration. The gas permeability is also evaluated by testing CO2, O2 and H2O at ambient temperature and laser irradiation. The effect of halogens on the gas transmission rates is also evaluated. The preliminary results obtained seem to show a trend in reducing O_2 and CO_2 gas permeability and the increasing steric hindrance of the *ortho* functional group. Moreover, by introducing a 532 nm green laser irradiation, CO_2 permeability can be dramatically reduced, while no effects are visible with other gases.

Firstly, an evaluation of the reactivity of each formulation was obtained from photorheology tests, switching on the UV irradiation after 60 s. For all samples, the same

very fast reactivity is noticed (Figure 61), employing a few seconds to be carried out, and the same observations remain valid also for the blank formulation. This means that no relevant delay in the start of the photopolymerization process and no intense absorbance competition between the photoinitiator and the dye occur during the polymerization process. The only sample that shows a slight delay in starting the process is compound **31**, as depicted in Figure 149 in Appendix VI, in which a zoom of the photorheology results is reported. However, this delay doesn't represent a problem for the 3D printing process.
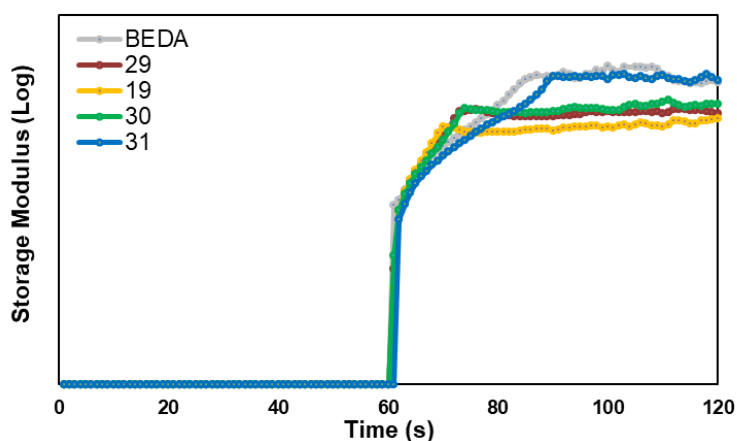
Figure 61 *– Photorheology tests for all formulations containing halogenated azodyes. The UV light is switched on at 60 seconds.*

Permeability tests were carried out to evaluate the possibility of different gases passing through the 3D printed polymeric membranes. These membranes were obtained using optimized 3D printing parameters (Table 26). As previously reported, the concentration of the azodyes used in all formulations is 0.1 wt.%, which is the optimal concentration to obtain a fast 3D printing process without reducing the mechanical properties.

Table 26 *- Optimized 3D printing parameters to obtain polymeric membranes.*

	BEDA	18	29	19	30	31
Slice thickness (µm)	25.0	25.0	25.0	25.0	25.0	25.0
Burn-In time (s)	1.5	3.5	3.5	3.5	3.5	3.5
Normal exposure time (s)	1.5	2.5	2.5	2.5	2.5	2.5

All membranes were cleaned from all residual gases, which can remain trapped in the polymeric matrix during printing, applying a constant nitrogen flux until the detector revealed no targeted gas signals. Initial transmission rate values for each gas employed (CO_2, O_2 and H_2O) were primarily obtained: from them, all parameters can be calculated considering the thickness of each sample.

In Figure 62, all results are depicted. It is of primary importance to point out that for CO_2 and O_2 gases, some samples (F, Br and I) show an increased Transmission Rate (Tr) concerning the BEDA blank sample. In contrast, others remain around zero or negative (the cleaning cycle doesn't remove all traces of residual gases). Instead, for H_2O Tr BEDA sample shows a reduced value, while all other azo-based samples have values around zero. Water tests are not considered in the following studies, and their permeability was not further investigated.
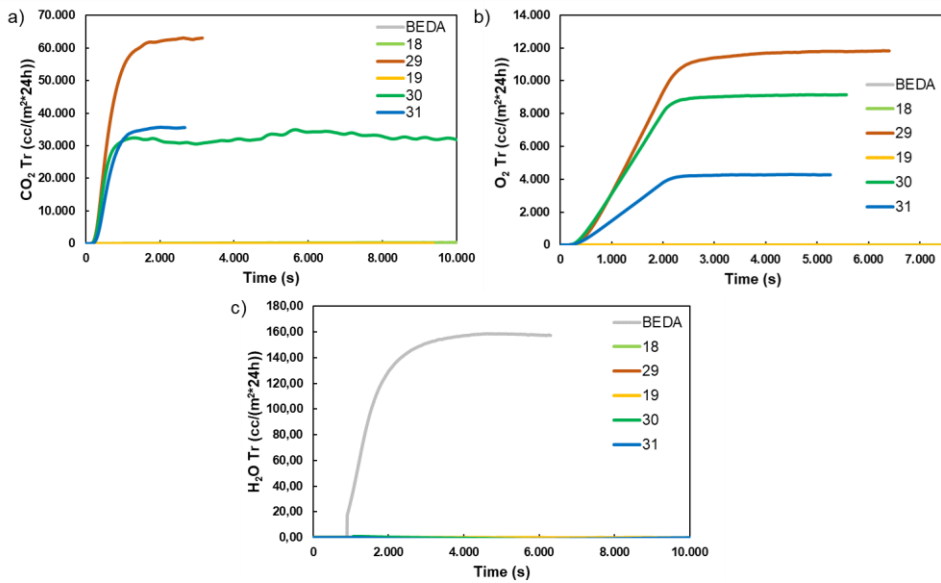
Figure 62 – a) CO₂, b) O₂, and c) H₂O transmission rate (Tr) for all samples.

We can consider the thickness of each sample, in order to evaluate permeability, diffusivity and solubility parameters, according to the following reported equations:

$$P = \frac{Tr(plateau) * l}{p} * 1.157e^{-9} \left[\frac{cm^3 * cm}{s * cm^2 * bar} \right] \quad (1)$$

$$D = \frac{l^2}{6 * t_{lag}} \left[\frac{cm^2}{s} \right] \quad (2)$$

$$S = \frac{P}{D} \left[\frac{cm^3}{cm^3 * bar} \right] \qquad\qquad (3)$$

Where $Tr_{(plateau)}$ is the transmission rate at the stable plateau (Figure 150 in Appendix VI), p is the compensation pressure (equal to 1 bar), l is the thickness of the sample, t_{lag} is calculated as reported in Figure 151 in Appendix VI. The thicknesses of all 3D printed membranes are reported in Table 27.

Table 27 – *Thickness of 3D printed polymeric membranes tested.*

	Thickness (cm)
Blank	0,08
H	0,06
F	0,30
Cl	0,05
Br	0,28
I	0,23

As demonstrated in Figure 63, the sample containing compound **29** shows the highest values of permeability and diffusivity for both gases. Both values decrease with the increase of the steric hindrance of the ortho functional group. Nevertheless, **18** and **19** seem not to follow this trend. Blank, **18,** and **19** samples might act as barriers against carbon dioxide and oxygen. However, all samples display very good CO_2 solubility, while the worst results were obtained for O_2 solubility, that is, in some cases, less than zero.
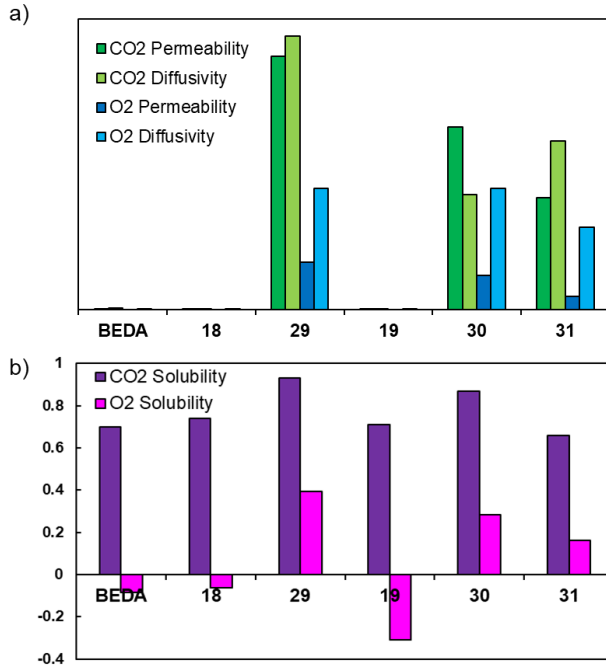
Figure 63 - a) Permeability, Diffusivity and b) Solubility values for all 3D printed samples.

The same results are reported in Table 28, in which only the Permeability values are considered, and the Barrer, a new unit measure, can be calculated from them according to the following equation:

$$Barrer = \frac{\left(\frac{P}{75.01}\right)}{10^{-10}} \qquad (4)$$

Table 28 – Barrer CO_2 and O_2 permeability values of 3D printed membranes.

	CO_2 Barrer	O_2 Barrer
BEDA	10,25	-0,94
H	5,83	-0,37
F	2906,28	547,40
Cl	8,97	-2,81
Br	2093,05	394,87
I	1283,83	154,43

Based on these results, the selectivity for each membrane to a combination of these gases can be calculated, finding that **29** and **30** show five times higher selectivity of CO_2 with respect to O_2, while **31** is eight times more selective (Table 29).

Table 29 – Selectivity values for each 3D printed membrane to a different couple of gases.

	CO_2/O_2 selectivity	CO_2/H_2O selectivity	O_2/H_2O selectivity
BEDA	-	5,26	-
18	-	100,08	-
29	5,31	72296,67	13617,15
19	-	131,21	-
30	5,30	18604,07	3509,83
31	8,31	5822,17	700,35

At the same time, all membranes show very high selectivity to CO_2 over H_2O and to O_2 over H_2O. The 532 nm green laser irradiation was introduced into the permeameter through a special transparent sample holder that allows focalising the spot directly on the polymeric membrane. In this way, we can increase the CO_2 permeability when the laser is switched on, in a reversible process, as demonstrated in Figure 64 for the sample containing compound **31**. Instead, no increasing effects are noticed on the other gases, which can be interesting in using these membranes to separate some gases selectively.
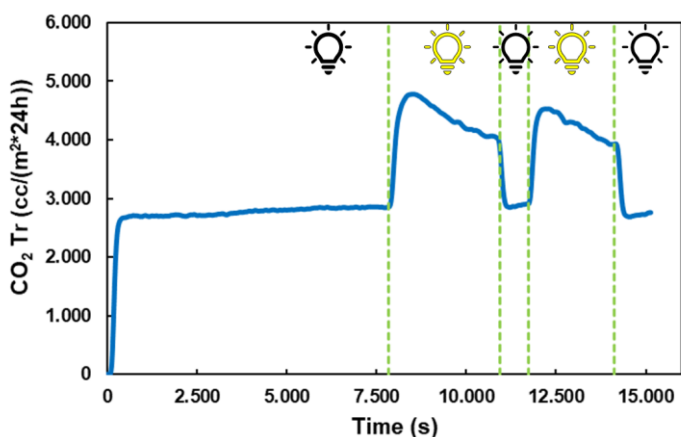
Figure 64 – Effect of 532 nm green laser irradiation on the CO_2 transmission rate and the reversible process when switched off.

The green laser irradiation was chosen to evaluate the absorption spectra of all azodyes in the solution. The 532 nm wavelength of the laser is located near all absorption maxima (Figure 152 in Appendix VI).

These results show a promising way to produce polymeric membranes that change their gas permeability by adding a very low quantity of a functional azodye, with possible uses in industrial applications to separate gases and vapours. Moreover, with laser irradiation, the CO_2 permeability can be reversible tuned, allowing the application of these devices as sensors. Next, investigations to explain these phenomena will be needed to investigate if the polymeric membranes are heated under laser irradiation and if temperature plays a crucial role in CO_2 permeability. Here, only some preliminary results are described, but a lot of work still needs to be done, particularly testing these membranes in real applications. The use of 3D printing allows adapting the final membrane to all devices, reaching at the same time very complex final geometries.

6.2.4 pH-responsive polymers based on NDI dyes

In the previous paragraphs, the only stimulus used is light that can be UV or visible, but it can also be dangerous for many molecules and challenging to manage. We focused here on pH stimulus, which can be exploited in many chemical reactions and sensor production. This research could represent an interesting application of this study in this field.

This project was carried out in collaboration with Politecnico di Torino. Ms.c. Beatrice Tosetto conducted preliminary tests and the 3D printing process to obtain good final resolved polymeric devices. They were tested in mechanical, chemical and permeability properties and the application as sensors in some reactions.

This work aims to produce 3D printed polymeric devices that can be used as optical sensors for acids or bases in aqueous or organic solutions and the vapour phase, giving a fast and reversible response with 3D complex geometries. In particular, in this work, the functional dye employed is compound **34,** which shows two hydroxyl functional groups that can give, in the presence of bases, two sequential processes of

deprotonation, changing at the same time colour and emission spectrum. This compound is exploited both as a functional dye that responds to an external stimulus, such as the pH change and as a photopolymerization controller through which polymerization processes can be avoided without introducing other moieties. Good final resolutions and fidelity to the CAD projects can be reached. Moreover, the reversible process can be activated by introducing an acid, which quantity can be controlled to obtain one or two deprotonated species or leave the device under air. This second process shows a very low recovery speed.

In the first part, the suitable polymeric matrix was chosen, in which the chromophore can be easily dispersed. Then, some tests are described, in which the matrix can be in contact with aqueous or organic solutions of bases and some vapours to test the response. At least some 3D printed complex devices are used as demonstrators in real applications.

Naphthalene diimides (NDIs) are a class of chromophores that show very interesting optical and chemical properties. The general formula is reported in Figure 65, in which the possible functionalizable positions are represented by numbers for the core-substituted NDIs, or by R that represent functional lateral groups.
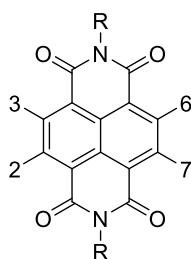
Figure 65 - *General scaffold of NDI compounds. The numbered positions described the possible core substitutions, while the R groups the possible functionalization on the imine-group.*

The R groups can be alkyl or aryl chains, and usually, these components don't show important modifications to the optical properties of the NDIs. For this reason, these positions can be appropriately functionalized according to the final desired uses of the molecule.[243] Conversely, core-substituted naphthalenediimides (cNDIs) represent a class of NDIs that show functional substitutions in positions 2,3,6 and 7. The addition of electron donor groups on the molecule's core transforms these compounds into

119

panchromatic fluorophores, and donor groups can confer a very strong π-acidity. Primary colours can be achieved by substituting oxygen with nitrogen.[244] The strong thermal and photostability joined with the strong π-acidity make these compounds suitable for many applications, such as photovoltaics.[243,244]

In this work, all formulations are obtained by adding the photoinitiator (HMBT) directly into the liquid monomer. Then, compound **34** was added, and the mixture was left under sonication until homogeneous solutions were obtained. All components and the relative time of sonication are reported in Table 30. For the BEMA-based formulation, 1 mL of acetone was added to enhance the solubilization and reduce the viscosity.

Table 30 - *Composition of each formulation and the relative time of sonication needed to reach a homogeneous solution.*

Monomer	Quantity (g)	Photoinitiator (mg)	34 (mg)	Acetone (mL)	Sonication (min)	Identification of the solution
PEGDA 250				-	60	A
PEGDA 575				-	60	B
PEGDA 700	1.00 ± 0.05	27.0 ± 0.5	1.0 ± 0.1	-	60	C
HDDA				-	60	D
BEDA				-	90	E
BEMA				1.0	115	F

The liquid formulations were photopolymerized under UV light to evaluate the most interesting and promising monomers. The so obtained solid samples were divided into three, and each part was used to test the variation of colour in contact with a base. In particular, one part was used as a reference, the second one was dipped into a solution of ammonium hydroxide (25 wt.%) at room temperature, and the last third one was used to evaluate the response under vapours of the same ammonium hydroxide solution, that was put in an over at 37°C. After 1 hour, an evaluation of the results obtained was carried out. We also tested the resistance in these basic conditions and the eventual leaching of the dye from the polymers during these tests.

Different polymers were chosen to test their hydrophobic/hydrophilic properties and the crosslinking network they can produce once photopolymerized. Both these variables can influence the chromic response of the dye. Compound **34** shows relative high hydrophobicity given by C_8 alkyl chains that allow us to avoid the leaching once dipped in an aqueous solution and the dye's leaching, which can be helped if the final polymer's mesh is too high. We tested the different molecular weights of PEGDA to evaluate if, increasing the hydrophilicity of the polymer with the increasing molecular weight, a good solubility of the dye can be obtained, avoiding leaching.[245]

HDDA produces a hydrophobic polymer that can solubilize the dye, while BEDA and BEMA produce hydrophobic and rigid polymers.[29]

We evaluated the dispersed dye's colour changes in the polymeric films composed of the previously reported monomer. In general, the protonated dye confers a yellow colour, but in basic conditions, they change colours from red to blue (see Figure 66).
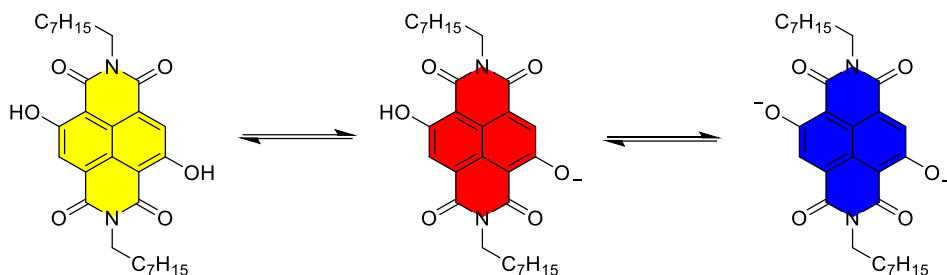
Figure 66 - *Different colours of compound* *34* *under sequentially deprotonation processes.*

Moreover, it can also change its emitting properties, as depicted in Figure 67, in which a comparison of the solution of compound **34** under ambient or UV illumination is given. Fin et al. reported all properties of this compound in all protonated and deprotonated species.[244] for a similar compound bearing different R groups. The most important aspect regards the pK_a of the different species. The authors reported a value of 6.3 for the first pK_a, while 11.1 for the second one.
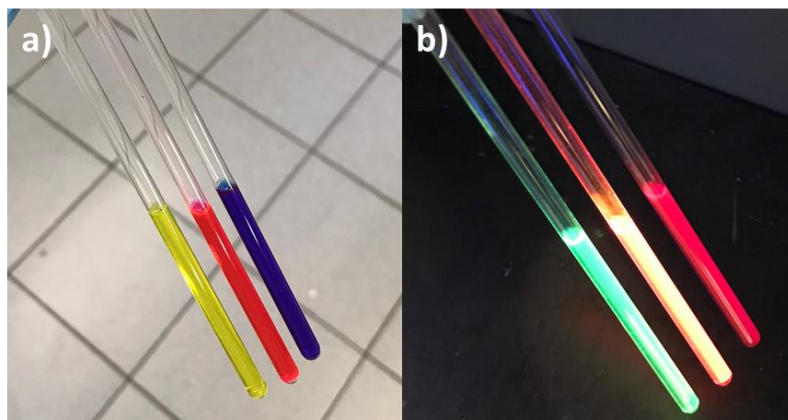
*Figure 67 – NMR tubes containing solutions of **34** with different pH under a) ambient illumination and b) under 365 nm UV lamp. The yellow acid solution emits green light, while the red form emits yellow and the blue in the red range.*

At the same time, Table 31 reports the wavelengths of absorption for all species of protonated, mono-deprotonated and bis-deprotonated compound **34**.

*Table 31 – Species and relative pH and wavelength (nm) of absorbance for all species of protonated, mono-deprotonated and bis-deprotonated compound **36**.*

Species	pH	λ of absorbance (nm)
Protonated	< 5	470
Mono-deprotonated	6 - 11	565
Bis-deprotonated	> 12	615

Moreover, an organic base was employed to test the reactivity of compound 34 and the time required to complete the process. DBU was chosen due to its high solubility in many organic solvents, and its structure is depicted in Figure 68.
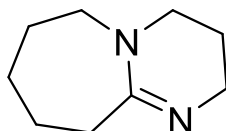
Figure 68 - Structure of DBU.

An instantaneous colour change was noticed once 118 eq of DBU dissolved in chloroform was added to a solution of **34**, as reported in Figure 69. The emission also changes in wavelength, from green to orange/red.
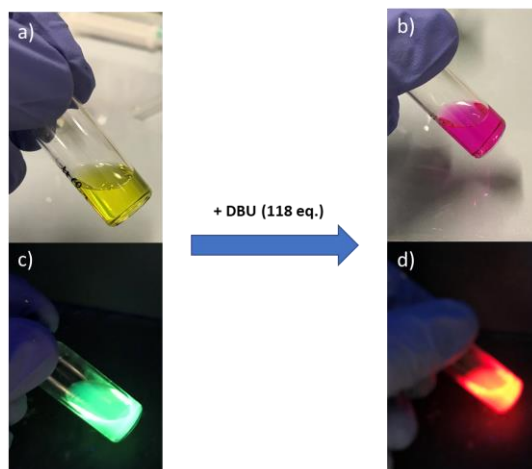
Figure 69 – Colour change from a) yellow (completely protonated form) of a 0.25 mM of a solution of 34 in chloroform to b) purple one (a combination of mono e bis deprotonated species). The compound changes its emission from c) green to d) red.

Other preliminary tests were conducted to evaluate the absorption and emission properties of compound **34** solubilized in different organic solvents (Figure 70).
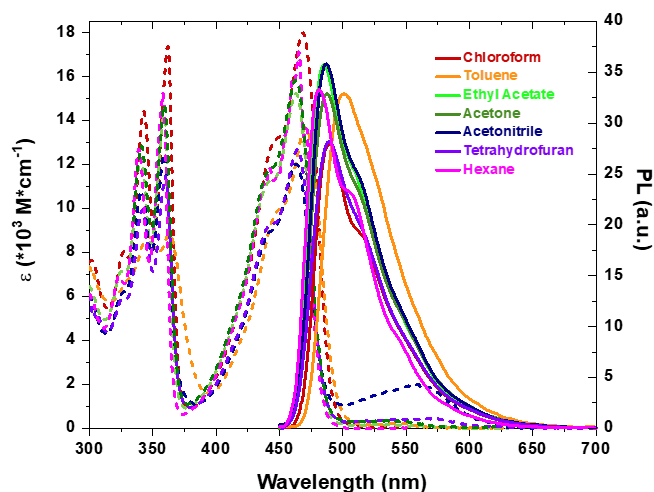
Figure 70 - Absorption (dashed) and emission (solid) spectra of 34 in several organic solvents. Emission spectra are normalized at 0.1 intensity at the excitation wavelength.

From these tests, some information about absorption and emission wavelength, as well as the Stokes shift, the quantum yield (ϕ_F) and molar extinction coefficient (ε) in all different organic solvents are reported (Table 32).

Table 32 – *Photophysical properties of **34** in different organic solvents. λ_{abs}, λ_{em}, Stokes shift and ε are reported in nm, 10^3 cm^{-1} and M^{-1} cm^{-1}, respectively. All photophysical values reflect the average of three independent measurements. Φ_F was measured, referring to Rhodamine 101 as standard.*

Solvent	$\lambda_{abs}{}^a$	$\lambda_{em}{}^a$	Stokes shift^a	ε^a	$\Phi_F{}^b$
Acetonitrile	463	486	1.02	12370	0.19
Acetone	462	486	1.07	16331	0.17
Chloroform	469	489	0.87	17996	0.16
Ethyl acetate	463	485	0.98	15624	0.19
Hexane	465	481	0.72	17020	0.17
Tetrahydrofuran	465	487	0.97	12306	0.17
Toluene	470	501	1.32	14709	0.21

The photophysical properties of **34** in solution were evaluated. The absorption spectrum of **34** shows a π-π^* transition around 360 nm and a charge-transfer band at 460 nm more sensitive to the environment polarity. Finally, a transition after 500 nm appears in all the solvents, excluding hexane and chloroform, probably due to the hydrogen bonding (HB) interaction between **34** hydroxyl groups (HB donor) and the solvent molecules (HB acceptor).[246,247] **34** displays a bright green emission with a fluorescent quantum yield (Φ_F) value of around 0.18 for all the investigated solvents.

From these results and the preliminary tests, we can exclude some matrices. Firstly, PEGDA 250 was degraded under basic conditions, bringing a blackened matrix. The same phenomenon was not observed in PEGDA 575 and 700, but while the first one maintained the same dimensions of the polymeric film, PEGDA 700 showed less stability and hygroscopicity. For these reasons, PEGDA 700 was excluded. Secondly, HDDA and BEDA showed a reduced response of the dye under basic conditions due to their marked hydrophobicity: only the surface can turn the colour orange/red, while the bulk remains yellow. Another interesting matrix was BEMA, which gives a sudden colour change when immersed in a basic solution and contact with basic vapours. From these tests, the most promising matrices are PEGDA and BEMA, on which further studies are focused.

To further investigate the material's behaviour, the reported formulations were prepared (Table 33), solubilizing **34** in acetone before the addition to the liquid formulation.

Table 33 – *Composition of the formulations to test the material's properties.*

Monomer	Photoinitiator (phr)	34 (phr)	Acetone (mL/$g_{monomer}$)	UV-absorber	Name
BEMA		0.1	0.2	-	BEMA-NDI
PEGDA 575	2.5	-	-	-	PEGDA
		0.1	-	-	PEGDA-NDI
		-	-	0.2	PEGDA-UV

Some tests were carried out on these formulations to evaluate the photopolymerization process and their photorheological behaviours. For the first test, a broad range UV lamp with an intensity of 5.3 mW/cm^2 was used to start the photopolymerization process. The photorheology films with a 0.2 mm thickness and diameter of about 2.5 cm were produced.

Testing the change colour of the so obtained samples, an effect of the addition of acetone can be noticed. In particular, investigating the BEMA matrix, the addition of acetone brings an increased rate of colour changes, as depicted in Figure 71. The first half (A) of the 3D printed object was immersed for 10 minutes in acetone and then put in a vacuum oven at 45°C for 10 minutes, while the second half (B) was only immersed in acetone for 10 minutes.
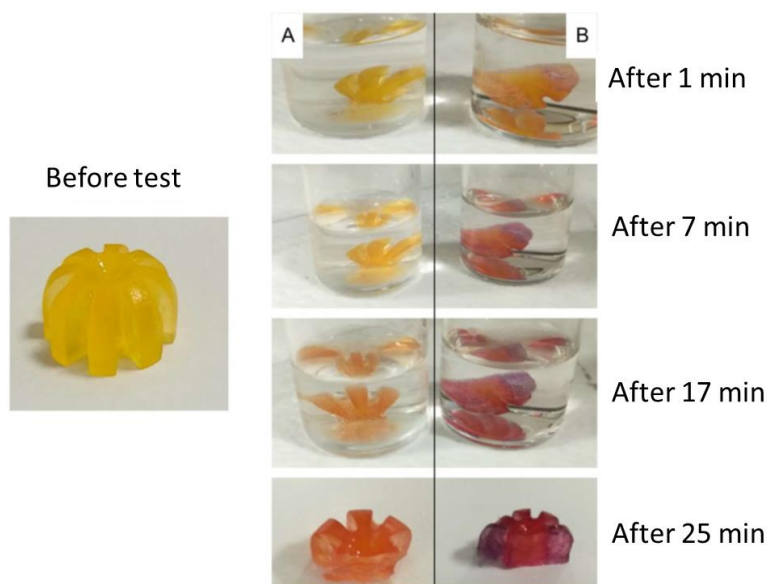
Figure 71 – Effects of acetone in the rate of colour changes process, which is faster for sample B, contains a high amount of acetone than A.

As can be noticed, the variation of colour is faster for the B half, while in A, reduced visible changes of colour are obtained. Moreover, a more evident purple/blue colour can be obtained when acetone remains in the polymeric matrix, while when it's absent, only a red colour can be noticed. An analogue test was also conducted on PEGDA 575, but no differences can be found between samples. For this reason, we decided to investigate only PEGDA 575 as a polymeric matrix to avoid the effect of acetone.

From the photorheology tests, a delay in the start of the polymerization process can be noticed when the intensity of the UV lamp is very low (0.5 mW/cm^2). At the same time, a reduced effect is obtained by increasing the irradiation intensity to 4.7 mW/cm^2. This can be due to the concurrent absorption in the UV range between the photoinitiator and the dye, causing an increased delay time needed to reach the gel point. At the same time, no differences in the final modulus are observed, meaning that the addition of the dye doesn't affect the kinetic of the photopolymerization but only the initial phase of propagation (Figure 153 in Appendix VII). DMA can confirm this hypothesis. The same glass transition temperature value is detected for both

formulations with and without the NDI-OH (Figures 154 and 155 in Appendix VII). The resulting T_g is about -16°C, which means that all samples are in the rubber state.

Furthermore, an evaluation of the resistance of PEGDA when immersed in different solvents and its permeability to aqueous solutions was carried out to study the possibility of using this polymer in the final demonstrators. All samples used in this part were obtained with the Asiga DLP 3D printer with a LED wavelength of 385 nm. The experimentally optimized parameters are reported in Table 34.

Table 34 – Optimized 3D printing parameters.

	Normal layers	Burn-In Layers
Layer thickness (mm)	0.1	0.1
Light intensity (mW/cm²)	40	40
Exposure time (s)	4	10

This test only evaluates the final polymer after 24 hours into the solution for aqueous solutions. Reduced resistance of this type of polymer in aqueous solutions is visible after a day of immersion. Some cracks reveal that water can easily destroy the matrix after a long contact time (Figure 72). Beyond water, other organic solvents were tested, producing the results reported in Table 35.
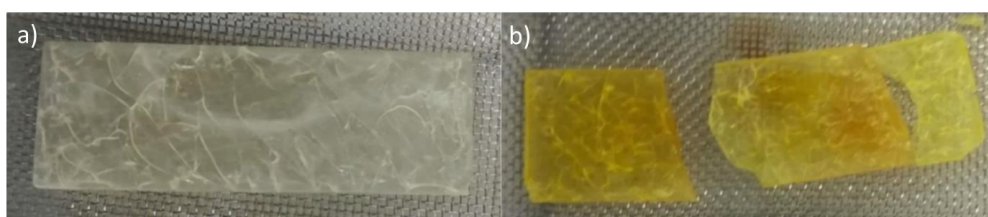
Figure 72 - PEGDA a) without and b) with compound **34** after 24 h in deionized water.

Table 35 – Solvents in which both samples (with and without **34**) were dipped with some observations about the process.

	Thickness variation (%)		
Solvent	PEGDA	PEGDA-NDI	Observations
DMSO	15.6	6.8	-
Ethylene glycol	0.0	0.0	-
Toluene	5.9	4.9	Cracks after 10 minutes
Acetonitrile	11.5	4.0	Cracks after 10 minutes
PC	4.5	6.8	-

n-hexane	0.0	0.0	-
DMF	7.5	7.8	Changes in colour
Acetone	5.0	5.3	Cracks after 20 minutes
Isopropanol	3.6	3.0	-
Ethanol	8.9	2.4	-

From these results, we excluded toluene, acetonitrile, DMF and acetone because they cause damage to the polymeric matrix and changes in the colour of **34**.

To test the results after the exposure to vapours, some permeability tests were performed, reaching the results synthetized in Table 36.

Table 36 *– Properties of a polymeric matrix with and without **34** under aqueous vapours exposure.*

	PEGDA	PEGDA-NDI
Permeability (cm^2/(s*bar))	1.31×10^{-10}	2.18×10^{-10}
Diffusivity (cm^2/s)	0.322×10^{-7}	3.47×10^{-7}
Solubility (bar^{-1})	4.05×10^{-3}	0.6×10^{-3}

We noticed better results for the sample containing compound **34**, in which the diffusivity is facilitated due to the low crosslinking density caused by the introduction of the dye. At the same time, the solubility is higher in the sample without **34**. From the so obtained results, a demonstration that these matrices can be used as sensors for both liquid and vapour applications is provided.

Evaluated the possible application as pH sensors, some tests about the values of pH at which the sample changes colours were carried out, using the following reported solutions (Table 37).

Table 37 *– Experimental conditions about tests on 3D printed polymeric samples at different pH and in different solvents.*

Base	NH_3		DBU
Solvent	H_2O		n-hexane
Physical state	Liquid	Vapor	Liquid
Concentration		pH 12	50 %$_{v/v}$
		pH 11	10 %$_{v/v}$
		pH 10	5.0 %$_{v/v}$
		pH 9	0.4 %$_{v/v}$
		pH 8	0.0 %$_{v/v}$
	Distilled water		

Temperature	RT	30°C	RT
Thickness	0.8 ± 0.1 mm	0.5 ± 0.03 mm	0.5 ± 0.03 mm

All samples were tested by leaving them in contact with basic water or vapours for 18 minutes, and then UV spectra were recorded (Figure 73).
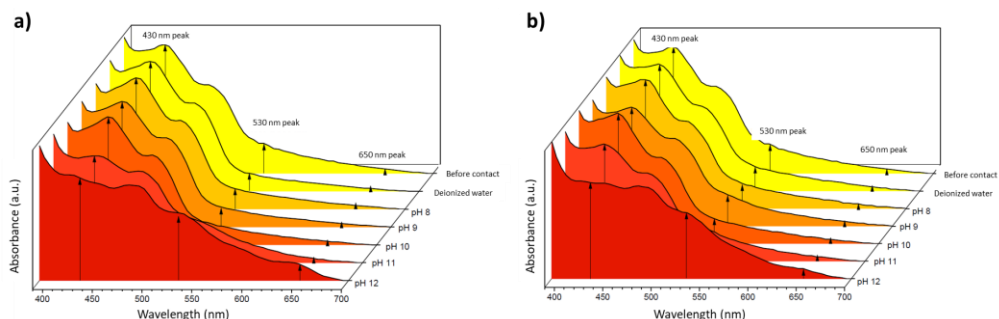

*Figure 73 – UV-visible spectra of 3D printed samples containing **34** after 18 minutes of a) NH$_3$ aqueous solution and b) NH$_3$ vapours at different pH values.*

In both cases, an increase in the 650 nm and 530 nm peaks is visible, with a relative reduction of 430 nm. This means that the protonated moiety starts to lose one or two protons at a rate that strongly depends on the pH: the higher the basicity, the faster the process. Leaving the samples for more time or increasing the pH values of the solution can bring a faster deprotonation reaction and a shifted equilibrium to the unprotonated moieties.

The process is reversible, and it can occur by employing two different methods: leaving the sample in contact with air or dipping it into an acid solution. The first method requires more than 30 days to be completed, while the second one is faster, and only 30 minutes are needed to return to its original colour when dipped in a solution of HCl in water (with pH=1). Same results were obtained employing acidic vapours, but the time required is a bit longer (about 50 minutes).

Some tests were also carried out employing a solution of DBU in *n*-hexane at two different concentrations of base (5.0% and 0.4%). As depicted in Figure 74, the less concentrated solution of DBU can turn the colour after 24 h from yellow to only red/purple. In comparison, only after 17 h the more concentrated solution turns the sample from yellow to blue, meaning complete double deprotonation of **34**.
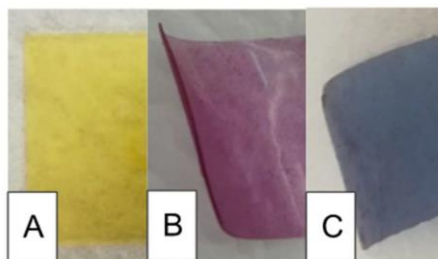
Figure 74 - A) PEGDA-NDI before the test. B) PEGDA-NDI after 24 h in a solution DBU/hexane 0.4% of concentration. C) PEGDA-NDI after 17 h in a solution DBU/hexane 5.0% of concentration.

Also, the process is reversible in this case, but it takes more than 30 days to recover the original yellow colour.

After these preliminary tests, compound **34** was used to obtain some 3D printed devices with a complex final shape. The honeycomb and a perforated cube were chosen as possible final structures to evaluate the fidelity between the real printed device and the CAD virtual version, reported in Figure 75.
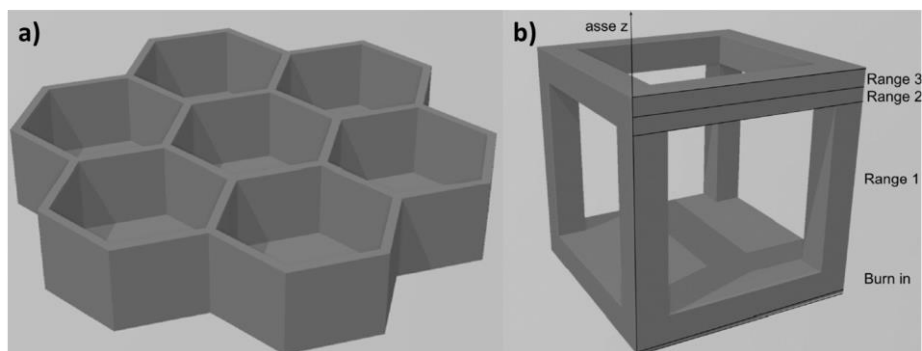

Figure 75 - CAD project of a) honeycomb and b) perforated cube.

In Table 38, all 3D printing optimized parameters for both structures are reported. No additional parameter optimizations were required for the honeycomb one, reaching good resolution on the *XY* plane in the *Z* direction. At the same time, for the perforated cube, the structure was divided into three parts: in this way, better final fidelity to the CAD project is obtained and a final self-standing device.

Table 38 - Optimized parameters for 3D printed structures.

	Honeycomb			Perforated cube		
	Normal layers	Burn-In Layers	Normal layers range 1	Normal layers range 2	Normal layers range 3	Burn-In Layers
Layer thickness (mm)	0.1	0.1	0.1	0.2	0.2	0.1
Number of layers	46	2	63	3	2	2
Light intensity (mW/cm²)	40	40	40	48.36	30	40
Exposure time (s)	2.5	5	3	0.7	2.5	5

Using the optimized reported parameters, good resolutions can be easily achieved. The displacements between the CAD project and the real 3D printed object can be evaluated using the 3D scanner, comparing the two objects. As reported in Figure 76, most of the device appears in green for the honeycomb device, which means that a displacement of about ± 0.050 mm was detected, and the only parts that show defects are the internal walls.
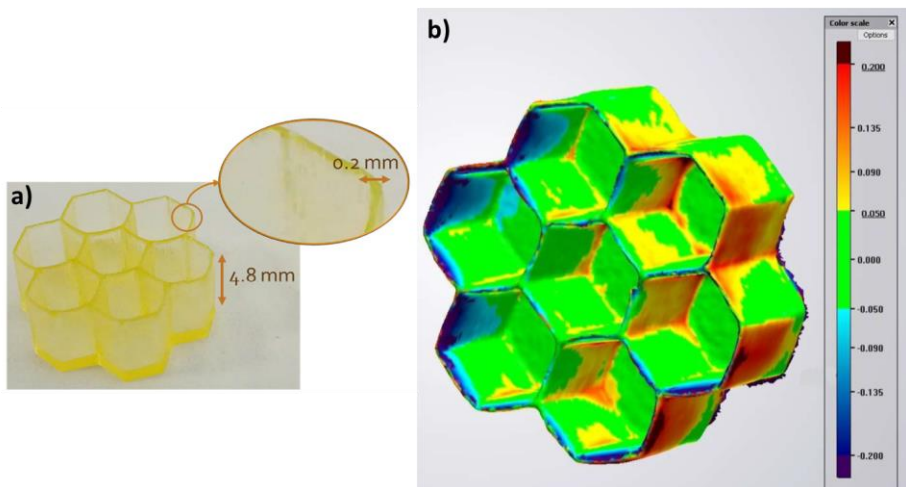

Figure 76 – a) 3D printed honeycomb structure and b) a comparison between its 3D image and the CAD project to evaluate displacements (the scale is in mm).

For the perforated cube, a structure in which the *Z* resolution is the most important one to obtain a self-standing structure, better final resolutions were achieved, as reported in Figure 77.
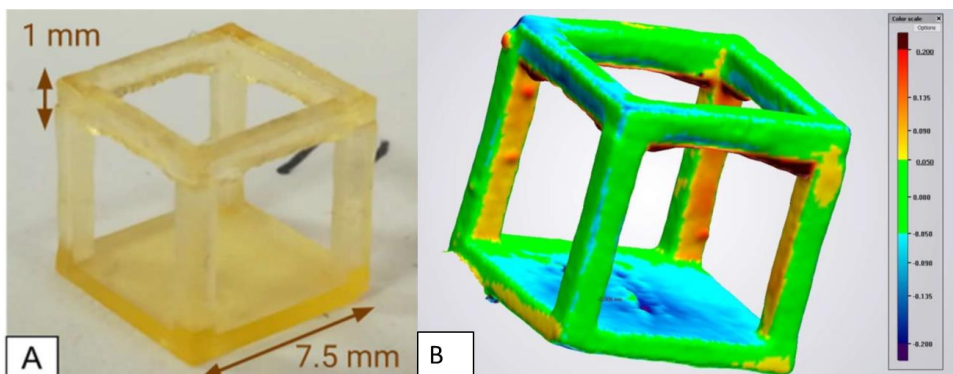
Figure 77 – a) 3D printed perforated cube and b) its comparison with the CAD project in which the displacement is highlighted (the scale is in mm).

Some final demonstrators were then produced to show some practical uses of these devices containing compound **34**, acting as a sensor. Both were designed as laboratory sensors to follow chemical reactions. The first device is composed of microfluidic channels in which reagents can flow: different colours can detect if a base is generated or consumed during the process. These variations help evaluate when the reaction is over and which conversions can be reached. In this case, we tested this device with solutions containing different concentrations of DBU to evaluate the applicability and the time required for the whole process to occur.

As reported in Figure 78, the CAD device was designed to obtain two channels where both reagents can be inserted. All channels were made of PEGDA and 0.1wt.% DBU, while the base was only in PEGDA without the dye. Both reagents can be inserted in the two IN-holes, they can react over the whole device, and the final products are pushed out at the end of the device.
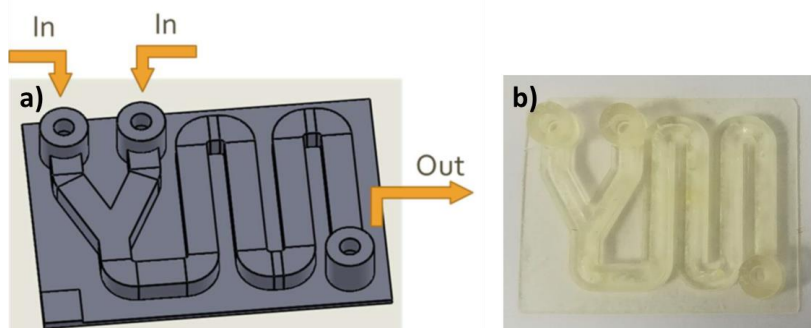

Figure 78 - a) CAD project for the microfluidic device and b) the 3D printed object.

Different solutions were used to test the final demonstrator, and all of them are reported in Table 39. The first formulation was used to test the maximum flow that two automatic syringes can apply. In contrast, in the others, an increasing concentration of DBU is used to evaluate the final colour of the matrix.

Table 39 – Solutions and their flow rate used to test the final microfluidic device.

	IN 1		IN 2		
	Solution	Flow rate (µl/min)	Solution	Flow rate (µl/min)	Time
A	Hexane	250	Hexane	250	30 s
B	Hexane	250	0.4% DBU	250	7 min 30 s
C	Hexane	250	5.0% DBU	250	7 min
D	-	-	5.0% DBU	500	8 min

Trial A, as expected, didn't produce any colour variations due to the absence of the DBU. In trials B and C, a colour change was noticed for both in 4 minutes, reaching a red/purple colour for the first one and deep blue for the second one. The most promising one is trial D, in which a highly concentrated solution of DBU in hexane was pumped into the device, blocking at the same time IN 1. As depicted in Figure 79, a complete colour change was observed, reaching a dark blue colour. This process is totally reversible, introducing a strong acid or washing with pure hexane.
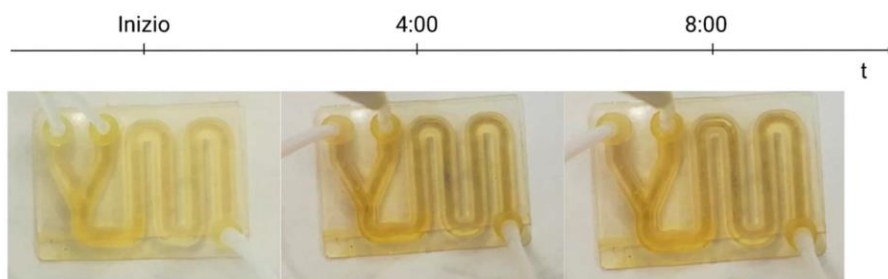

Figure 79 – Introduction of a solution of 5.0 wt.% DBU in n-hexane at 500 µl/min. After 4 minutes, a complete colouration of the device is visible.

A similar device was produced to evaluate the emission of basic vapours during a chemical reaction. In particular, it was shaped to fit as a chimney on the top part of a 10 mL Becher a reaction can take place, as depicted in Figure 80.

Figure 80 - 3D printed device able to respond to basic ammonia vapour.

The reaction was monitored by the development of ammonia vapours that were originated from the following reaction that can start under heating:

$$Ca(OH)_2 + 2NH_4Cl \longrightarrow 2NH_3 + CaCl_2$$

All reagents were introduced into the Becher, and it was heated to 80°C under vigorous stirring. The evolution of the colour from yellow to dark red/blue was followed with a camera, as reported in Figure 81, over more than 25 minutes.
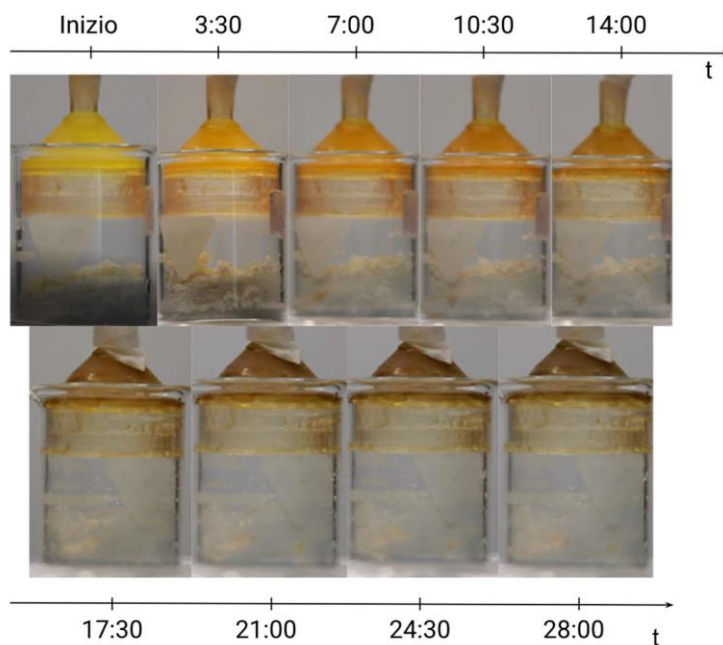

*Figure 81 - 3D printed device that changes its colour due to the reaction between compound **34** and the ammonia vapours that originated during the reaction.*

In this project, the printability of PEGDA with compound **34** solubilized into a functional moiety has been demonstrated. It shows promising results in reduced printing times required, good quality of the final devices, complex shapes achievable through 3D printing and the fast and reversible response of the final demonstrators in everyday life applications, such as pH sensors for liquid and gas basic species. The same process can be reversed: the device can be put in contact with a strong base, and its colour change from yellow to blue, then it can detect the presence of an acid species. In the future, implementing a mathematical model that correlates the final colour with the conversion of the deprotonation reaction might become possible and determining how many cycles are possible with this type of material. Finally, improvements in the synthetic pathway and the molecule's structure (inserting some photopolymerizable groups that can avoid the leaching of the dye during use) will be necessary before real possible industrial applications.

7. Conclusions and perspectives

In this thesis, different projects aim to obtain innovative functional and 3D printable materials that respond to external stimuli, changing mechanical or chemical properties quickly and reversibly. Starting from results reported in the literature for inorganic fillers, some organic and metalorganic chromophores have been investigated as active species to confer innovative properties to polymeric materials. Preliminary results are then provided to demonstrate that merging innovative production techniques, such as 3D printing, with dyes results in innovative and functional polymeric materials with complex shapes, usually impossible to be reached with the traditional production methods. These results will help widen the availability of printable polymers and their uses as reversible sensors, maintaining low costs and saving raw materials.

Traditionally, introducing inorganic fillers in the FFF printing technique is the most exploited way in literature to confer innovative properties to polymers. For this reason, in the first part of this thesis, I investigated their use as species able to confer

piezoresistive properties to a non-conductive polymeric matrix. Promising results can have been obtained with CNTs, but their high costs and elevated quantities make this way less appealing from an industrial point of view. Limits in the 3D printing process have been found due to possible degradations of fillers when high temperatures are required, and inhomogeneous devices with reduced mechanical properties can be obtained. In this case, an optimization of the printing parameters has to be found, and a comparison between 3D printed devices with one produced traditionally.

To overcome these drawbacks, I moved on to another 3D printing method that is more suitable for introducing organic dyes as a soluble component in a liquid photoreactive resin. The attention was mainly focused on the DLP 3D printing method and the use of engineered dyes to give fast and reversible changes in mechanical and chemical properties once activated by external stimuli. In recent years, the use of DLP as a printing technique has been increasing but only recently the use of dyes for aesthetical reasons or to improve the final resolutions and fidelity has been reported. Moreover, this method turned out to be the most versatile one, in which reduced costs and savings of raw materials represent the main advantages over other techniques. According to the final application, improvements can be obtained by introducing dyes to obtain tailor-made materials with different mechanical and chemical properties. The introduction of dyes requires fewer concerns than other printing techniques. They are preserved over the whole printing process, maintaining the temperature low and using low intensity LED as a light source. Furthermore, the experimental optimisation process can achieve suitable printing parameters to obtain the best results. In this way, the use of expensive inorganic fillers, such as the usually exploited CNTs, can be avoided, overcoming at the same time dispersion and homogeneity problems that can limit the final properties of the device.

Firstly, the choice of suitable dyes was made according to the data reported in the literature and based on these results. The chosen molecules were appropriately engineered to be more soluble in the liquid resins and photoreactive to be covalently connected to polymeric chains. Studies on the best concentration of active moiety for

all projects were carried out, finding that the best results in fast response and printability were obtained with very low quantities. Finally, the optimal printing parameters were found to obtain fast printing processes, high resolutions and fidelity to the CAD project, and fast and reversible responses of final devices under external stimulations.

A wide range of materials and dyes are here applied to demonstrate the range of possible applications and the variety of organic and metalorganic species that can be exploited. From the post-curing process, in which photosensitive species can be applied without any degradations, to introducing soluble dyes into liquid inks, 3D printing can be applied to obtain complex-shaped devices with rapid and reversible external stimuli. Moreover, engineering dyes in suitable ways make their covalent bonding with polymeric matrix possible, avoiding leaching phenomena during use.

The post-functionalization process aims to demonstrate an innovative way to introduce photosensitive dyes into polymeric devices by exploiting reactive groups that remain unreacted on the surface. At the same time, thiol-yne chemistry represents a useful method to obtain high resolved 3D printed structures that can expose different functional groups on the surface, which can be used to connect the desired moieties. Both mechanical and chemical properties of the matrix and the dye are preserved, and this path the way in the use of different fluorophores with applications in biomedicine.

Organic and metalorganic light-emitting dyes can also be exploited as soluble species in liquid monomers to obtain downshifter devices, absorb UV light and emit in the visible range. Metalorganic complexes are more promising than organic dyes due to their high photo and thermal stability, the very high Stokes shift and high quantum yields. Polymeric waveguides can be easily produced, with reduced lateral dispersions, giving the appropriate shape to the final materials. The low toxicity and concentration required and easy synthesis make these compounds suitable moieties for low-cost and efficient waveguides. The preliminary results reported can path the future way of using these devices.
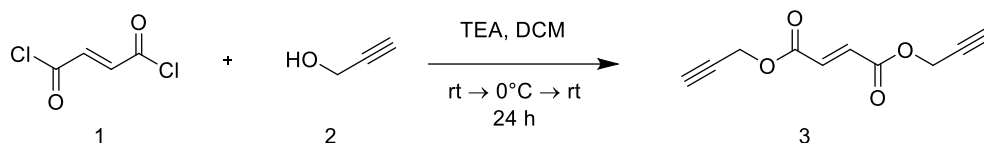
Other classes of chromophores here exploited are azodyes that can confer fast and reversible responses under laser or UV LED irradiations thanks to their optical properties. Fast heating without thermal and photodegradation can be achieved with low quantities of azodyes and confer light-induced shape-memory properties simultaneously. Inorganic fillers usually give this characteristic, and no examples are reported about the use of dyes as shape-recovery activators. Moreover, azodyes also confer innovative gas permeabilities to usually non-permeable polymeric matrices. Changes in permeability values are first noticed by introducing azodyes and then changing their ortho functional groups. More interestingly, permeabilities can be tuned for some selective gases under green laser irradiation. This property is of primary importance in producing smart and light-controllable sensors.

Finally, pH-responsive species have been employed here, demonstrating that fast and reversible responses can be reached using different external stimulations. Final examples of laboratory-scale applications are then described to demonstrate the use of these final devices as sensors for reactions.

With all these applications, I would like to demonstrate how the application of engineered dyes can join new 3D printing production methods and how innovative polymeric materials are found by exploiting both of them. Light, pH, and mechanical stresses are investigated here, aiming to prove that almost all external changes can impact this type of material's mechanical or chemical properties. Many limits have yet to be overcome regarding the possibility of applying these devices on industrial scales. Many variables must be investigated, such as the optimal concentrations, type of materials, shapes even the final properties of the devices. Through the reported examples and the promising results reported in this thesis, the path in the innovative use of dyes is open, and it can encourage other research in the future. Thinking about the wide range of organic dyes reported in the literature, it appears clear that numerous functionalities can be conferred to a wide range of polymeric materials.

Appendix I: Synthesis and characterizations

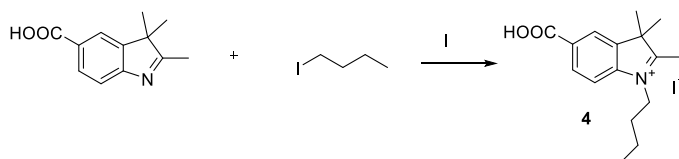**Synthesis of di(prop-2-yn-1-yl) fumarate (3):**

All synthetical steps were carried out in dried glassware under an inert Argon atmosphere. Propargyl alcohol (**2**) (7.55 mL, 131 mmol) was solubilized in anhydrous dichloromethane (DCM) in a three-neck round-bottom flask under stirring. Triethylamine (TEA) (21.88 ml, 157.2 mmol) was added, and the mixture was cooled to 0 °C. A solution of fumaryl chloride (**1**) (5.65 mL, 52.4 mmol) in anhydrous DCM (30 mL) was added dropwise over 45 minutes through a dropping funnel. Then the temperature was raised to 25°C, and the reaction was stirred for 24 h, washed sequentially with a saturated solution of ammonium chloride (3 x 250 mL), and saturated sodium bicarbonate (2 x 240 mL) and brine (1 x 80 mL). The organic fractions were collected, dried under Na_2SO_4, filtered, and the solvent was evaporated under reduced pressure. The crude material was recovered as a dark brown solid, and it was purified with silica gel flash chromatography (100% ethyl ether, isocratic eluent) to obtain a brown-white solid.

Yield 81.0% (42.44 mmol, 8.16 g).

^{1}H NMR (600 MHz, Chloroform-*d*): δ 6.93 (s, 2H), 4.80 (d,J = 2.5 Hz, 4H), 2.52 (t, J = 2.5 Hz, 2H).

^{13}C NMR (151 MHz, Chloroform-*d*): δ 163.99, 133.69, 75.89, 75.39, 52.64.

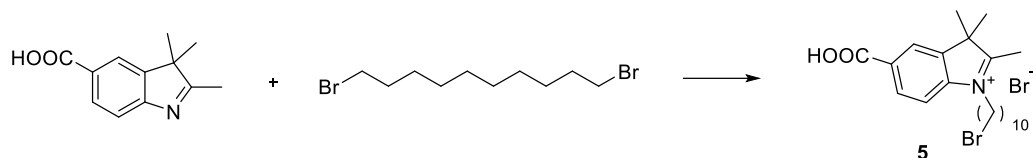**Synthesis of 1-butyl-5-carboxy-2,3,3-trimethyl-3H-indol-1-ium iodide (4):**

2,3,3-Trimethyl-3H-indole-5-carboxylic acid (2.50 g, 12.3 mmol), 1-iodobutane (5.6 ml, 49.2 mmol) and 9 ml ACN.

Yield: 86% (4.10 g, 10.6 mmol).

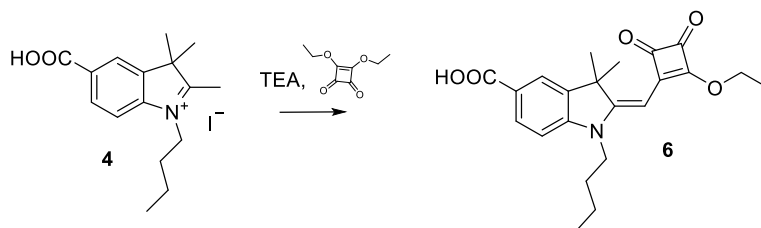Characterizations are in agreement with the reported literature.[112]

Synthesis of 1-(10-bromodecyl)-5-carboxy-2,3,3-trimethyl-3H-indol-1-ium bromide (5).

2,3,3-trimethyl-3H-indole-5-carboxylic acid (0.500 g, 2.46 mmol) was inserted in a vial equipped with a magnetic stirrer. The vial was sealed, and 1,10-dibromodecane (3.69 g, 2.76 ml, 12.3 mmol) and 8 ml of anhydrous ACN were added dropwise. Argon was fluxed for 15 minutes. Then the reaction was carried out in a microwave (165°C, 60 minutes). The solvent was removed under vacuum, and the product was recovered with ethyl ether, filtered and washed five times with ethyl ether. Yield 73% (0.903 g, 1.80 mmol).

^{1}H NMR (200 MHz, DMSO-d_6) δ (ppm) = 8.40 (s, 1H), 8.13 (m, 2H), 4.48 (t, 2H), 3.51 (t, 2H), 2.89 (s, 3H), 1.77 (t, 2H), 1.58 (s, 6H), 1.26 (m, 14H).

Synthesis of 1-butyl-2-((2-ethoxy-3,4-dioxocyclobut-1-en-1-yl)methylene) -3,3-dimethylindoline-5-carboxylic acid (6).

1-butyl-5-carboxy-2,3,3-trimethyl-3H-indol-1-ium (0.100 g, 0.258 mmol) was inserted in a vial equipped with a magnetic stirring. Ethanol (3 ml), 3,4-diethoxycyclobut-3-ene-1,2-dione (0.088 g, 0.08 ml, 0.52 mmol) and triethylamine (0.078 g, 0.11 ml, 0.78 mmol)
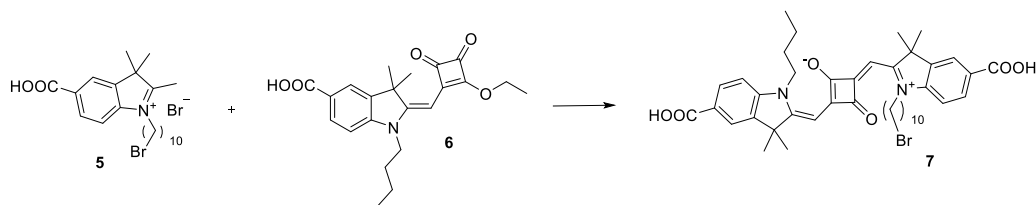
were added. The reaction was carried out with the microwave (90°C, 13 minutes). The resulting mixture was evaporated under vacuum, and ethyl ether was added to recover the product. The solvent was evaporated under reduced pressure, and the so obtained solid was washed with ethyl ether (3x15 ml). The filtrate was evaporated, the liquid was diluted with DCM, and purified by flash column chromatography (EtOAc/Petroleum ether 3:7). Yield: 49% (48.5 mg, 0.126 mmol).

^{1}H NMR (200 MHz, DMSO-d_6) δ (ppm) = 7.93 (s, 1H), 7.865 (d, 1H, J = 6.0 Hz), 7.24 (d, 1H, J = 8.0 Hz), 5.44 (s, 1H), 4.82 (m, 2H), 3.93 (t, 2H, J = 8.0 Hz), 1.56 (s, 6H), 1.41 (m, 4H), 0.88 (t, 3H, J = 8.0 Hz).

^{13}C NMR (50 MHz, DMSO-d_6) δ (ppm) = 192.88, 188.93, 187.24, 172.51, 167.10, 146.40, 140.28, 130.38, 124.42, 122.76, 108.67, 82.192, 70.04, 46.962, 42.12, 28.05, 26.47, 19.39, 15.56, 13.54.

ESI-MS: 382.44 (M-1).

Synthesis of 4-((1-(10-bromodecyl)-5-carboxy-3,3-dimethyl-3H-indol-1-ium-2-yl)methylene)-2-((-1-butyl-5-carboxy-3,3-dimethylindolin-2-ylidene)methyl)-3-oxocyclobut-1-en-1-olate (7).

1-(10-bromodecyl)-5-carboxy-2,3,3-trimethyl-3H-indol-1-ium bromide (0.145 g, 0.289 mmol) and 1-butyl-2-((2-ethoxy-3,4-dioxocyclobut-1-en-1-yl)methylene)-3,3-dimethylindoline-5-carboxylic acid (0.111 g, 0.289 mmol) were dissolved in a vial employing a solution of 2 mL of butanol and toluene (1:1). The vial was sealed, and the reaction was carried out with the microwave (160°C, 1 hour). The green-blue liquid was recovered with ethyl ether, and the solvent was evaporated. The product was re-crystallised by butanol, and the obtained solid was filtered under vacuum, washed with
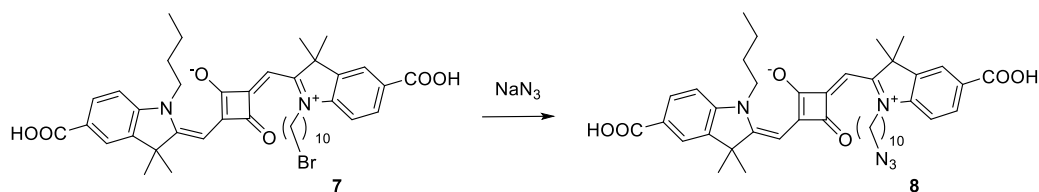
ethyl ether and dried on the vacuum stove (40°C, 2 hours). Yield: 24% (0.052 g, 0.069 mmol).

^{1}H NMR (200 MHz, DMSO-d_6) δ (ppm) = 8.03 (s, 2H), 7.96 (d, 2H, J = 8.0 Hz), 7.43 (d, 2H, J = 8.0 Hz), 5.90 (s, 2H), 4.12 (t, 4H, J = 6.0 Hz), 3.47 (t, 2H, J = 7.0 Hz), 1.70 (m, 12H), 1.23 (m, 20H), 0.94 (t, 3H, J = 8.0 Hz).

^{13}C NMR (50 MHz, DMSO-d_6) δ (ppm) = 180.92, 170.18, 167.46, 146.35, 141.96, 130.69, 126.29, 123.66, 119.66, 110.67, 88.04, 48.97, 35.55, 32.66, 29.16, 28.46, 27.92, 26.90, 26.45, 20.04, 14.16.

ESI-MS: 759.20 (M-1).

Synthesis of 4-((1-(10-azidodecyl)-5-carboxy-3,3-dimethyl-3H-indol-1-ium-2-yl)methylene)-2-((-1-butyl-5-carboxy-3,3-dimethylindolin-2-ylidene)methyl)-3-oxocyclobut-1-en-1-olate (8):

4-((1-(10-bromodecyl)-5-carboxy-3,3-dimethyl-3H-indol-1-ium-2-yl)methylene)-2-((-1-butyl-5-carboxy-3,3-dimethylindolin-2-ylidene)methyl)-3-oxocyclobut-1-en-1-olate (0.025 g, 0.033 mmol) and sodium azide (0.0024 g, 0.036 mmol) were added in a vial and dissolved in 1 mL of DMF. The vial was sealed and the reaction was carried out with the microwave (100°C, 20 minutes). The product was recovered with DCM and it was washed with deionized water (2x50 mL) and brine (1x50 mL). Then the product was dried with Na$_2$SO$_4$, filtered and the solvent was evaporated under vacuum. Yield: 63% (0.016 g, 0.021 mmol)

^{1}H NMR (200 MHz, DMSO-d_6) δ (ppm) = 8.03 (s, 2H), 7.96 (d, 2H, J = 8.0 Hz), 7.43 (d, 2H, J = 8.0 Hz), 5.90 (s, 2H), 4.12 (t, 4H, J = 6.0 Hz), 3.47 (t, 2H, J = 7.0 Hz), 1.70 (m, 12H), 1.23 (m, 20H), 0.94 (t, 3H, J = 8.0 Hz)

The compound solubility in CDCl$_3$ proved too low to record a ^{13}C NMR spectrum.

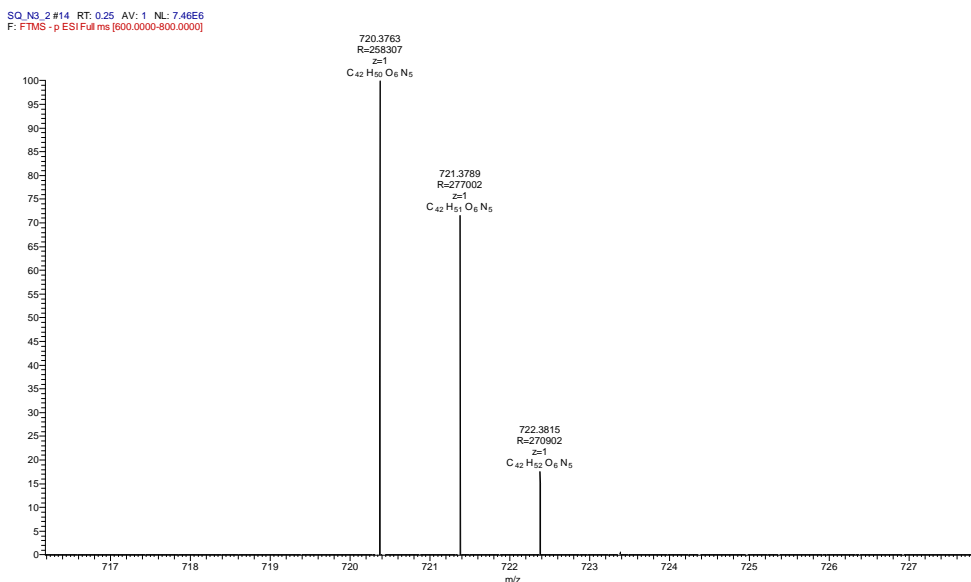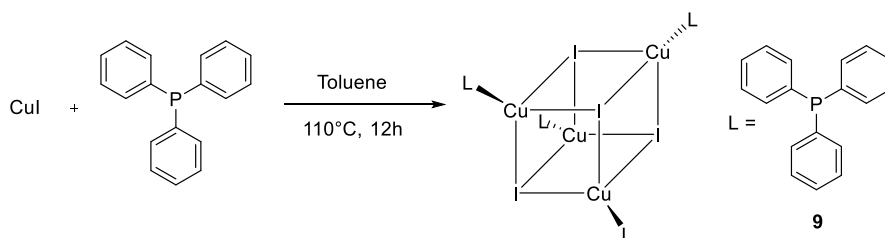HR-ESI-MS: calculated 720.3839, found 720.3763 (M-1).
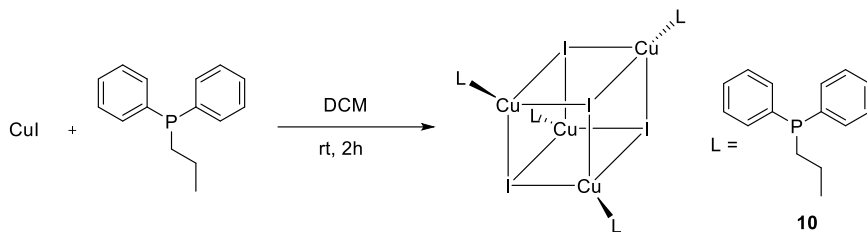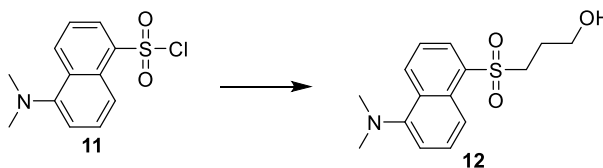

Figure 82 - HRMS of *8*.

Synthesis of copper-iodine based complex with triphenylphosphine as ligand (9):

The procedure is the same as previously reported.[114] All glassware was dried overnight before use, and the air was removed with Schlenk equipment. CuI (2.6 mmol, 0.500 g) was suspended in 50 mL of toluene, and triphenylphosphine (2.6 mmol, 0.700 mg) was added. The reaction was left for 12 hours at 110°C under stirring, then the mixture was filtered, the solvent was removed under vacuum, and the solid was recovered as white crystals. Yield 52.4% (0.343 mmol, 0.617 g).

The NMR characterization matches the one reported in the literature.

Synthesis of copper-iodine based complex with diphenylpropylphosphine as ligand (10):

The procedure is the same as previously reported.[115] All glassware was dried overnight before use, and the air was removed with Schlenk equipment. CuI (4.4 mmol, 0.840 g) was suspended in 20 mL of DCM and diphenylpropylphosphine (4.4 mmol, 1.0 g) was added. The solution was stirred for 2 hours, then it was filtered, and the solvent was removed under vacuum. The resulting white powder was purified by flash chromatography (PE/EtOAc 4:1). Yield 65.1% (0.859 mmol, 1.99 g).

The NMR characterization matches the one reported in the literature.

Synthesis of 3-((5-(dimethylamino)naphthalen-1-yl)sulfonyl)propan-1-ol (12):

Na_2SO_3 (11.12 mmol, 1.402 g) and $NaHCO_3$ (11.12 mmol, 0.934 g) were dissolved in 15 mL of H_2O in a round bottom flask. The temperature was raised to 95°C, and under vigorous stirring, **11** (5.56 mmol, 1.50 g) was added dropwise over an hour. After the last addition, the mixture was left for one hour under reflux, and then the flask was cooled to room temperature and water was removed employing a freeze drier. The solid product was dissolved in 25 mL of ethanol under stirring, and 3-bromopropanol (5.56 mmol, 0.773 g) was added dropwise. The mixture was left for 24 h under reflux, and the reaction was monitored by TLC (DCM : EtOAc 7:3, Rf = 0.4). Once the complete reaction was reached, the solvent was removed under vacuum, and the solid was dissolved in DCM (30 mL) and washed with brine (4 x 20 mL). The organic fractions are collected, dried with Na_2SO_4 and filtered. The solvent was removed under vacuum to obtain a yellow solid purified by crystallization from DMF and ethyl ether. The yellow solid

obtained after the crystallization was washed with ethyl ether. Yield 46.8% (2.60 mmol, 0.763 g).

^{1}H NMR (600 MHz, Chloroform-*d*): δ 8.60 (d, J = 8.5 Hz, 1H), 8.37 (d, J = 8.6 Hz, 1H), 8.29 (dd, J = 7.3; 1.3 Hz, 1H), 7.59 (m, 2H), 7.20 (d, J = 7.6 Hz, 1H), 3.72 (q, J = 5.7 Hz, 2H), 3.45 (m, 2H), 2.89 (s, 6H), 1.98 (m, 2H).

^{13}C NMR (151 MHz, Chloroform-*d*): δ 152.29, 134.26, 131.59, 130.62, 130.45, 129.96, 128.92, 123.51, 118.47, 115.44, 60.72, 52.85, 45.48, 25.84.

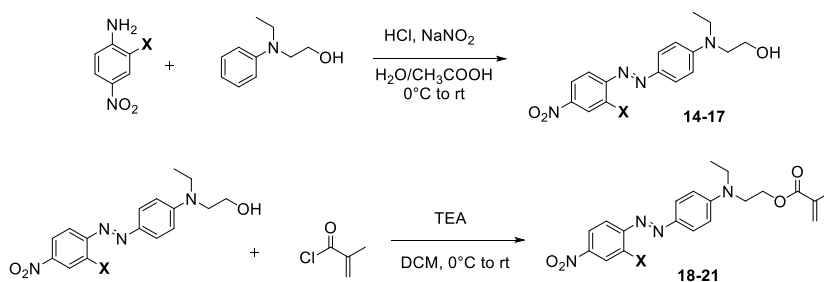ESI-MS (m/z): calculated 293.11, found 294.04 [M + H]$^+$

λ (EtOH abs.) = 342 nm

ε (EtOH abs.) = 3.548*10^3 L mol^{-1} cm^{-1}

Emission: 522 nm (Excitation 325 nm)

Quantum yield (φ): 47.15% (excitation 345 nm, emission 370-650 nm)

Stokes shift: 180 nm

Synthesis of 3-((5-(dimethylamino)naphthalen-1-yl)sulfonyl)propyl methacrylate (13):

In an anhydrous round bottom flask under argon atmosphere, **12** (0.68 mmol, 0.200 g) was dissolved in 8 mL of anhydrous THF under stirring. The temperature was cooled down to 0°C then TEA (0.82 mmol, 0.11 mL) and freshly distilled methacryloyl chloride (0.89 mmol, 0.086 mL) were added. The reaction was left for 12 h at room temperature, and it was monitored by TLC (DCM:MeOH 95:5, Rf = 0.84). Once the complete conversion was reached, EtOAc (50 mL) was added, and the mixture was filtered. The solvents were removed under vacuum, and the resulting solid product was dissolved in DCM and washed with brine (3 x 30 mL). The aqueous fractions were extracted with DCM, and all organic fractions were collected, dried with Na$_2$SO$_4$ and filtered. The

organic solvent was removed under vacuum, and the water residues were removed by freeze-drying. The product was recovered as a yellow solid. Yield 45.9% (0.313 mmol, 0.113 g).

^{1}H NMR (600 MHz, Chloroform-*d*): δ 8.61 (dt, J = 8.5, 1.1 Hz, 1H), 8.35 (dt, J = 8.6, 0.9 Hz, 1H), 8.30 (dd, J = 7.3, 1.3 Hz, 1H), 7.59 (ddd, J = 8.6, 7.4, 1.2 Hz, 2H), 7.20 (dd, J = 7.7, 0.9 Hz, 1H), 5.95 (dq, J = 2.0, 1.0 Hz, 1H), 5.50 (dq, J = 2.0, 1.0 Hz, 1H), 4.15 (t, J = 6.2 Hz, 2H), 3.44 – 3.39 (m, 2H), 2.90 (s, 6H), 2.13 – 2.06 (m, 2H), 2.01 (dd, J = 1.6, 1.0 Hz, 1H), 1.83 (dd, J = 1.6, 1.0 Hz, 3H).

^{13}C NMR (151 MHz, Chloroform-*d*): δ 167.00, 152.37, 135.90, 133.94, 131.72, 130.76, 130.40, 129.99, 128.95, 125.98, 123.53, 118.30, 115.45, 62.24, 52.54, 45.48, 22.62, 18.26.

ESI-MS (m/z): calculated 361.456, found 362.11 [M + H]$^+$

λ (EtOH abs.) = 344 nm

ε (EtOH abs.) = 4.393*10^3 L mol^{-1} cm^{-1}

Emission: 522 nm (Excitation 325 nm)

Quantum yield (φ): 41.55% (excitation 345 nm, emission 370-650 nm)

Stokes shift: 178 nm

-X	Disperse-X	Methacrylated-X
-H	14	18
-Cl	15	19
-OCH$_3$	16	20
-NO$_2$	17	21

2-(ethyl(4-((4-nitrophenyl)diazenyl)phenyl)amino)ethan-1-ol (14):

Compound **14** is commercially available, and it was purchased from Sigma-Aldrich and used without further purifications.

Synthesis of 2-((4-((2-chloro-4-nitrophenyl)diazenyl)phenyl)(ethyl)amino)ethan-1-ol (15):

The procedure is reported in the literature[116,117], and all characterizations were in agreement with the reported data.

Synthesis of 2-(ethyl(4-((2-methoxy-4-nitrophenyl)diazenyl)phenyl)amino)ethan-1-ol (16):

Compound **16** was synthetized as follows. 2-Methoxy-4-nitroaniline (2.0 g, 11.9 mmol) was dissolved in 50 mL of a 1:1 solution of H_2O and acetic acid under stirring. Then the temperature was brought to 0°C. Sodium nitrite (0.985 g, 14.3 mmol) was dissolved in 5 mL of water and added dropwise. After 30 minutes, a solution of N-ethyl-N-hydroxyethylaniline in 10 mL of water and 2 mL of methanol was added under vigorous stirring. After 30 minutes from the last addition, the temperature was brought to room temperature, and after 2 hours, the product was filtrated, washed with cold water and dried. The product was then purified on a silica gel column with an eluent PE/EtOAc 7:3. The product was recovered as a dark red powder with a yield of 90% (3.53 g, 10.7 mmol).

^{1}H-NMR (600 MHz, Chloroform-*d*) δ 7.92 – 7.87 (m, 4H), 7.71 – 7.66 (m, 1H), 6.79 (d, J = 9.0 Hz, 2H), 4.09 (s, 3H), 3.89 (t, J = 5.9 Hz, 2H), 3.61 (t, J = 5.9 Hz, 2H), 3.56 (q, J = 7.1 Hz, 2H), 1.25 (t, J = 7.1 Hz, 3H).

^{13}C-NMR (151 MHz, Chloroform-*d*) δ 155.79, 151.67, 148.39, 147.01, 144.55, 126.54, 117.53, 116.70, 111.68, 107.79, 60.45, 56.85, 52.52, 46.12, 12.25.

λ_{max} (EtOH): 490 nm

ε (L mol^{-1} cm^{-1}): 30.5 x 10^3

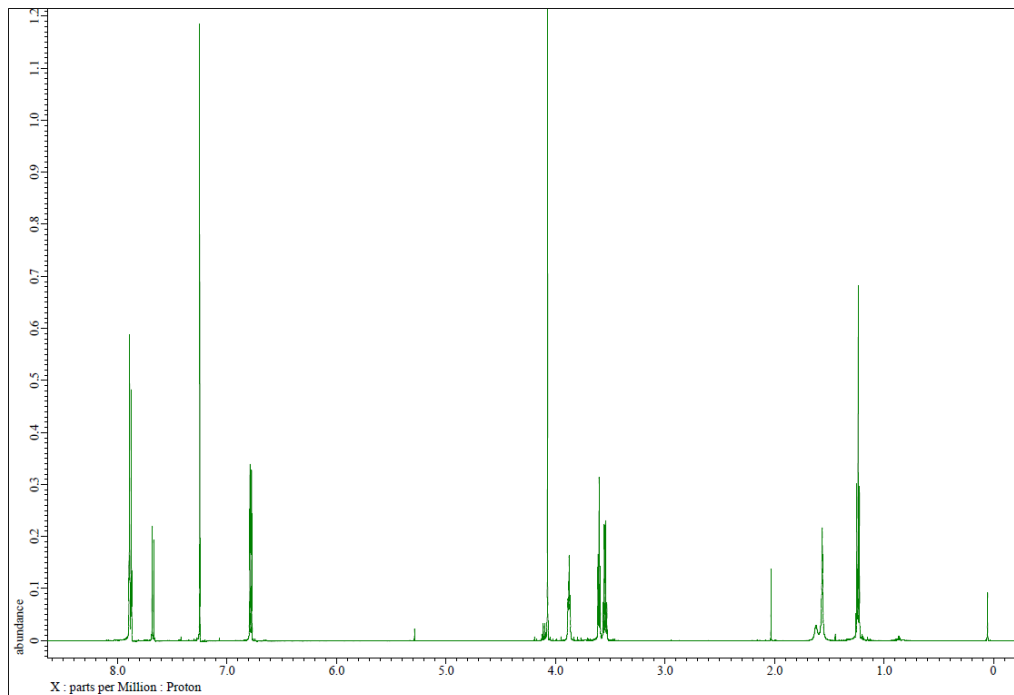HRMS: calculated 344.1485, found 345.1557 (M+1)
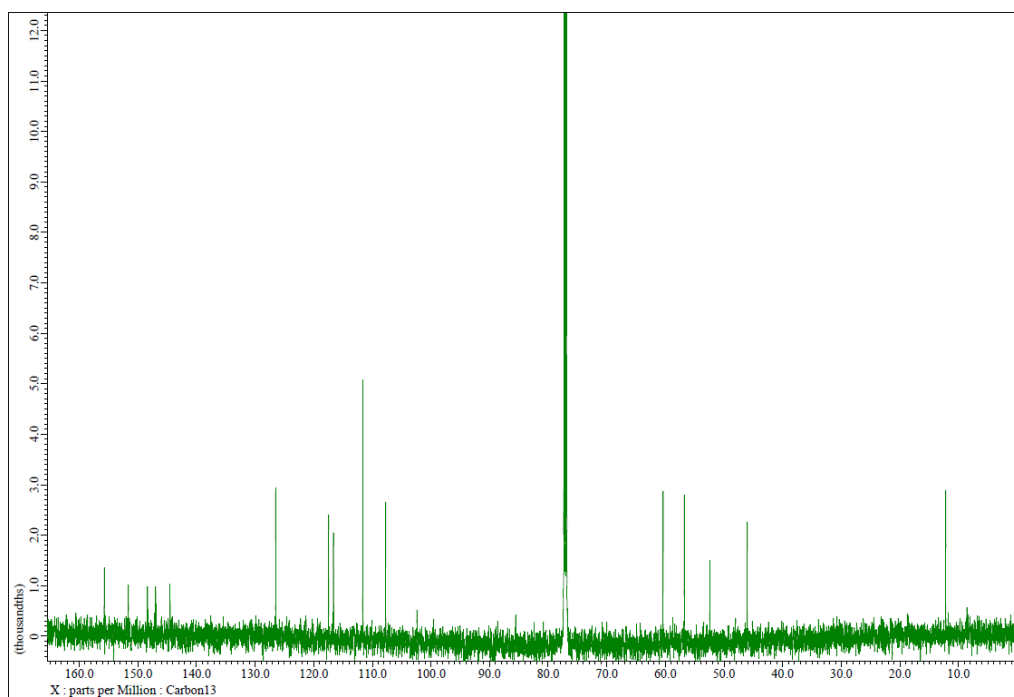
Figure 83 - ^{1}H-NMR of **16** (CDCl$_3$).

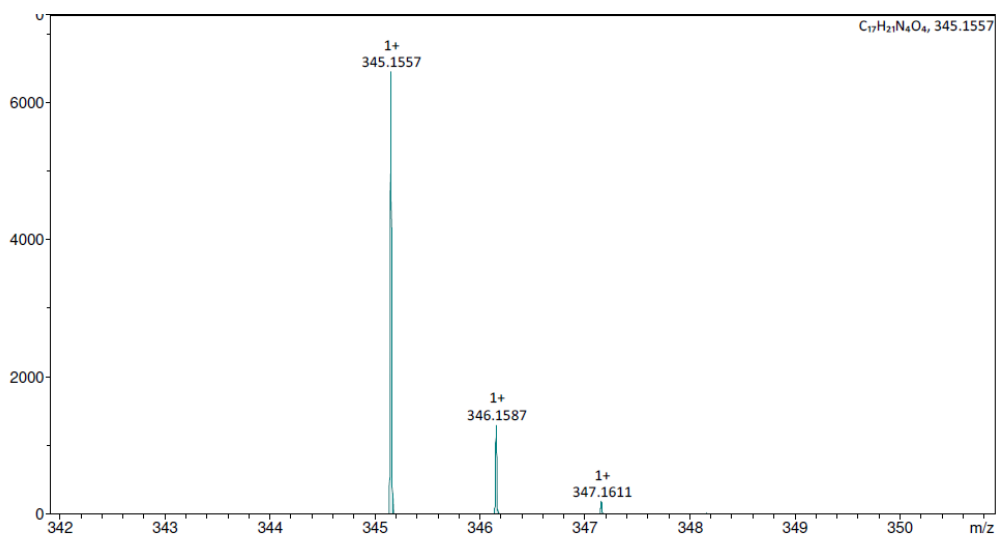*Figure 84* – ^{13}C-NMR of **16** (CDCl$_3$).

Figure 85 - *HRMS of* **16**.

Synthesis of 2-((4-((2,4-dinitrophenyl)diazenyl)phenyl)(ethyl)amino)ethan-1-ol (17):

The procedure is reported in the literature[116,117], and all characterizations were in agreement with the reported data.

Synthesis of 2-(ethyl(4-((4-nitrophenyl)diazenyl)phenyl)amino)ethyl methacrylate (18):

Compound **18** was synthetized according to the procedures reported in the literature, and its characterizations were in agreement with the results reported.[118,119]

Synthesis of 2-((4-((2-chloro-4-nitrophenyl)diazenyl)phenyl)(ethyl)amino)ethyl methacrylate (19):

Compound **19** was synthetized according to the procedures reported in the literature, and its characterizations were in agreement with the results reported.[118,119]

Synthesis of 2-(ethyl(4-((2-methoxy-4-nitrophenyl)diazenyl)phenyl)amino)ethyl methacrylate (20):

150

All glassware was dried before use, and all reactions were performed under an inert atmosphere (Ar). The azodye was dissolved in anhydrous THF, and the solution was put in an ice bath to reach 0°C. Methacryloyl chloride (1.1 eq.) and TEA (1.2 eq.) were added through a syringe, and after 20 minutes, the ice bath was removed, and the temperature was brought to room temperature. The reaction was left under stirring overnight and was monitored with TLC (PE:EtOAc 7:3). The solution was filtered, the solvent was removed under vacuum, maintaining the temperature below 30°C, and then EtOAc was added and extracted three times with water and one time with brine. The organic fractions were collected, dried with Na_2SO_4 and filtered. The product was then purified on a silica gel column with an eluent PE/EtOAc 7:3. The product was recovered as dark red powders.

Yield 93%.

^{1}H-NMR (600 MHz, Chloroform-*d*) δ 7.93 − 7.86 (m, 4H), 7.69 (d, *J* = 8.6 Hz, 1H), 6.81 (d, *J* = 1.5 Hz, 2H), 6.14 − 5.59 (m, 2H), 5.59 (p, *J* = 1.6 Hz, 1H), 4.37 (t, *J* = 6.2 Hz, 2H), 4.09 (s, 3H), 3.73 (t, *J* = 6.2 Hz, 2H), 3.54 (q, *J* = 7.1 Hz, 2H), 1.94 (t, *J* = 1.3 Hz, 3H), 1.26 (t, *J* = 7.1 Hz, 4H).

^{13}C-NMR (151 MHz, Chloroform-*d*) δ 167.41, 155.76, 151.24, 148.37, 146.94, 144.58, 135.96, 126.49, 117.50, 116.63, 111.54, 107.74, 61.83, 56.80, 48.85, 45.70, 18.45, 12.36.

λ_{max} (EtOH): 490 nm
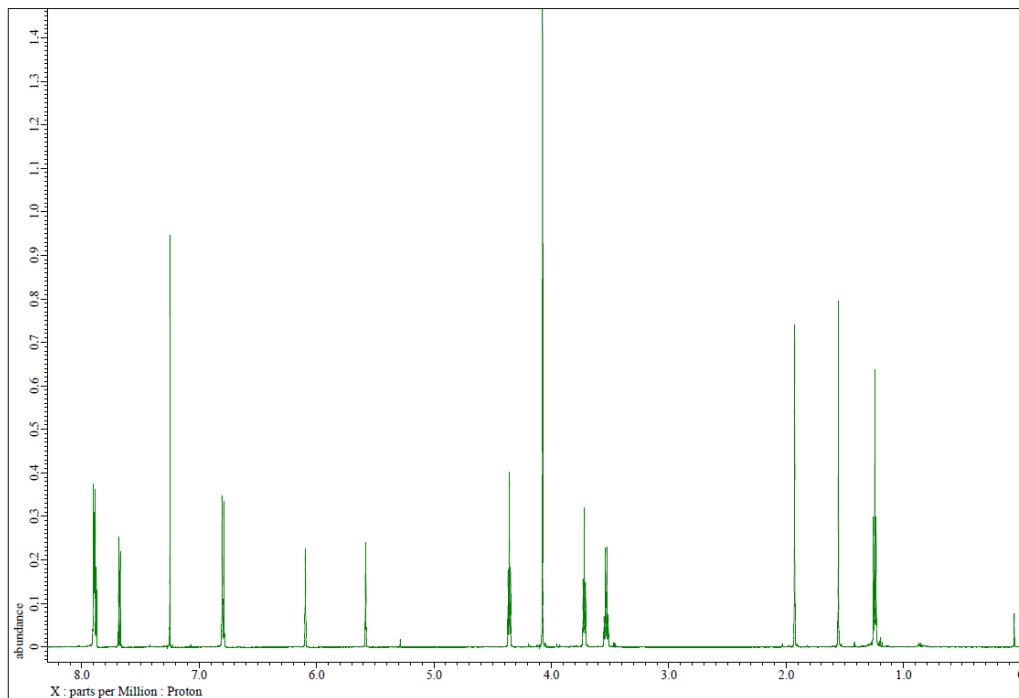
HRMS: calculated 412.1747, found 413.1819 (M+1)

Figure 86 - ^1H-NMR of **20** (CDCl$_3$).
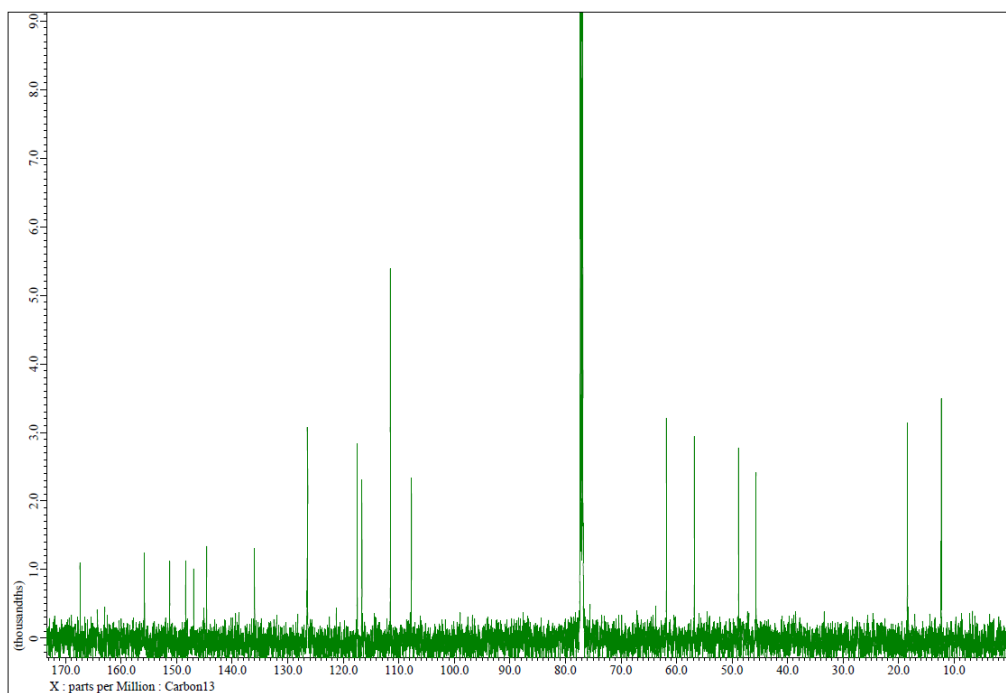

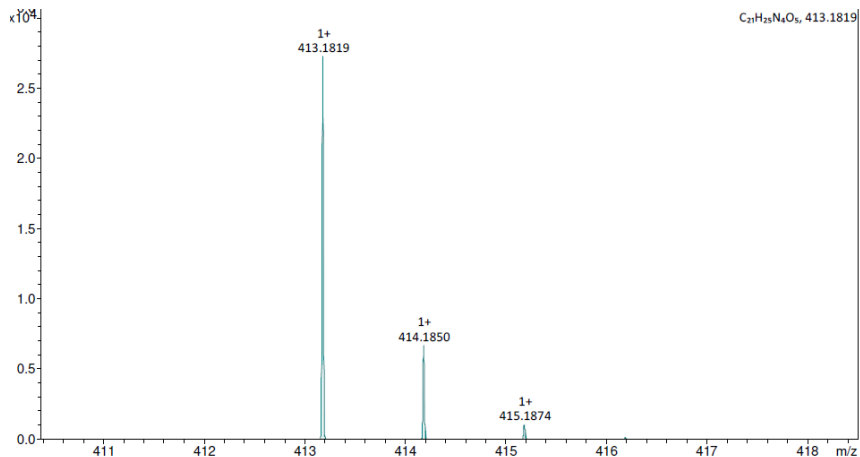*Figure 87* - ^{13}C-NMR of **20** (CDCl$_3$).

Figure 88 – HRMS of **20**.

Synthesis of 2-((4-((2,4-dinitrophenyl)diazenyl)phenyl)(ethyl)amino)ethyl methacrylate (21):

Yield 82%

^{1}H-NMR (600 MHz, Chloroform-*d*) δ 8.39 (d, *J* = 2.4 Hz, 1H), 8.15 (dd, *J* = 8.9, 2.4 Hz, 1H), 7.97 – 7.92 (m, 2H), 7.78 (d, *J* = 8.9 Hz, 1H), 6.85 – 6.80 (m, 2H), 6.14 – 5.59 (m, 2H), 4.38 (t, *J* = 6.3 Hz, 2H), 3.75 (t, *J* = 6.3 Hz, 2H), 3.56 (q, *J* = 7.1 Hz, 2H), 1.94 (s, 3H), 1.27 (t, *J* = 7.1 Hz, 3H).

^{13}C-NMR (151 MHz, Chloroform-d) δ 167.44, 153.21, 151.85, 147.30, 144.56, 135.95, 134.14, 127.10, 126.50, 126.17, 122.76, 118.17, 111.68, 77.37, 61.74, 48.91, 45.86, 18.49, 12.41.

λ$_{max}$ (EtOH): 520 nm

HR-ESI-MS: calculated 427.1492, found 450.1384 (M + Na^{+})

153
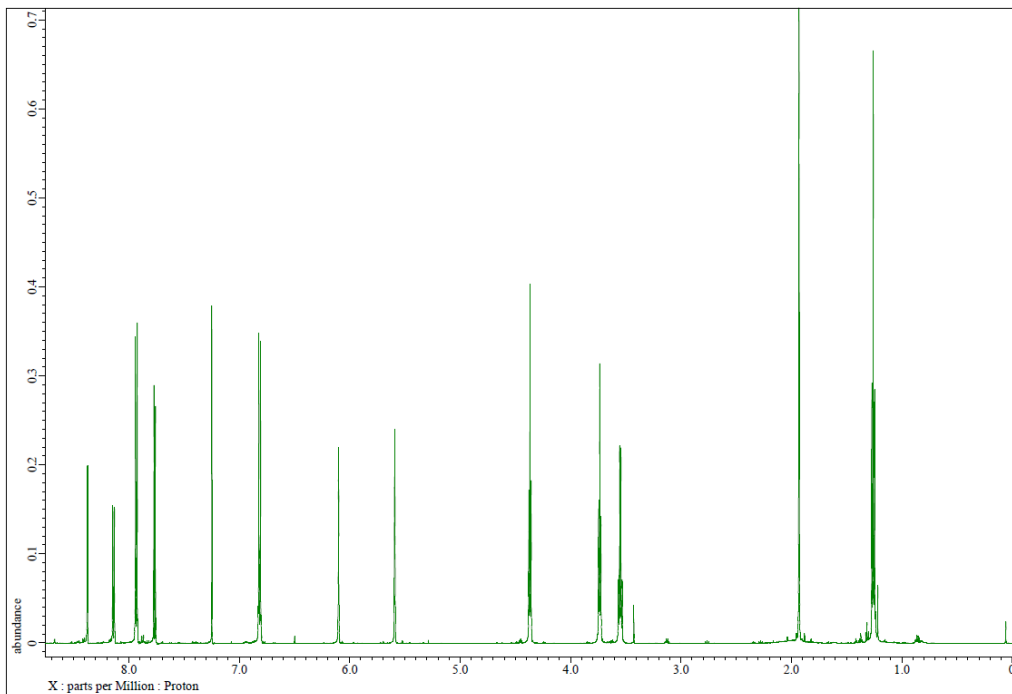
Figure 89 - ^{1}*H-NMR of* **21** *(CDCl$_3$).*
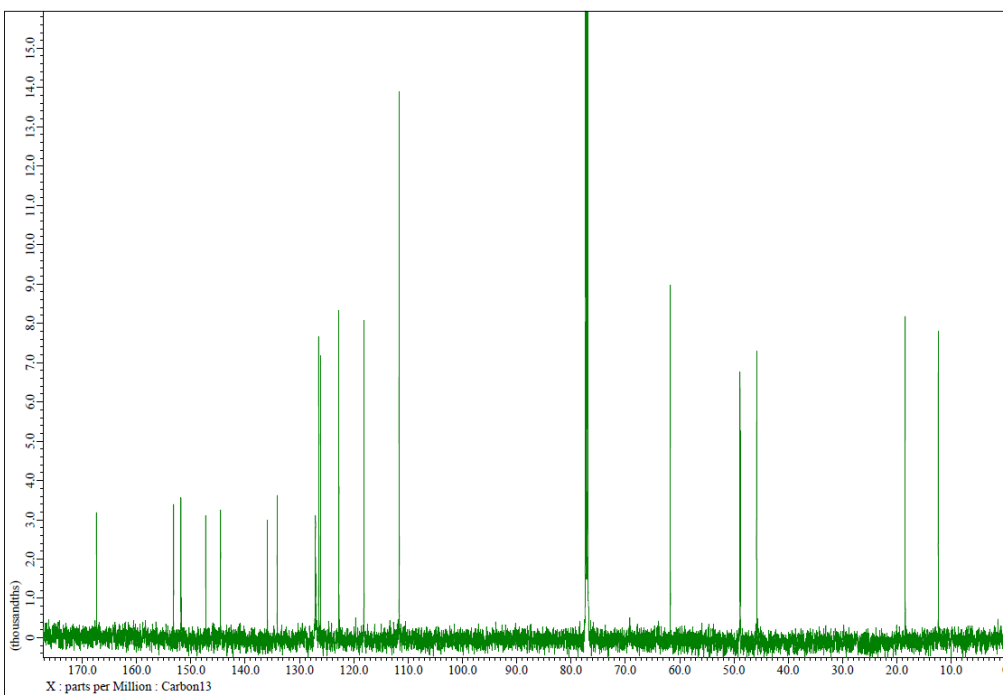
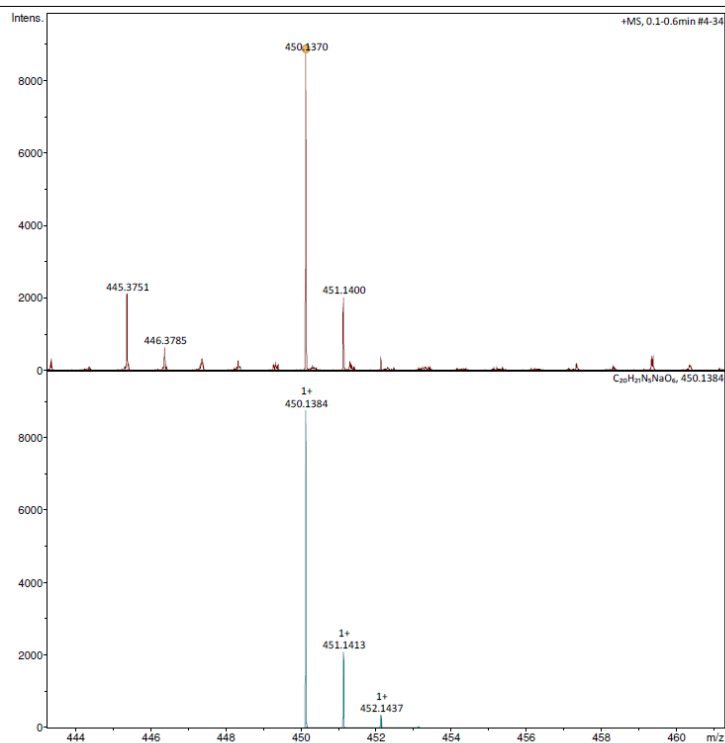*Figure 90* - ^{13}*C-NMR of* **21** *(CDCl$_3$).*

Figure 91 - *HRMS of **21**.*

Synthesis of 2-(ethyl(4-((4-nitrophenyl)diazenyl)phenyl)amino)ethyl acrylate (22):

Compound **22** was synthetized following the reported procedure[120], and its characterization agrees with the reported data. Yield: 92%

Synthesis of 2-((4-((2-chloro-4-nitrophenyl)diazenyl)phenyl)(ethyl)amino)ethyl acrylate (23):

Compound **23** was synthetized following the reported procedure[120], and its characterization agrees with the reported data. Yield 90%.

Synthesis of (E)-2-(ethyl(4-((2-methoxy-4-nitrophenyl)diazenyl)phenyl)amino)ethyl acrylate (24):

The azodye **16** was put in a dried round bottom flask under an inert Ar atmosphere and completely dissolved with anhydrous THF under stirring. The flask was put in an ice bath, and 1.1 eq of triethylamine (TEA) was added by a syringe. Then freshly distilled

acryloyl chloride (1.2 eq) was added dropwise over 15 minutes, and after 30 minutes from the last addition, the ice bath was removed, and the reaction was left for 24 h, monitoring with TLC (EP/EtOAc 1:1). The solution is filtrated and washed with EtOAc to recover the desired product when the reaction is completed. The solvents were distilled under vacuum at a temperature below 30°C. The solid was recovered with EtOAc, put in a separation funnel, and extracted 3 times with water and 2 times with brine. The organic fractions were combined, and the solvent was distilled under vacuum at 30°C; instead, the aqueous fractions were extracted again with EtOAc until they became clear. The final product was obtained as a dark red solid.

Yield: 92%.

^{1}H-NMR (600 MHz, Chloroform-*d*) δ 7.96 – 7.86 (m, 4H), 7.69 (d, *J* = 8.6 Hz, 1H), 6.83 – 6.79 (m, 2H), 6.41 (dd, *J* = 17.2, 1.4 Hz, 1H), 6.12 (dd, *J* = 17.3, 10.4 Hz, 1H), 5.86 (dd, *J* = 10.4, 1.3 Hz, 1H), 4.38 (t, *J* = 6.2 Hz, 2H), 4.08 (s, 3H), 3.72 (t, *J* = 6.2 Hz, 2H), 3.54 (q, *J* = 7.1 Hz, 2H), 1.26 (t, *J* = 7.1 Hz, 3H).

^{13}C-NMR (151 MHz, Chloroform-*d*) δ 166.11, 155.77, 151.19, 148.38, 146.93, 144.60, 131.66, 128.03, 126.48, 117.49, 116.63, 111.52, 107.75, 61.56, 56.81, 48.91, 45.80, 12.38.

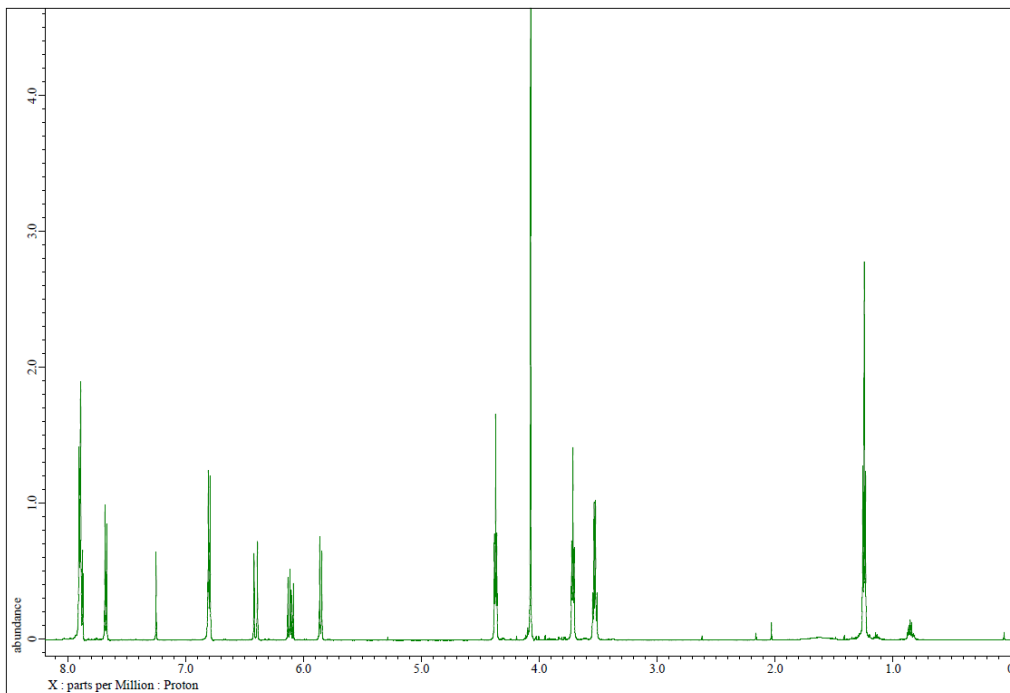HR-ESI-MS: calculated 398.1590, found 399.1663 (M + 1)
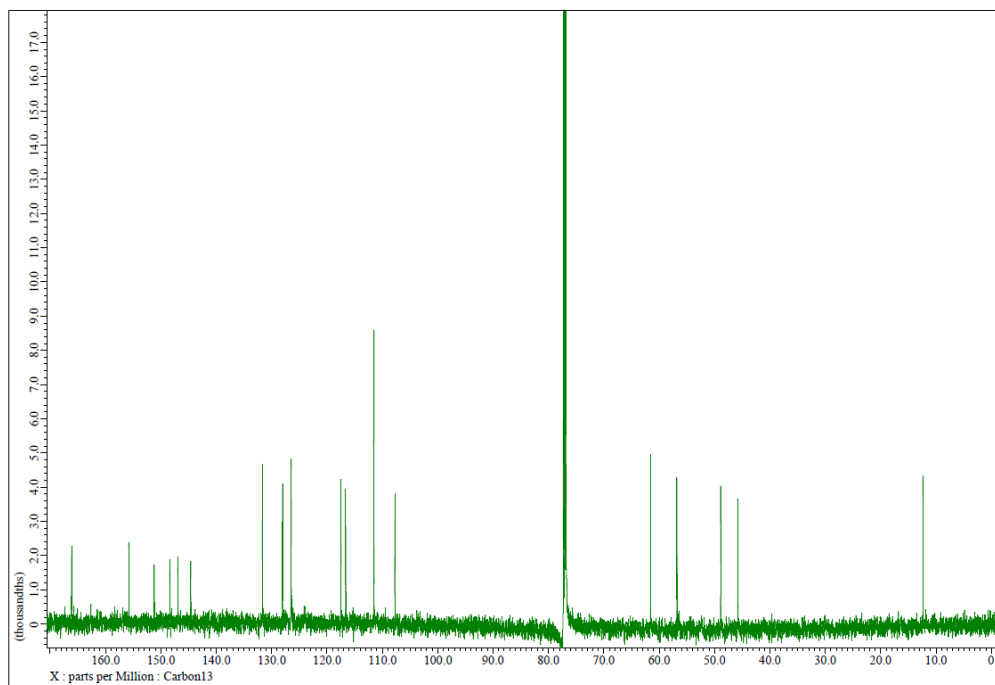
Figure 92 - ^{1}*H-NMR of compound* **24** *(CDCl$_3$).*

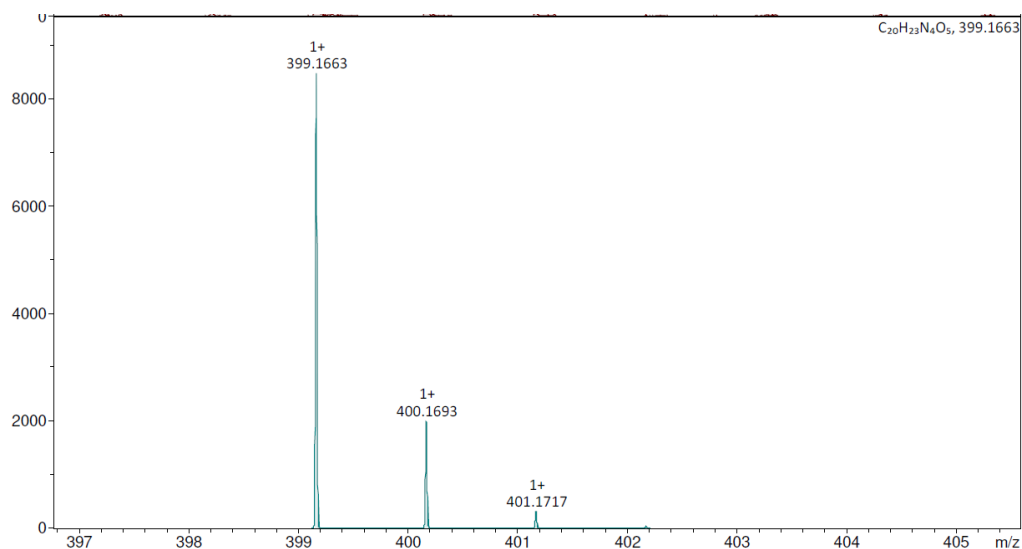*Figure 93* – ^{13}*C-NMR of compound* **24**.

157

Figure 94 - HRMS of compound *24*.

Synthesis of 2-((4-((2,4-dinitrophenyl)diazenyl)phenyl)(ethyl)amino)ethyl acrylate (25):

The azodye **17** was put in a dried round bottom flask under an inert Ar atmosphere and completely dissolved with anhydrous THF under stirring. The flask was put in an ice bath, and 1.1 eq of triethylamine (TEA) was added by a syringe. Then freshly distilled acryloyl chloride (1.2 eq) was added dropwise over 15 minutes, and after 30 minutes from the last addition, the ice bath was removed, and the reaction was left for 24 h, monitoring with TLC (EP/EtOAc 1:1). The solution is filtrated and washed with EtOAc to recover the desired product when the reaction is completed. The solvents were distilled under vacuum at a temperature below 30°C. The solid was recovered with EtOAc, put in a separation funnel, and extracted 3 times with water and 2 times with brine. The organic fractions were combined, and the solvent was distilled under vacuum at 30°C; instead, the aqueous fractions were extracted again with EtOAc until they became clear. The final product was obtained as a dark red solid.

Yield: 87%.

¹H-NMR (600 MHz, Chloroform-*d*) δ 8.39 (d, 1H), 8.15 (dd, *J* = 8.9, 2.4 Hz, 1H), 7.94 (d, *J* = 9.1 Hz, 2H), 7.77 (d, *J* = 8.9 Hz, 1H), 6.82 (d, *J* = 9.2 Hz, 2H), 6.42 (dd, *J* = 17.4, 1.3 Hz, 1H), 6.13 (dd, *J* = 17.3, 10.5 Hz, 1H), 5.87 (dd, *J* = 10.4, 1.3 Hz, 1H), 4.39 (t, *J* = 6.3 Hz, 2H), 3.74 (t, *J* = 6.3 Hz, 2H), 3.56 (q, *J* = 7.1 Hz, 2H), 1.27 (t, *J* = 7.1 Hz, 3H).

¹³C-NMR (151 MHz, Chloroform-*d*) δ 166.06, 152.55, 149.42, 146.60, 146.06, 144.52, 131.84, 127.91, 127.31, 120.06, 119.70, 111.80, 61.38, 49.00, 46.02, 12.39.

HR-ESI-MS: calculated 413.1335, found 436.1228 (M + Na⁺)

Figure 95 *- ¹H-NMR of compound **25** (CDCl₃).*

^{1}H-NMR (600 MHz, Chloroform-*d*) δ 8.39 (d, 1H), 8.15 (dd, *J* = 8.9, 2.4 Hz, 1H), 7.94 (d, *J* = 9.1 Hz, 2H), 7.77 (d, *J* = 8.9 Hz, 1H), 6.82 (d, *J* = 9.2 Hz, 2H), 6.42 (dd, *J* = 17.4, 1.3 Hz, 1H), 6.13 (dd, *J* = 17.3, 10.5 Hz, 1H), 5.87 (dd, *J* = 10.4, 1.3 Hz, 1H), 4.39 (t, *J* = 6.3 Hz, 2H), 3.74 (t, *J* = 6.3 Hz, 2H), 3.56 (q, *J* = 7.1 Hz, 2H), 1.27 (t, *J* = 7.1 Hz, 3H).

^{13}C-NMR (151 MHz, Chloroform-*d*) δ 166.06, 152.55, 149.42, 146.60, 146.06, 144.52, 131.84, 127.91, 127.31, 120.06, 119.70, 111.80, 61.38, 49.00, 46.02, 12.39.

HR-ESI-MS: calculated 413.1335, found 436.1228 (M + Na^{+})

Figure 95 *- ^{1}H-NMR of compound **25** (CDCl$_3$).*

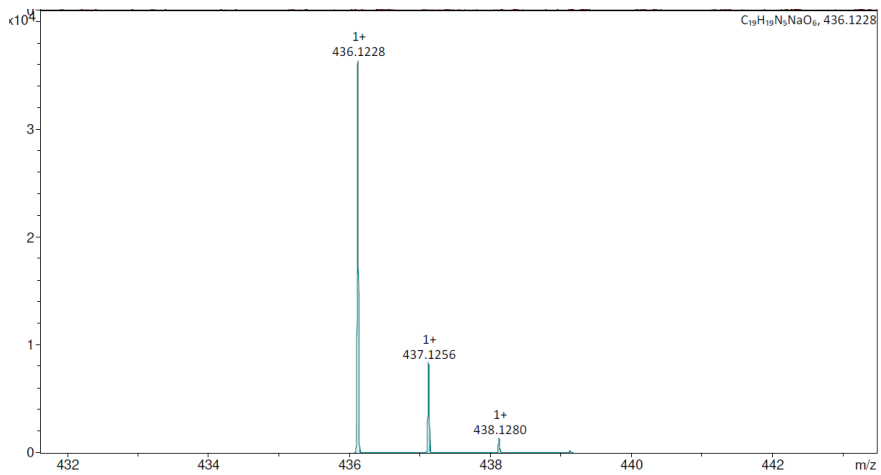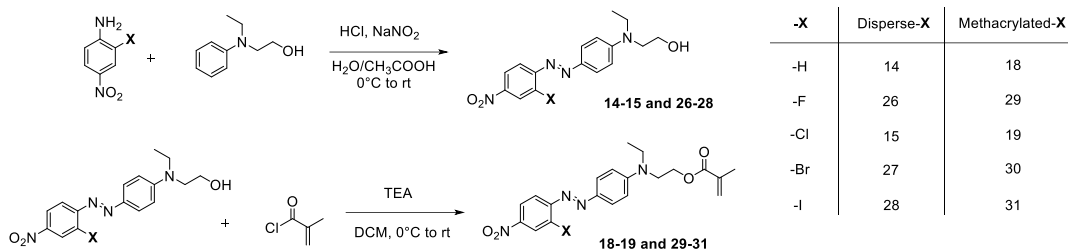**Figure 96** –¹³C-NMR of compound **25** (CDCl₃).

Figure 97 - HRMS of compound **25**.

Synthesis of 2-(ethyl(4-((2-fluoro-4-nitrophenyl)diazenyl)phenyl)amino)ethan-1-ol (26):

The aniline was dissolved in 50 ml of H2O/CH3COOH (1:4) solution under stirring in a round bottom flask. The mixture was heated until it became clear, then the flask was put in an ice bath, and the temperature was monitored to reach 0-5°C. NaNO$_2$ (1.1 eq) was dissolved in deionized water, brought to 0-5°C and added dropwise to the aniline solution. After 30 minutes, the N-Ethyl-N-hydroxyethylaniline (1.2 eq) was dissolved in H$_2$O, and 1 mL of HCl was added: this solution was dripped in the first one under vigorous stirring. The reaction was left for 3 h and then was poured into crushed ice to obtain a red precipitate that was filtered, washed with cold water and dried.

Yields 84%

^{1}H NMR (600 MHz, Chloroform-*d*) δ 8.09 − 8.03 (m, 2H), 7.89 (d, *J* = 9.3 Hz, 2H), 7.82 (dd, *J* = 8.8, 7.5 Hz, 1H), 6.79 (d, *J* = 9.4 Hz, 2H), 3.90 (t, *J* = 6.0 Hz, 2H), 3.62 (t, *J* = 6.0 Hz, 2H), 3.57 (q, *J* = 7.2 Hz, 2H), 1.26 (t, *J* = 7.1 Hz, 3H).

^{13}C-NMR (151 MHz, Chloroform-*d*) δ 159.03, 157.31, 152.18, 147.54, 145.54, 144.36, 126.87, 119.89, 118.40, 113.04, 112.88, 111.66, 60.37, 52.47, 46.14, 12.20.

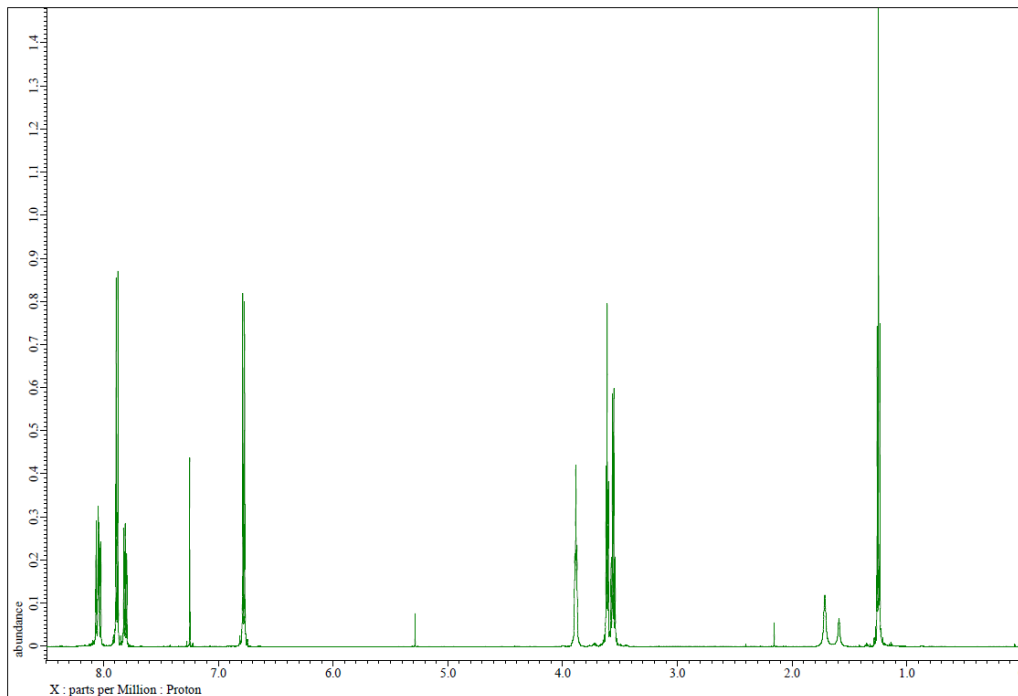HR-ESI-MS: calculated 332.1285, found 333.1357 (M + 1)
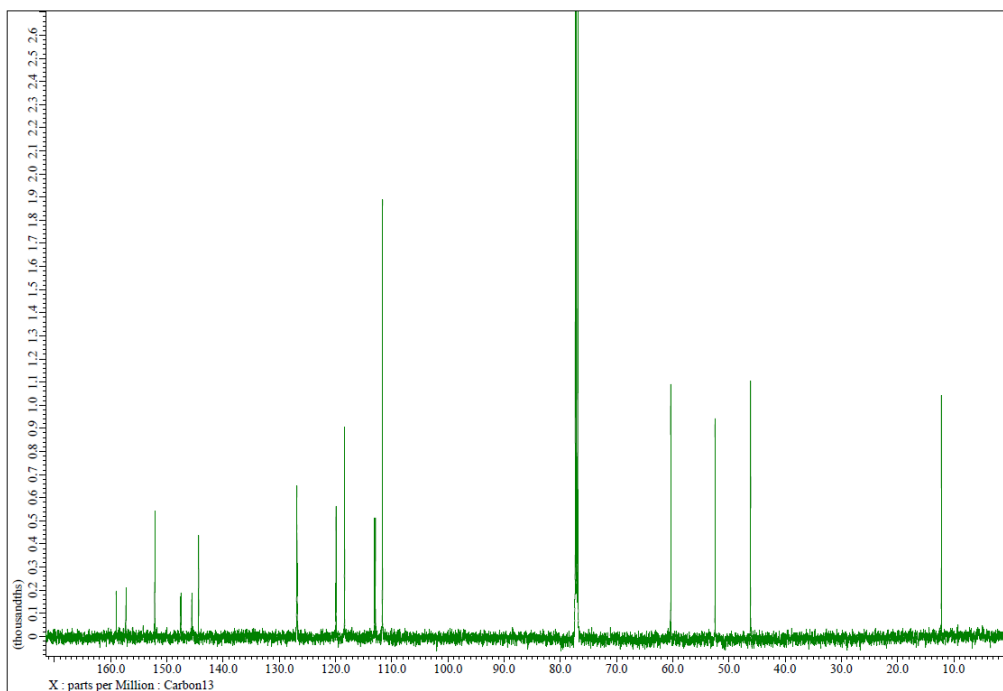
Figure 98 - ^{1}H-NMR of compound **26** (CDCl$_3$).

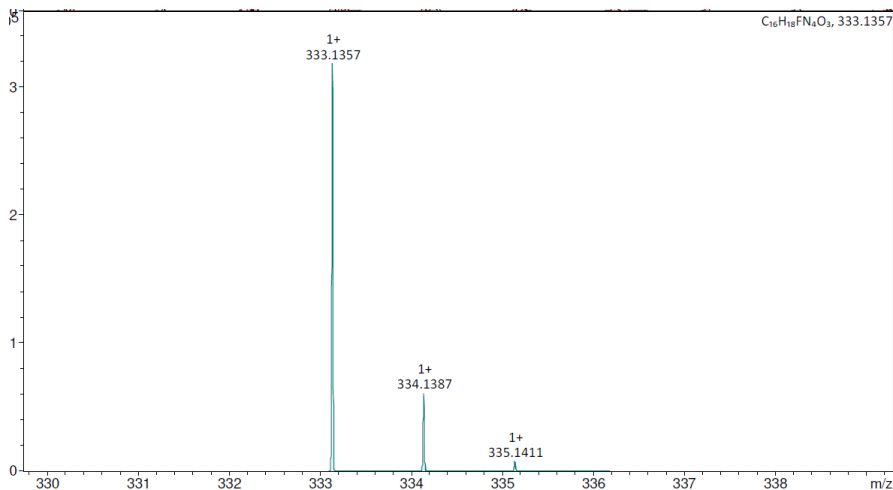*Figure 99* - ^{13}C-NMR of compound **26** (CDCl$_3$).

Figure 100 - *HRMS of compound **26**.*

Synthesis of 2-((4-((2-bromo-4-nitrophenyl)diazenyl)phenyl)(ethyl)amino)ethan-1-ol (27):

The aniline was dissolved in 50 ml of H_2O/CH_3COOH (1:4) solution under stirring in a round bottom flask. The mixture was heated until it became clear, then the flask was put in an ice bath, and the temperature was monitored to reach 0-5°C. $NaNO_2$ (1.1 eq) was dissolved in deionized water, brought to 0-5°C and added dropwise to the aniline solution. After 30 minutes, the N-Ethyl-N-hydroxyethylaniline (1.2 eq) was dissolved in H_2O, and 1 mL of HCl was added: this solution was dripped in the first one under vigorous stirring. The reaction was left for 3 h and then was poured into crushed ice to obtain a red precipitate that was filtered, washed with cold water and dried.

Yields: 92%.

^{1}H-NMR (600 MHz, Chloroform-*d*) δ 8.53 (d, *J* = 2.4 Hz, 1H), 8.16 (dd, *J* = 8.7, 2.4 Hz, 1H), 7.91 (d, *J* = 9.4 Hz, 2H), 7.71 (d, *J* = 8.9 Hz, 1H), 6.79 (d, *J* = 9.5 Hz, 2H), 3.90 (t, *J* = 4.2 Hz, 2H), 3.62 (t, *J* = 5.9 Hz, 2H), 3.57 (q, *J* = 7.2 Hz, 2H), 1.26 (t, *J* = 7.1 Hz, 3H).

^{13}C-NMR (151 MHz, Chloroform-*d*) δ 154.12, 152.26, 147.29, 144.33, 129.12, 123.97, 123.40, 118.08, 111.75, 60.42, 52.54, 46.22, 12.25.

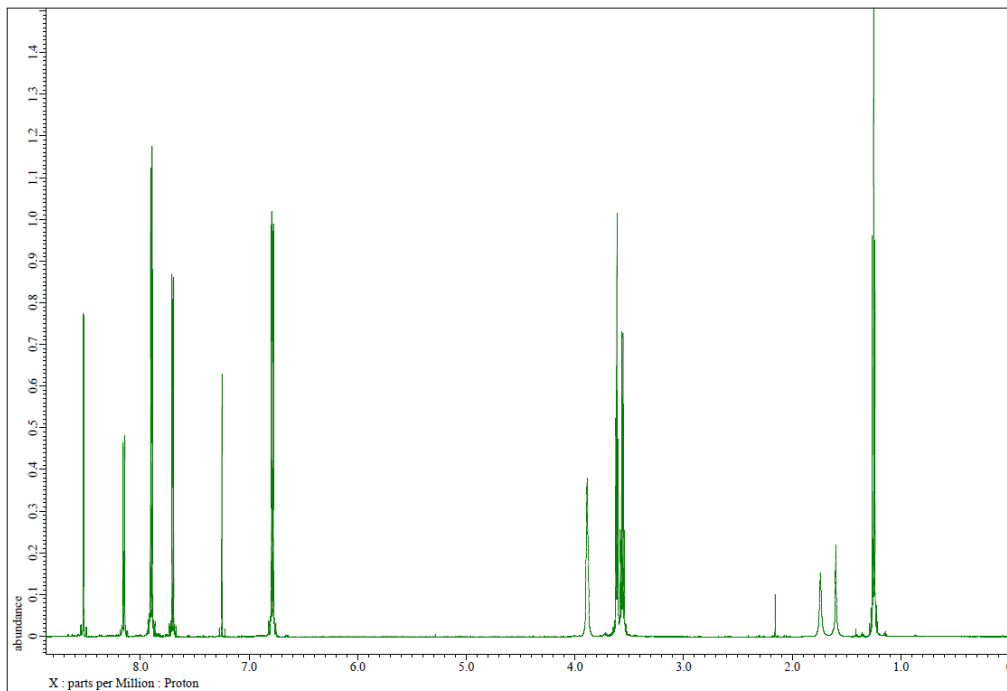HR-ESI-MS: calculated 392.0484 and 394.0464 ($M^{79}Br$ and $M^{81}Br$), found 393.0557 395.0538 [($M^{79}Br$ + 1) and ($M^{81}Br$ + 1)].
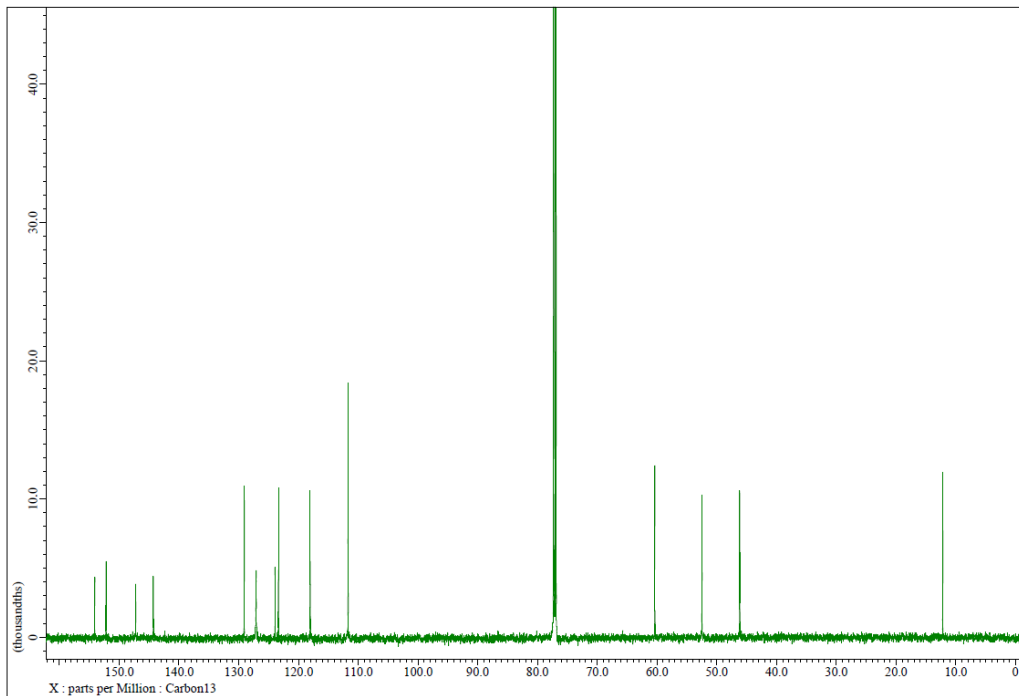
Figure 101 - ^{1}H-NMR of compound *27* (CDCl$_3$).

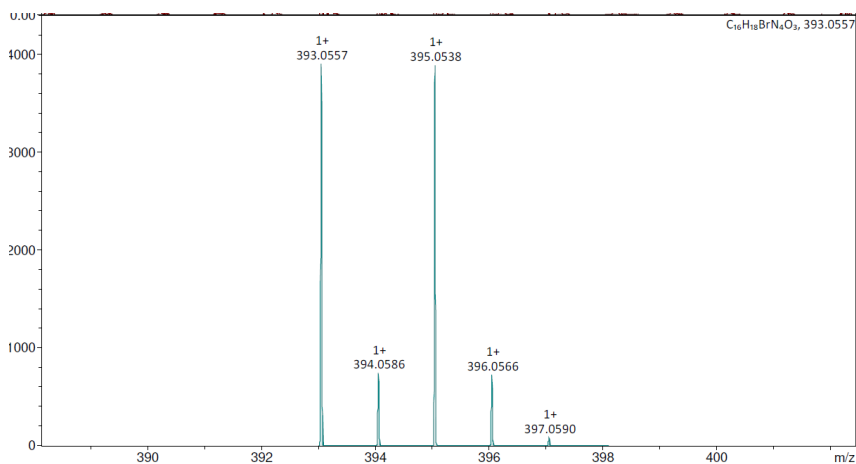*Figure 102 – ^{13}C-NMR of compound 27 (CDCl₃).*

Figure 103 - HRMS of compound 27.

Synthesis of 2-(ethyl(4-((2-iodo-4-nitrophenyl)diazenyl)phenyl)amino)ethan-1-ol (28):

The aniline was dissolved in 50 ml of H_2O/CH_3COOH (1:4) solution under stirring in a round bottom flask. The mixture was heated until it became clear, then the flask was put in an ice bath, and the temperature was monitored to reach 0-5°C. $NaNO_2$ (1.1 eq)

was dissolved in deionized water, brought to 0-5°C and added dropwise to the aniline solution. After 30 minutes, the N-Ethyl-N-hydroxyethylaniline (1.2 eq) was dissolved in H_2O, and 1 mL of HCl was added: this solution was dripped in the first one under vigorous stirring. The reaction was left for 3 h and then was poured into crushed ice to obtain a red precipitate that was filtered, washed with cold water and dried.

Yields: 81%.

^{1}H NMR (600 MHz, Chloroform-*d*) δ 8.80 (d, *J* = 2.4 Hz, 1H), 8.24 (dd, *J* = 8.8, 2.4 Hz, 1H), 7.95 (d, *J* = 9.4 Hz, 2H), 7.66 (d, *J* = 8.9 Hz, 1H), 6.82 (d, *J* = 9.3 Hz, 2H), 3.90 (t, *J* = 6.9 Hz, 2H), 3.64 (t, *J* = 5.9 Hz, 2H), 3.59 (q, *J* = 7.1 Hz, 2H), 1.27 (t, *J* = 7.1 Hz, 3H).

^{13}C NMR (151 MHz, Chloroform-*d*) δ 155.70, 152.24, 147.47, 144.11, 134.99, 127.29, 124.35, 117.22, 111.82, 99.92, 60.46, 52.56, 46.24, 12.28.

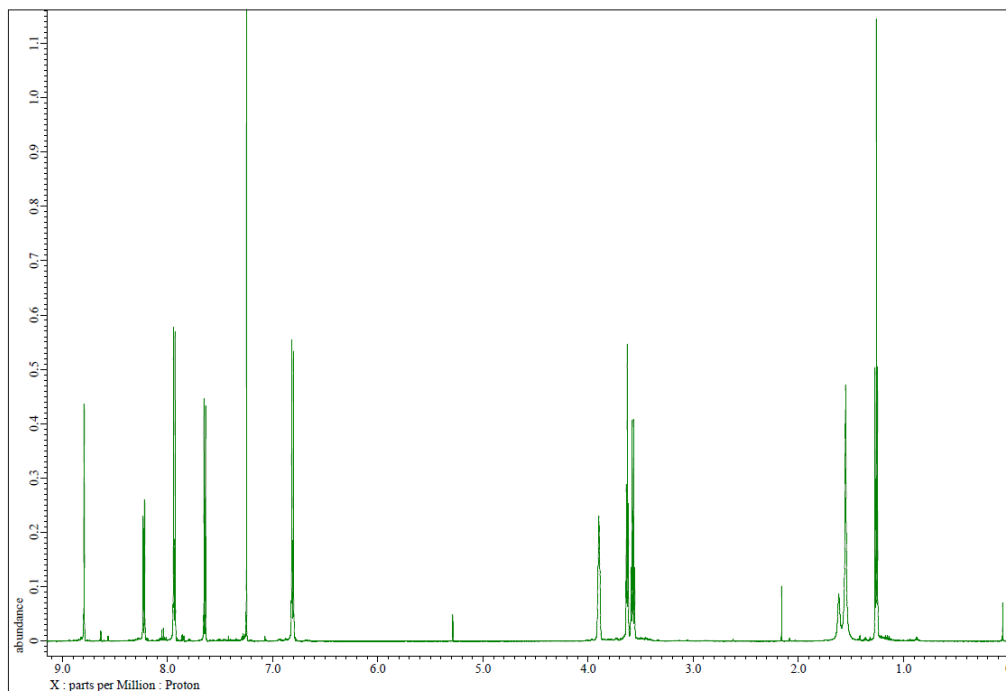HR-ESI-MS: calculated 440.0345, found 441.0418 (M + 1)

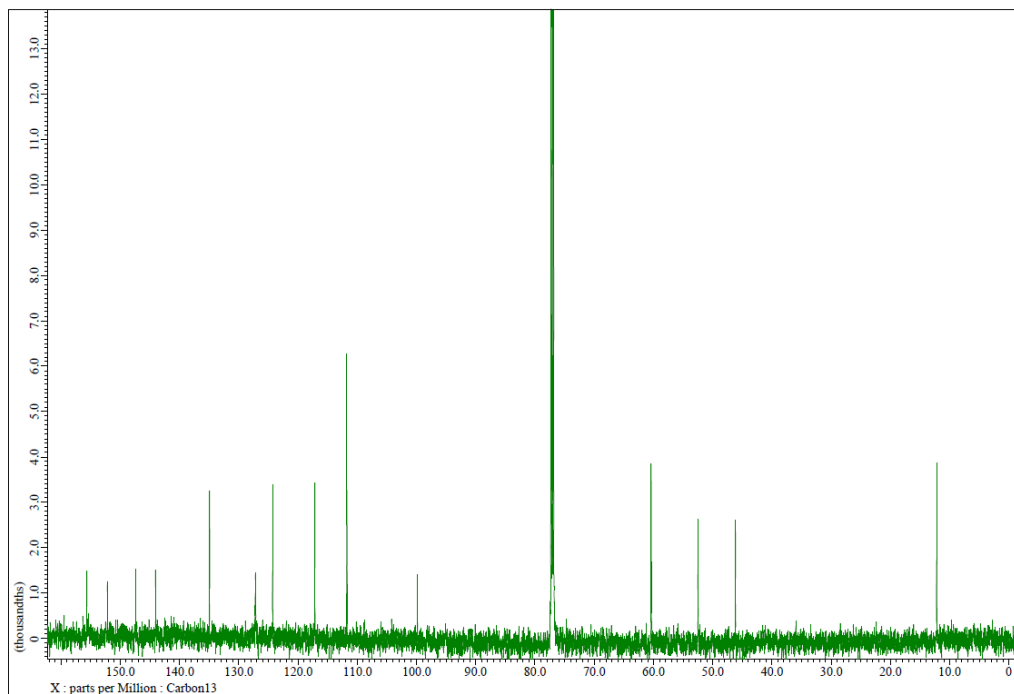***Figure 104*** - [1]*H-NMR of compound **28** (CDCl₃).*

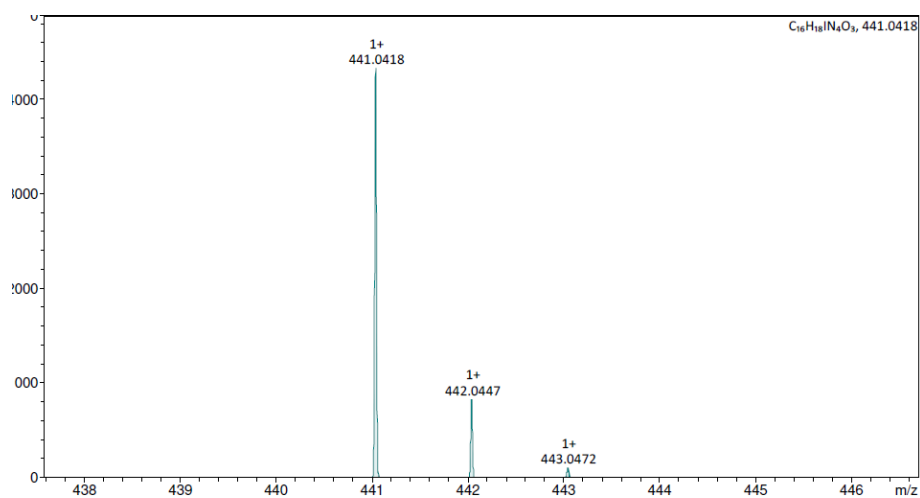*Figure 105* – ^{13}C-NMR of compound *28* (CDCl$_3$).

Figure 106 – HRMS of compound *28*.

Synthesis of 2-(ethyl(4-((2-fluoro-4-nitrophenyl)diazenyl)phenyl)amino)ethyl methacrylate (29):

Compound **26** was put in a dried round bottom flask under an inert Ar atmosphere and completely dissolved with anhydrous THF under stirring. Then the flask was put in an ice bath, and 1.1 eq of triethylamine (TEA) was added by a syringe. Then freshly distilled methacryloyl chloride (1.2 eq) was added dropwise for 15 minutes, and after 30 minutes from the last addition, the ice bath was removed, and the reaction was left for 24 h monitoring with TLC (EP/EtOAc 1:1). The solution is filtrated and washed with EtOAc to recover the desired product when the reaction is completed. The solvents were distilled under vacuum at a temperature below 25°C. The solid was recovered with EtOAc, put in a separation funnel, and extracted 3 times with water and 2 times with brine. The organic fractions were combined, and the solvent was distilled under vacuum at 25°C; instead, the aqueous fractions were extracted again with EtOAc until they became clear. The final product was obtained as a dark red solid.

Yield: 88%.

29:

^{1}H-NMR (600 MHz, Chloroform-*d*) δ 8.12 – 8.04 (m, 2H), 7.92 (d, J = 8.6 Hz, 2H), 7.87 – 7.81 (m, 1H), 6.82 (d, J = 9.3 Hz, 2H), 6.13 – 6.08 (m, 1H), 5.63 – 5.57 (m, 1H), 4.37 (t, J = 6.2 Hz, 2H), 3.74 (t, J = 6.2 Hz, 2H), 3.56 (q, J = 7.1 Hz, 2H), 1.94 (dd, J = 1.6, 1.0 Hz, 3H), 1.27 (t, J = 7.1 Hz, 3H).

^{13}C-NMR (151 MHz, Chloroform-d) δ 167.43, 159.13, 157.41, 151.84, 144.53, 135.97, 126.91, 126.45, 119.96, 112.94, 111.66, 61.79, 48.91, 45.82, 18.47, 12.41.

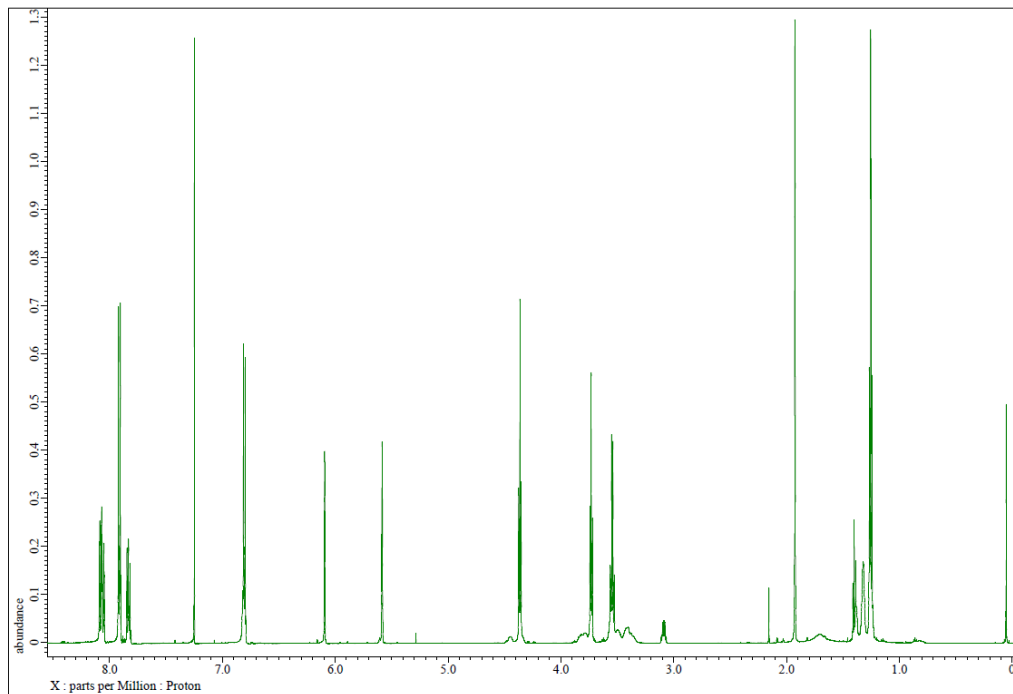HR-ESI-MS: calculated 400.1547, found 401.1620 (M + 1)
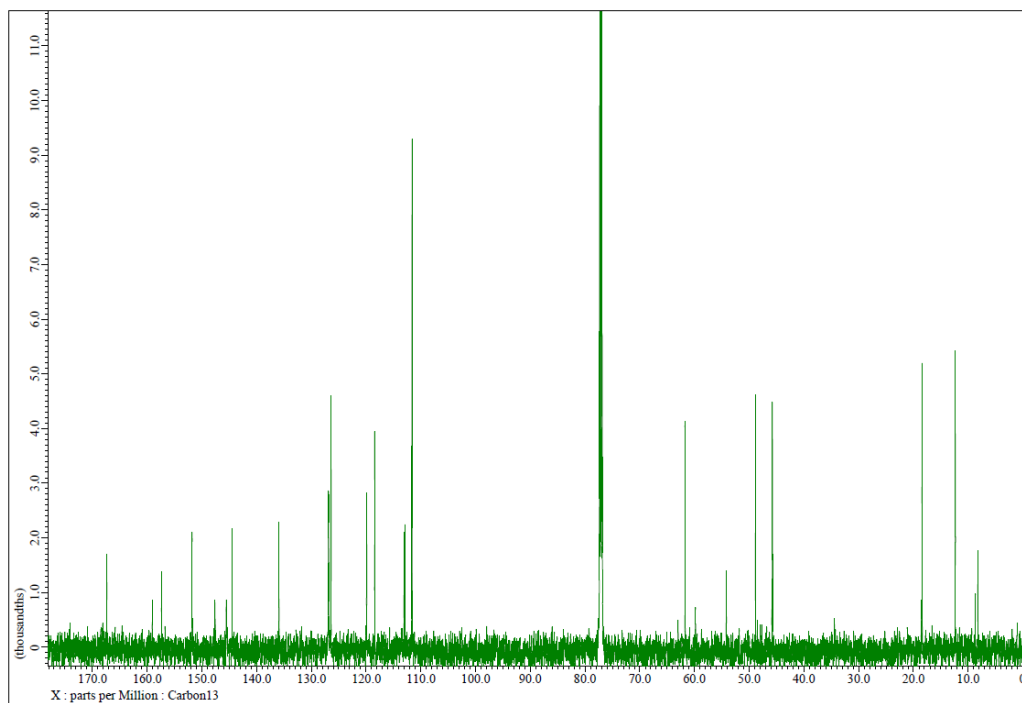
Figure 107 - ¹H-NMR of compound **29** (CDCl₃).

Figure 108 - ¹³C-NMR of compound **29** (CDCl₃).
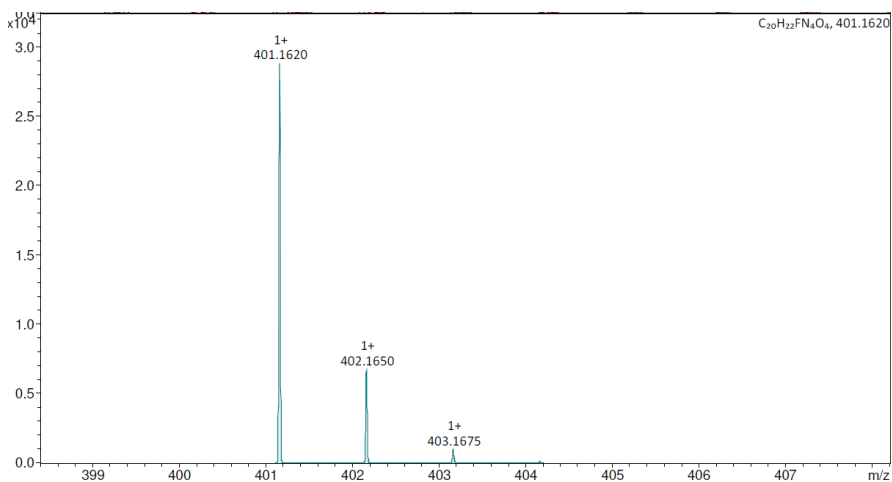
Figure 109 - HRMS of compound **29**.

Synthesis of 2-((4-((2-bromo-4-nitrophenyl)diazenyl)phenyl)(ethyl)amino)ethyl methacrylate (30):

Compound **27** was put in a dried round bottom flask under an inert Ar atmosphere and completely dissolved with anhydrous THF under stirring. Then the flask was put in an ice bath, and 1.1 eq of triethylamine (TEA) was added by a syringe. Then freshly distilled methacryloyl chloride (1.2 eq) was added dropwise for 15 minutes, and after 30 minutes from the last addition, the ice bath was removed, and the reaction was left for 24 h monitoring with TLC (EP/EtOAc 1:1). The solution is filtrated and washed with EtOAc to recover the desired product when the reaction is completed. The solvents were distilled under vacuum at a temperature below 25°C. The solid was recovered with EtOAc, put in a separation funnel, and extracted 3 times with water and 2 times with brine. The organic fractions were combined, and the solvent was distilled under vacuum at 25°C; instead, the aqueous fractions were extracted again with EtOAc until they became clear. The final product was obtained as a dark red solid.

Yields: **30**: 91%.

^{1}H-NMR (600 MHz, Chloroform-*d*) δ 8.55 (d, *J* = 2.4 Hz, 1H), 8.18 (dd, *J* = 8.8, 2.4 Hz, 1H), 7.94 (d, *J* = 8.9 Hz, 2H), 7.73 (d, *J* = 8.9 Hz, 1H), 6.82 (d, *J* = 8.7 Hz, 2H), 6.11 (s, 1H),

5.60 (s, 1H), 4.38 (t, J = 6.2 Hz, 2H), 3.74 (t, J = 6.3 Hz, 2H), 3.56 (q, J = 7.1 Hz, 2H), 1.94 (s, 3H), 1.27 (t, J = 7.1 Hz, 4H).

^{13}C-NMR (151 MHz, Chloroform-d) δ 167.40, 154.06, 151.83, 147.34, 144.43, 135.94, 129.09, 127.11, 126.45, 124.01, 123.38, 118.09, 111.69, 61.70, 48.91, 45.87, 18.46, 12.40.

HR-ESI-MS: calculated 460.0746 and 462.0726 ($M^{79}Br$ and $M^{81}Br$), found 461.0819 and 463.0801 [($M^{79}Br$ + 1) and ($M^{81}Br$ + 1)].
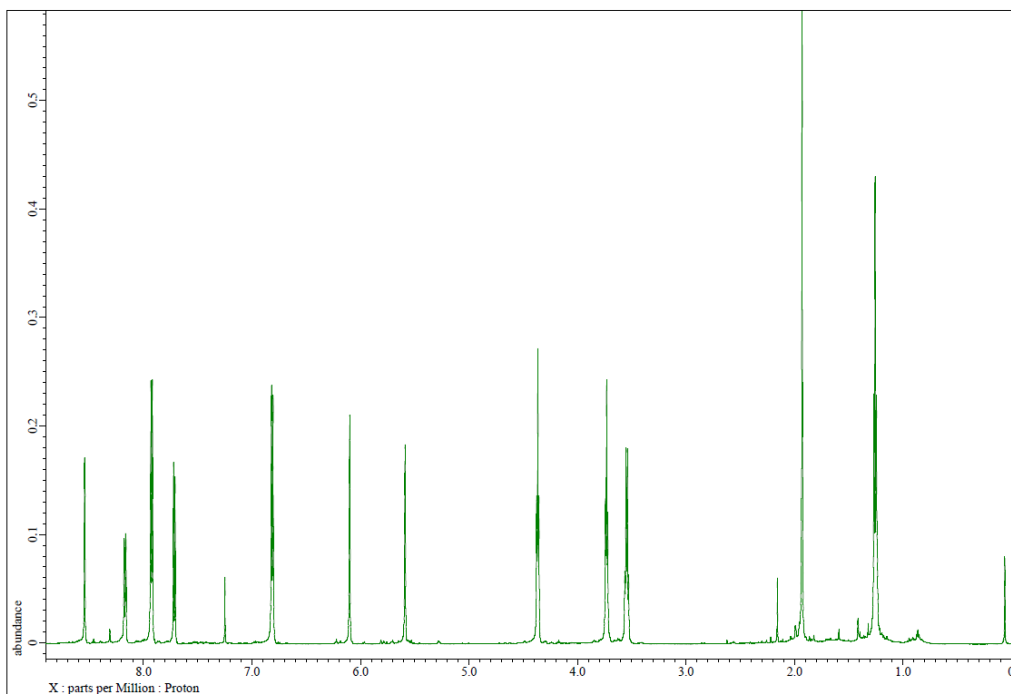

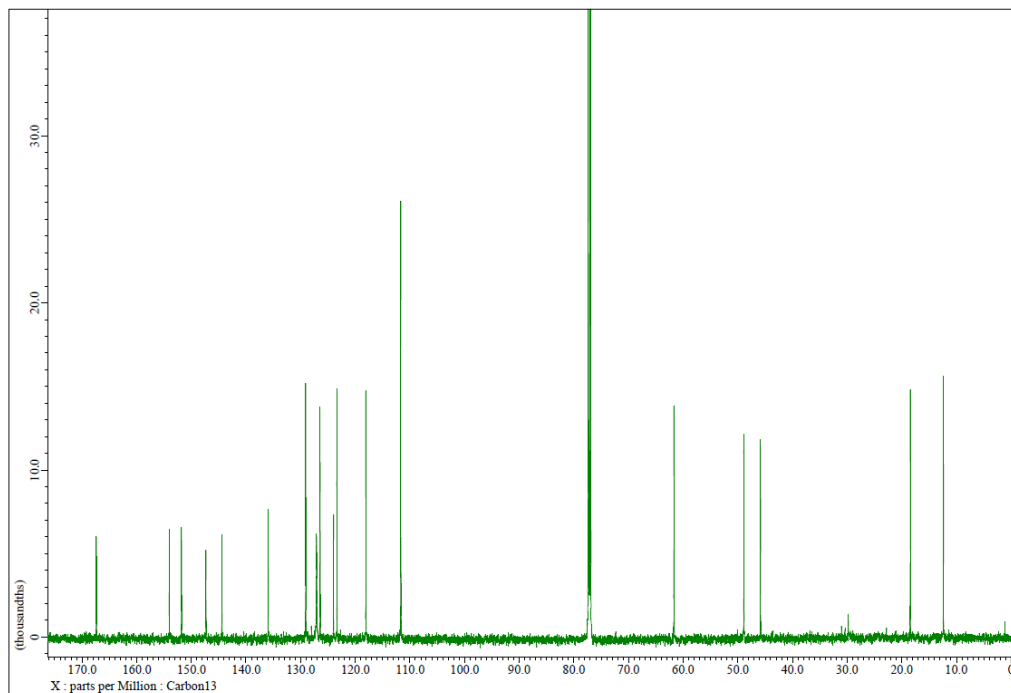*Figure 110 – ^{1}H-NMR of compound 30 (CDCl₃).*

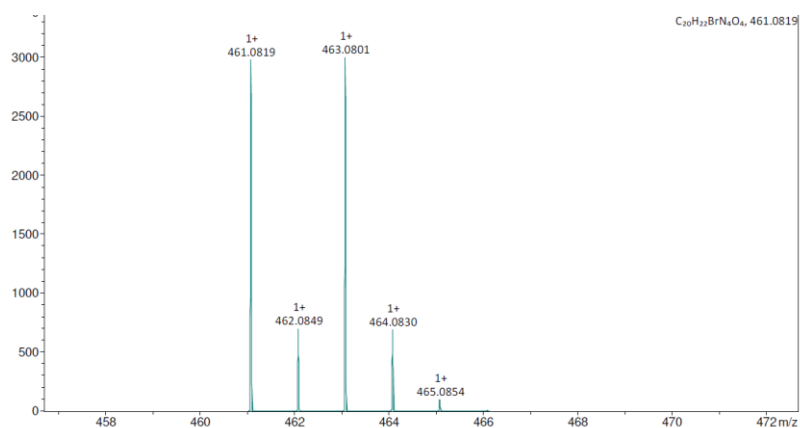*Figure 111 – ^{13}C-NMR of compound **30** (CDCl$_3$).*

*Figure 112 - HRMS of compound **30**.*

Synthesis of 2-(ethyl(4-((2-iodo-4-nitrophenyl)diazenyl)phenyl)amino)ethyl methacrylate (31):

Azodyes **28** were put in a dried round bottom flask under an inert Ar atmosphere and completely dissolved with anhydrous THF under stirring. Then the flask was put in an

ice bath, and 1.1 eq of triethylamine (TEA) was added by a syringe. Then freshly distilled methacryloyl chloride (1.2 eq) was added dropwise for 15 minutes, and after 30 minutes from the last addition, the ice bath was removed, and the reaction was left for 24 h monitoring with TLC (EP/EtOAc 1:1). The solution is filtrated and washed with EtOAc to recover the desired product when the reaction is completed. The solvents were distilled under vacuum at a temperature below 25°C. The solid was recovered with EtOAc, put in a separation funnel, and extracted 3 times with water and 2 times with brine. The organic fractions were combined, and the solvent was distilled under vacuum at 25°C; instead, the aqueous fractions were extracted again with EtOAc until they became clear. The final product was obtained as a dark red solid.

Yields: **31**: 85%.

^{1}H NMR (600 MHz, Acetone-d_6) δ 8.79 (d, J = 2.4 Hz, 1H), 8.34 (dd, J = 8.9, 2.4 Hz, 1H), 7.95 (d, J = 9.5 Hz, 2H), 7.74 (d, J = 8.8 Hz, 1H), 7.03 (d, J = 9.3 Hz, 2H), 6.08 (dq, J = 1.9, 1.0 Hz, 1H), 5.64 (p, J = 1.6 Hz, 1H), 4.43 (t, J = 5.9 Hz, 2H), 3.90 (t, J = 5.9 Hz, 2H), 3.69 (q, J = 7.1 Hz, 2H), 1.93 – 1.87 (m, 3H), 1.28 (t, J = 7.1 Hz, 3H).

^{13}C NMR (151 MHz, Acetone-d_6) δ 166.70, 155.65, 152.47, 147.59, 143.83, 136.34, 134.68, 126.96, 125.38, 124.48, 117.09, 111.99, 99.26, 61.90, 48.59, 45.44, 17.62, 11.65.
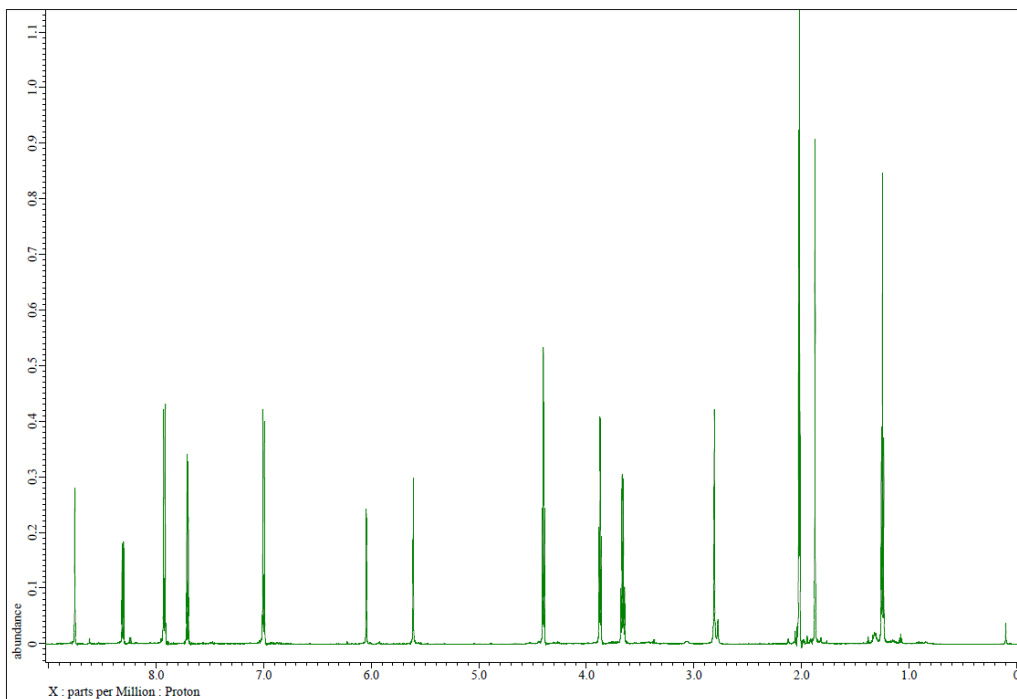
HR-ESI-MS: calculated 508.0607, found 531.0500 (M + Na$^+$).

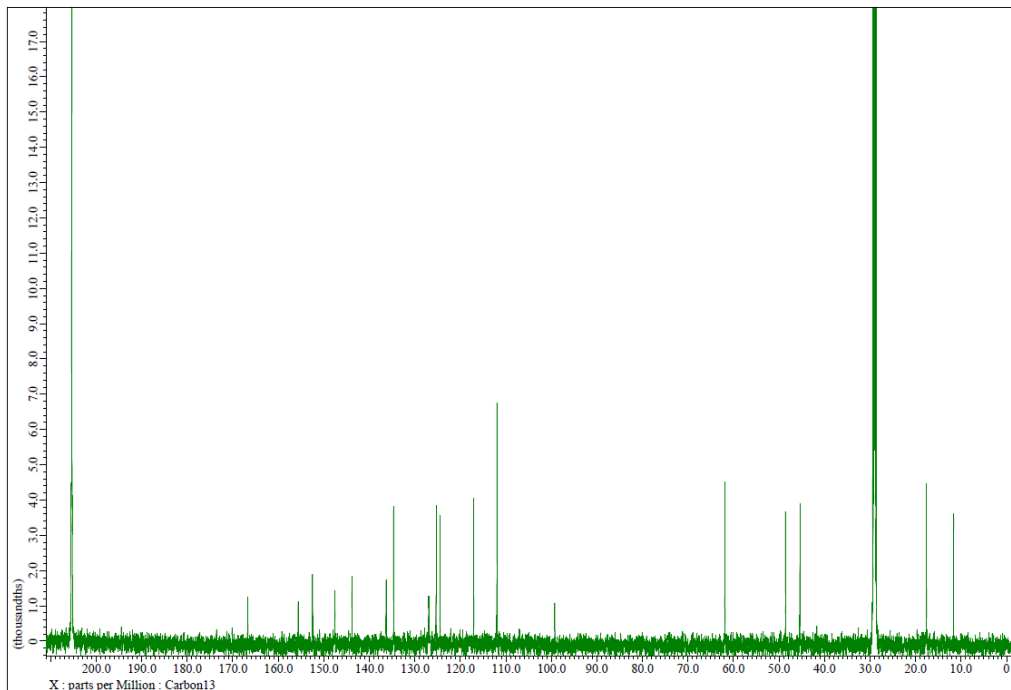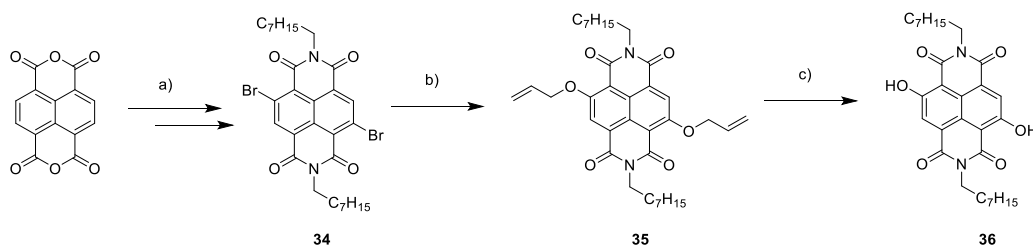**Figure 113** – ^{1}H-NMR of compound **31** (Acetone-d$_6$).

Figure 114 – ^{13}C-NMR of compound *31* (Acetone-d_6).

Synthesis of 4,9-dibromo-2,7-dioctylbenzo[lmn][3,8]phenanthroline-1,3,6,8(2H,7H)-tetraone (32).

Compound **32** was synthetized following the same procedure reported by Modarelli et al.[121] The chemical characterization was in agreement with the reported data.

Synthesis of 4,9-bis(allyloxy)-2,7-dioctylbenzo[lmn][3,8]phenanthroline-1,3,6,8 (2H,7H)-tetraone (33).

A freshly prepared solution of AllylONa in allyl alcohol (240 μL of a solution 1 M of NaH in allyl alcohol) was added dropwise to a solution of **32** (50 mg, 0.08 mmol) in dry CH_2Cl_2

175

(8 mL). The mixture was stirred at rt for 7 h. Then, CH_2Cl_2 was added, and the organic layer was washed with brine and water, dried over Na_2SO_4 and concentrated *in vacuo*. The crude was purified by flash chromatography (CH_2Cl_2/Hexane 3:2), affording **33** as a yellow solid (13 mg, 28%).

^{1}H-NMR (600 MHz, $CDCl_3$): 8.47 (s, 2H), 6.18 (ddt, $^3J(H,H)$ = 17.2, 10.6, 5.2 Hz, 2H), 5.72 (dq, $^3J(H,H)$ = 17.2 Hz, $^2J(H,H)$ = 1.2 Hz, $^4J(H,H)$ = 1.4 Hz, 2H), 5.45 (dq, , $^3J(H,H)$ = 10.6 Hz, $^2J(H,H)$ = 1.2 Hz, $^4J(H,H)$ = 1.4 Hz, 2H), 5.02 (dt, , $^3J(H,H)$ = 5 Hz, $^4J(H,H)$ = 1.5 Hz, 4H), 4.15 (t, $^3J(H,H)$ = 7.8 Hz, 4H), 1.73 (qt, $^3J(H,H)$ = 7.8 Hz, 4H), 1.42 (qt, $^3J(H,H)$ = 7.7 Hz, 4H), 1.36 (qt, $^3J(H,H)$ = 7.6 Hz, 4 H), 1.32-1.25 (m, 12 H), 0.87 (t, $^3J(H,H)$ = 6.8 Hz, 6H).

^{13}C-NMR (150 MHz, $CDCl_3$): δ 162.53, 161.27, 159.80, 131.60, 127.80, 123.88, 120.12, 119.47, 111.36, 71.61, 43.44, 31.96, 29.46, 29.36, 28.14, 27.31, 22.79, 14.79.

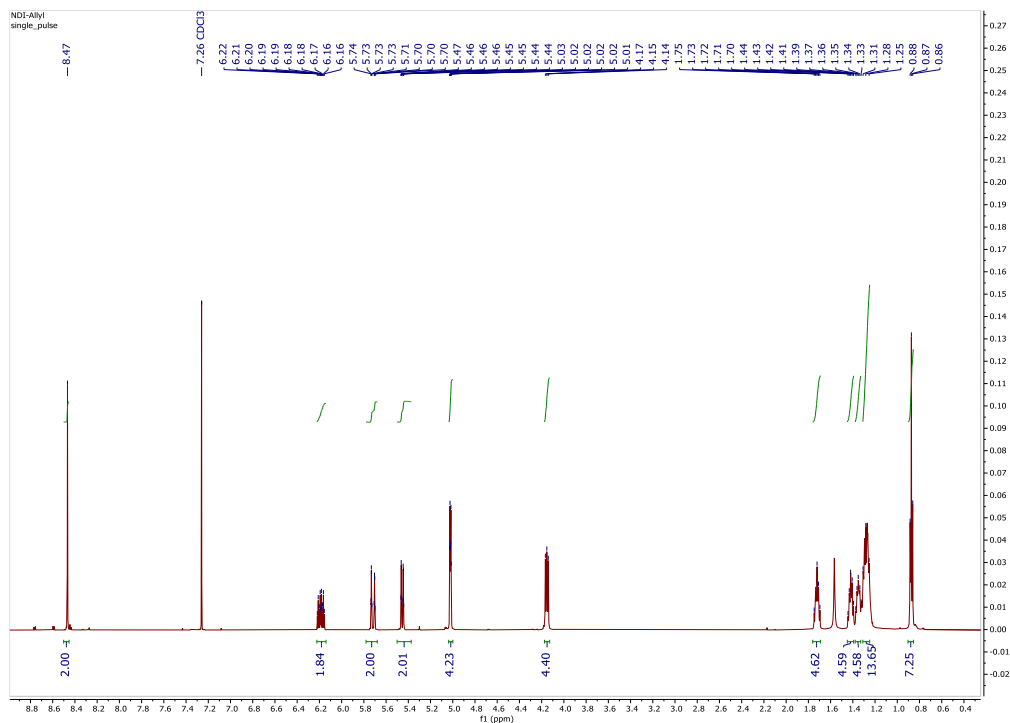MS (ESI, CH_2Cl_2/MeOH): 603 ([M+H]$^+$), 1204 ([2M]$^+$), 1227 ([2M + Na$^+$]).

ù

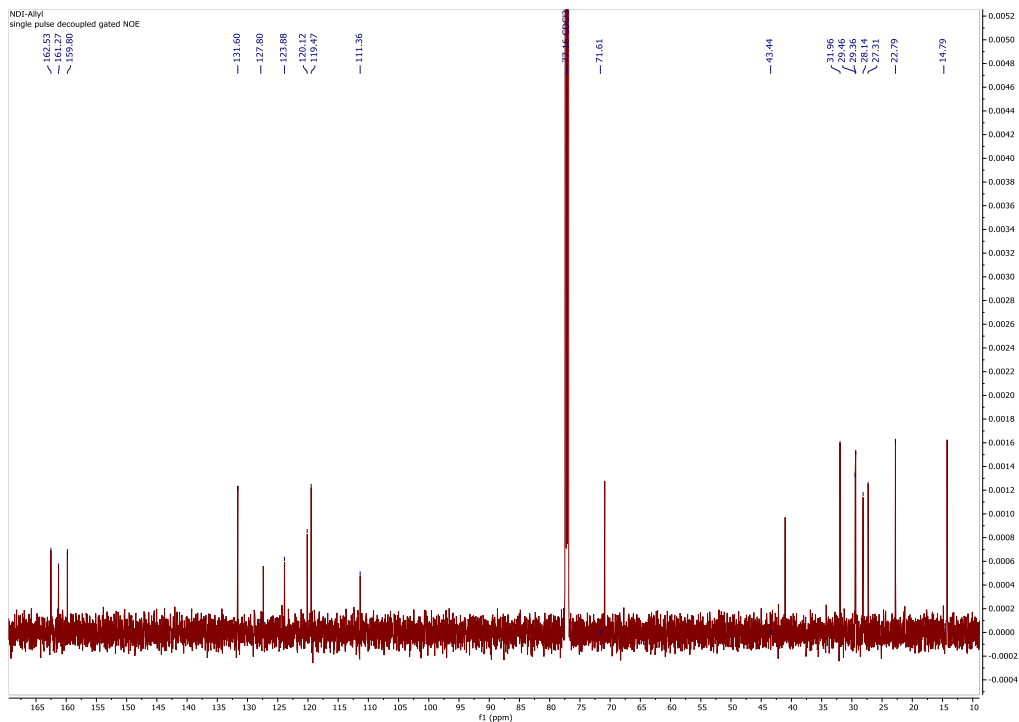***Figure 115*** *– ^{1}H-NMR spectrum of **33** ($CDCl_3$).*

Figure 116 - ^{13}C-NMR spectrum of compound **33** (CDCl₃).

Synthesis of 4,9-dihydroxy-2,7-dioctylbenzo[*lmn*][3,8]phenanthroline-1,3,6,8 (2*H*,7*H*)-tetraone (34).

To a solution of **33** (13 mg, 0.02 mmol) and Pd(PPh₃)₄ (1.3 mg, 0.001 mmol) in dry CH₂Cl₂ (3 mL), phenylsylane (17.3 mg, 0.16 mmol) was added. The mixture was stirred under Argon at rt for 12 h. Volatiles were removed *in vacuo,* and the reaction crude was purified by flash chromatography (CH₂Cl₂/Hexane 1:1), affording **34** as a yellow solid (6 mg, 53%).

^{1}H-NMR (600 MHz, CDCl₃): 12.38 (s, 2H), 8.30 (s, 2H), 4.17 (t, ^{3}J(H,H) = 7.7 Hz, 4H), 1.73 (qt, ^{3}J(H,H) = 7.6 Hz, 4H), 1.42 (qt, ^{3}J(H,H) = 7.6 Hz, 4H), 1.36 (qt, ^{3}J(H,H) = 7.4 Hz, 4 H), 1.32-1.25 (m, 12 H), 0.87 (t, ^{3}J(H,H) = 6.9 Hz, 6H).

^{13}C-NMR (150 MHz, CDCl₃): δ 168.55, 166.42, 161.92, 160.68, 127.25, 123.94, 106.96, 40.75, 31.93, 29.38, 29.32, 28.09, 27.19, 22.77, 14.24.
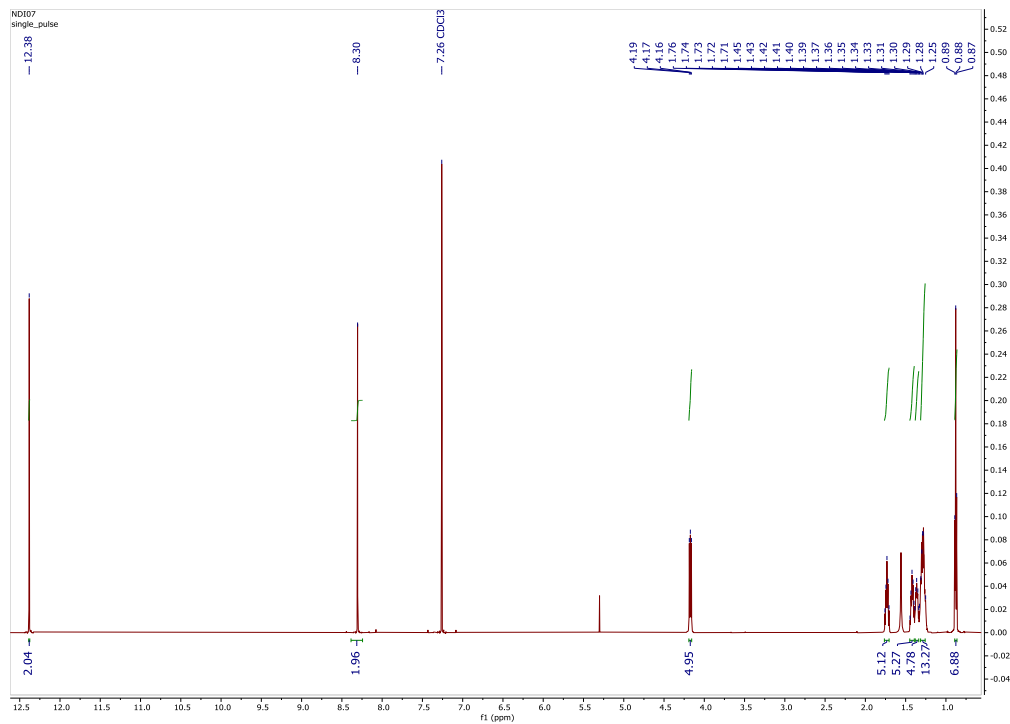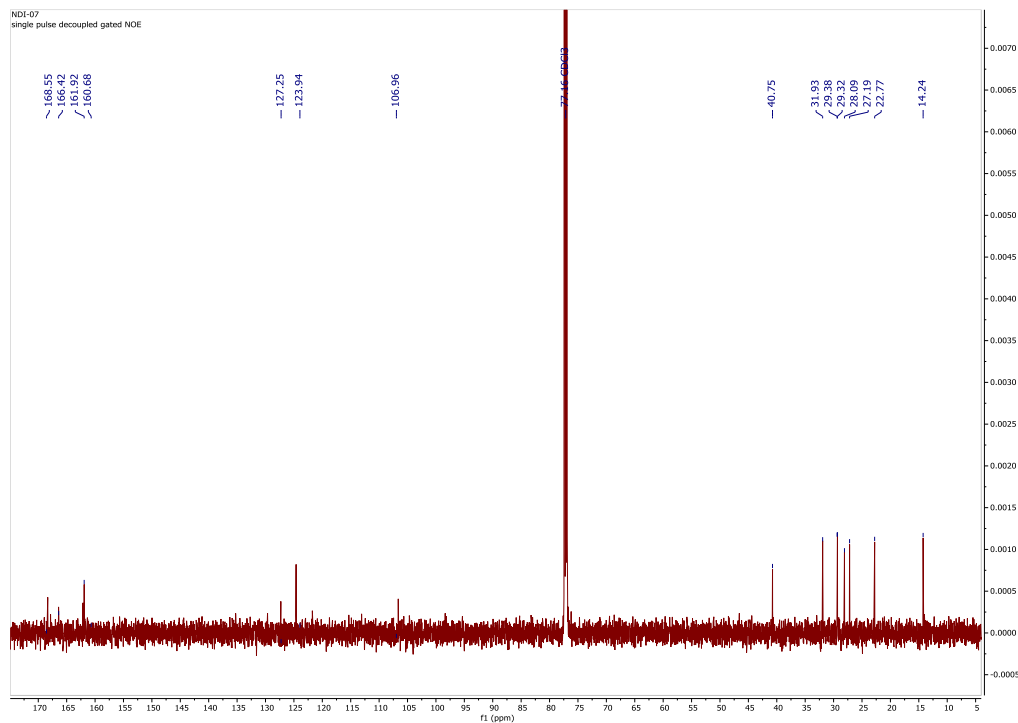
***Figure 117** -¹H-NMR spectrum of **34** (CDCl₃).*

***Figure 118** -¹³C-NMR spectrum of compound **34** (CDCl₃).*

178

Appendix II: Piezoresistivity
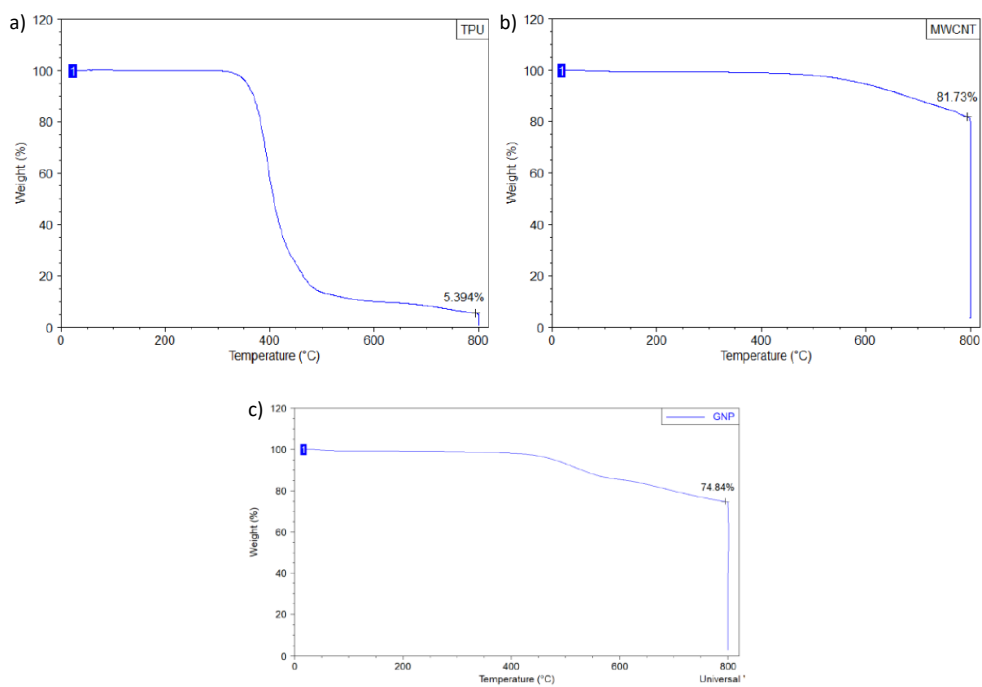

Figure 119 - *Thermograms of a) pure TPU, b) pure MWCNTs, and c) pure GNPs.*

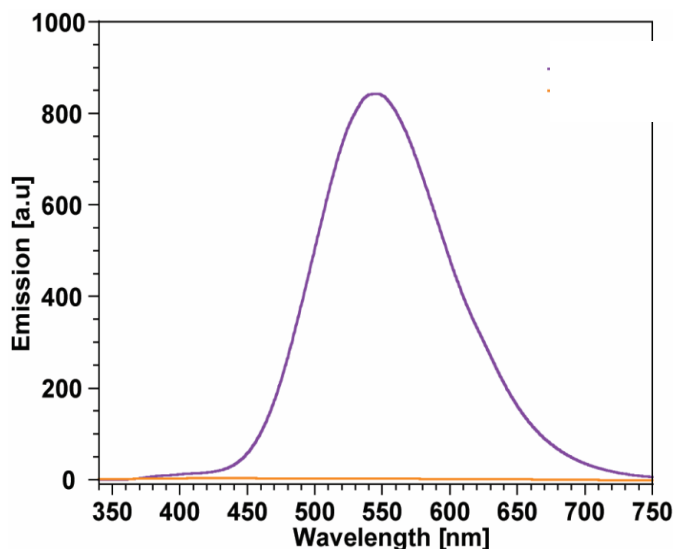# Appendix III: Fluorophores for 3D printing

Figure 120 - *Emission spectra of liquid formulations containing 1.0 wt.% of **9** (purple) and **10** (orange) copper-iodine based clusters. The insolubility of **9** is visible by the emission spectrum, while the soluble **10** doesn't emit light (excitation wavelength 330 nm). Material from: M. Gastaldi, I. Roppolo, A. Chiappone, C. Garino, A. Fin, M. Manachino, P. Sirianni, G. Viscardi, L. Scaltrito, M. Zanetti, S. Bordiga, C. Barolo, Additive Manufacturing **2022**, 49, 102504.*

Figure 121 *– UV-vis absorption spectra of 3D printed before (orange) and after (purple) the post-curing process under UV over irradiation for 5 minutes on each side. Material from: M. Gastaldi, I. Roppolo, A. Chiappone, C. Garino, A. Fin, M. Manachino, P. Sirianni, G. Viscardi, L. Scaltrito, M. Zanetti, S. Bordiga, C. Barolo, Additive Manufacturing **2022**, 49, 102504.*

*Figure 122 - DSC thermograms of 3DP polymeric waveguides with an increasing concentration of **9**. a) Blank, b) 0.1 %, c) 1.0 % and d) 5.0 % w w⁻¹. Material from: M. Gastaldi, I. Roppolo, A. Chiappone, C. Garino, A. Fin, M. Manachino, P. Sirianni, G. Viscardi, L. Scaltrito, M. Zanetti, S. Bordiga, C. Barolo, Additive Manufacturing **2022**, 49, 102504.*
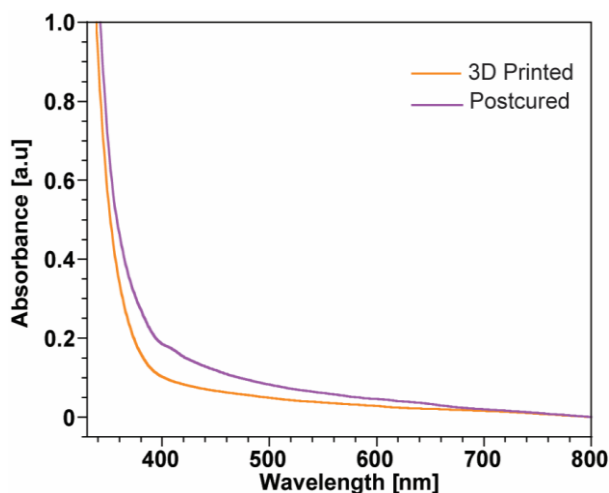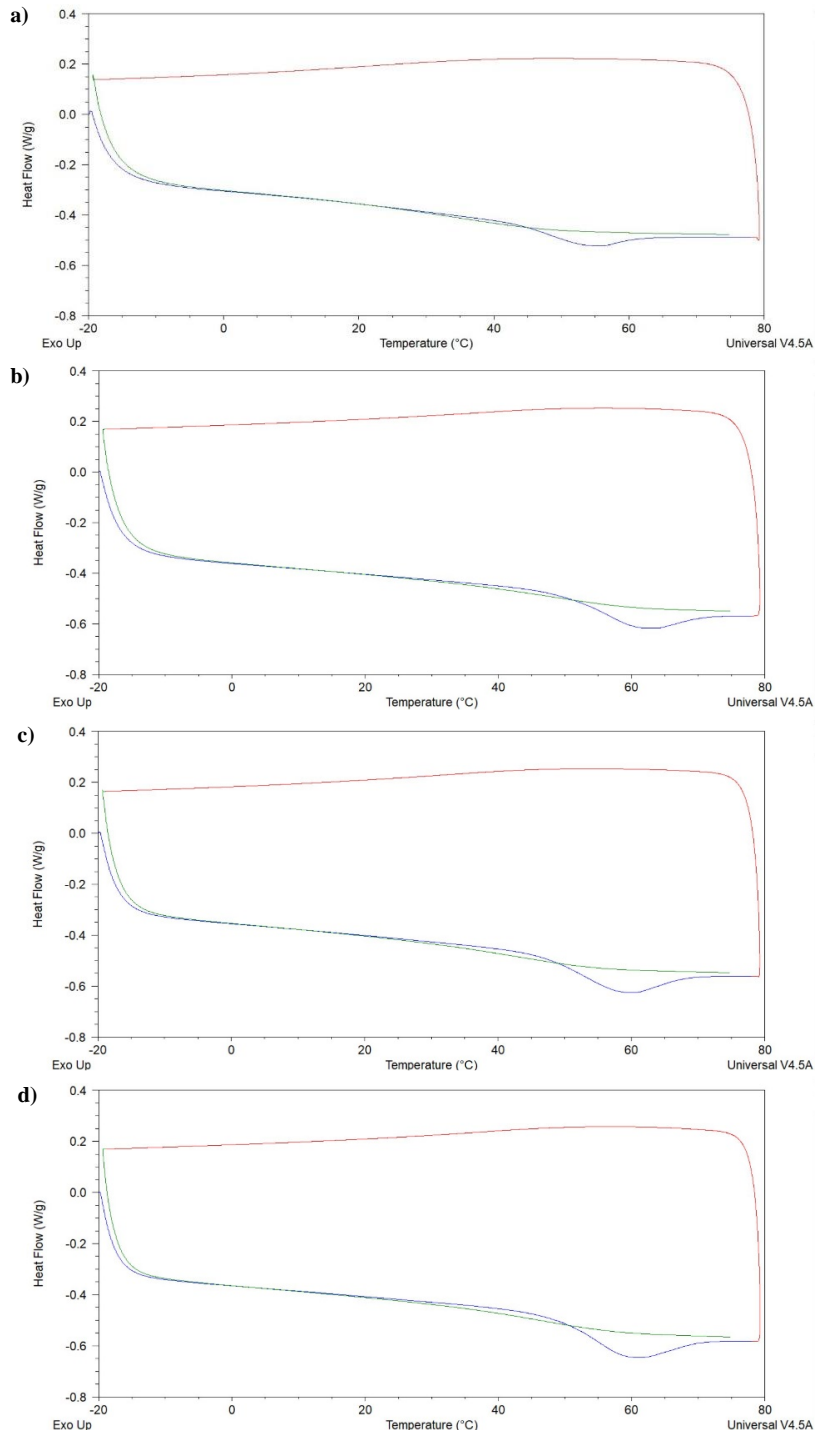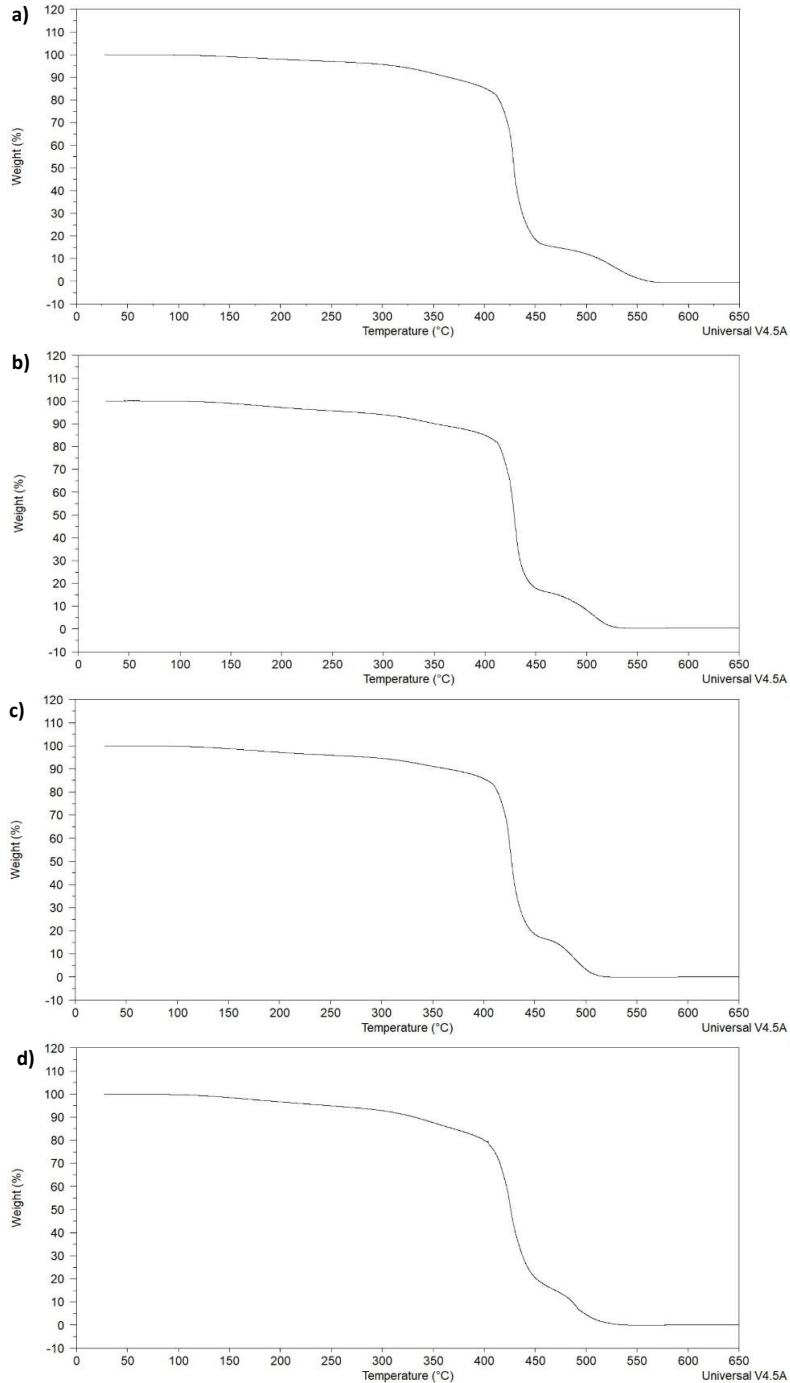
Figure 123 *- TGA thermograms of 3DP polymeric waveguides with an increasing concentration of **10**. a) Blank, b) 0.1 %, c) 1.0 % and d) 5.0 % w w^{-1}. Material from: M. Gastaldi, I. Roppolo, A. Chiappone, C. Garino, A. Fin, M. Manachino, P. Sirianni, G. Viscardi, L. Scaltrito, M. Zanetti, S. Bordiga, C. Barolo, Additive Manufacturing **2022**, 49, 102504.*

*Figure 124 - Emission spectrum of liquid BEDA without dyes or photoinitiator. Material from: M. Gastaldi, I. Roppolo, A. Chiappone, C. Garino, A. Fin, M. Manachino, P. Sirianni, G. Viscardi, L. Scaltrito, M. Zanetti, S. Bordiga, C. Barolo, Additive Manufacturing **2022**, 49, 102504.*

*Figure 125 - CAD project for a 3D printed luminescent device. Material from: M. Gastaldi, I. Roppolo, A. Chiappone, C. Garino, A. Fin, M. Manachino, P. Sirianni, G. Viscardi, L. Scaltrito, M. Zanetti, S. Bordiga, C. Barolo, Additive Manufacturing **2022**, 49, 102504.*
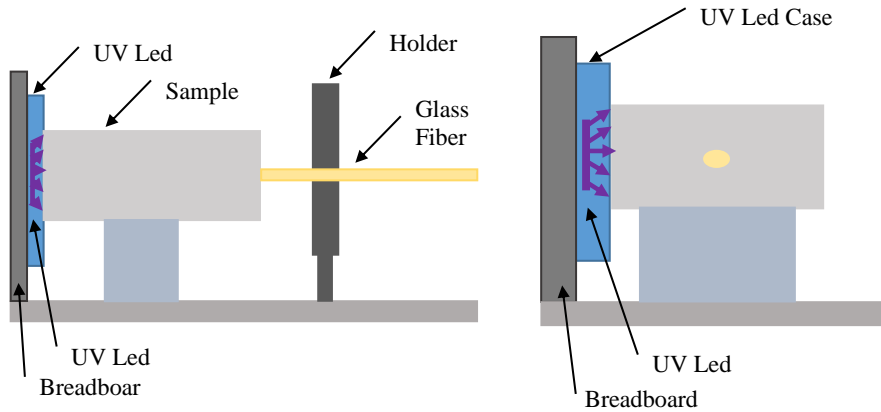
Figure 126 - *Direct (left) and side (right) experimental configurations to evaluate the efficiency in guiding light through the polymeric matrix of 3D printed waveguides. Material from: M. Gastaldi, I. Roppolo, A. Chiappone, C. Garino, A. Fin, M. Manachino, P. Sirianni, G. Viscardi, L. Scaltrito, M. Zanetti, S. Bordiga, C. Barolo, Additive Manufacturing **2022**, 49, 102504.*
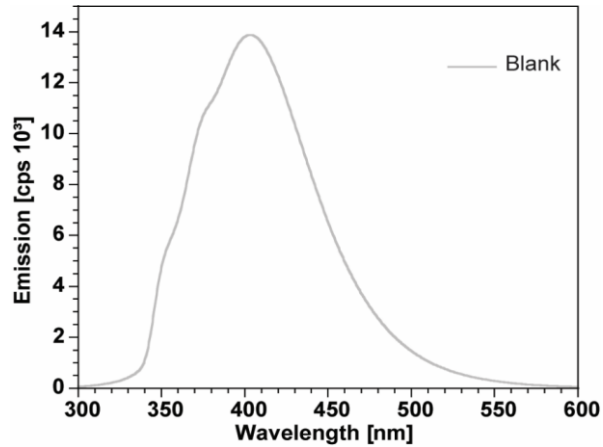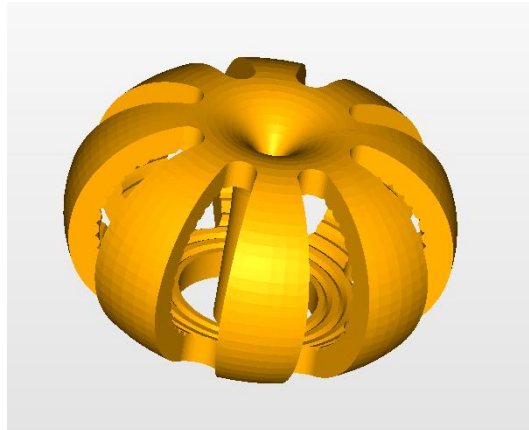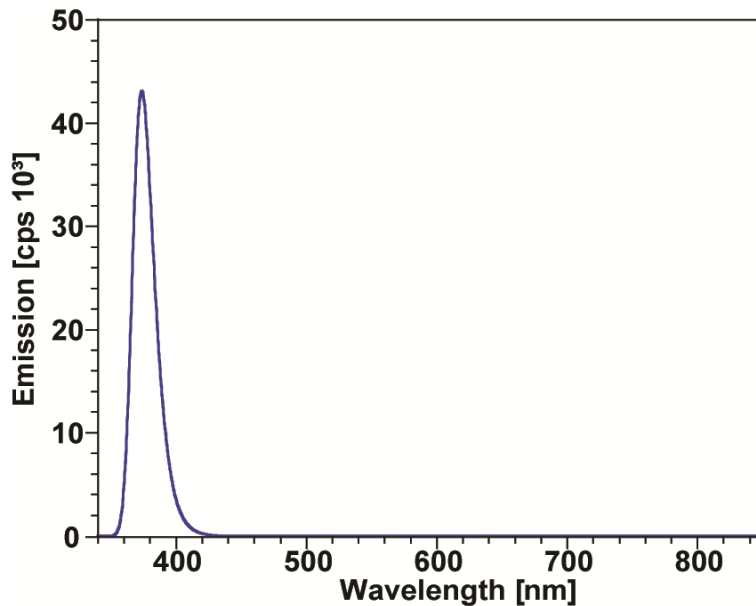

Figure 127 – *Emission spectrum of 365 nm centred LED. Material from: M. Gastaldi, I. Roppolo, A. Chiappone, C. Garino, A. Fin, M. Manachino, P. Sirianni, G. Viscardi, L. Scaltrito, M. Zanetti, S. Bordiga, C. Barolo, Additive Manufacturing **2022**, 49, 102504.*

Table 40 - *Measurement conditions of the LED spectrum and for each configuration used to evaluate the emitting properties of the PWGs at different lengths.*

Measurement type	Measure	Excitation Current [mA]	Led Voltage Drop [V]	Incident power density [mW/mm²]

LED	Led Spectrum	8	3.09	-
DIRECT PUMPING	Sample 2 cm	300	4.35	94.97
	Sample 3 cm	300	4.01	94.97
	Sample 5 cm	300	4.15	94.97
SIDE PUMPING	Sample 2 cm	800	5.29	223.74
	Sample 3 cm	800	5.29	223.74
	Sample 5 cm	800	5.28	223.74
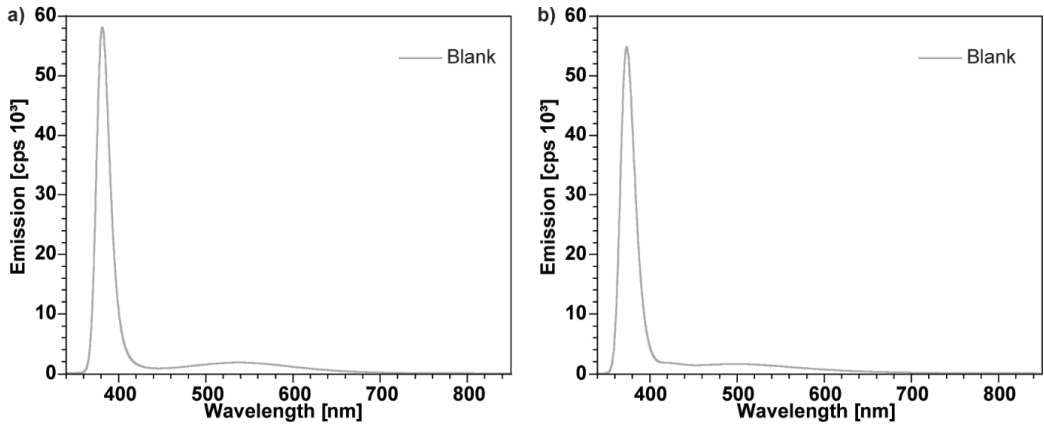
Figure 128 *– Emission of blank polymeric waveguides for (a) direct and (b) side pumping configurations. Material from: M. Gastaldi, I. Roppolo, A. Chiappone, C. Garino, A. Fin, M. Manachino, P. Sirianni, G. Viscardi, L. Scaltrito, M. Zanetti, S. Bordiga, C. Barolo, Additive Manufacturing **2022**, 49, 102504.*
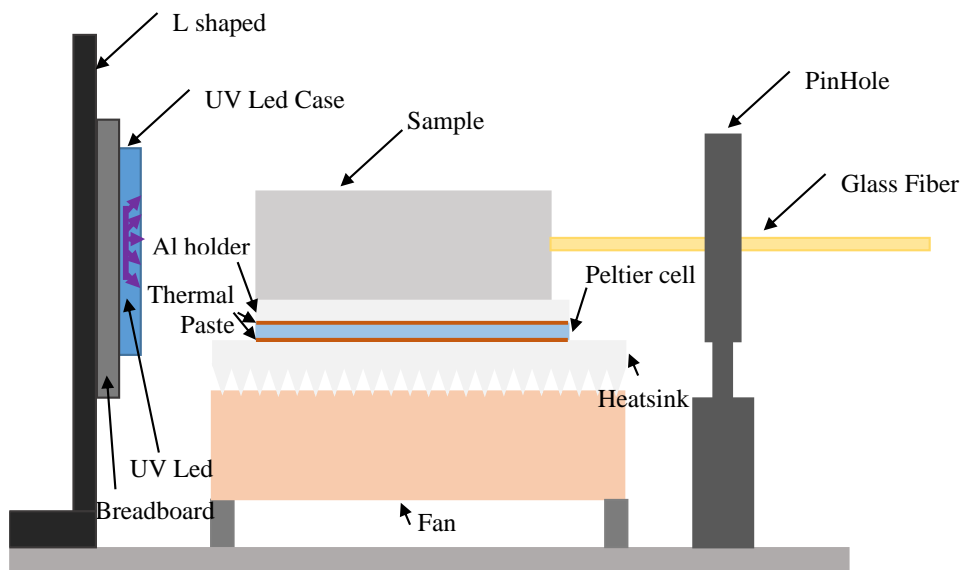
*Figure 129 -Experimental setup to evaluate the effects of changes in temperature on the emitting properties of polymeric waveguides. The Peltier cell is used to regulate the working temperature of the waveguide. Material from: M. Gastaldi, I. Roppolo, A. Chiappone, C. Garino, A. Fin, M. Manachino, P. Sirianni, G. Viscardi, L. Scaltrito, M. Zanetti, S. Bordiga, C. Barolo, Additive Manufacturing **2022**, 49, 102504.*
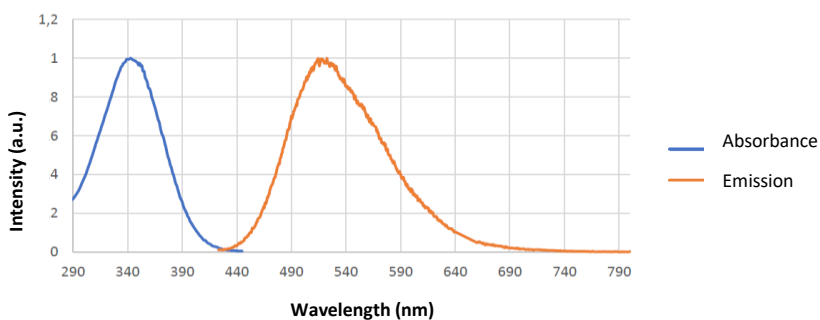
Figure 130 – Absorbance (blue) and emission (orange) spectra of 3D printed films in which compound 12 was dispersed.
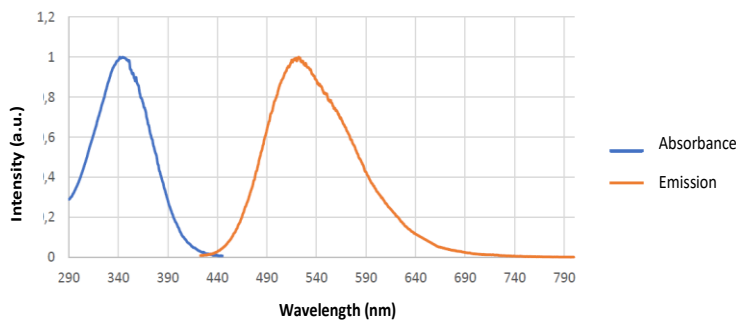
Figure 131 *- Absorbance (blue) and emission (orange) spectra of 3D printed films in which compound **13** was copolymerized as a side-functional group.*
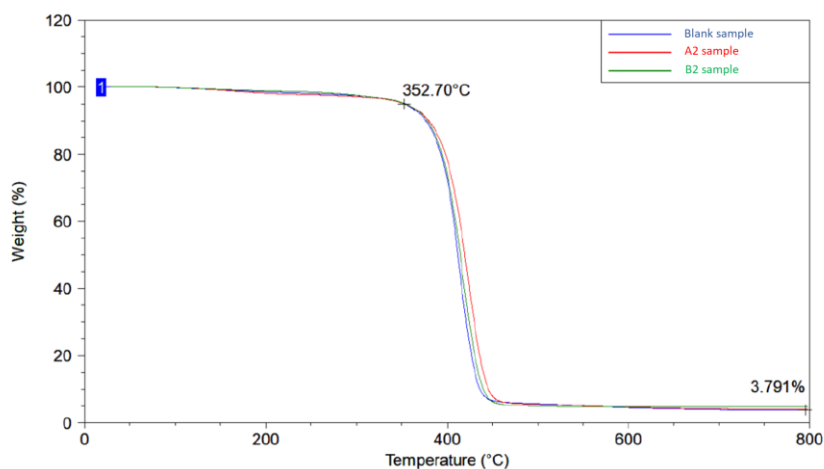

Figure 132 *– TGA thermograms of 3D printed blank samples (blue) without the introduction of any functional dyes, A1 sample (red) and B1 sample (green). All thermograms were registered under an N_2 atmosphere and a heating ramp of 10°C/min. 352.70°C represents the temperature when the blank sample loses 5% of the initial weight, while 3.791% represents the final residues at 800°C.*

Appendix IV: Photoinduced tunable properties polymers with azobenzene dyes.
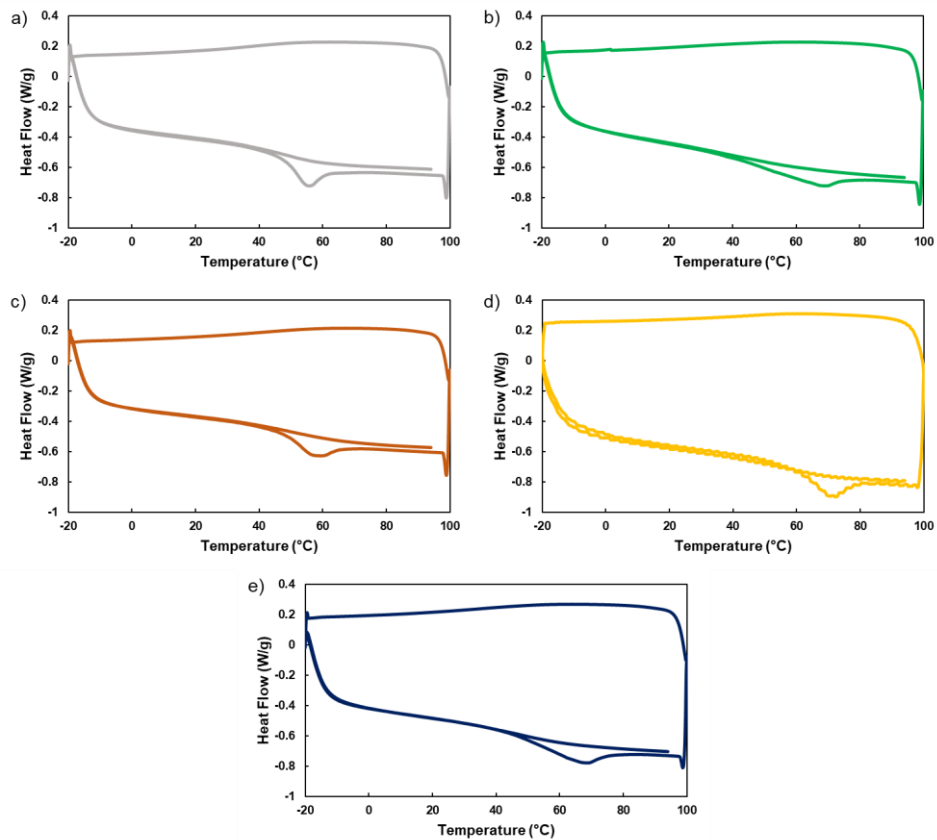
Figure 133 - *DSC of 3D printed polymeric films made of a) BEDA, b) **18**, c) **19**, d) **20**, e) **21**.*
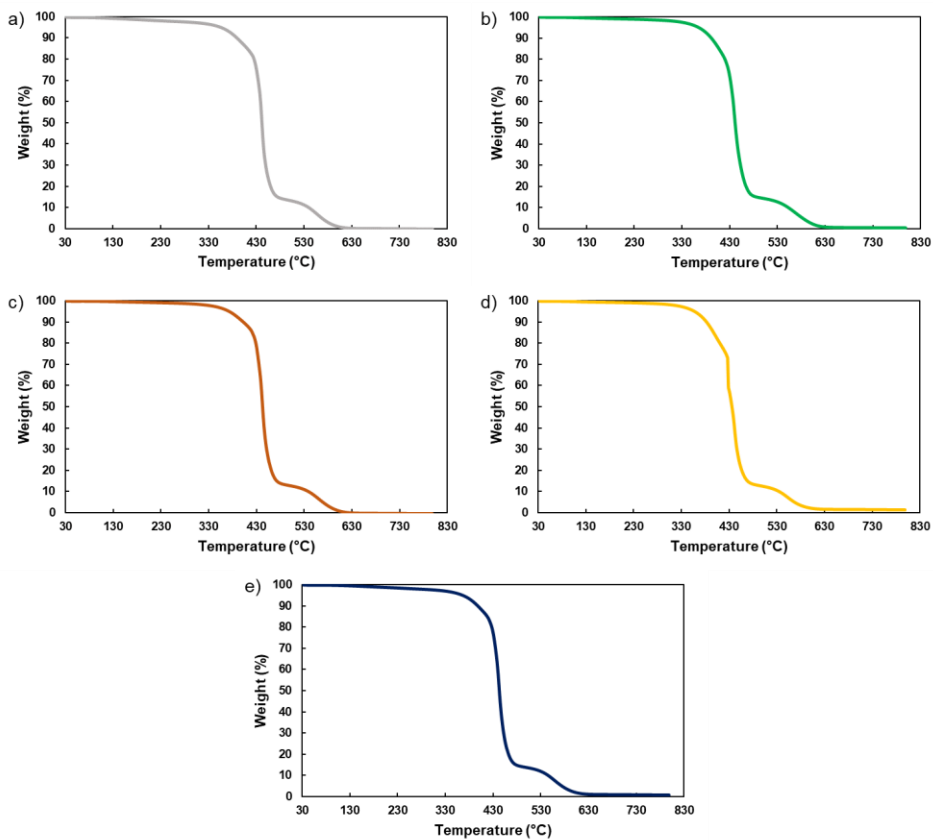
Figure 134 - TGA of 3D printed polymeric films made of a) BEDA, b) **18**, c) **19**, d) **20**, e) **21**.
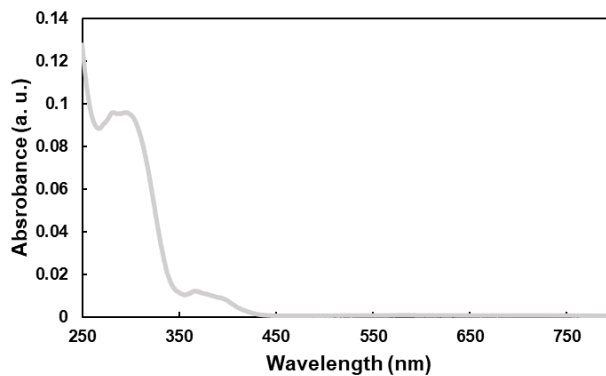
Figure 135 - UV-Vis spectrum of BAPO photoinitiator in EtOH.
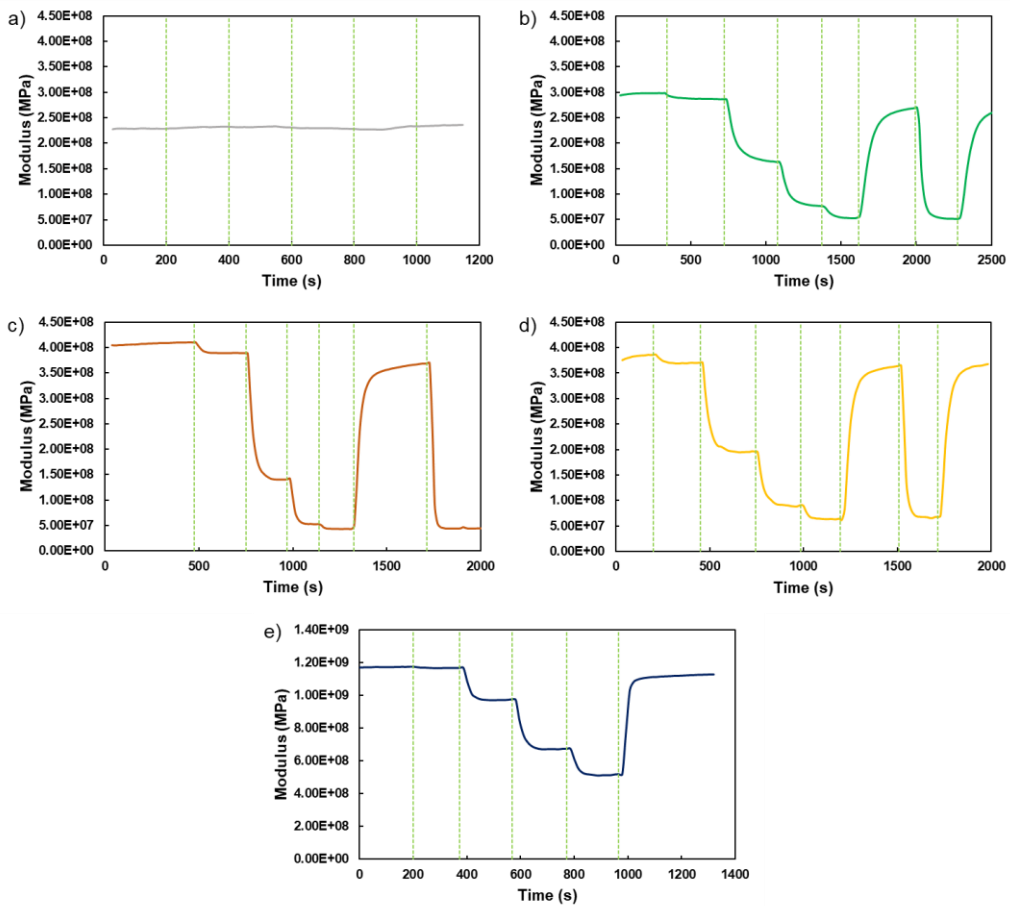
Figure 136 *- TGA of 3D printed polymeric films made of a) BEDA, b)* ***18****, c)* ***19****, d)* ***20****, e)* ***21****.*
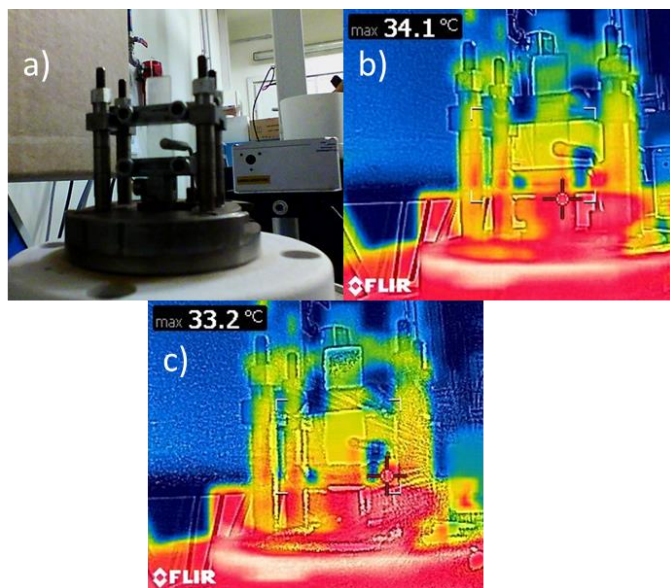
Figure 137 - *a) Experimental setup for BEDA sample into DMA. Thermal images of BEDA sample under b) 0% and c) 100% of laser power irradiation.*
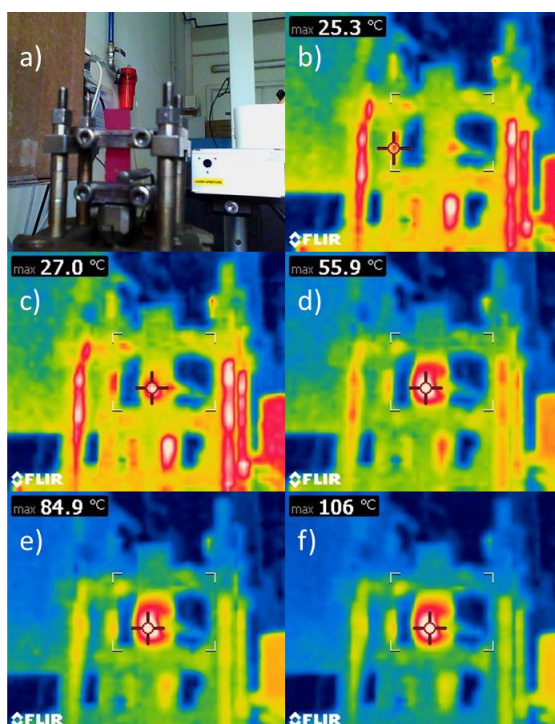
Figure 138 - *a) Experimental setup for DMA under laser irradiation for the azo-based sample containing compound **21**. b) Laser OFF, c) 25% of laser power, d) 50%, e) 75%, f) 100%.*
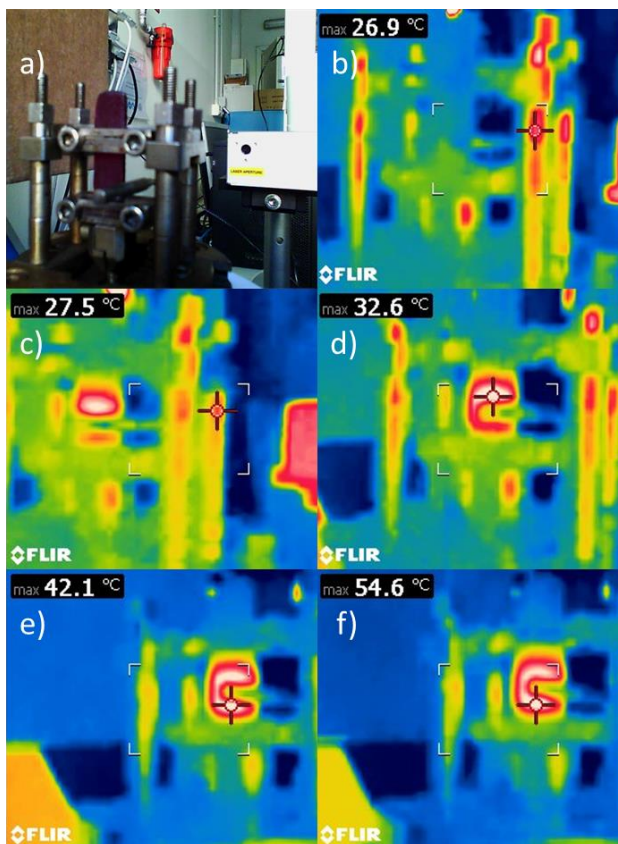
Figure 139 *- a) Experimental setup for DMA under laser irradiation for the azo-based sample containing compound **17**. b) Laser OFF, c) 25% of laser power, d) 50%, e) 75%, f) 100%.*
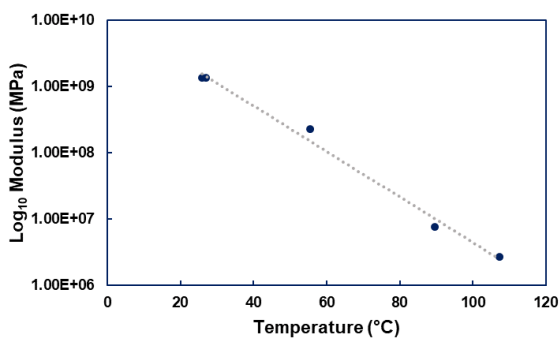
Figure 140 *- Linear interpolation of modulus reduction with an increasing temperature for a 3D printed film containing compound **21**.*

Appendix V: Light-induced shape-memory 3D printed polymers
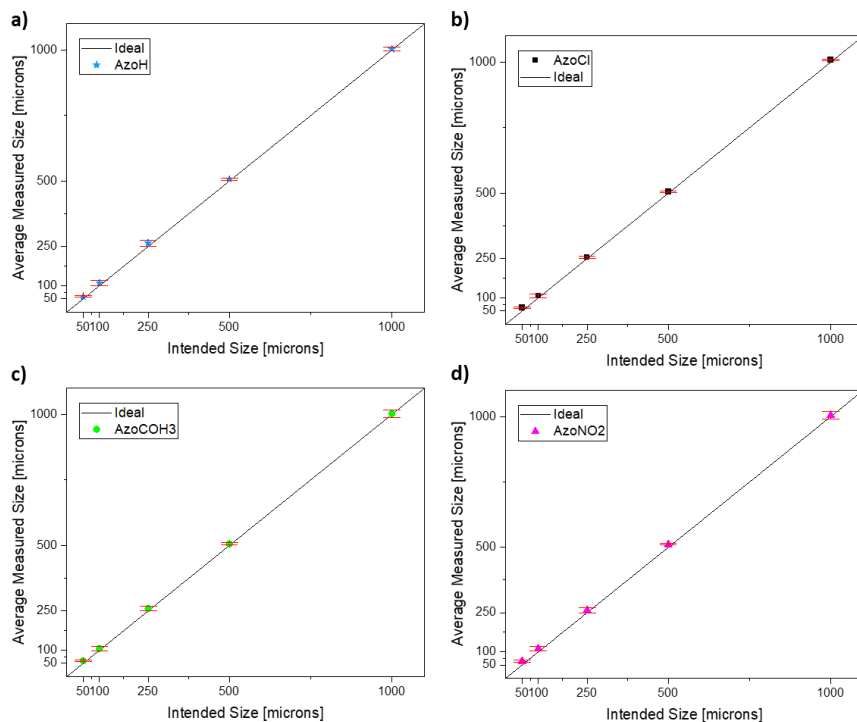
Figure 141 *- Final XY resolutions for all 3D printed samples containing compounds a)* ***22****, b)* ***23****, c)* ***24****, and d)* ***25****.*
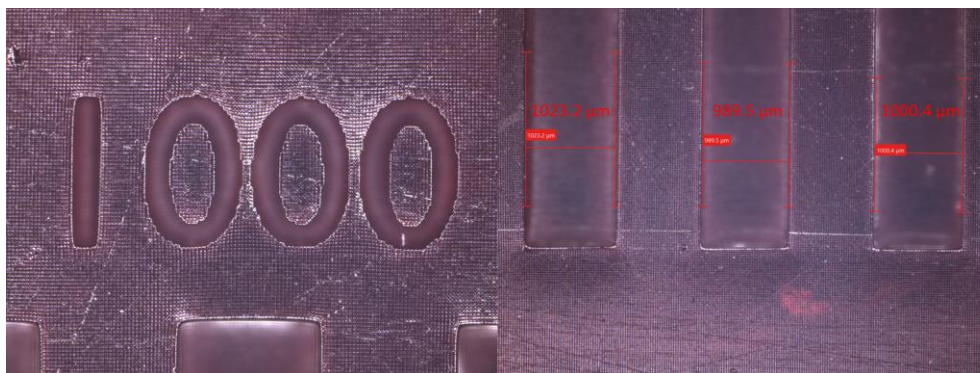
Figure 142 *- XY resolution of 1000 μm sample containing compound* ***25****.*
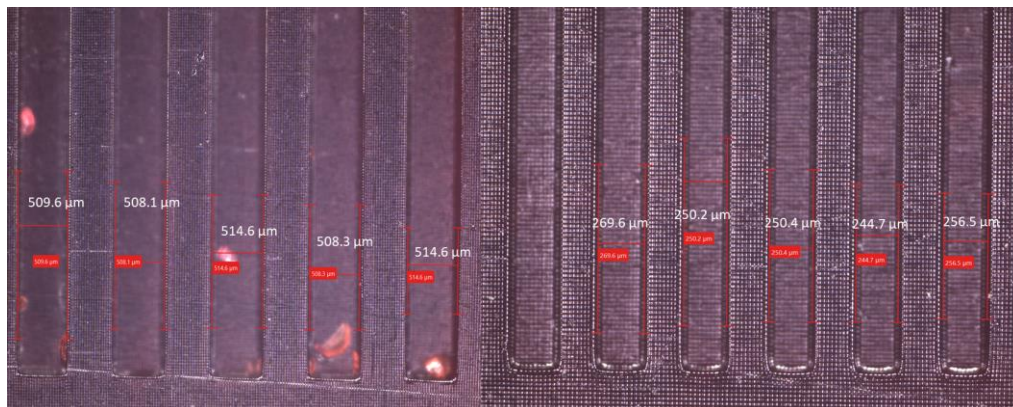
Figure 143 - *XY resolution of 500 μm and 250 μm samples containing compound* **25**.
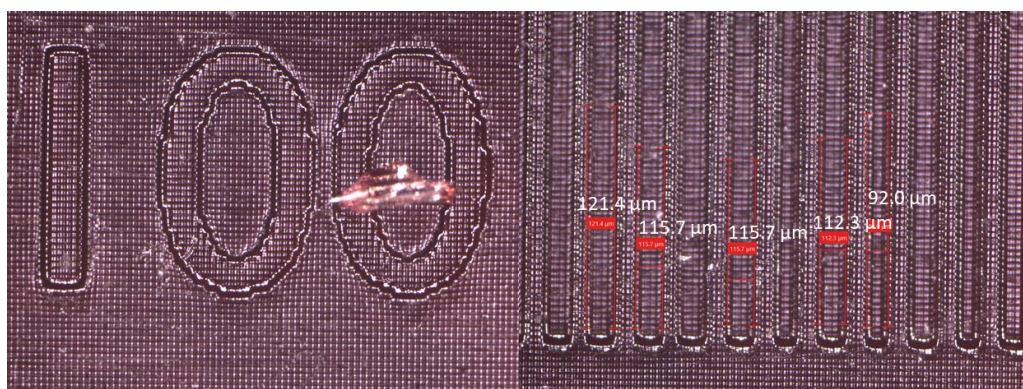
Figure 144 - *XY resolution of 100 μm sample containing compound* **25**.
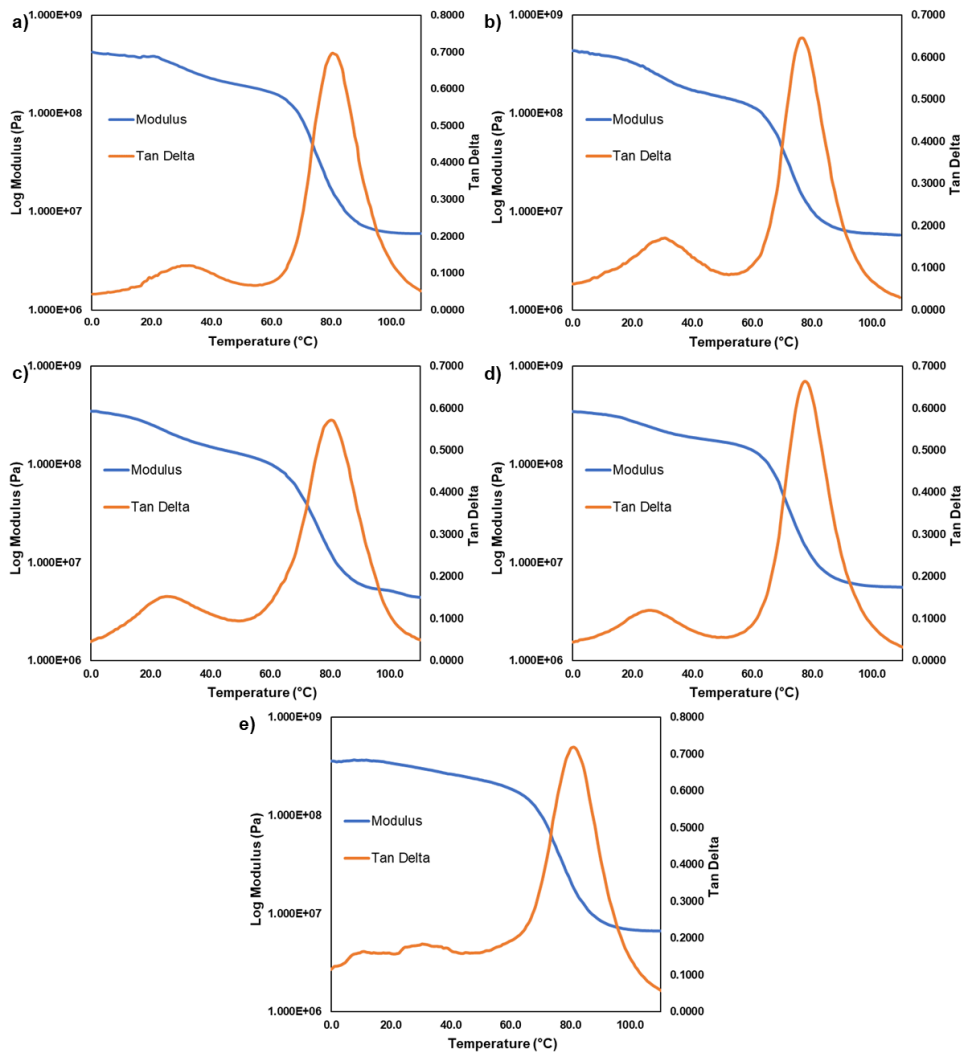
Figure 145 - *DMA thermograms for all 3D printed samples made of a) BEDA, b) **22**, c) **23**, d) **24**, e) **25**.*
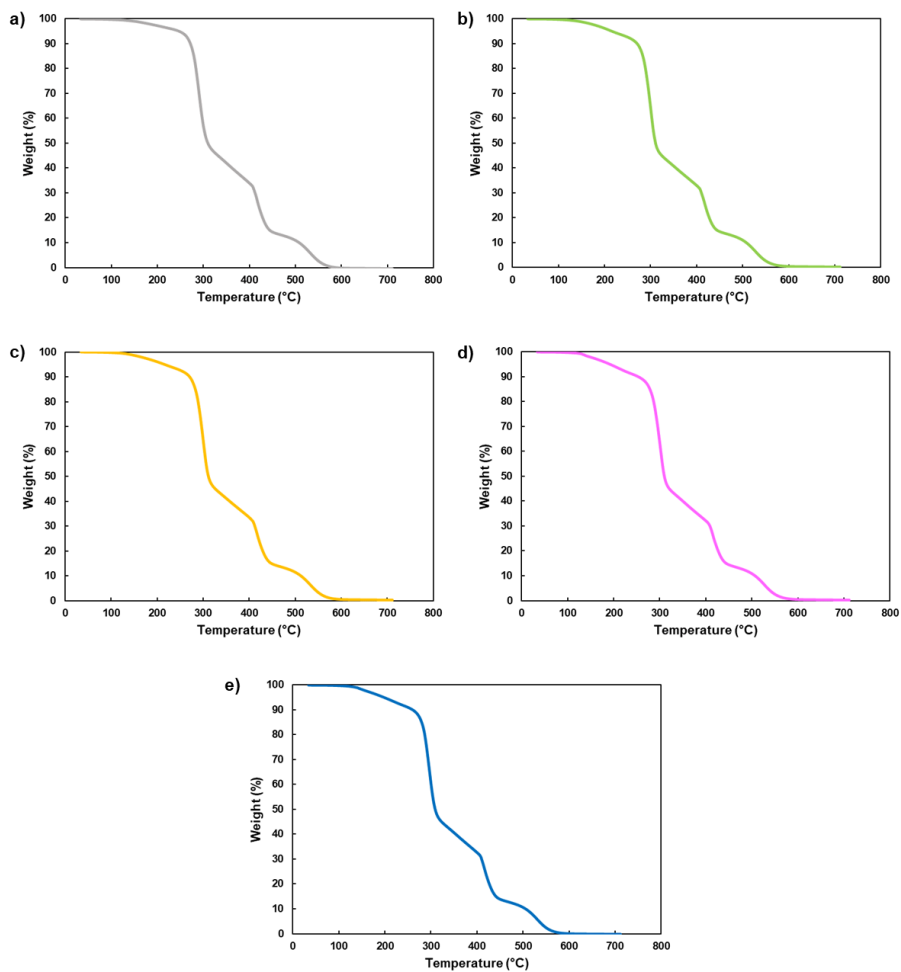
Figure 146 - *TGA thermograms for all 3D printed samples. a) Blank, b)* **22***, c)* **23***, d)* **24***, e)* **25***.*
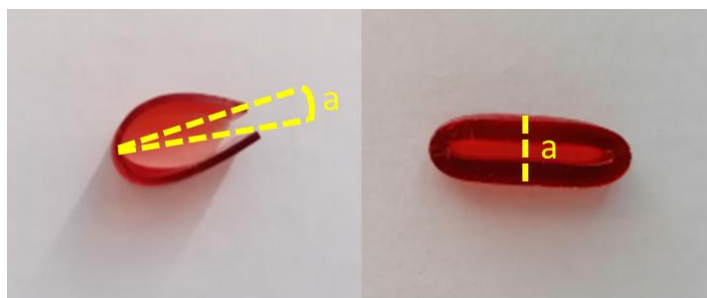
Figure 147 - *Calculation of the* **a** *parameter for 3D printed polymeric strips.*

Figure 148 - *3D printed chain after 2 minutes of LED irradiation. The LED was focused on the second transparent-white ring from the left. All white rings remain unopened, while the two central rings were opened under LED irradiation.*

Appendix VI: 3D printed azo-based membranes for gas permeability
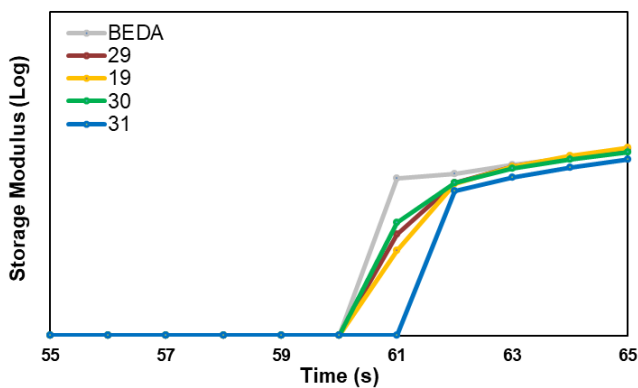
Figure 149 – The photorheology test highlights a delay of 1 second at the start of the polymerization process.
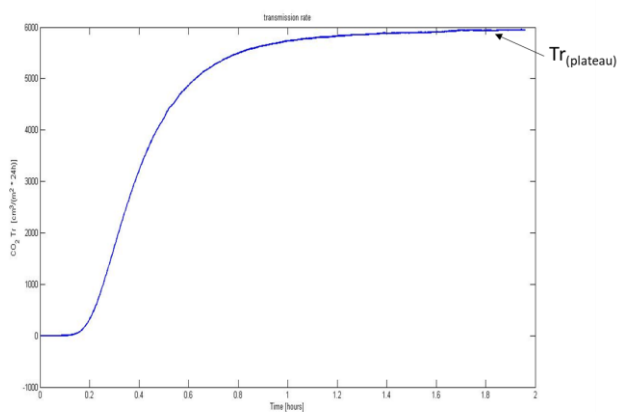
Figure 150 – Calculation of $Tr_{(plateau)}$ value.
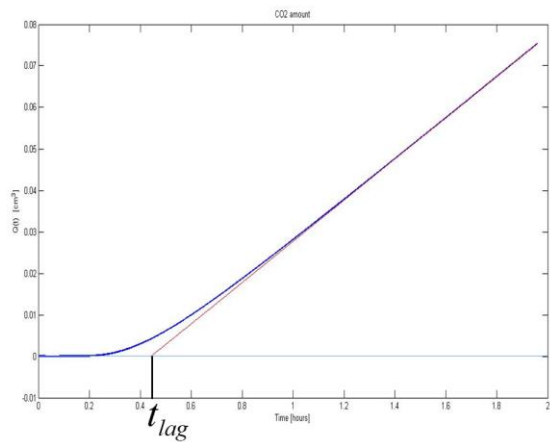
Figure 151 - *Calculation of t_{lag} value.*
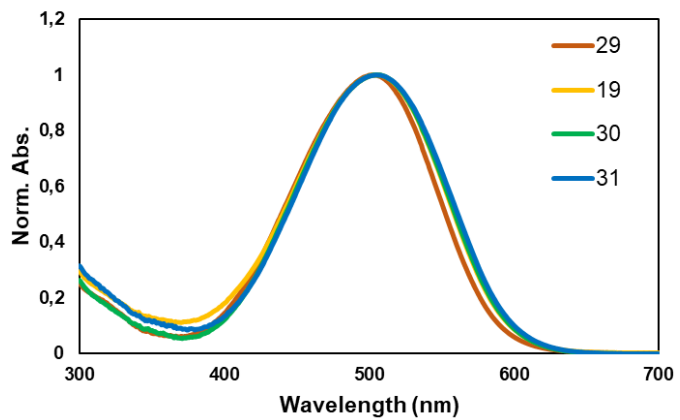
Figure 152 - *Normalized UV-vis spectra in solution (EtOH).*

Appendix VII: 3D printed polymeric sensors based on NDI-OH
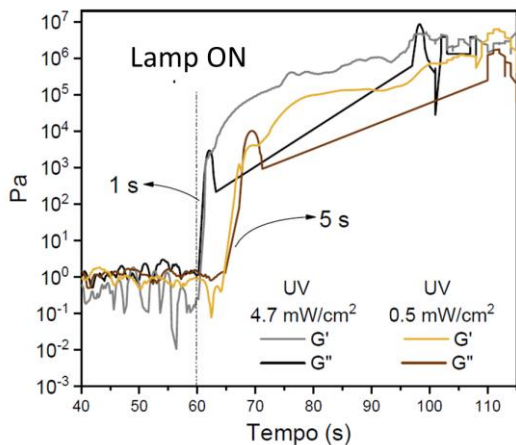
Figure 153 *- Photorheology test in which two different intensities of the UV light are employed. The delay in the start of the photopolymerization process is about 5 seconds. This time can be reduced to 1 second, increasing the light irradiation's power.*
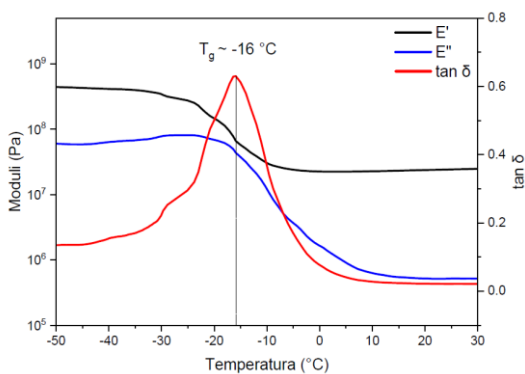
Figure 154 *– DMA analysis on PEGDA 575 without **36**.*
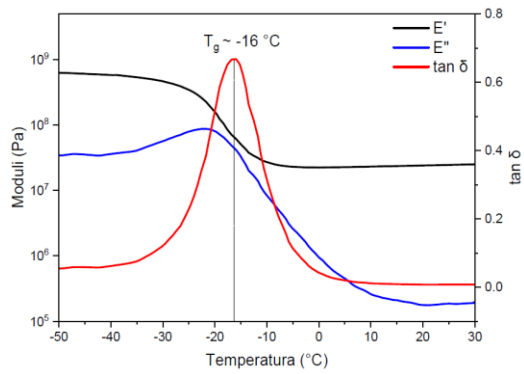
Figure 155 – *DMA analysis on PEGDA 575 with* **36**.

References

[1]   V. Mazzanti, L. Malagutti, F. Mollica, *Polymers (Basel)* **2019**, *11*.
[2]   S. C. Daminabo, S. Goel, S. A. Grammatikos, H. Y. Nezhad, V. K. Thakur, *Materials Today Chemistry* **2020**, *16*, 100248.
[3]   A. A. Vaidya, C. Collet, M. Gaugler, G. Lloyd-Jones, *Materials Today Communications* **2019**, *19*, 286.
[4]   J. Wu, C. Yuan, Z. Ding, M. Isakov, Y. Mao, T. Wang, M. L. Dunn, H. J. Qi, *Sci Rep* **2016**, *6*, 24224.
[5]   D. Filgueira, S. Holmen, J. K. Melbø, D. Moldes, A. T. Echtermeyer, G. Chinga-Carrasco, *Polymers* **2018**, *10*, 314.
[6]   U. D'Amora, M. D'Este, D. Eglin, F. Safari, C. M. Sprecher, A. Gloria, R. De Santis, M. Alini, L. Ambrosio, *J Tissue Eng Regen Med* **2018**, *12*, 321.
[7]   V. Yu. Krakhmatova, A. I. Zakharov, D. V. Andreev, A. F. Krivoshchepov, *Glass Ceram* **2019**, *75*, 479.
[8]   P. Anant Pidge, H. Kumar, *Materials Today: Proceedings* **2020**, *21*, 1689.
[9]   S. C. Ligon, R. Liska, J. Stampfl, M. Gurr, R. Mülhaupt, *Chem. Rev.* **2017**, *117*, 10212.
[10]   A. J. Boydston, B. Cao, A. Nelson, R. J. Ono, A. Saha, J. J. Schwartz, C. J. Thrasher, *J. Mater. Chem. A* **2018**, *6*, 20621.
[11]   R. T. Shafranek, S. C. Millik, P. T. Smith, C.-U. Lee, A. J. Boydston, A. Nelson, *Progress in Polymer Science* **2019**, *93*, 36.
[12]   H. W. Tan, J. An, C. K. Chua, T. Tran, *Advanced Electronic Materials* **2019**, *5*, 1800831.
[13]   E. Fantino, A. Chiappone, I. Roppolo, D. Manfredi, R. Bongiovanni, C. F. Pirri, F. Calignano, *Advanced Materials* **2016**, *28*, 3712.
[14]   A. Cortés, A. Cosola, M. Sangermano, M. Campo, S. González Prolongo, C. F. Pirri, A. Jiménez-Suárez, A. Chiappone, *Adv. Funct. Mater.* **2021**, 2106774.
[15]   M. Milazzo, N. C. Negrini, S. Scialla, B. Marelli, S. Farè, S. Danti, M. J. Buehler, *Advanced Functional Materials* **2019**, *29*, 1903055.
[16]   Y. Li, Z. Feng, L. Huang, K. Essa, E. Bilotti, H. Zhang, T. Peijs, L. Hao, *Composites Part A: Applied Science and Manufacturing* **2019**, *124*, 105483.
[17]   H. Yang, W. R. Leow, T. Wang, J. Wang, J. Yu, K. He, D. Qi, C. Wan, X. Chen, *Advanced Materials* **2017**, *29*, 1701627.
[18]   C. Credi, A. Fiorese, M. Tironi, R. Bernasconi, L. Magagnin, M. Levi, S. Turri, *ACS Applied Materials & Interfaces* **2016**, *8*, 26332.
[19]   S. Tibbits, *Architectural Design* **2014**, *84*, 116.
[20]   R. Suriano, R. Bernasconi, L. Magagnin, M. Levi, *J. Electrochem. Soc.* **2019**, *166*, B3274.
[21]   F. Momeni, J. Ni, *arXiv:1811.12609 [physics]* **2018**.
[22]   Y. Yue, Y. Norikane, R. Azumi, E. Koyama, *Nature Communications* **2018**, *9*.
[23]   C. W. Hull, S. Gabriel, 16.

[24] J. W. Stansbury, M. J. Idacavage, *Dental Materials* **2016**, *32*, 54.

[25] J. Frketic, T. Dickens, S. Ramakrishnan, *Additive Manufacturing* **2017**, *14*, 69.

[26] P. Han, *Engineering* **2017**, *3*, 648.

[27] A. Bhargav, V. Sanjairaj, V. Rosa, L. W. Feng, J. F. Yh, *Journal of Biomedical Materials Research Part B: Applied Biomaterials* **2018**, *106*, 2058.

[28] J. M. Korde, M. Shaikh, B. Kandasubramanian, *Polymer-Plastics Technology and Engineering* **2018**, *57*, 1828.

[29] B. C. Gross, J. L. Erkal, S. Y. Lockwood, C. Chen, D. M. Spence, *Analytical Chemistry* **2014**, *86*, 3240.

[30] K. Chen, X. Kuang, V. Li, G. Kang, H. J. Qi, *Soft Matter* **2018**, *14*, 1879.

[31] S. S. Crump, A. E.-P. D. Muir, **1992**, 15.

[32] O. A. Mohamed, S. H. Masood, J. L. Bhowmik, *Adv. Manuf.* **2015**, *3*, 42.

[33] H. Zhao, X. Liu, W. Zhao, G. Wang, B. Liu, *J. Phys.: Conf. Ser.* **2019**, *1213*, 052037.

[34] J. M. Chacón, M. A. Caminero, E. García-Plaza, P. J. Núñez, *Materials & Design* **2017**, *124*, 143.

[35] M. Gastaldi, F. Cardano, M. Zanetti, G. Viscardi, C. Barolo, S. Bordiga, S. Magdassi, A. Fin, I. Roppolo, *ACS Materials Lett.* **2020**, 1.

[36] B. Brenken, E. Barocio, A. Favaloro, V. Kunc, R. B. Pipes, *Additive Manufacturing* **2018**, *21*, 1.

[37] H. I. Medellin-Castillo, J. Zaragoza-Siqueiros, *Chinese Journal of Mechanical Engineering* **2019**, *32*, 53.

[38] C. R. Deckard, J. F. Darrah, **1992**, 12.

[39] M. Singh, S. Jonnalagadda, *European Journal of Pharmaceutical Sciences* **2020**, *143*, 105167.

[40] B. Wendel, D. Rietzel, F. Kühnlein, R. Feulner, G. Hülder, E. Schmachtenberg, *Macromolecular Materials and Engineering* **2008**, *293*, 799.

[41] M. Schmid, A. Amado, K. Wegener, *Journal of Materials Research* **2014**, *29*, 1824.

[42] A. Ghilan, A. P. Chiriac, L. E. Nita, A. G. Rusu, I. Neamtu, V. M. Chiriac, *J Polym Environ* **2020**, *28*, 1345.

[43] H. N. Chia, B. M. Wu, *J Biol Eng* **2015**, *9*.

[44] J. A. Lewis, *Advanced Functional Materials* **2006**, *16*, 2193.

[45] L. Li, Q. Lin, M. Tang, A. J. E. Duncan, C. Ke, *Chemistry – A European Journal* **2019**, *25*, 10768.

[46] M. O. Aydogdu, B. Mutlu, M. Kurt, A. T. Inan, S. E. Kuruca, G. Erdemir, Y. M. Sahin, N. Ekren, F. N. Oktar, O. Gunduz, *J Aust Ceram Soc* **2019**, *55*, 849.

[47] Z. Ji, D. Jiang, X. Zhang, Y. Guo, X. Wang, *Macromolecular Rapid Communications* **2020**, *41*, 2000064.

[48] M. A. Skylar-Scott, J. Mueller, C. W. Visser, J. A. Lewis, *Nature* **2019**, *575*, 330.

[49] Y. Guo, J. Xu, C. Yan, Y. Chen, X. Zhang, X. Jia, Y. Liu, X. Wang, F. Zhou, *Advanced Engineering Materials* **2019**, *21*, 1801314.

[50] T. Mohan, A. Dobaj Štiglic, M. Beaumont, J. Konnerth, F. Gürer, D. Makuc, U. Maver, L. Gradišnik, J. Plavec, R. Kargl, K. Stana Kleinschek, *ACS Appl. Bio Mater.* **2020**, *3*, 1197.

[51] X. Wan, F. Zhang, Y. Liu, J. Leng, *Carbon* **2019**, *155*, 77.

[52] H. Quan, T. Zhang, H. Xu, S. Luo, J. Nie, X. Zhu, *Bioactive Materials* **2020**, *5*, 110.

[53] P. Garra, J. P. Fouassier, S. Lakhdar, Y. Yagci, J. Lalevée, *Progress in Polymer Science* **2020**, *107*, 101277.

[54] J. Shao, Y. Huang, Q. Fan, *Polym. Chem.* **2014**, *5*, 4195.

[55] J. Zhu, Q. Zhang, T. Yang, Y. Liu, R. Liu, *Nature Communications* **2020**, *11*, 3462.

[56] B. Strehmel, C. Schmitz, T. Bromme, A. Halbhuber, D. Oprych, J. S. Gutmann, *Journal of Photopolymer Science and Technology* **2016**, *29*, 111.

[57] F. P. W. Melchels, J. Feijen, D. W. Grijpma, *Biomaterials* **2010**, *31*, 6121.

[58] J. Wang, A. Goyanes, S. Gaisford, A. W. Basit, *International Journal of Pharmaceutics* **2016**, *503*, 207.

[59] X. Kuang, D. J. Roach, J. Wu, C. M. Hamel, Z. Ding, T. Wang, M. L. Dunn, H. J. Qi, *Advanced Functional Materials* **2019**, *29*, 1805290.

[60] I. Roppolo, A. Chiappone, A. Angelini, S. Stassi, F. Frascella, C. F. Pirri, C. Ricciardi, E. Descrovi, *Materials Horizons* **2017**, *4*, 396.

[61] T. D. Ngo, A. Kashani, G. Imbalzano, K. T. Q. Nguyen, D. Hui, *Composites Part B: Engineering* **2018**, *143*, 172.

[62] M. P. Lee, G. J. T. Cooper, T. Hinkley, G. M. Gibson, M. J. Padgett, L. Cronin, *Scientific Reports* **2015**, *5*.

[63] M. Göppert-Mayer, *Ann. Phys.* **2009**, *18*, 466.

[64] W. Kaiser, C. G. B. Garrett, *Phys. Rev. Lett.* **1961**, *7*, 229.

[65] S. Maruo, O. Nakamura, S. Kawata, *Opt. Lett., OL* **1997**, *22*, 132.

[66] Y. Lin, J. Xu, *Advanced Optical Materials* **2018**, *6*, 1701359.

[67] C. Barner-Kowollik, M. Bastmeyer, E. Blasco, G. Delaittre, P. Müller, B. Richter, M. Wegener, *Angewandte Chemie International Edition* **2017**, *56*, 15828.

[68] J. T. Fourkas, In *Three-Dimensional Microfabrication Using Two-Photon Polymerization (Second Edition)* (Ed.: Baldacchini, T.), William Andrew Publishing, **2020**, pp. 57–76.

[69] W. Qiu, P. Hu, J. Zhu, R. Liu, Z. Li, Z. Hu, Q. Chen, K. Dietliker, R. Liska, *ChemPhotoChem* **2019**, *3*, 1090.

[70] B. Derkowska-Zielinska, L. Skowronski, M. Sypniewska, D. Chomicki, V. Smokal, O. Kharchenko, M. Naparty, O. Krupka, *Optical Materials* **2018**, *85*, 391.

[71] M. Nadgorny, A. Ameli, *ACS Applied Materials & Interfaces* **2018**, *10*, 17489.

[72] S. A. M. Tofail, E. P. Koumoulos, A. Bandyopadhyay, S. Bose, L. O'Donoghue, C. Charitidis, *Materials Today* **2018**, *21*, 22.

[73] A. Pappu, V. K. Thakur, R. Patidar, S. R. Asolekar, M. Saxena, *Journal of Cleaner Production* **2019**, *240*, 118249.

[74] E. M. Palmero, D. Casaleiz, J. de Vicente, J. Hernández-Vicen, S. López-Vidal, E. Ramiro, A. Bollero, *Composites Part A: Applied Science and Manufacturing* **2019**, *124*, 105497.

[75] R. Matsuzaki, M. Ueda, M. Namiki, T.-K. Jeong, H. Asahara, K. Horiguchi, T. Nakamura, A. Todoroki, Y. Hirano, *Sci Rep* **2016**, *6*, 23058.

[76] X. Gao, D. Zhang, S. Qi, X. Wen, Y. Su, *Journal of Applied Polymer Science* **2019**, *136*, 47824.

[77] W. Zhong, F. Li, Z. Zhang, L. Song, Z. Li, *Materials Science and Engineering: A* **2001**, *301*, 125.

[78] G. Ehrmann, A. Ehrmann, *Journal of Applied Polymer Science* **2021**, *138*, 50847.

[79] M. Nikzad, S. H. Masood, I. Sbarski, *Materials & Design* **2011**, *32*, 3448.

[80] M. L. Shofner, K. Lozano, F. J. Rodríguez-Macías, E. V. Barrera, *Journal of Applied Polymer Science* **2003**, *89*, 3081.

[81] G. C. Pidcock, M. in het Panhuis, *Advanced Functional Materials* **2012**, *22*, 4790.

[82] V. Mazzanti, F. Mollica, N. El Kissi, *Polymer Composites* **2016**, *37*, 3460.

[83] M. Barczewski, O. Mysiukiewicz, A. Kloziński, *Iran Polym J* **2018**, *27*, 677.

[84] V. Mazzanti, F. Mollica, *J Polym Environ* **2017**, *25*, 1044.

[85] M. J. A. van den Oever, B. Beck, J. Müssig, *Composites Part A: Applied Science and Manufacturing* **2010**, *41*, 1628.

[86] F. Ciardelli, G. Ruggeri, A. Pucci, *Chem. Soc. Rev.* **2013**, *42*, 857.

[87] G. I. Peterson, M. B. Larsen, M. A. Ganter, D. W. Storti, A. J. Boydston, *ACS Appl. Mater. Interfaces* **2015**, *7*, 577.

[88] M. Dharmarwardana, B. S. Arimilli, M. A. Luzuriaga, S. Kwon, H. Lee, G. A. Appuhamillage, G. T. McCandless, R. A. Smaldone, J. J. Gassensmith, *CrystEngComm* **2018**, *20*, 6054.

[89] M. Dharmarwardana, R. P. Welch, S. Kwon, V. K. Nguyen, G. T. McCandless, M. A. Omary, J. J. Gassensmith, *Chem. Commun.* **2017**, *53*, 9890.

[90] B. M. Boyle, T. A. French, R. M. Pearson, B. G. McCarthy, G. M. Miyake, *ACS Nano* **2017**, *11*, 3052.

[91] A. Vitale, J. T. Cabral, *Materials (Basel)* **2016**, *9*.

[92] C. J. Kloxin, T. F. Scott, C. N. Bowman, *Macromolecules* **2009**, *42*, 2551.

[93] H. Lu, J. A. Carioscia, J. W. Stansbury, C. N. Bowman, *Dental Materials* **2005**, *21*, 1129.

[94] T. Y. Lee, J. Carioscia, Z. Smith, C. N. Bowman, *Macromolecules* **2007**, *40*, 1473.

[95] P. Hu, W. Qiu, S. Naumov, T. Scherzer, Z. Hu, Q. Chen, W. Knolle, Z. Li, *ChemPhotoChem n/a*.

[96] X. Zhang, X. N. Jiang, C. Sun, *www.elsevier.nlrlocatersna Micro-stereolithography of polymeric and ceramic microstructures*, **1998**.

[97] F. Wang, Y. Chong, F. Wang, C. He, *Journal of Applied Polymer Science* **2017**, *134*, 44988.

[98] G. Gonzalez, A. Chiappone, I. Roppolo, E. Fantino, V. Bertana, F. Perrucci, L. Scaltrito, F. Pirri, M. Sangermano, *Polymer* **2017**, *109*, 246.

[99] H. Wei, Q. Zhang, Y. Yao, L. Liu, Y. Liu, J. Leng, *ACS Appl. Mater. Interfaces* **2017**, *9*, 876.

[100] H. Meng, J. Hu, *Journal of Intelligent Material Systems and Structures* **2010**, *21*, 859.

[101] G. Taormina, C. Sciancalepore, F. Bondioli, M. Messori, *Polymers (Basel)* **2018**, *10*.

[102] J. Thévenot, H. Oliveira, O. Sandre, S. Lecommandoux, *Chem. Soc. Rev.* **2013**, *42*, 7099.

[103] R. U. Hassan, S. Jo, J. Seok, *Journal of Applied Polymer Science* **2018**, *135*, 45997.

[104] E. Fantino, A. Chiappone, F. Calignano, M. Fontana, F. Pirri, I. Roppolo, *Materials (Basel)* **2016**, *9*.

[105] Y. Han, F. Wang, H. Wang, X. Jiao, D. Chen, *Composites Science and Technology* **2018**, *154*, 104.

[106] X. Shen, B. Jia, H. Zhao, X. Yang, Z. Liu, *IOP Conf. Ser.: Mater. Sci. Eng.* **2019**, *563*, 022029.

[107] N. Maldonado, V. G. Vegas, O. Halevi, J. I. Martínez, P. S. Lee, S. Magdassi, M. T. Wharmby, A. E. Platero-Prats, C. Moreno, F. Zamora, P. Amo-Ochoa, *Advanced Functional Materials* **2019**, *29*, 1808424.

[108] L. G. Blok, M. L. Longana, H. Yu, B. K. S. Woods, *Additive Manufacturing* **2018**, *22*, 176.

[109] B. Peng, Y. Yang, K. Gu, E. J. Amis, K. A. Cavicchi, *ACS Materials Lett.* **2019**, *1*, 410.

[110] M. Gillono, I. Roppolo, F. Frascella, L. Scaltrito, C. F. Pirri, A. Chiappone, *Applied Materials Today* **2020**, *18*, 100470.

[111] H. Xie, K.-K. Yang, Y.-Z. Wang, *Materials Today: Proceedings* **2019**, *16*, 1524.

[112] N. Barbero, C. Magistris, J. Park, D. Saccone, P. Quagliotto, R. Buscaino, C. Medana, C. Barolo, G. Viscardi, *Organic Letters* **2015**, *17*, 3306.

[113] O. D. Montagnat, G. Lessene, A. B. Hughes, *Tetrahedron Letters* **2006**, *47*, 6971.

[114] S. Perruchas, C. Tard, X. F. Le Goff, A. Fargues, A. Garcia, S. Kahlal, J.-Y. Saillard, T. Gacoin, J.-P. Boilot, *Inorg. Chem.* **2011**, *50*, 10682.

[115] C. Tard, S. Perruchas, S. Maron, X. F. Le Goff, F. Guillen, A. Garcia, J. Vigneron, A. Etcheberry, T. Gacoin, J.-P. Boilot, *Chem. Mater.* **2008**, *20*, 7010.

[116] H. Jiang, G. Guo, W. Chen, Z. Cui, *Dyes and Pigments* **2021**, *194*, 109555.

[117] E. Schab-Balcerzak, M. Siwy, M. Kawalec, A. Sobolewska, A. Chamera, A. Miniewicz, *The Journal of Physical Chemistry A* **2009**, *113*, 8765.

[118] P. A. Ribeiro, D. T. Balogh, J. L. C. Fonseca, J. A. Giacometti, *Macromolecules* **2004**, *37*, 2618.

[119] N. Li, J. Lu, H. Li, E.-T. Kang, *Dyes and Pigments* **2011**, *88*, 18.

[120] L. De Smet, G. Vancoillie, P. Minshall, K. Lava, I. Steyaert, E. Schoolaert, E. Van De Walle, P. Dubruel, K. De Clerck, R. Hoogenboom, *Nature Communications* **2018**, *9*.

[121] H. S. Mehr, N. C. Romano, R. Altamimi, J. M. Modarelli, D. A. Modarelli, *Dalton Transactions* **2015**, *44*, 3176.

[122] S. Yuan, J. Bai, C. K. Chua, J. Wei, K. Zhou, *Composites Part A: Applied Science and Manufacturing* **2016**, *90*, 699.

[123] R. Megha, F. A. Ali, Y. T. Ravikiran, C. H. V. V. Ramana, A. B. V. Kiran Kumar, D. K. Mishra, S. C. Vijayakumari, D. Kim, *Inorganic Chemistry Communications* **2018**, *98*, 11.

[124] C. Li, E. T. Thostenson, T.-W. Chou, *Composites Science and Technology* **2008**, *68*, 1227.

[125] A. de la Vega, J. Sumfleth, H. Wittich, K. Schulte, *J Mater Sci* **2012**, *47*, 2648.

[126] S. Kumar, T. K. Gupta, K. M. Varadarajan, *Composites Part B: Engineering* **2019**, *177*, 107285.

[127] N. Hu, Y. Li, T. Nakamura, T. Katsumata, T. Koshikawa, M. Arai, *Composites Part B: Engineering* **2012**, *43*, 3.

[128] Alamusi, N. Hu, H. Fukunaga, S. Atobe, Y. Liu, J. Li, *Sensors (Basel)* **2011**, *11*, 10691.

[129] B. Li, W.-H. Zhong, *J Mater Sci* **2011**, *46*, 5595.

[130] H. Kim, A. A. Abdala, C. W. Macosko, *Macromolecules* **2010**, *43*, 6515.

[131] R. M. Sankar, K. S. Meera, A. B. Mandal, S. N. Jaisankar, *High Performance Polymers* **2013**, *25*, 135.

[132] S. A. Abdullah, A. Iqbal, L. Frormann, *Journal of Applied Polymer Science* **2008**, *110*, 196.

[133] H. Xia, M. Song, *Soft Matter* **2005**, *1*, 386.

[134] F. Abbasi, H. Mirzadeh, A.-A. Katbab, *Polymer International* **2001**, *50*, 1279.

[135] S. Stassi, E. Fantino, R. Calmo, A. Chiappone, M. Gillono, D. Scaiola, C. F. Pirri, C. Ricciardi, A. Chiadò, I. Roppolo, *ACS Appl. Mater. Interfaces* **2017**, *9*, 19193.

[136] X. Wang, X. Cai, Q. Guo, T. Zhang, B. Kobe, J. Yang, *Chem. Commun.* **2013**, *49*, 10064.

[137] J. M. Goddard, J. H. Hotchkiss, *Progress in Polymer Science* **2007**, *32*, 698.

[138] R. M. Arnold, N. E. Huddleston, J. Locklin, *J. Mater. Chem.* **2012**, *22*, 19357.

[139] I. Roppolo, F. Frascella, M. Gastaldi, M. Castellino, B. Ciubini, C. Barolo, L. Scaltrito, C. Nicosia, M. Zanetti, A. Chiappone, *Polym. Chem.* **2019**, *10*, 5950.

[140] A. B. Lowe, C. E. Hoyle, C. N. Bowman, *J. Mater. Chem.* **2010**, *20*, 4745.

[141] K. Griesbaum, *Angewandte Chemie International Edition in English* **1970**, *9*, 273.

[142] A. B. Lowe, *Polymer* **2014**, *55*, 5517.

[143] A. Massi, D. Nanni, *Org. Biomol. Chem.* **2012**, *10*, 3791.

[144] J. W. Chan, C. E. Hoyle, A. B. Lowe, *J. Am. Chem. Soc.* **2009**, *131*, 5751.

[145] C. E. Hoyle, C. N. Bowman, *Angewandte Chemie International Edition* **2010**, *49*, 1540.

[146] B. D. Fairbanks, T. F. Scott, C. J. Kloxin, K. S. Anseth, C. N. Bowman, *Macromolecules* **2009**, *42*, 211.

[147] David. Briggs, Graham. Beamson, *Anal. Chem.* **1992**, *64*, 1729.

[148] N. S. Bhairamadgi, S. Gangarapu, M. A. C. Campos, J. M. J. Paulusse, C. J. M. van Rijn, H. Zuilhof, *Langmuir* **2013**, *29*, 4535.

[149] D. G. Castner, K. Hinds, D. W. Grainger, *Langmuir* **1996**, *12*, 5083.

[150] J. Jia, A. Kara, L. Pasquali, A. Bendounan, F. Sirotti, V. A. Esaulov, *J. Chem. Phys.* **2015**, *143*, 104702.

[151] L. Pasquali, F. Terzi, R. Seeber, S. Nannarone, D. Datta, C. Dablemont, H. Hamoudi, M. Canepa, V. A. Esaulov, *Langmuir* **2011**, *27*, 4713.

[152] A. Hoffmann, H. Leonards, N. Tobies, L. Pongratz, K. Kreuels, F. Kreimendahl, C. Apel, M. Wehner, N. Nottrodt, *J Tissue Eng* **2017**, *8*, 2041731417744485.

[153] F. Frascella, G. González, P. Bosch, A. Angelini, A. Chiappone, M. Sangermano, C. F. Pirri, I. Roppolo, *ACS Appl. Mater. Interfaces* **2018**, *10*, 39319.

[154] J. Alamán, M. López-Valdeolivas, R. Alicante, C. Sánchez-Somolinos, *Sensors (Basel)* **2019**, *19*.

[155] K. Jakubowski, W. Kerkemeyer, E. Perret, M. Heuberger, R. Hufenus, *Materials & Design* **2020**, *196*, 109131.

[156] D. Niu, L. Wang, Q. Xu, M. Jiang, X. Wang, X. Sun, F. Wang, D. Zhang, *Appl. Opt., AO* **2019**, *58*, 1276.

[157] S.-H. Oh, K.-D. Ahn, H.-Y. Choi, *Opt. Eng.* **2019**, *58*, 1.

[158] J. W. Choi, Y. M. Ha, S. H. Lee, K. H. Choi, *J Mech Sci Technol* **2006**, *20*, 2094.

[159] H. Ma, A. K.-Y. Jen, L. R. Dalton, *Advanced Materials* **2002**, *14*, 1339.

[160] J. Feng, Q. Jiang, P. Rogin, P. W. de Oliveira, A. del Campo, *ACS Appl. Mater. Interfaces* **2020**, *12*, 20287.

[161] J. Guo, C. Yang, Q. Dai, L. Kong, *Sensors (Basel)* **2019**, *19*.

[162] C.-L. Sun, Z. Gao, K.-X. Teng, L.-Y. Niu, Y.-Z. Chen, Y. S. Zhao, Q.-Z. Yang, *ACS Appl. Mater. Interfaces* **2018**, *10*, 26526.

[163] C. A. Briehn, M.-S. Schiedel, E. M. Bonsen, W. Schuhmann, P. Bäuerle, *Angewandte Chemie International Edition* **2001**, *40*, 4680.

[164] C. Gu, N. Huang, Y. Chen, L. Qin, H. Xu, S. Zhang, F. Li, Y. Ma, D. Jiang, *Angewandte Chemie International Edition* **2015**, *54*, 13594.

[165] A. Garreau, J.-L. Duvail, *Advanced Optical Materials* **2014**, *2*, 1122.

[166] H. Xia, T. Chen, C. Hu, K. Xie, *Polymers (Basel)* **2018**, *10*.

[167] R. Stach, J. Haas, E. Tütüncü, S. Daboss, C. Kranz, B. Mizaikoff, *ACS Sens.* **2017**, *2*, 1700.

[168] S. Khan, N. Vahabisani, M. Daneshmand, *IEEE Transactions on Components, Packaging and Manufacturing Technology* **2017**, *7*, 70.

[169] F. Zhao, D. Cambié, J. Janse, E. W. Wieland, K. P. L. Kuijpers, V. Hessel, M. G. Debije, T. Noël, *ACS Sustainable Chem. Eng.* **2018**, *6*, 422.

[170] Q. Mu, C. K. Dunn, L. Wang, M. L. Dunn, H. J. Qi, T. Wang, *Smart Mater. Struct.* **2017**, *26*, 045008.

[171] N. Huby, J. Bigeon, Q. Lagneaux, M. Amela-Cortes, A. Garreau, Y. Molard, J. Fade, A. Desert, E. Faulques, B. Bêche, J.-L. Duvail, S. Cordier, *Optical Materials* **2016**, *52*, 196.

[172] Y. Xia, B. Xue, M. Qin, Y. Cao, Y. Li, W. Wang, *Scientific Reports* **2017**, *7*, 1.

[173] Y. Ren, J. Feng, *ACS Appl. Mater. Interfaces* **2020**, *12*, 6797.

[174] S. Moynihan, R. Van Deun, K. Binnemans, G. Redmond, *Optical Materials* **2007**, *29*, 1821.

[175] Z. Li, P. Liu, X. Ji, J. Gong, Y. Hu, W. Wu, X. Wang, H.-Q. Peng, R. T. K. Kwok, J. W. Y. Lam, J. Lu, B. Z. Tang, *Advanced Materials n/a*, 1906493.

[176] D. Ahn, L. M. Stevens, K. Zhou, Z. A. Page, *ACS Cent Sci* **2020**, *6*, 1555.

[177] M. Gastaldi, I. Roppolo, A. Chiappone, C. Garino, A. Fin, M. Manachino, P. Sirianni, G. Viscardi, L. Scaltrito, M. Zanetti, S. Bordiga, C. Barolo, *Additive Manufacturing* **2022**, *49*, 102504.

[178] I. Roppolo, E. Celasco, A. Fargues, A. Garcia, A. Revaux, G. Dantelle, F. Maroun, T. Gacoin, J.-P. Boilot, M. Sangermano, S. Perruchas, *Journal of Materials Chemistry* **2011**, *21*, 19106.

[179] S. Perruchas, X. F. Le Goff, S. Maron, I. Maurin, F. Guillen, A. Garcia, T. Gacoin, J.-P. Boilot, *Journal of the American Chemical Society* **2010**, *132*, 10967.

[180] B. Li, H.-T. Fan, S.-Q. Zang, H.-Y. Li, L.-Y. Wang, *Coordination Chemistry Reviews* **2018**, *377*, 307.

[181] B. Xin, J. Sang, Y. Gao, G. Li, Z. Shi, S. Feng, *RSC Adv.* **2018**, *8*, 1973.

[182] E. Cariati, E. Lucenti, C. Botta, U. Giovanella, D. Marinotto, S. Righetto, *Coordination Chemistry Reviews* **2016**, *306*, 566.

[183] F. De Angelis, S. Fantacci, A. Sgamellotti, E. Cariati, R. Ugo, P. C. Ford, *Inorg Chem* **2006**, *45*, 10576.

[184] E. Pantuso, G. D. Filpo, F. P. Nicoletta, *Advanced Optical Materials* **2019**, *7*, 1900252.

[185] H. Y. Jiang, S. Kelch, A. Lendlein, *Advanced Materials* **2006**, *18*, 1471.

[186] P. Weis, S. Wu, *Macromol Rapid Commun* **2018**, *39*.

[187] O. S. Bushuyev, M. Aizawa, A. Shishido, C. J. Barrett, *Macromol Rapid Commun* **2018**, *39*.

[188] V. Y. Chang, C. Fedele, A. Priimagi, A. Shishido, C. J. Barrett, *Advanced Optical Materials* **2019**, *7*, 1900091.

[189] E. Merino, *Chemical Society Reviews* **2011**, *40*, 3835.

[190] A. Priimagi, A. Shevchenko, *Journal of Polymer Science Part B: Polymer Physics* **2014**, *52*, 163.

[191] S. Yang, J. D. Harris, A. Lambai, L. L. Jeliazkov, G. Mohanty, H. Zeng, A. Priimagi, I. Aprahamian, *Journal of the American Chemical Society* **2021**.

[192] H. Zhou, C. Xue, P. Weis, Y. Suzuki, S. Huang, K. Koynov, G. K. Auernhammer, R. Berger, H.-J. Butt, S. Wu, *Nature Chemistry* **2017**, *9*, 145.

[193] A. Goulet-Hanssens, T. C. Corkery, A. Priimagi, C. J. Barrett, *J. Mater. Chem. C* **2014**, *2*, 7505.

[194] J. V. Accardo, J. A. Kalow, *Chem. Sci.* **2018**, *9*, 5987.

[195] C. Liu, H. Qin, P. T. Mather, *J. Mater. Chem.* **2007**, *17*, 1543.

[196] J. Hu, Y. Zhu, H. Huang, J. Lu, *Progress in Polymer Science* **2012**, *37*, 1720.

[197] L. C. Chang, T. A. Read, *JOM* **1951**, *3*, 47.

[198] F. El Feninat, G. Laroche, M. Fiset, D. Mantovani, *Advanced Engineering Materials* **2002**, *4*, 91.

[199] J. Van Humbeeck, *Advanced Engineering Materials* **2001**, *3*, 837.

[200] K. Otsuka, X. Ren, *Progress in Materials Science* **2005**, *50*, 511.

[201] E. Farber, J.-N. Zhu, A. Popovich, V. Popovich, *Materials Today: Proceedings* **2020**, *30*, 761.

[202] M. Behl, M. Y. Razzaq, A. Lendlein, *Advanced Materials* **2010**, *22*, 3388.

[203] Y. Shi, M. Yoonessi, R. A. Weiss, *Macromolecules* **2013**, *46*, 4160.

[204] J. Kunzelman, T. Chung, P. T. Mather, C. Weder, *J. Mater. Chem.* **2008**, *18*, 1082.

[205] C. Zeng, H. Seino, J. Ren, N. Yoshie, *ACS Appl. Mater. Interfaces* **2014**, *6*, 2753.

[206] F. Castro, K. K. Westbrook, J. Hermiller, D. U. Ahn, Y. Ding, H. J. Qi, *Journal of Engineering Materials and Technology* **2011**, *133*.

[207] R. Mohr, K. Kratz, T. Weigel, M. Lucka-Gabor, M. Moneke, A. Lendlein, *PNAS* **2006**, *103*, 3540.

[208] A. M. Schmidt, *Macromolecular Rapid Communications* **2006**, *27*, 1168.

[209] J. W. Cho, J. W. Kim, Y. C. Jung, N. S. Goo, *Macromolecular Rapid Communications* **2005**, *26*, 412.

[210] N. G. Sahoo, Y. C. Jung, N. S. Goo, J. W. Cho, *Macromolecular Materials and Engineering* **2005**, *290*, 1049.

[211] W. M. Huang, B. Yang, L. An, C. Li, Y. S. Chan, *Appl. Phys. Lett.* **2005**, *86*, 114105.

[212] B. Yang, W. M. Huang, C. Li, C. M. Lee, L. Li, *Smart Mater. Struct.* **2003**, *13*, 191.

[213] H. Du, J. Zhang, *Soft Matter* **2010**, *6*, 3370.

[214] D. Aoki, Y. Teramoto, Y. Nishio, *Biomacromolecules* **2007**, *8*, 3749.

[215] M. Herath, J. Epaarachchi, M. Islam, L. Fang, J. Leng, *European Polymer Journal* **2020**, *136*, 109912.

[216] H. Zhang, Y. Zhao, *ACS Appl. Mater. Interfaces* **2013**, *5*, 13069.

[217] N. Yenpech, V. Intasanta, S. Chirachanchai, *Polymer* **2019**, *182*, 121792.

[218] S. Ishii, K. Uto, E. Niiyama, M. Ebara, T. Nagao, *ACS Appl Mater Interfaces* **2016**, *8*, 5634.

[219] S. V. Ahir, E. M. Terentjev, *Nature Mater* **2005**, *4*, 491.

[220] H. M. C. M. Herath, J. A. Epaarachchi, M. M. Islam, W. Al-Azzawi, J. Leng, F. Zhang, *Composites Science and Technology* **2018**, *167*, 206.

[221] Y. Liu, G. Zhu, W. Liu, H. Liu, Y. Huo, T. Ren, X. Hou, *Smart Mater. Struct.* **2018**, *27*, 095008.

[222] J. Loomis, X. Fan, F. Khosravi, P. Xu, M. Fletcher, R. W. Cohn, B. Panchapakesan, *Sci Rep* **2013**, *3*, 1900.

[223] L. Fang, S. Chen, T. Fang, J. Fang, C. Lu, Z. Xu, *Composites Science and Technology* **2017**, *138*, 106.

[224] A. Lendlein, H. Jiang, O. Jünger, R. Langer, *Nature* **2005**, *434*, 879.

[225] Y. Li, O. Rios, J. K. Keum, J. Chen, M. R. Kessler, *ACS Appl. Mater. Interfaces* **2016**, *8*, 15750.

[226] K. M. Lee, H. Koerner, R. A. Vaia, T. J. Bunning, T. J. White, *Soft Matter* **2011**, *7*, 4318.

[227] N. Hurduc, B. C. Donose, A. Macovei, C. Paius, C. Ibanescu, D. Scutaru, M. Hamel, N. Branza-Nichita, L. Rocha, *Soft Matter* **2014**, *10*, 4640.

[228] A. S. Kuenstler, K. D. Clark, J. Read de Alaniz, R. C. Hayward, *ACS Macro Lett.* **2020**, *9*, 902.

[229] G. J. Fang, J. E. Maclennan, Y. Yi, M. A. Glaser, M. Farrow, E. Korblova, D. M. Walba, T. E. Furtak, N. A. Clark, *Nat Commun* **2013**, *4*, 1521.

[230] J. Vapaavuori, A. Laventure, C. G. Bazuin, O. Lebel, C. Pellerin, *J. Am. Chem. Soc.* **2015**, *137*, 13510.

[231] Q. Mu, L. Wang, C. K. Dunn, X. Kuang, F. Duan, Z. Zhang, H. J. Qi, T. Wang, *Additive Manufacturing* **2017**, *18*, 74.

[232] D. Martella, S. Nocentini, F. Micheletti, D. S. Wiersma, C. Parmeggiani, *Soft Matter* **2019**, *15*, 1312.

[233] Y. Norikane, E. Uchida, S. Tanaka, K. Fujiwara, E. Koyama, R. Azumi, H. Akiyama, H. Kihara, M. Yoshida, *Org. Lett.* **2014**, *16*, 5012.

[234] C. A. Spiegel, M. Hackner, V. P. Bothe, J. P. Spatz, E. Blasco, *Advanced Functional Materials n/a*, 2110580.

[235] A. P. Piedade, *J Funct Biomater* **2019**, *10*.

[236] M. Ulbricht, *Polymer* **2006**, *47*, 2217.

[237] S. Hassan, R. Anandakathir, M. J. Sobkowicz, B. M. Budhlall, *Polym. Chem.* **2016**, *7*, 1452.

[238] M. Kameda, K. Sumaru, T. Kanamori, T. Shinbo, *Journal of Applied Polymer Science* **2003**, *88*, 2068.

[239] E. Głowacki, K. Horovitz, C. W. Tang, K. L. Marshall, *Advanced Functional Materials* **2010**, *20*, 2778.

[240] W. Shi, J. Deng, H. Qin, D. Wang, C. Zhao, *Journal of Membrane Science* **2014**, *455*, 357.

[241] Z. Wang, A. Knebel, S. Grosjean, D. Wagner, S. Bräse, C. Wöll, J. Caro, L. Heinke, *Nature Communications* **2016**, *7*, 1.

[242] N. Prasetya, B. C. Donose, B. P. Ladewig, *J. Mater. Chem. A* **2018**, *6*, 16390.

[243] M. Al Kobaisi, S. V. Bhosale, K. Latham, A. M. Raynor, S. V. Bhosale, *Chem. Rev.* **2016**, *116*, 11685.

[244] A. Fin, I. Petkova, D. A. Doval, N. Sakai, E. Vauthey, S. Matile, *Org. Biomol. Chem.* **2011**, *9*, 8246.

[245] H. Lin, T. Kai, B. D. Freeman, S. Kalakkunnath, D. S. Kalika, *Macromolecules* **2005**, *38*, 8381.

[246] J. Zheng, K. Kwak, X. Chen, J. B. Asbury, M. D. Fayer, *J. Am. Chem. Soc.* **2006**, *128*, 2977.

[247] E. S. Kryachko, M. T. Nguyen, *J. Phys. Chem. A* **2002**, *106*, 4267.